Investigating the Role of the Inhibitor of Apoptosis Proteins (IAPs) in Metastasis Formation

Thesis

Maria Teresa Majorini

Degree in Biological Sciences

OU personal identifier: D1934968

Investigating the Role of the Inhibitor of Apoptosis Proteins (IAPs) in Metastasis Formation

Thesis presented for the Degree of Doctor of Philosophy

The Open University, Milton Keynes (UK)

Faculty of Science Technology Engineering and Mathematics (STEM)

Discipline: School of Life, Health and Chemical Sciences

Date of submission: November 2017

Affiliated Research Centre:

Fondazione IRCCS Istituto Nazionale dei Tumori, Milan (Italy)

Director of studies: Dr. Domenico Delia

Internal supervisor: Dr. Daniele Lecis

External supervisor: Prof. Mads Gyrd-Hansen

ACKNOWLEDGEMENTS

"*Knowledge is in the end based on acknowledgement*"-Ludwig Wittgenstein.

This thesis has become a reality not only because of my dedication but also thanks to the kind support of many people who encouraged me during this PhD period. First and foremost, I would like to thank my Director of Studies, Dr. Domenico Delia, for supervising my PhD project, encouraging my work and for allowing me to grow as a scientist. I would like to express my sincere gratitude to my supervisor Dr. Daniele Lecis for his patient guidance, motivation, advice and immense knowledge. I have been extremely lucky to have a supervisor who cared so much about my work, and who responded to my questions and queries so promptly. His support helped me in all the time of my course of research and in writing this thesis. I am also extremely grateful to my External Supervisor, Prof. Mads Gyrd-Hansen, for his insightful comments and encouragement, but also for his hard questions that have always incentivised me to widen my research from various perspectives.

I wholeheartedly thank my best lab mate and friend, Annalisa, for the stimulating discussions and for all the fun we had in the last four years. She greatly supported me and was always willing to help me. Other past and present colleagues, which I had the pleasure to work with or alongside: Alessandro, Raina, Matteo, Antonio, Luigi, Enrico, Michela, Martina, Laura, Clara, Alice, Maria Chiara, Paola and Vincenzo. They have been unwavering in their personal and professional support during my PhD period.

It is my fortune to gratefully acknowledge the support of my friends, Alessandra, Roberta, Ramona and Serena for always encouraging, helping, and standing by me. They were always beside me during the happy and hard moments to push and motivate me.

Finally, there is my family. No words can express the feelings that I have for my parents: they gave me their constant unconditional love, taught me determination and helped me in whatsoever way they could do during this challenging period. I could not have done this without them. This thesis is dedicated to my beloved sister, Anna, and to her husband Andrea, wishing them to have a future filled with all the blessings and joys of life. *Thank you.*

DECLARATION OF AUTHORSHIP

I hereby certify that the thesis I am submitting is my own original work, except for experiments and analyses listed below:

- *In vivo* experiments performed using MDA-MB231 cells subcutaneously engrafted in NOD/SCID mice were performed by Dr. Daniele Lecis and Dr. Giacomo Manenti.
- Gene expression profiling and bioinformatics analyses were performed in collaboration with the Functional Genomics and Bioinformatic core facility of Fondazione IRCCS Istituto Nazionale dei Tumori.
- IHC staining was performed by the Immunohistochemistry facility of Fondazione IRCCS Istituto Nazionale dei Tumori.
- *In vivo* experiments performed using 4T1 cells injected in immuno-competent BALB/c mice were carried out by Dr. Claudia Chiodoni.

TABLE OF CONTENTS

1 ABSTRACT

Inhibitor of apoptosis proteins (IAPs) constitute a conserved family of molecules, which regulate both apoptosis and receptor signalling. They are often deregulated in cancer cells and represent potential targets for therapy. In my work, I investigated the effect of IAP inhibition *in vivo* to identify novel down-stream genes expressed in an IAP-dependent manner that could contribute to cancer aggressiveness. To this end, immunocompromised mice engrafted subcutaneously with the triple negative breast cancer (TNBC) cell line MDA-MB231 were treated with SM83, a Smac mimetic developed in our laboratory that acts as a pan-IAP inhibitor, and tumour nodules were profiled for gene expression. The analysis revealed that the inhibition of IAPs significantly reduces the expression of SNAI2, a zinc finger transcriptional repressor often associated with cancer aggressiveness, resistance to therapy and metastatic potential, especially in breast cancer. By testing several TNBC cell lines, I found that SNAI2 levels is promoted specifically by cellular IAP1 (cIAP1), and not by other IAPs, and that SM83-dependent down-regulation of SNAI2 reduces cancer cell motility. Accordingly, cIAP1 depletion blocks epidermal growth factor receptor (EGFR)-dependent activation of the mitogen-activated protein kinase (MAPK) pathway causing the reduction of SNAI2 transcription levels. The inhibition of EGFR signalling stems from the block of receptor signalling and from the down-regulation of its levels, but paradoxically the silencing of cIAP1 promotes EGFR stability rather than its degradation. Nonetheless, EGFR levels decrease upon cIAP1 silencing due to reduced NF-kB-dependent gene expression supporting the notion that cIAP1 controls EGFR in an opposite fashion, promoting its gene expression while causing its degradation. In conclusion, my work indicates that IAP-targeted therapy could contribute to

EGFR inhibition and to the reduction of its down-stream mediators. This approach could be particularly effective in tumours characterized by high levels of EGFR and SNAI2, such as TNBCs.

2 INTRODUCTION

2.1 Apoptosis: a process of programmed cell death

Apoptosis is the most studied type of programmed cell death; it is regulated by molecular pathways, which are evolutionarily conserved among the species (Degterev and Yuan, 2008). Apoptosis is crucial during embryonic development of multicellular organisms and, therefore, its deregulation is responsible for several diseases (Favaloro *et al.*, 2012). For instance, excessive apoptosis leads to neurodegeneration (Mattson, 2000), while insufficient activation of the apoptotic machinery results in autoimmune disorders (Nagata, 2010) and many cancer types. Accordingly, pathological inhibition of apoptosis has been shown to favour cancer development. Therefore, several approaches have been designed to induce apoptosis or prevent its inhibition in tumours in order to eradicate them.

Resistance to apoptosis is one of the hallmarks of cancer, which were proposed by Hannah and Weinberg (Hanahan and Weinberg, 2011; Figure 2.1). In fact, aggressive tumours develop various strategies to escape the apoptotic process, and there is therefore the need to target the apoptotic blocks in order to promote the activity of therapeutic treatments, which usually rely on apoptotic activation to be effective (Gimenez-Bonafe *et al.*, 2009).

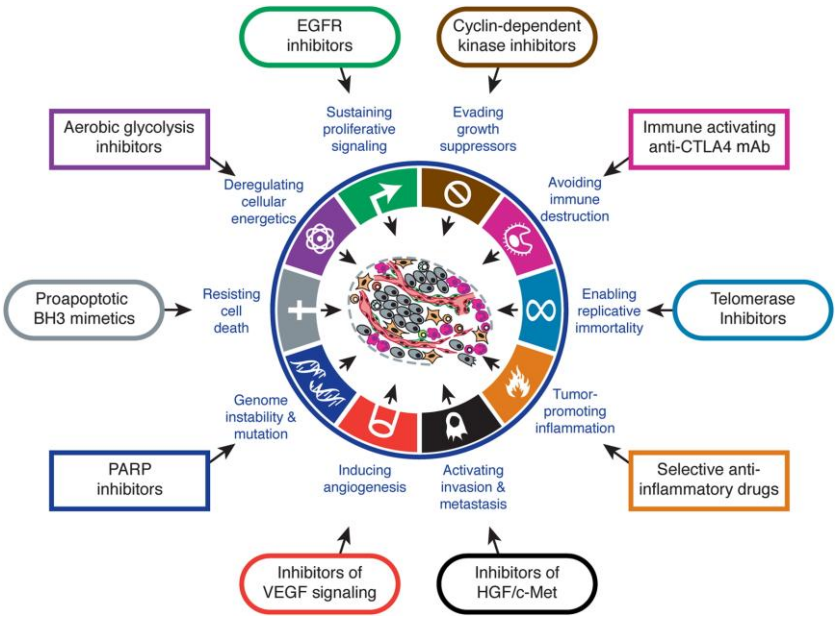

Figure 2.1 - Hallmarks of cancer (Hanahan and Weinberg, 2011)**.** The figure shows the hallmarks of cancer that characterize neoplastic cells compared to normal cells.

2.1.1 Mechanisms of apoptosis

Two main pathways constitute the apoptotic machinery: the extrinsic and the intrinsic apoptotic programs, which both depend on the balance between pro- and anti-apoptotic effectors. The extrinsic pathway senses and propagates death-inducing signals and soluble factors originated from the microenvironment outside the cells, while the intrinsic circuit is triggered by a variety of intra-cellular signals (Fulda and Debatin, 2006; Galluzzi *et al.*, 2012). Importantly, these two pathways are tightly linked and culminate in the activation of normally inactive proteases (caspases-8 and -9, respectively), which, in turn, trigger the effector caspases (caspases-3, -6 and -7). The final step is then the execution phase of apoptosis, thus leading to the cell disruption.

Although different mechanisms regulate programmed cell death, all the apoptosis pathways converge in the activation of caspases, which are therefore executioners of

apoptosis (Figure 2.2). Caspases are conserved cysteine proteases that, in the absence of apoptosis signals, are expressed as inactive zymogens (pro-caspases) and, upon strictly controlled activation, acquire the capability to cleave their substrates after an aspartate residue (Thornberry and Lazebnik, 1998). Caspases are classified in initiator and effector depending whether they are apical activators of the apoptotic pathway or if they amplify an up-stream stimulus received by another caspase. Of note, initiator and effector caspases are characterized by a different structure. Initiator caspases display a long pro-domain that interacts with the up-stream adapter molecules through two different motifs: the caspase recruitment domain (CARD; caspase-2, -9) and the death effector domain (DED; caspase-8 and -10). On the contrary, a short pro-domain defines effector caspases (caspase-3, -6 and -7) and allows the cleavage of diverse substrates, which have already been processed by up-stream caspases, leading to the apoptosis demolition phase. A vast number of substrates can be cleaved by caspases (Fischer *et al.*, 2003), such as nuclear lamin, inhibitor of caspase activated DNase (ICAD) and especially cleaved poly(adenosine diphosphate–ribose)polymerase (PARP), which, upon cleavage, is universally exploited as a marker for apoptotic cells (Nosseri *et al.*, 1994).

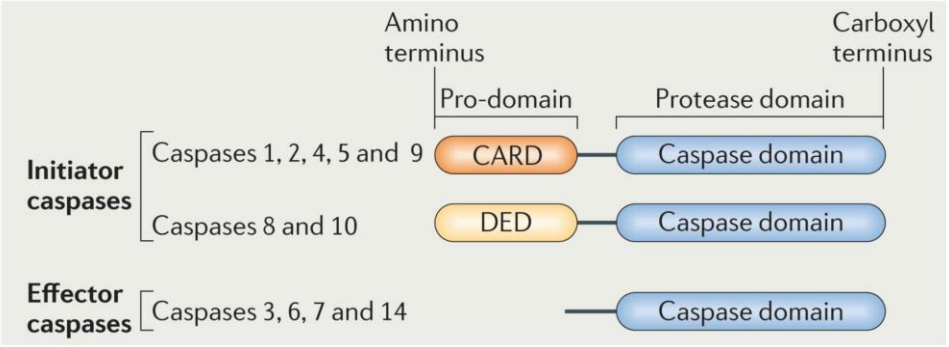

Figure 2.2 - Human caspase-mediated apoptosis (Lamkanfi, 2011). Based on their mechanism of action, caspases are distinguished in initiator caspases and effector caspases. Initiator caspase-8 and -10 comprise a DED motif in their long pro-domain, while the other initiator caspases show the CARD motif.

Importantly, the caspase-mediated proteolytic process is accompanied by discrete morphological changes resulting from various events, including DNA fragmentation, chromatin condensation and nuclear remodelling (Figure 2.3). Interestingly, apoptotic cells, on the basis of morphological alterations, can be distinguished from cells dying by diverse types of death, such as necrosis, necroptosis and autophagy (Degterev and Yuan, 2008; Galluzzi *et al.*, 2015).

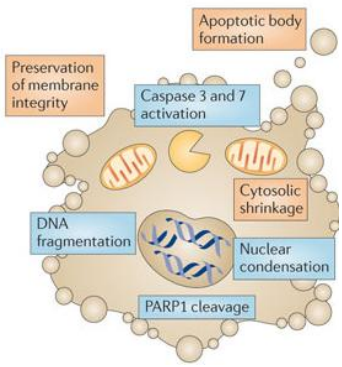

Figure 2.3 - Morphological changes in apoptotic cells. Adapted from (Lamkanfi, 2011). Apoptosis is accompanied by a variety of biochemical and morphological features, including nuclear condensation and oligo-nucleosomal DNA fragmentation, shrinkage of the cell, cytoplasmic packing in apoptotic bodies and rapid phagocytosis by neighbouring cells. Cleaved PARP is commonly used as marker of apoptosis. All these features uniquely identify the apoptosis process.

2.1.2 The intrinsic apoptotic pathway

The activation of the intrinsic apoptosis pathway is mediated by diverse non-receptor-induced stimuli that produce intracellular signals leading to mitochondrial-

dependent death. In response to the mitochondrial outer membrane permeabilization (MOMP), cytochrome c is released from the inter-mitochondrial membrane space to the cytosol, where forms the apoptosome by interacting with the initiator caspase-9 and apoptotic protease activating factor 1 (APAF-1; Reubold and Eschenburg, 2012). This event is tightly controlled by the B-cell lymphoma-2 (BCL-2) family members (Figure 2.4), and, in particular, it is inhibited by the anti-apoptotic (BCL-2, BCL-XL and myeloid cell leukaemia 1-MCL-1) proteins, whereas it is promoted by the pro-apoptotic (BCL-2 antagonist killer 1 –BAK, BCL-2-associated X protein –BAX and BH3-only protein -BID) ones. Following apoptosome formation, caspase-9 is cleaved and activates the effector caspases-3, -6 and -7. These caspases, in turn, cleave diverse cellular substrates hence causing the biochemical and morphological changes, which are classically associated with the apoptotic phenotype (Danial and Korsmeyer, 2004).

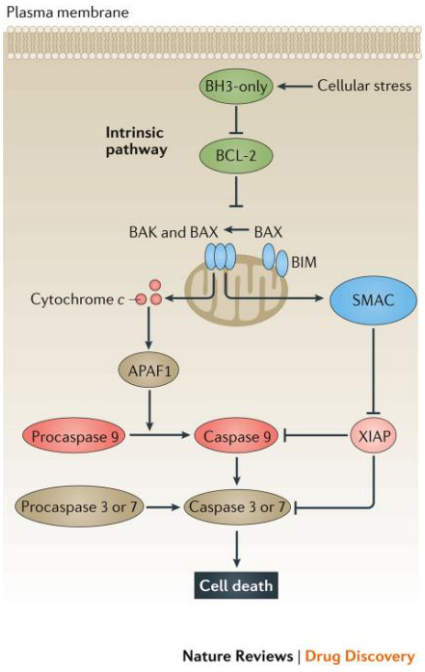

Figure 2.4 - The intrinsic apoptosis signalling pathway (Ashkenazi *et al.*, 2017). Cellular stress, either DNA damage or endoplasmic reticulum (ER) stress, induces the intrinsic apoptosis pathway with consequent

inhibition of the anti-apoptotic proteins, BCL-2, BCL-XL, BCL-W and MCL-1, and subsequent activation of the pro-apoptotic ones, BAK and BAX. This event results in MOMP, which allows the release of cytochrome c from the mitochondria. Once in the cytosol, cytochrome c forms a complex with pro-caspase-9 and APAF-1, thus activating the caspase-9. The latter promotes the induction of pro-caspase-3 and -7, and consequently cell death.

2.1.3 The extrinsic apoptotic pathway

The extrinsic apoptotic program, also named death receptor-dependent pathway, is activated by the binding of death ligands belonging to the tumour necrosis factor (TNF) superfamily to its cognate receptors, the TNF-Receptors (TNF-Rs), which are localized in the cell surface (Walczak, 2013). The stimulation of the TNF-Rs leads to rapid activation of the initiator caspase-8 and -10 (Barnhart *et al.*, 2003; Dickens *et al.*, 2012; Ganten *et al.*, 2004), which are critically involved in the activation of apoptosis signalling. In details, upon binding to its ligand, the adaptor proteins Fas-associated protein with death domain (FADD) and TNF receptor-associated protein with death domain (TRADD) are recruited to the receptor (Figure 2.5). The formed complex, named death-inducing signalling complex (DISC; Scaffidi *et al.*, 1998), allows pro-caspases-8 and -10 dimerization and activation, which results in the processing of their down-stream effector caspases-3, -6 and -7 (McIlwain *et al.*, 2013).

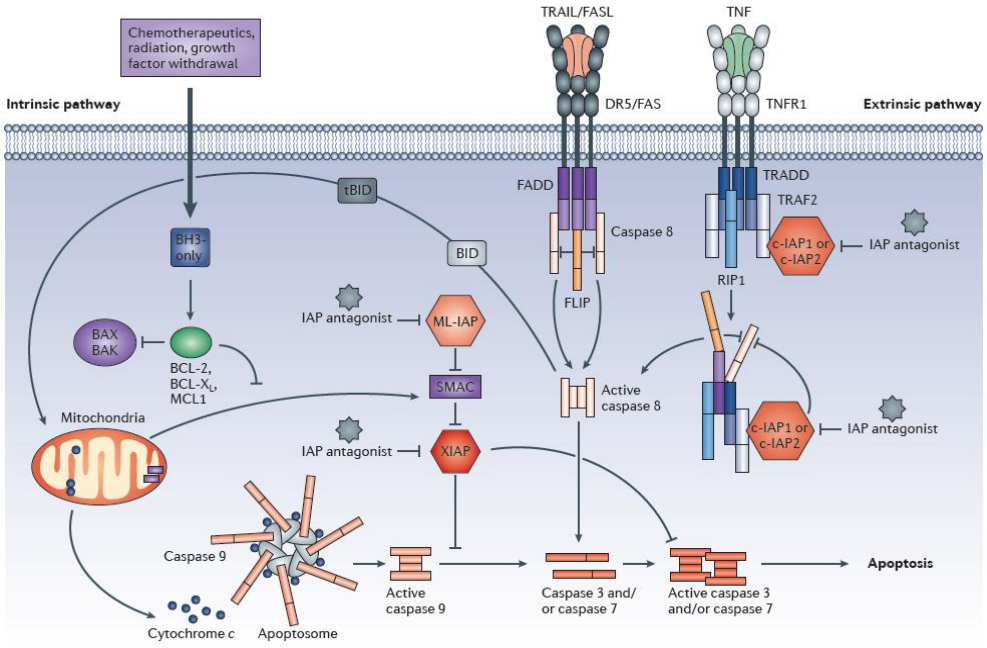

Figure 2.5 - Overview of the apoptosis pathways (Fulda and Vucic, 2012)**.** Both external and internal stimuli are responsible for apoptosis pathway activation. The extrinsic pathway is induced by binding of death ligands to the cognate receptors. Upon ligand binding, cytoplasmic adapter proteins are recruited, thus forming the DISC. This complex is responsible for the auto-catalytic activation of initiator caspases triggering to the execution phase of apoptosis. The cross-talk between extrinsic and intrinsic pathways occurs at the mitochondria. When mitochondria undergo MOMP, the apoptosome is formed and activates the initiator caspase-9 thus propagating the apoptotic process.

Although caspase-3 is capable of cleaving a number of substrates necessary for cell viability, the activation of caspase-8 and -3 is not always sufficient to kill cells. Cells are therefore divided in two groups: “type I” and “type II” (Ozoren and El-Deiry, 2002). While in “type I” cells the activation of the extrinsic pathway is sufficient to induce irreversible damage that crucially compromises cell viability, “type II” cells require the involvement of mitochondria to efficiently activate apoptosis (Figure 2.6). In these cells, caspase-8 cleaves BID, thereby generating the activated truncated form of BID, t-BID (Kantari and Walczak,

2011), which leads to MOMP via the direct activation of BAX and BAK. This step is therefore in common between the extrinsic and intrinsic pathways and allows their cross-talk.

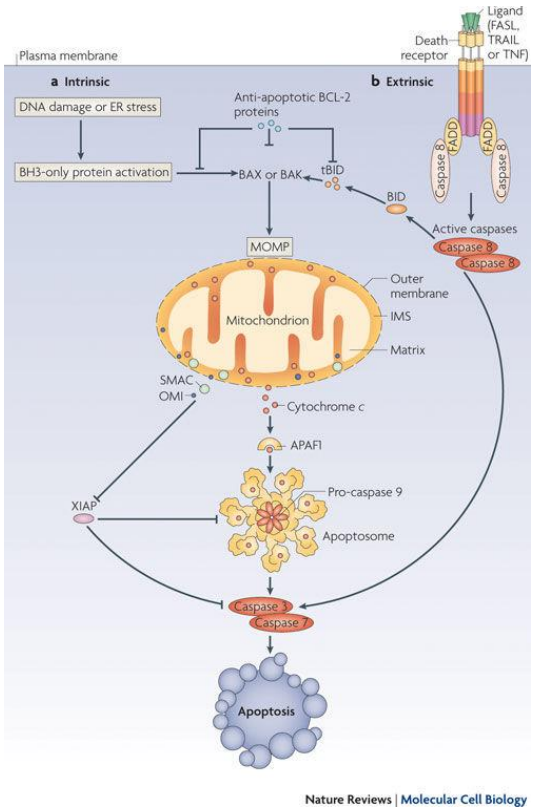

Figure 2.6 - Regulation of cell death by mitochondria (Tait and Green, 2010)**.** The cross-talk between intrinsic and extrinsic apoptosis pathways is mediated by mitochondria and occurs after caspase-8-mediated cleavage and subsequent activation of BID (t-BID, hereafter). T-BID causes MOMP, which favours the release of various proteins from the mitochondrial intermembrane space, thus promoting caspase activation and apoptosis.

2.2 IAPs: Inhibitors of apoptosis proteins

Extrinsic and intrinsic apoptotic signals are controlled by the inhibitor of apoptosis protein (IAP) family, which consists of eight members, called X-linked IAP (XIAP), cIAP1, cIAP2, neuronal-IAP (NAIP), Survivin, Livin (ML-IAP), Apollon (BRUCE) and ILP-2 (Figure 2.7). Although IAPs were initially described as being negative regulators of apoptosis, later works have clarified their role also in controlling several other cell features and mechanisms (Rothe

et al., 1995; Damgaard and Gyrd-Hansen, 2011). The activity on caspases has been confirmed only for 2-3 members of the family and it is likely to be restricted to limited settings (Choi *et al.*, 2009; Eckelman *et al.*, 2006). IAPs are ubiquitously expressed and their expression is deregulated in diseases and cancer cells, where they contribute to chemoresistance and poor prognosis (Gyrd-Hansen and Meier, 2010). For this reason, IAPs are considered potential targets in clinical oncology and many pharmacological approaches have been designed to inhibit the members of this family.

2.2.1 IAP structure and conserved domains

IAPs are characterized by the presence of one or three conserved motifs of about 70 aminoacids, named baculoviral IAP repeat (BIR) domains (Birnbaum *et al.*, 1994), originally identified in the baculoviral genome. Through this domain, IAPs, also called BIR-containing proteins (BIRCs), interact with other proteins. XIAP, cIAP1, and cIAP2 are among the most characterized IAPs and contain three BIR domains (Figure 2.7) that mediate protein-protein interactions. Moreover, XIAP and cIAP1/2 bear a domain named really interesting new gene (RING), which confers the E3 ubiquitin ligase activity that allows the binding with the E2 ubiquitin-conjugating enzymes and catalyzes the transfer of ubiquitin to a target substrate (Vaux and Silke, 2005). Therefore, the RING domain provides IAPs with the capability to polyubiquitinate proteins, such as caspases and many other substrates, and also to self-ubiquitinate. Ubiquitination can induce either proteasomal degradation or regulation of the target proteins in several signalling cascades (Chen, 2012). Other two additional domains identify some IAPs: a caspase-associated recruitment domain (CARD) and an ubiquitin-associated (UBA) domain. CARD regulates the E3 activity preventing RING domain

dimerization, which is essential for cIAP1 to exert its activity (Lopez *et al.*, 2011). While cIAPs affect the apoptotic process only indirectly, XIAP is considered as a direct inhibitor of caspases. In particular, the BIR3 domain of XIAP interacts with caspase-9, preventing its activation, whereas activated caspase-3 and -7 are sequestered after the interaction with the BIR2 and the up-stream linker region (Chai *et al.*, 2001; Datta *et al.*, 2000; Riedl *et al.*, 2001).

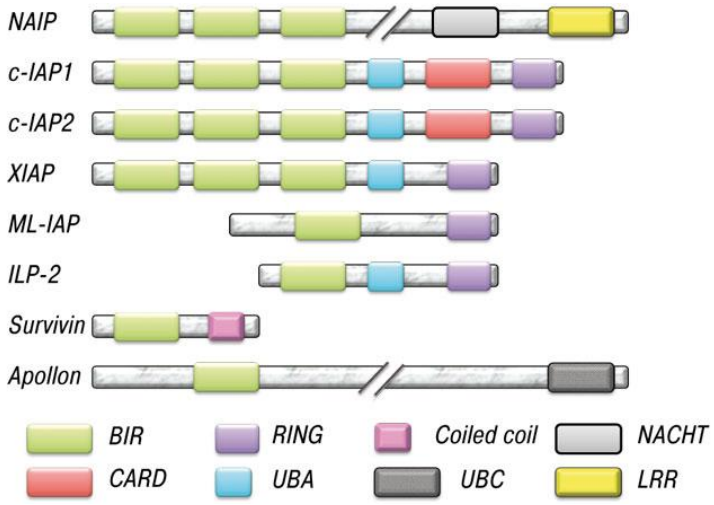

Figure 2.7 - Structural domains of IAP family members. Adapted from (de Almagro and Vucic, 2012). The IAP family is constituted by eight members characterized by one or three BIR domains, typically located in the protein amino(N)-terminus. Several mammalian IAPs share the presence of the additional structural domain RING, which functions as an E3 ubiquitin ligase, while only cIAP1 and cIAP2 show the presence of CARD motif. UBA motif is shared by XIAP, cIAP1/2 and ILP-2. Survivin has a single BIR domain combined with a COOH-terminal alpha-helix coiled-coil domain. While, NAIP structure shows three BIR motifs together with the nucleotide-binding oligomerization (NACHT) and leucine-rich repeats (LRR) domains.

Based on the capability to regulate caspases, BIR domains can be divided into two classes, I and II, where only type II can interact to caspases, while type I is responsible for the binding with other proteins, including TRAF1 and 2 (Gyrd-Hansen and Meier, 2010). Notably, type II BIRs are characterized by a conserved groove, which allows the interaction with a

region within caspases, called IAP binding motif (IBM; Wu *et al.*, 2000). An example of IBM is constituted by the AVPI (Ala-Val-Pro-Ile) sequence which is located at the N terminus of the second mitochondria-derived activator of caspase/direct inhibitor of apoptosis-binding protein with low pI (Smac/DIABLO), a mammalian natural antagonist of IAPs (Figure 2.8). Interestingly, after apoptotic stimuli, Smac/DIABLO is released from the mitochondria into the cytosol, where it binds to the XIAP-BIR3 domain thus relieving the inhibition of caspase-9 and eventually allowing the activation of the executioner caspases-3 and -7.

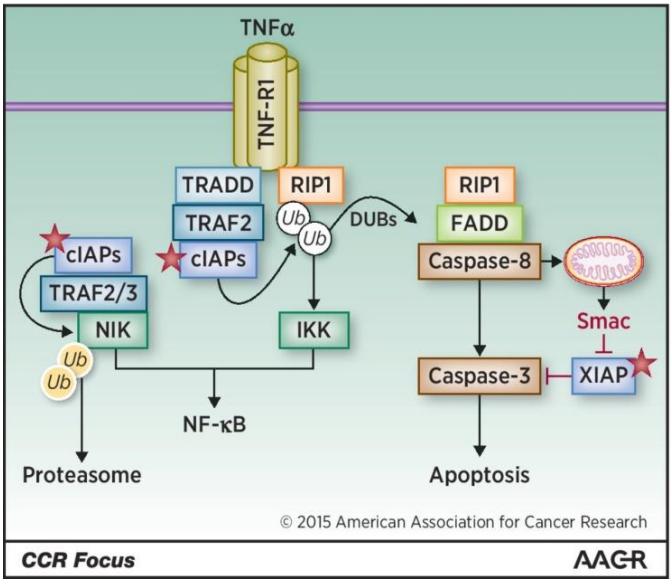

Figure 2.8 - Smac/DIABLO: the IAP natural antagonist (Fulda, 2015). The binding of Smac/DIABLO to XIAP neutralizes XIAP-mediated caspase inhibition, resulting in apoptosis cell death.

2.2.2 The role of IAPs in cancer

The crucial role of IAPs in oncogenesis derives from their capability to promote resistance against cell death and control many survival pathways. Not surprisingly, IAPs have been found aberrantly expressed in diverse types of tumour (Che *et al.*, 2012; Hundsdoerfer *et al.*, 2010). However, the prognostic significance of IAP over-expression remains not

completely clear. This is the case of XIAP, whose expression levels correlate with disease severity and prognosis in acute myelogenous leukemia (AML) and renal cell carcinoma, but not in non-small cell lung carcinoma or cervical carcinoma (LaCasse *et al.*, 2008). Deregulated expression of IAPs can be a result of different events, such as gene amplifications, mutations or deletions and chromosomal translocations. For instance, amplification of 11q21-q23, in which both cIAP1 and cIAP2 are located, has been found in several tumours, including, glioblastoma, hepatocellular carcinoma, esophageal carcinoma, cervical cancer, liver cancer, non-small-cell lung cancer (NSCLC), and pancreatic cancer (LaCasse *et al.*, 2008). Moreover, trans-activation and post-translational events are often responsible for the increase of IAP expression in tumours. For example, the t(11;18)(q21;q21) translocation event has been found in mucosa-associated lymphoid tissue (MALT) lymphoma and causes the fusion of the BIR domains of cIAP2 with the paracaspase MALT1 (Rosebeck *et al.*, 2011). As a consequence of this phenomenon, the constitutive activation of the NF-κB signalling pathway (Darding *et al.*, 2011) occurs thereby promoting oncogenesis and tumour progression.

2.2.3 Smac mimetic-mediated targeting of IAPs

Based on the capability to prevent apoptosis, IAPs represent possible targets for cancer therapy and this leads to the development of small compounds, which are specific for IAP domains. Hence, the elucidation of the biochemical structures involved in the IAP–Smac/DIABLO interaction allowed the development of Smac-like molecules, called Smac mimetics (SMs). SMs resemble the N-terminal region of Smac/DIABLO and, in particular, mimic the IBM motif (Eckelman *et al.*, 2008), which is directed against the XIAP BIR2- and BIR3-caspase interaction pocket, and prevent XIAP-mediated caspase inhibition. While

initially designed to target XIAP, SMs have been shown to affect cIAP1/2 E3 activity, driving their self-ubiquitination and proteasomal degradation (Figure 2.9).

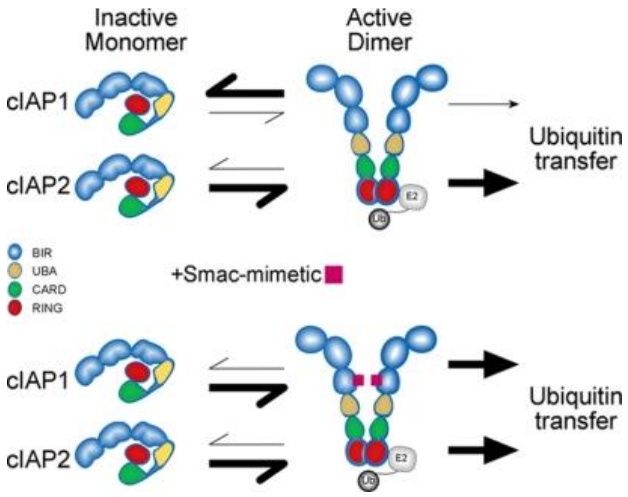

Figure 2.9 - SM-mediated activation of cIAPs (Feltham *et al.*, 2011). The binding of SMs with cIAPs promotes the RING dimerization and activates the cIAP E3 ligase function, self- ubiquitination and proteasomal degradation.

Notably, about 10-15 % of cancer cell lines are efficiently killed *in vitro* by SMs as standalones (Petersen *et al.*, 2007; Figure 2.10) with low nanomolar EC50s, depending on the molecules used. In 2007, it has been reported by several groups that the cytotoxic effect of the SMs in monotherapy does not depend on their activity against XIAP, but it stems from a rapid SM-dependent depletion of cIAP1 and cIAP2. This event results in the autocrine production of TNF and subsequent cancer cell death (Petersen *et al.*, 2007; Varfolomeev *et al.*, 2007; Vince *et al.*, 2007).

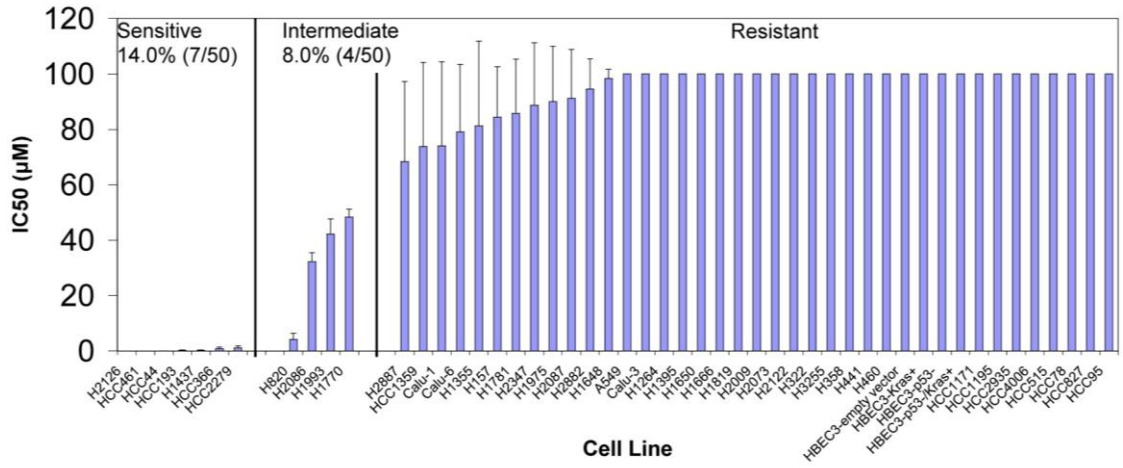

Figure 2.10 - SM response in a panel of lung cancer cell lines. Adapted from (Petersen *et al.*, 2007). About the 14 % of NSCLC cell lines is responsive to the SM treatment administered alone.

SMs are usually considered not toxic in normal tissues and the anti-tumour activity of several SMs has been tested in phase I/II clinical trials (Fulda, 2015). They were developed either as monovalent compounds containing one tetrapeptide mimicking endogenous Smac/DIABLO, or as bivalent molecules having two mimicking sequences connected together by a chemical linker. Since the natural Smac/DIABLO protein acts as a dimer, bivalent SMs were realized to enhance the binding affinity compared to a monomer Smac AVPI-mimicking peptide. Of note, the binding of the Smac/DIABLO AVPI motif is stronger towards BIR3 compared to BIR2, but the presence of two AVPI-like motifs ensures the formation of a very stable interaction between SMs and IAPs by targeting simultaneously two BIR domains within the same IAP (Lecis *et al.*, 2012). As a consequence of this stable interaction (Cossu *et al.*, 2009b; Cossu *et al.*, 2012), dimeric SMs have been shown to be much more effective both *in vitro* and *in vivo* (Fulda, 2014b) compared to monomeric ones. In addition, dimeric compounds are more efficient in causing the depletion of cIAP1 and cIAP2 (Varfolomeev *et al.*, 2007). However, dimeric SMs are less “drug-like” compared to monomeric ones from a pharmacological viewpoint (Fulda, 2015). In fact, being smaller molecules, movalent SMs can

even be endowed with a good oral bioavailability, which provides an important advantage for their clinical application. Conversely, the bioavailability of bivalent SMs is limited by their molecular weight that requires the employment of other administration routes, such as intravenous injection.

Unfortunately, the vast majority of cancer cells are usually resistant to SM employed in monotherapy, but the reason for this resistance is not fully understood. It has been reported that cIAP2 degradation occurs in a cIAP1 dependent manner (Darding *et al.*, 2011). Upon SM treatment, cIAP2 is quickly replaced by newly synthesized protein that cannot be degraded anymore in the absence of cIAP1. Importantly, cIAP2 displays some common features with cIAP1 and its presence is sufficient to confer resistance to SM treatment (Darding *et al.*, 2011). As SMs are very rarely cytotoxic in monotherapy, the efficacy should be enhanced by the combination with either death agonists, such as TNFα, TNF-related apoptosis-inducing ligand (TRAIL; Lecis *et al.*, 2010), and FasL, or chemotherapy (Greer *et al.*, 2011), resulting in synergistic activity (Moller *et al.*, 2014). SMs have been reported to synergise with chemotherapeutic drugs in solid tumours and hematologic malignancies. However, some side effects and unwanted toxicity caused especially by immune system activation and cytokine production have been revealed by *in vivo* experiments and the first clinical trials (Amaravadi *et al.*, 2011; Infante *et al.*, 2014; Sikic *et al.*, 2011).

SM efficacy has been tested in phase I/II clinical trials for solid and hematologic malignancies (Fulda, 2015), as monotherapy or in rational combinations with gemcitabine, daunorubicin, cytarabine, or Paclitaxel. Importantly, phase I trials indicate SM administration as a safety and well tolerated treatment, even if inducing an increase of cytokines in patients

(Fulda, 2014b). For instance, the up-regulation of inflammatory cytokines, that are NF-kB target genes, has been reported by Infante and colleagues after the administration of LCL161 for the treatment of human advanced solid tumours (Infante *et al.*, 2014). In the attempt to reduce possible risks linked to SM administration, the new compound Birinapant has been designed with reduced affinity for XIAP, but still conserving the same effect on cIAP1 and cIAP2 (Obexer and Ausserlechner, 2014). In fact, it has been reported that SM-triggered cytokine release stems from the inhibition of XIAP. Intriguingly, Birinapant treatment does not promote TNF production and results well tolerated (Allensworth *et al.*, 2013; Condon *et al.*, 2014). The efficacy of this compound has been also assessed together with other chemotherapeutics to analyse whether some clinical benefits may be obtained from the combinations (Krepler *et al.*, 2013). Among SMs, the two monovalent compounds: LCL161 (Novartis) and AT-406/Debio1143 (Ascenta Therapeutics; Figure 2.11) are currently tested in clinical trials, for the treatment of refractory multiple myeloma and advanced solid malignacies or metastatic NSCLC, respectively.

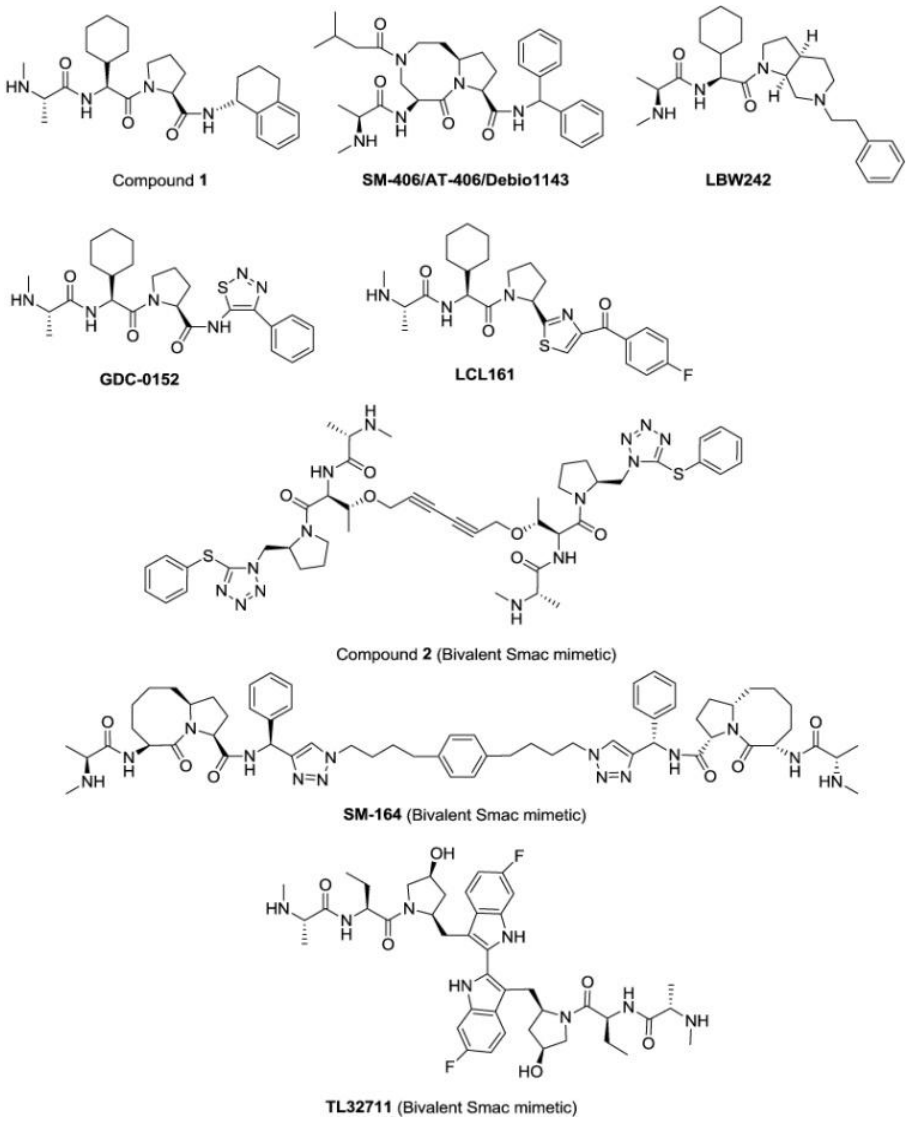

Figure 2.11 - Chemical structures of SMs (Bai *et al.*, 2014).

2.3 The TNF/TNF-R superfamily

As already mentioned, SM-mediated autocrine production of TNF occurs in response of cIAP depletion leading to cell death. TNF is a member of a large family of cytokines that exert pleiotropic functions among whom regulation of the immune system, control of cell proliferation, differentiation and apoptosis (Ashkenazi and Dixit, 1998). TNF is expressed as a transmembrane protein, membrane TNF (mTNF), which can be shed by the metalloprotease

TNF-converting enzyme (TACE) into a soluble factor (sTNF). While mTNF can activate both TNF-R1 and TNF-R2, the soluble form fully activates only TNF-R1, despite the high binding affinity with TNF-R2 (Richter *et al.*, 2012).

The members of the TNF-R superfamily are classified into two groups based on the presence of the death domain (DD; Walczak, 2013). Receptors belonging to the first group display an intracellular DD, which confers the capability to induce cell death. Conversely, members belonging to the second class lack this domain and cannot directly activate cell death, but need to interact with additional adaptor molecules, such as TNF-receptor-associating factors (TRAFs) through the receptor TRAF-interacting motif (TIM; Dempsey *et al.*, 2003). The recruitment of adaptor proteins is crucial for the activation of the intracellular pathways triggered by the TNF superfamily ligands. Of note, the DDs are present only in a few adaptor proteins (MacEwan, 2002). In fact, TRADD and FADD exploit their DD to interact with the receptors and activate cell death, whilst other interactors, such as TRAFs, bind to the receptors either directly via the receptor TIM domain or indirectly by recruiting other adaptor proteins as intermediates (Hehlgans and Pfeffer, 2005). For its increased capability to induce cell death, TNF-R1 signalling has been studied more deeply than TNF-R2 in the cancer field. Therefore, several functions of the latter receptor still remain unclear.

2.3.1 TNF-R1 complex and its signal transduction

While the carboxyl (C)-terminal end of TNF-R1 is occupied by DD motif for the apoptosis signal transduction, the N-terminal region contains a cysteine-rich domain that favours the preassembly of the receptor into a trimeric complex (Hehlgans and Pfeffer, 2005). TNF-R1 is constitutively expressed in all tissue and can activate a variety of cellular

processes, including cell proliferation, apoptosis or necroptosis, based on the cellular context (Wajant *et al.*, 2003). Even though TNF-R1 usually activate the nuclear factor κB (NF-κB) and mitogen-activated protein kinase (MAPK) signalling pathways, TNF-R1 activation can result in different scenarios determined by the formation of two diverse complexes, named Complex I and II (Figure 2.7; Micheau and Tschopp, 2003). In the first scenario, TNF-R1 trimerizes within a few minutes upon TNF stimulation and recruits TRADD to the DD. Then, additional mediators, namely receptor-interacting protein 1 (RIP1; Wong *et al.*, 2010), TRAF2 and/or TRAF5, are added to the complex and, in turn, cIAP1 and cIAP2 are assembled. The activation of NF-kB signalling pathway occurs after the recruitment of NF-κB essential modulator (NEMO; also known as IKKγ), TGFβ-activated kinase 1 (TAK1; also known as MAP3K7) and the TAK1-binding proteins (TAB1 and TAB2; Figure 2.12; Wajant and Scheurich, 2011).

The second scenario occurs at late time-points of TNF-R1 stimulation or when NF-kB activation is specifically inhibited (Varfolomeev and Ashkenazi, 2004). Importantly, two different types of Complex II can be distinguished, named Complex IIa and IIb. Complex IIa requires the dissociation of RIP1, TRAF2, and TRADD from the receptor and the subsequent recruitment of FADD and caspase-8 (Micheau and Tschopp, 2003). Differently from Complex IIa, which drives to apoptosis, the Complex IIb is responsible for a distinct type of cell death, named necroptosis, which has recently been object of high interest. Necroptosis is both mechanistically and morphologically distinct from apoptosis. When caspase-8 is activated in Complex IIa, it cleaves and halts the activities of RIP1, RIP3, and the deubiquitinating enzyme CYLD. However, caspase-8 inhibitors (e.g. zVAD) or genetic deletion of caspase-8 or FADD impair RIP1 and RIP3 cleavage and lead to the Complex IIb formation and subsequent necroptosis. Importantly, the activation of necroptosis is tightly controlled by cIAPs, which

are responsible for the proteasome-dependent degradation of active RIP1/3 complexes, and therefore can block the execution of this process (Oberst, 2016).

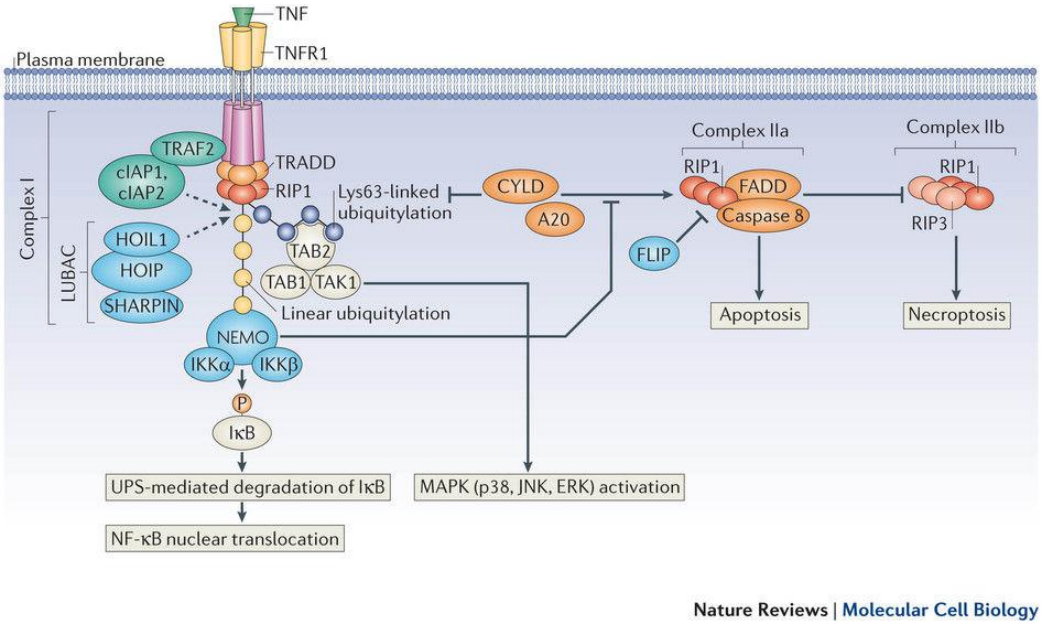

Figure 2.12 - Model of TNF-R1 signal transduction (Ofengeim and Yuan, 2013). Upon ligand binding, TNF-R1 forms the Complex I through the recruitment of several factors, including TRADD, RIP1, TRAF2, cIAP1 and 2. This Complex leads to the recruitment of TAK1 and IKK and drives either to the activation of NF-κB, mediating IκB degradation, or to MAPK activation. Importantly, within 10–15 min after TNF stimulation, the deubiquitylation enzymes disrupt Complex I mediating the deubiquitination of its members. This results in the formation of alternative complexes, named Complex IIa or Complex IIb. Complex IIa includes FADD, caspase-8 and RIP1, and mediates apoptosis. However, the inhibition of caspase-8 leads to Complex IIb, which triggers necroptosis.

2.3.2 TNF-R2 complex and its signal transduction

Differently from TNF-R1, TNF-R2 expression is more restricted to specific cell types, including neurons, oligodendrocytes, microglia and astrocytes in the brain (McCoy and Tansey, 2008), endothelial cells, CD4+ and CD8+ T cells (Ware *et al.*, 1991), cardiac myocytes (Irwin *et al.*, 1999), thymocytes and human mesenchymal cells (Bocker *et al.*, 2008). Even

though TNF-R2 lacks DD, it still interacts with TRAF2 and also this receptor can activate the NF-kB pathway in a TNF-R1-independent manner (Borghi *et al.*, 2016). In details, TNF-R2 trimerization allows the recruitment of TRAF2 and consequently of the TRAF2-associated proteins: TRAF1 and cIAPs, thus forming a complex, which interacts with TRAF3 (Figure 2.13). Most of the biological activities triggered by TNF-R2 depend on its interaction with TRAF2, which provides a mechanism for activation of NF-kB, whose translocation to the nucleus promotes the expression of pro-survival target genes, including IAPs and pro-survival BCL-2 proteins (Pahl, 1999). Importantly, inhibition of TRAF2/3 or IAPs reverses the classical NF-κB activation pathway to the non-canonical one (Zarnegar *et al.*, 2008).

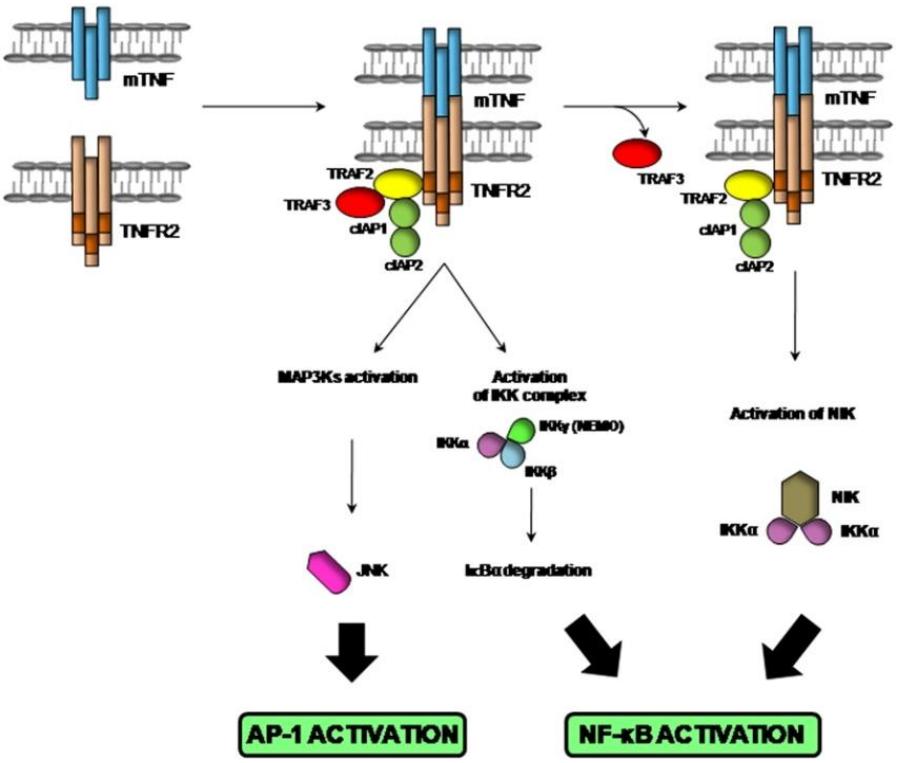

Figure 2.13 - TNF-R2 signal transduction (Cabal-Hierro and Lazo, 2012). TNF-R2 signalling is triggered by the binding with mTNF. This event prompts to the recruitment of TRAF2, which enables the generation of a signalling complex composed by TRAF3, cIAP1 and cIAP2.

2.4 The NF-kB signalling pathway

It is generally accepted that the most important contribution of cIAPs to cell survival and tumourigenesis resides in their ability to regulate NF-κB signal transduction (Zarnegar *et al.*, 2008). Despite its major role in cell survival, NF-κB is also recognised in the modulation of the inflammatory state and innate immunity, and in the control of different steps of cancer initiation and progression (Grilli *et al.*, 1993). The NF-κB family is composed by p65 (RelA), RelB, c-Rel, NF-κB1 and NF-κB2 that associate to form homo- and hetero-dimeric complexes in almost any combination (Figure 2.14; Hayden and Ghosh, 2004). They all share structural features, including a Rel homology domain (RHD; Hoesel and Schmid, 2013), which is required for dimerization, DNA binding, interaction with IκBs, as well as nuclear translocation. In contrast, the transcription activation domain (TA) necessary for the target gene expression is present only in the C-terminus of p65, c-Rel, and RelB subunits (Figure 2.13). Among the 15 potential homo-hetero dimers, three are not able to bind DNA (RelA:RelB, cRel:RelB and RelB:RelB), while other three bind DNA but lack the transcriptional activity (p50:p50, p52:p52, and p50:p52; O'Dea and Hoffmann, 2010). Upon stimulation, NF-κB1 and NF-κB2, which are synthesized as pro-forms (p105 and p100), are proteolytically processed to p50 and p52, respectively. Since neither NF-kB1 nor NF-kB2 contains a TA domain, homo-dimers of p50 and p52 binding to gene promoters act as transcriptional repressors (Chen *et al.*, 2000). However, when p50 or p52 are bound to other NF-κB family members containing a TA domain, such as p65 or RelB, they form a transcriptional activator (Wan and Lenardo, 2009). Different NF-kB subunits are responsible not only for the activation of diverse target genes, but also contain sites for phosphorylations and other post-translational modifications, which enable the cross-talk with other signalling pathways.

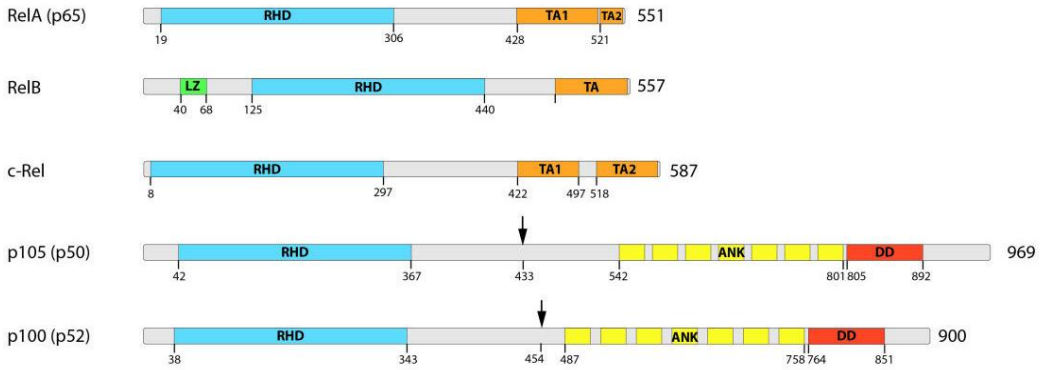

Figure 2.14 - NF-kB family members. Adapted from (Hoesel and Schmid, 2013)**.** NF-κB family is composed by five members, namely RelA (p65), RelB, c-Rel, NF-κB1 (p105), and NF-κB2 (p100). All the members contain a RHD, which allows their binding with DNA and the homo- and hetero-dimerization. The C-terminal TA domain is harboured only by the three members: RelA, RelB and c-Rel and mediates their transcriptional activity. The p105 and p100 members show the presence of ankyrin (ANK) repeats motif, which mediates the binding of IκBs to the NF-κB family of proteins and DD motif. The leucin-zipper-like domain (LZ) characterizes only RelB structure.

2.4.1 Activation of the canonical NF-kB pathway

In the canonical pathway, the activation can be mediated by binding of immune receptors including Toll-like receptors (TLRs), Interleukin-1 receptor (IL-1R), TNF-R and antigen receptors with their ligands, such as TNF and lipopolysaccharides (LPS; Ghosh and Hayden, 2008; Perkins, 2007). This interaction drives to the IκBα degradation, with the consequent release of NF-kB and nuclear translocation of p65-containing hetero-dimers, which results in the regulation of target genes (Figure 2.15).

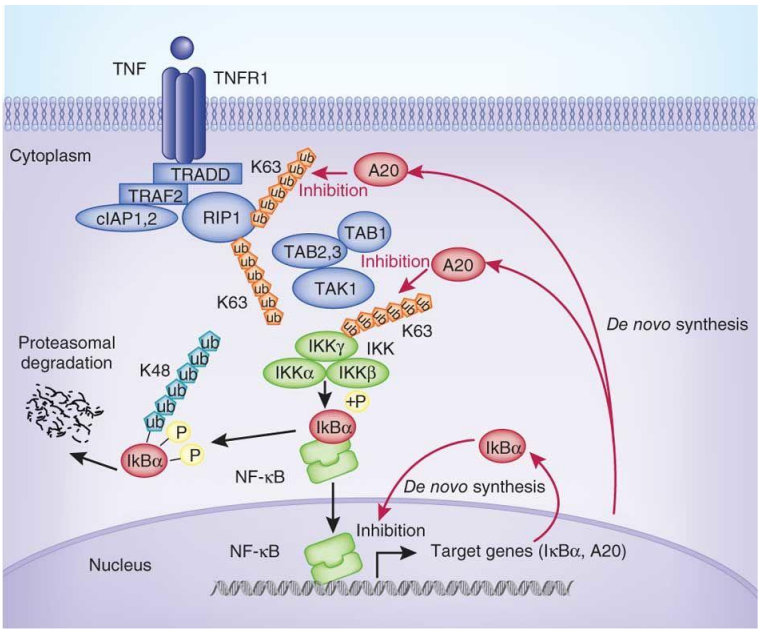

Figure 2.15 - The canonical NF-kB signalling pathway (Ruland, 2011). After TNF binding, the recruitment of TRADD, TRAF2 and cIAP1/2 and RIP1 occurs at the receptor level. This event mediates the activation of IKK complex, which in turn phosphorylates IκBα, thus triggering its degradation. The loss of IκBα allows NF-κB nuclear translocation resulting in the activation of gene transcription. Among the NF-κB target genes there are those that encode for its negative regulators as IκBα.

2.4.2 Non-canonical NF-kB pathway

The molecular mechanisms underlying the non-canonical NF-kB signalling pathway have been investigated only recently. Differently from the canonical one, the activation of the non-canonical NF-kB signalling is slow (within hours) and responds to a different set of stimuli (Razani *et al.*, 2011), e.g. B-cell activation factor (BAFFR), CD40, receptor activator for nuclear factor kappa B (RANK) or lymphtoxin β-receptor (LTβR). Upon stimulation, NIK, the apical inducer of non-canonical NF-kB signalling, phosphorylates and activates IKKα (Figure 2.16), which in turn mediates the phosphorylation of p100 associated with RelB. This event leads to the partial processing of p100 and generation of p52-RelB complex (Sun, 2011). More in-depth, after receptor activation, the complex responsible for NIK degradation,

comprising TRAF3, TRAF2 and cIAP1/2, undergoes cIAP-mediated degradation with the consequent stabilization of NIK. Both TRAFs are responsible for the recruitment of cIAPs, but TRAF3 binds to NIK in a TRAF2-independent manner, while TRAF2 mainly interacts with cIAP1/2.

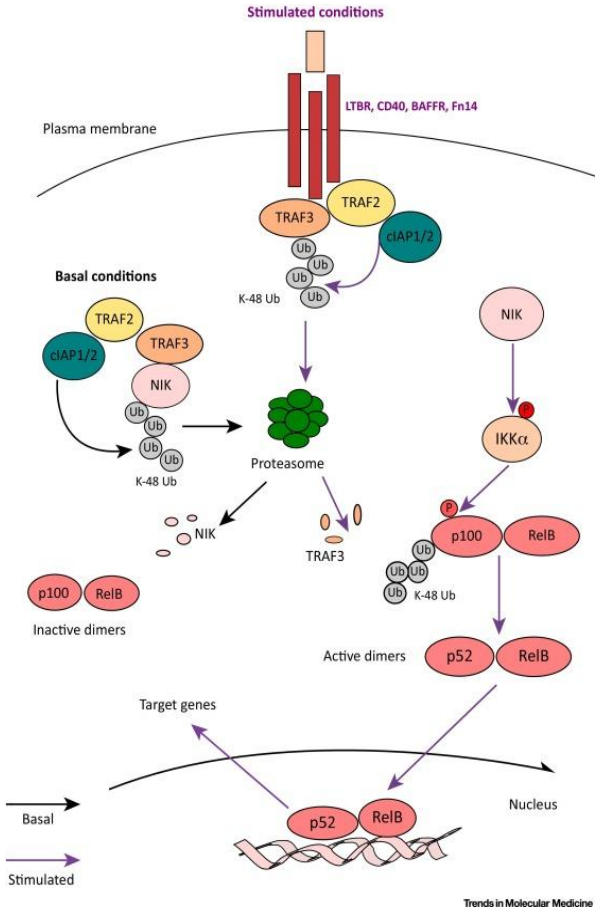

Figure 2.16 - Non-canonical NF-kB signalling (Cildir *et al.*, 2016)**.** Under resting conditions, NIK is degraded by proteasome in a TRAF2/3-dependent manner. In fact, TRAF2 recruits cIAP1 and 2 and promotes NIK ubiquitination and degradation. Then, after the activation of the non-canonical NF-kB pathway, cIAP1 and 2 mediate TRAF3 degradation therefore resulting in the stabilization of NIK. Once stabilized, NIK phosphorylates IKKα, which in turn phosphorylates p100 leading to its partial degradation to p52. Nuclear translocation of RelB–p52 hetero-dimers allows the expression of target genes.

2.5 IAPs and metastasis

A still less described role of IAPs regards their involvement in the metastatic process. Through the regulation of NF-kB and MAPK signalling pathways, IAPs are able to modulate cell plasticity, motility and invasion (Fulda, 2014c), which are key steps in metastasization. The metastatic process consists of several steps that allow cancer spread from the primary site into the surrounding tissues, and eventually resulting in the colonisation of a secondary site where cells can grow and give secondary tumours (Figure 2.17). During the malignant progression, cancer cells acquire the ability to invade the basal lamina, surrounding tissues and capillaries as single cells (Giampieri *et al.*, 2009) or clumps (Friedl and Gilmour, 2009), extravasate and colonise distant organs whose function is then compromised.

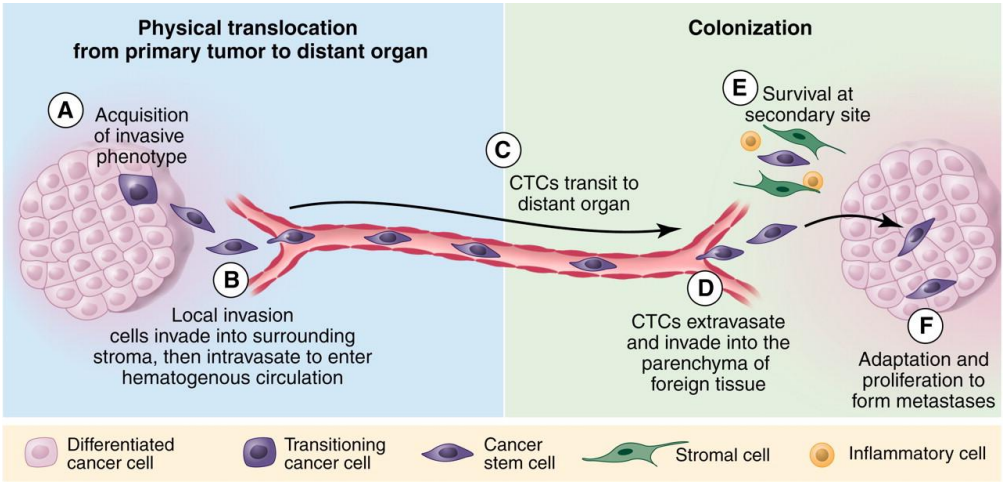

Figure 2.17 - Cancer cell metastatic process (Chaffer and Weinberg, 2011)**.** (A) First, the metastatic cascade initiates with cell detachment from the primary tumour. (B) Cancer cells invade the surrounding tissues and intravasate. (C) Once into the blood vessel, cells (CTCs) transit through the circulation to reach the distant organ. (D) At the distant organ, cells extravasate and invade the microenvironment of this secondary site to colonise the new tissue. (E) Cells evade the innate immune response and survive as a single cell or cluster. (F) To give macrometastasis, cancer cells must be able to proliferate and grow.

IAPs have been shown to regulate migration, invasion and metastasis, but the mechanisms underlying these processes are still controversial. On the one hand, several studies support the idea that the targeting of IAPs causes a reduction of cancer cell metastatic potential. These findings would therefore encourage the employment of SMs for the treatment of those types of tumour that are particularly aggressive. This is the case, for example, of triple negative breast cancers (TNBCs). Accordingly, Lopez J *et al.* (Lopez *et al.*, 2011) showed that cIAP1 deregulated activity can increase cell proliferation and migration, but SM administration is able to prevent this effect. Moreover, they demonstrated that cIAP1 depletion results in vascular tree degeneration *in vivo*, indicating a possible role of cIAP1 in the maintenance of vascular integrity, which is essential for tumour growth and favours the migratory capacity of cancer cells. Nonetheless, it has also been reported that cIAPs regulate Ras related C3 botulinum toxin substrate (Rac1), which is a member of Ras family of small GTPases involved in the control of cell migration and invasion. Notably, XIAP and cIAP1 were shown to interact with Rac1 and lead to its proteasomal degradation (Oberoi-Khanuja *et al.*, 2013). In these settings, IAP depletion mediated by pharmacological or genetic tools would increase Rac1 protein levels, eventually enhancing cell motility and migration. Consistently, Fulda's group (Tchoghandjian *et al.*, 2013) published the effect of SM BV6 at non-toxic concentrations in glioblastoma cell lines, showing that its administration activates the non-canonical NF-kB signalling and promotes cytoskeleton changes that enhance cell motility.

2.5.1 Role of MAPKs in the metastatic process

The activation of MAPK signalling pathways acts in a variety of cellular responses and mediates several processes such as growth, proliferation, differentiation, migration and

apoptosis (Dhillon *et al.*, 2007). Notably, three distinct MAPK pathways have been characterized: extracellular signal-regulated kinase 1 and 2 (ERK1/2), c-Jun N-terminal kinase/stress-activated protein kinase (JNK/SAPK) and p38 (Figure 2.18).

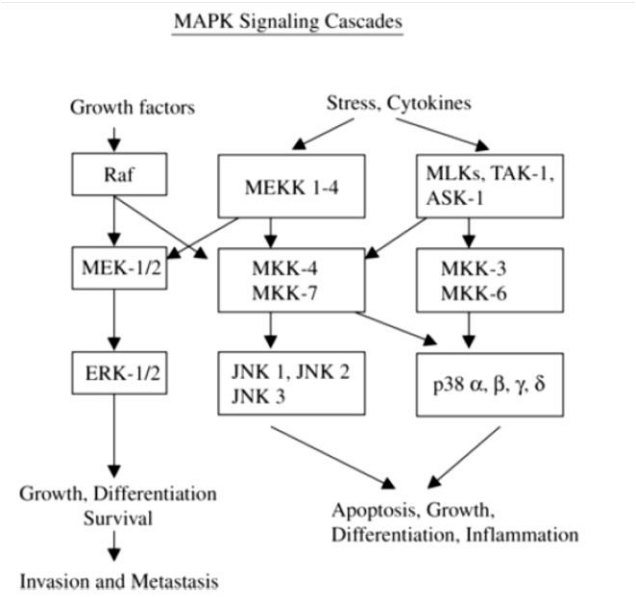

Figure 2.18 - Schematic representation of the MAPK role in tumours (Reddy *et al.*, 2003). A possible cross-talk exists among the three major MAPK cascades. Despite ERK is mainly responsible for cell invasion and metastasis, it also regulates other cellular processes such as tumour growth and inflammation. At the same times, other pathways besides ERK affect the metastatic process.

Beyond their predominant role in the regulation of the NF-κB signalling pathway, IAPs, and in particular cIAP1 and 2, are also involved in the modulation of the MAPK cascade. Several reports demonstrate that the ubiquitin ligase activity of cIAPs plays a critical role for the efficient activation of MAPK signalling (Gardam *et al.*, 2011; Karin and Gallagher, 2009). Indeed, it has been reported by Varfolomeev and colleagues (Varfolomeev *et al.*, 2012) that the loss of cIAP1 and 2 upon treatment with the IAP antagonist BV6 drastically affects the activation of p38 and JNK.

Among MAPKs, the role of the ERK signalling pathway in the metastatic process has been widely studied. ERK controls a large variety of cellular processes, including proliferation, differentiation, survival, migration, angiogenesis and chromatin remodelling (Dunn *et al.*, 2005; Yoon and Seger, 2006), depending on the cellular settings. Focusing on the metastatic process, it has been shown that sustained ERK signalling enhances the accumulation of genes responsible for angiogenesis, cell migration and invasion. This pathway also favours metastasis formation (Reddy *et al.*, 2003; Giehl, 2005) exerting profound effects on actin cytoskeleton organisation and adhesive structures. Moreover, the metastatic process is favoured by ERK signalling pathway in a double manner: via the apoptosis inhibition and through the increase of tumour cell migration. In the first case, MEK/ERK phosphorylate the pro-apoptotic protein BAD, which dissociates from BCL-2 and allows its anti-apoptotic response. Furthermore, ERK pathway favours the anti-apoptotic MCL-1 protein and inhibits the pro-apoptotic BIM protein, through their phosphorylation (Pachmayr *et al.*, 2017). In the second case, MEK/ERK signalling enhances cell migration by promoting cell movement and contraction through the expression of genes involved in the epithelial mesenchimal transition (EMT) or in the remodelling of tumour microenvironment, such as matrix-degrading proteases (Bae *et al.*, 2013). Therefore, tumour initiation and progression are often caused by the aberrant activation of ERK signalling pathway, which is often caused by the epidermal growth factor receptor (EGFR) hyper-activation.

2.6 EGFR signalling pathway in the metastatic process

EGFR (also named ErbB-1, HER1) is a well-known proto-oncogene, in fact, many reports indicate its crucial role in cancer progression and metastasis. This receptor belongs to

the EGFR family, which comprises other three structurally similar receptors, namely HER2 (ErbB-2), HER3 (ErbB-3), and HER4 (ErbB-4; Wieduwilt and Moasser, 2008). Particular interest has been focused on EGFR since its over-expression and/or hyper-activation characterize about 15–30 % breast carcinomas and is associated with poor patient outcomes (Sirkisoon *et al.*, 2016).

2.6.1 EGFR structure and down-stream pathways

EGFR is endowed with a tyrosine kinase activity, which is crucial for the modulation of cellular pathways, which are essential in both normal and cancerous cells. The EGFR activation depends on its binding with specific ligands including epidermal growth factor (EGF), transforming growth factor α (TGFα), amphiregulin or neuregulin (Purba *et al.*, 2017). This event can lead either to the formation of EGFR homo-dimers or hetero-dimers with the other three members of the family (Figure 2.19).

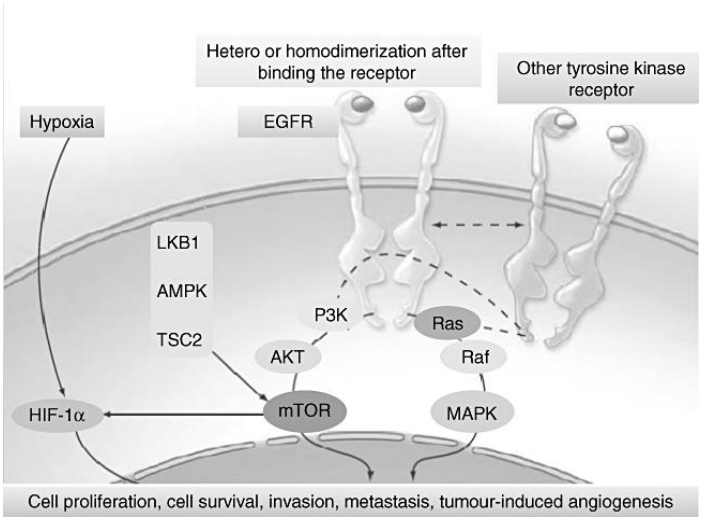

Figure 2.19 - EGFR signal transduction (Martinelli *et al.*, 2009)**.** EGFR signalling pathway initiates upon ligand binding, which drives the formation of homo-dimer or hetero-dimer with other members of the family. The receptor dimerization causes conformational changes, which induces the EGFR tyrosine kinase activity and

results in the phosphorylation of specific tyrosine residues within the intracellular C-terminal domain. Upon phosphorylation, EGFR acquires the capability to enhance several cellular processes, such as cell proliferation, loss of differentiation, invasion and angiogenesis and block of apoptosis.

The binding of the ligand activates the intracellular tyrosine kinase domain of the dimerized receptor, thus leading to the phosphorylation of specific tyrosine residues within the EGFR intracellular C- terminal domain (Martinelli *et al.*, 2009). Upon phosphorylation, the tyrosine residues provide a docking site for proteins containing Src homology 2 (SH2) domains, such as Grb2, Shc1, p85, PLCγ and JAK1, and trigger the activation of down-stream signalling cascades including the Phosphatidylinositol 4,5-bisphosphate 3-kinase (PI3K/Akt), JAK/STAT, NF-κB, PLCγ/protein kinase-C (PKC), and RAS/MAPK/ERK (Lindsey and Langhans, 2015). These effectors affect several cellular functions such as cell proliferation, loss of differentiation, motility, invasion, angiogenesis and blocking of apoptosis.

Although in normal tissues the presence of EGFR ligands is tightly regulated to ensure the maintenance of cell homeostasis, EGFR is often chronically stimulated in tumour cells. In some cases, the aberrant activation of EGFR, and consequently of its down-stream effectors, is caused by the sustained production of EGFR ligands in the tumour microenvironment. Moreover, in cancer cells, EGFR can be either over-expressed or mutated, causing its constitutive activation. This is the case, for example of head and neck, breast, lung, colorectal, prostate, kidney, pancreas, ovary, brain and bladder tumours (Woodburn, 1999). Remarkably, the correlation between high EGFR expression and poor patient survival renders this receptor a strong prognosis factor in breast, ovarian and head and neck cancers (Fischer-Colbrie *et al.*, 1997; Ishitoya *et al.*, 1989; Sebastian *et al.*, 2006). Not surprisingly, EGFR has emerged as an important target for therapeutic intervention.

2.7 Breast cancer classification

Breast cancers can be classified in five intrinsic subtypes called Luminal A, Luminal B, HER2-enriched, claudin-low and basal-like on the basis of expression levels of hormone estrogen (ER) and progesterone (PR) receptors, HER2, cytokeratins (CKs) 5/6, and claudins 3/4/7 (Prat and Perou, 2011). Tumours positive for ERα and/or PR, but with a low expression of Ki67, are generally defined Luminal A and are responsive to hormone therapy and chemotherapy. Differently, a variable response to chemotherapy has been assessed for Luminal B tumours, which are distinguished from Luminal A tumours due to the higher levels of Ki67. Moreover, the negative expression of ERα and PR characterize both the HER2-enriched tumours and the TNBCs, with HER-enriched tumours expressing high levels of this receptor, while TNBCs are negative. The majority of TNBCs display a basal subtype characterized by strong expression of basal markers such as CK 5, 6 and 17 (Alluri and Newman, 2014).

2.7.1 TNBC: molecular characterization and targeted therapies

TNBCs accounts for about 20 % of the invasive breast cancer cases, characterized by high grade tumours, distant metastasis and low survival. Since TNBCs lack ER, PR and HER2 (Figure 2.20), patients do not benefit from hormonal or trastuzumab-based therapies. Consequently, therapeutic intervention for TNBC women is very limited and patients often show a high risk of recurrence and disease progression. Additionally, TNBC is considered a highly heterogeneous disease and many attempts have been made for its classification. Recently, six molecular subtypes of TNBC have been identified, including basal-like 1, basal-like 2, immunomodulatory, mesenchymal-like (ML), mesenchymal stem–like (MSL), and

luminal androgen receptor, with distinct gene expression profiles and canonical pathways (Lehmann *et al.*, 2011). The high molecular heterogeneity of TNBC disease represents a further barrier in improving survival and in developing targeted therapy for patients (Figure 2.20; Ahn *et al.*, 2016). Currently, TNBC remains the only major type of breast tumour for which U.S. Food and Drug Administration (FDA)- or European Medicines Agency (EMA)-approved targeted therapy is not available, making invasive measures, such as surgery and chemotherapy, the only approaches for the treatment of TNBC patients (Lehmann and Pietenpol, 2015).

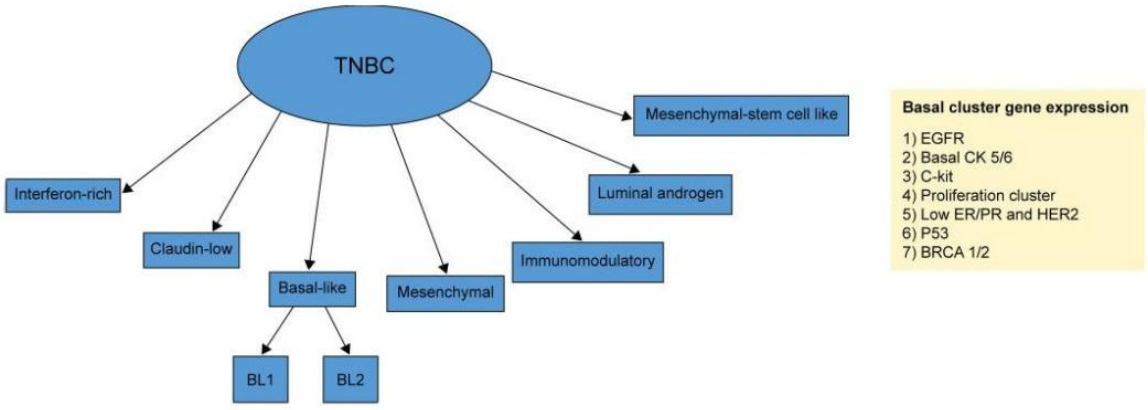

Abbreviations: TNBC, triple-negative breast cancer; BL, basal like; EGFR, epidermal growth factor receptor; CK, cytokeratin; ER, estrogen receptor; PR, progesterone receptor; BRCA, breast cancer susceptibility gene; HER2, human epidermal growth factor receptor 2.

Figure 2.20 - TNBC molecular classification (Zeichner *et al.*, 2016).

2.7.2 Targeting EGFR for anti-cancer treatment

So far, two pharmacological approaches have been proposed to inhibit EGFR activity: neutralizing monoclonal antibodies and small tyrosine kinase inhibitor molecules.

2.7.2.1 Monoclonal antibodies

Among the monoclonal antibodies that have been developed, cetuximab (C225, Erbitux) and panitumumab are currently widely employed in cancer treatment. Cetuximab is

a chimeric IgG1 monoclonal antibody that targets the ligand-binding domain of the EGFR (Figure 2.21). Through its binding with EGFR, cetuximab prevents the receptor activation and subsequent dimerization, and therefore inhibits its signal transduction and hyper-proliferative effects (Ferraro *et al.*, 2013). This drug has been shown to prevent EGFR-dependent primary tumour growth and metastasis. Hence, the employment of cetuximab for clinical use has been approved by FDA for the treatment of patients with *wild-type (wt)* KRAS, EGFR-expressing metastatic colorectal cancer (mCRC) and recurrent or metastatic head and neck cancers. Activity of cetuximab has been further tested for the treatment of metastatic NSCLC and breast tumours. Panitumumab is a fully human IgG2 targeting the extracellular domains of EGFR. It has been evaluated in clinical trials both in monotherapy and in combination with other agents for the treatment of various cancer types (colorectal and kidney tumours). Along with cetuximab, also panitumumab employment has been approved for treatment of colorectal cancer.

2.7.2.2 Small-molecule EGFR tyrosine kinase inhibitors

Structural studies have identified the ATP-binding site of the intracellular domain of EGFR as responsible for the receptor activity. This observation allowed the development of small-molecule EGFR tyrosine kinase inhibitors (Zhang *et al.*, 2006; Yun *et al.*, 2007). These compounds were designed to compete with the Adenosine 5’ triphosphate and inhibit the intracellular catalytic domain, eventually preventing the EGFR autophosphorylation and its down-stream signalling. These molecules differ in their abilities to bind the ATP-binding pocket—either reversibly or irreversibly—and in their capacities to interfere not only with EGFR but also with other members of the family (Janmaat and Giaccone, 2003). Among the

proposed EGFR inhibitors, gefitinib (Figure 2.21) and erlotinib, have been investigated in preclinical studies and exhibited an encouraging clinical response.

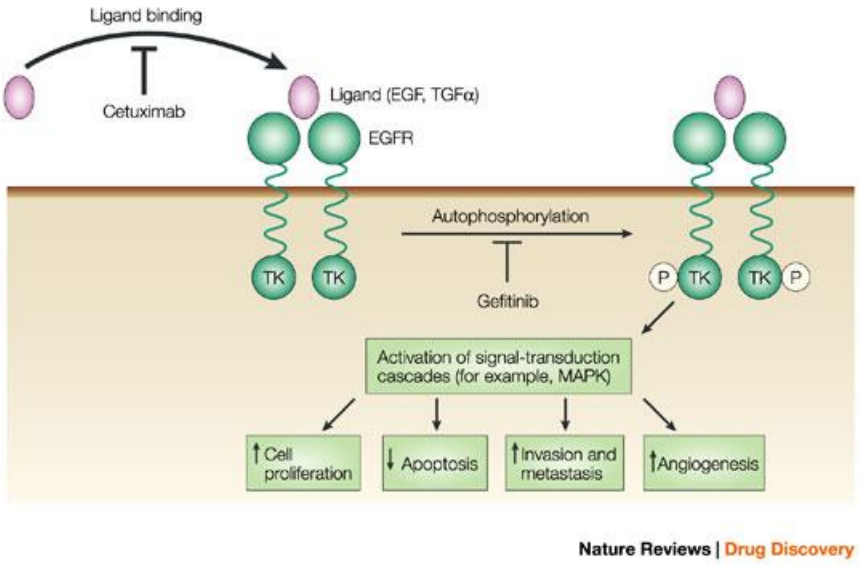

Figure 2.21 - Blocking the EGFR signalling transduction (Graham *et al.*, 2004). After dimerization, EGFR phosphorylated sites residues act as docking sites for several molecules, which cause the activation of diverse signalling pathways. To prevent this event, two strategies have been developed by designing EGFR-specific monoclonal antibodies and small-molecule tyrosine kinase inhibitors.

2.8 EGFR drives metastasis via MAPK signalling pathways

EGFR orchestrates several cellular responses including proliferation, cell motility, angiogenesis, cell survival, and differentiation through the activation of the RAS/MAPK cascade, together with the PI3K/Akt pathway (Schlessinger, 2000). Importantly, many findings provide evidence that MAPKs, and especially ERKs, are involved in cancer initiation and progression (Figure 2.22). In fact, EGFR leads to the activation of the RAS/RAF-MEK1/2-ERK1/2 axis. These signalling pathways are deregulated in approximately one-third of all human cancers and are consequently intensively studied (Dhillon *et al.*, 2007).

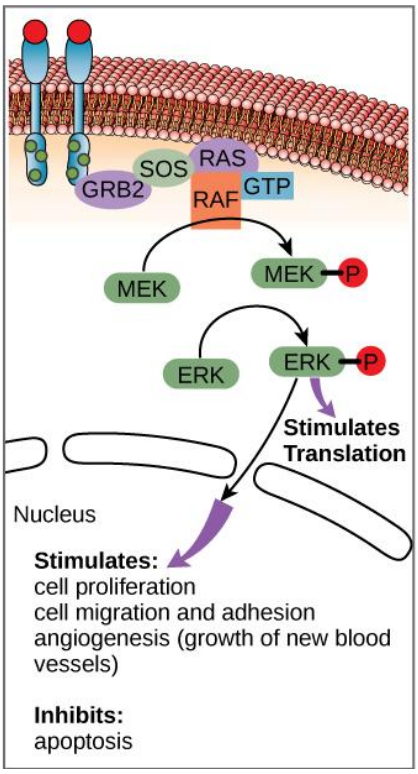

Figure 2.22 - EGFR regulation of cellular processes via ERK pathway. Modified from (https://courses.lumenlearning.com/wmopen-biology1/chapter/propagation-of-the-signal/). EGF activates the receptor intrinsic kinase, which in turn induces a large variety of down-stream intracellular signalling pathways. Among these, ERK activation strongly affects cancer behaviour, influencing cell growth, wound healing and tissue repair.

Constitutive activation of ERK signalling, which is found in the vast majority of cancer-associated lesions, is caused by: over-expressed or mutated receptor, sustained autocrine or paracrine production of activating ligands and mutated RAS or BRAF (Figure 2.23). Aberrant activation of the EGFR/MEK/ERK signalling pathway and high levels of ERK1/2 phosphorylation, indicating an elevated activity, have been observed in metastatic sites of breast tumours (Adeyinka *et al.*, 2002). In line with this consideration, MAPK signalling pathway is hyper-activated in TNBCs, where it is associated with both deregulated

proliferation and capability to migrate of malignant cells (Bartholomeusz *et al.*, 2012). Moreover, activation of this pathway has also been linked to higher recurrence rate (Eralp *et al.*, 2008). Finally, emerging evidence links the activation of ERK signalling pathway to the induction of EMT (Xie *et al.*, 2004).

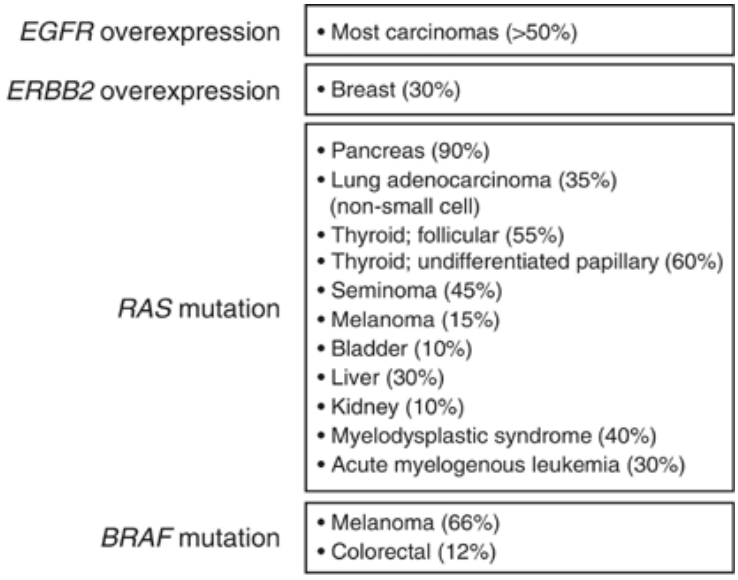

Figure 2.23 - Cancer lesions associated with ERK signalling pathway deregulation (Dhillon *et al.*, 2007).

2.9 EMT process in tumour progression

The essential features of EMT are associated with loss of cell-cell contact and decrease of epithelial features with gain of mesenchymal properties. Several studies have focused on the mechanisms underlying the EMT process supporting its role in tumour cell progression, invasion and metastasis. However, the importance of this process for tumour metastasis is still controversial (Fischer *et al.*, 2015). During the EMT, the down-regulation of E-Cadherin is a crucial step (Acloque *et al.*, 2008) for the reduction of intercellular adhesion junctions and consequent increase of cell detachment. This event is mediated by several E-Cadherin repressors, such as SNAIL, SNAI2 (Batlle *et al.*, 2000), twist family BHLH

transcription factor (TWIST) 1 and 2 (Yang *et al.*, 2004), and the zinc-finger E box-binding homeobox (ZEB) 1 and 2 (Vandewalle *et al.*, 2005). However, it is not clear if these EMT factors function independently or coordinately to activate the program. Notably, the most malignant cancers, including breast cancer, express high levels of Vimentin (mesenchymal marker) along with the decrease of E-Cadherin (epithelial-related), which correlates with poor prognosis (Thiery, 2002). TNBC tumours show high expression of genes associated with EMT (Jang *et al.*, 2015) that are induced by several mediators and, in particular, by the constitutive activation of ERK (Figure 2.24), which sustains cell migration (Huang *et al.*, 2004).

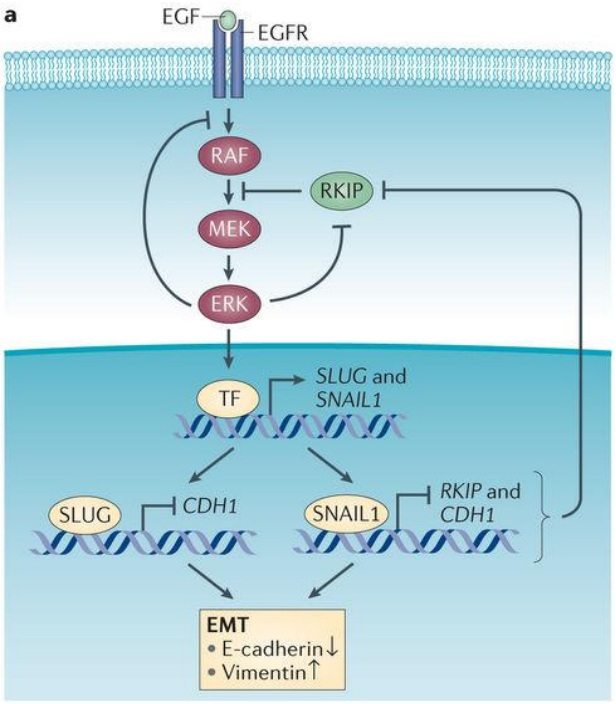

Figure 2.24 - ERK-mediated regulation of SNAI2 expression. Adapted from (Kolch *et al.*, 2015). ERK signalling pathway governs EMT by favouring the expression of genes, which are responsible for the regulation of this process, such as SNAIL1 and SNAI2/SLUG. Accordingly, the expression of SNAIL1 and SNAI2/SLUG is accompanied by the decrease of epithelial markers (E-Cadherin), along with the increase of mesenchymal ones (Vimentin).

2.9.1 The ERK signalling pathway promotes tumour aggressiveness

ERK chemical and genetic inhibition results in the reduction of cell migration (Huang *et al.*, 2004). Accordingly, tumour aggressiveness often relies on ERK-mediated phosphorylation of numerous targets, including kinases, phosphatases, transcription factors and cytoskeletal proteins (Dhillon *et al.*, 2007). Notably, several mediators of the EMT process are found among these targets, e.g. SNAIL1, SNAI2 (Chang *et al.*, 2011), TWIST1 and ZEB1, which are commonly high expressed in TNBCs (Figure 2.25).

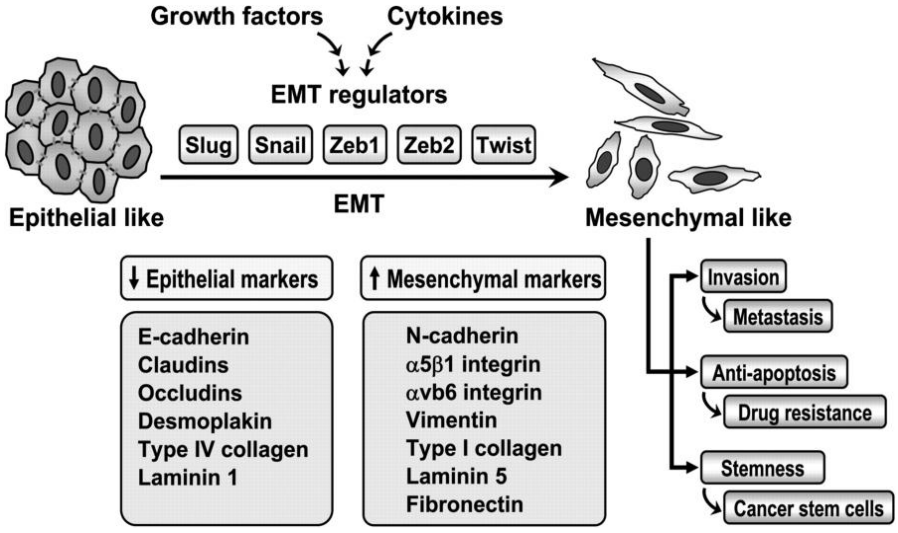

Figure 2.25 - EMT features and molecular portrait (Shih and Yang, 2011). EMT is a crucial step for tumour progression and invasion and promotes metastasis formation, because of the increased cell motility that follows the acquisition of mesenchymal features. Furthermore, EMT favours apoptosis resistance to chemotherapeutic drugs and the expression of stem cell-like features.

2.9.2 The role of SNAI2 in cancer metastasis

The expression of the transcription factor SNAI2 is sustained by EGFR down-stream pathways, including PI3K-Akt and RAS-MAPK. SNAI2 belongs to the highly conserved

Snail/Scratch superfamily and it is characterized by two domains: the highly conserved SNAG (Snail/Gfi) domain in the N-terminal region and the C2H2 type zinc fingers in its C-terminal region (Nieto, 2002) Figure 2.26).

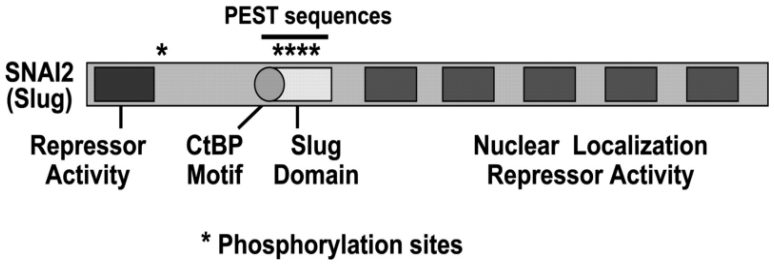

Figure 2.26 - Structural domains of SNAI2. Modified from (Shih and Yang, 2011). The zinc finger transcriptional factor SNAI2 contains an N-terminal SNAG domain and C-terminal zinc finger domains. Both of these domains are responsible for SNAI2 repressor activity. The NES domain allows the nuclear export signal.

Several agents, including EGF, fibroblast growth factor (FGF), hepatocyte growth factor (HGF), transforming growth factor β (TGFβ), bone morphogenetic proteins (BMPs), WNTs and Notch (Figure 2.27), activate SNAI2 expression. Among these factors, EGF is important for SNAI2 high expression in TNBCs, which enhances cell motility, metastatic potential (Bailey *et al.*, 2012; Phillips and Kuperwasser, 2014) and resistance to detachment-induced cell death.

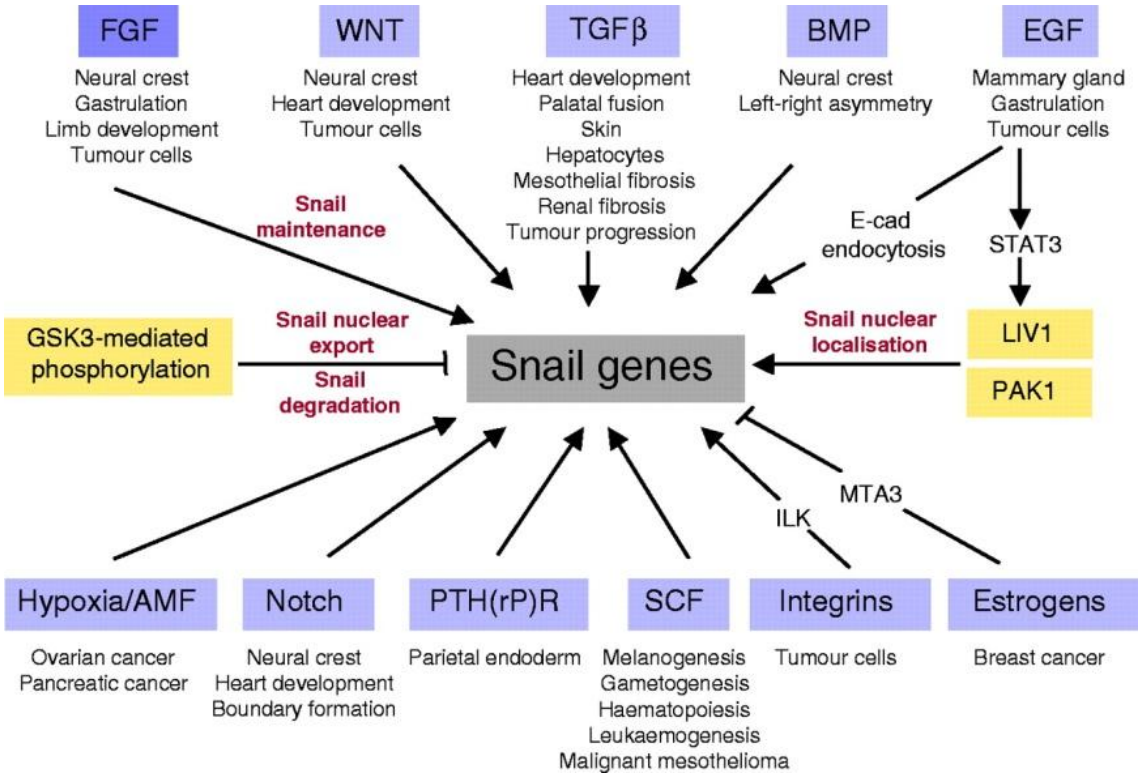

Figure 2.27 - Pathways responsible for SNAI2 expression (Barrallo-Gimeno and Nieto, 2005). The transcription factor SNAI2 is controlled by several pathways. Its modulation occurs not only at the transcriptional levels, but also through the regulation of its subcellular localization.

Therefore, the association of SNAI2 with cancer aggressiveness and resistance to therapy renders this protein an attractive therapeutic target in breast cancers (Figure 2.28). However, only few compounds have been designed to directly target SNAI2 (Harney *et al.*, 2009) and some indirect approaches have been developed to inhibit its expression and/or activity (Ferrari-Amorotti *et al.*, 2014; Ferrari-Amorotti *et al.*, 2013). In this way, the invasive and migratory behaviours of cancer cells have been attenuated.

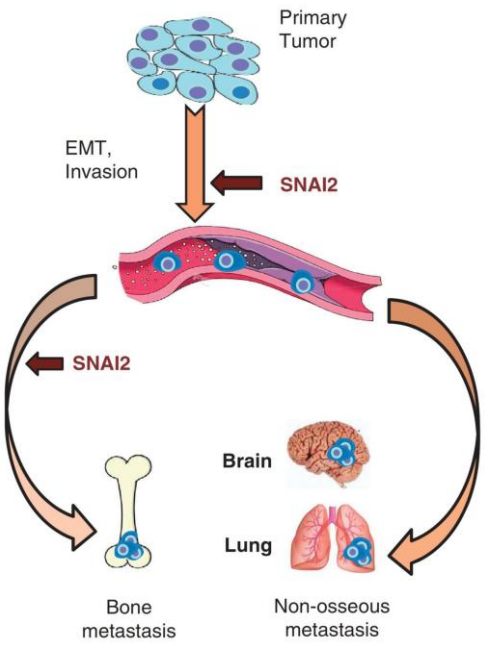

Figure 2.28 - Role of SNAI2 in tumour metastasis. Adapted from (Chimge and Frenkel, 2013). SNAI2 controls both early metastatic events including EMT, invasion, intravasation and late stages, thus favouring cancer cell colonisation of secondary sites.

Beyond EMT regulation, SNAI2 increases cancer aggressiveness favouring cancer cell stem-like features (Luanpitpong *et al.*, 2016). In fact, a correlation exists between EMT and cancer stem-like cell (CSC) enrichment, and in line with this findings, it has been reported that SNAI2 controls the levels of SOX2 (Samanta *et al.*, 2016) and SOX9 (Luanpitpong *et al.*, 2016). These proteins belong to the SOX (Sry-related HMG Box) family, which is involved in the maintenance of self-renewal and pluripotency in embryonic stem cells, as well as in adult tissue progenitors (Sarkar and Hochedlinger, 2013). Therefore, SNAI2 plays a pivotal role in the regulation of cell motility, survival and cancer cell "stemness" and contributes to the dissemination of cancer cells from the primary tumours to the secondary sites. In light of these observations, it would be important to understand the molecular mechanisms of

action and regulation of SNAI2 in order to design novel approaches to interfere with its expression and contrast the metastatic process.

2.10 EGFR intracellular trafficking

So far, the mechanisms leading to EGFR over-expression in TNBCs are not completely clear. Increased levels of this receptor have been linked to the presence of mutated BRCA (Nakai *et al.*, 2016), but also other aspects contribute to EGFR levels. For example, it has been shown that a reduced degradation can sustain its levels (Zhang *et al.*, 2013). EGFR down-regulation occurs at the end of an intricate process resulting in signal attenuation, which derives from the removal of the receptor from the cell surface (Peschard and Park, 2003). Upon ligand-binding, the major mechanism of EGFR internalization is clathrin-mediated endocytosis (CME), through which the receptor is internalized by clathrin-coated pits and then directed to early endosomes where the cargo is delivered after fusion. Following the delivery to the early endosome, the receptor can be either recycled to the cell surface or sorted to late endosomes and lysosomes for being degraded. An alternative pathway for EGFR internalization is clathrin-independent and it is therefore called clathrin-independent endocytosis (CIE; Sigismund *et al.*, 2005). It has been published that high concentrations of EGF drives to CIE rather than CME (Figure 2.29).

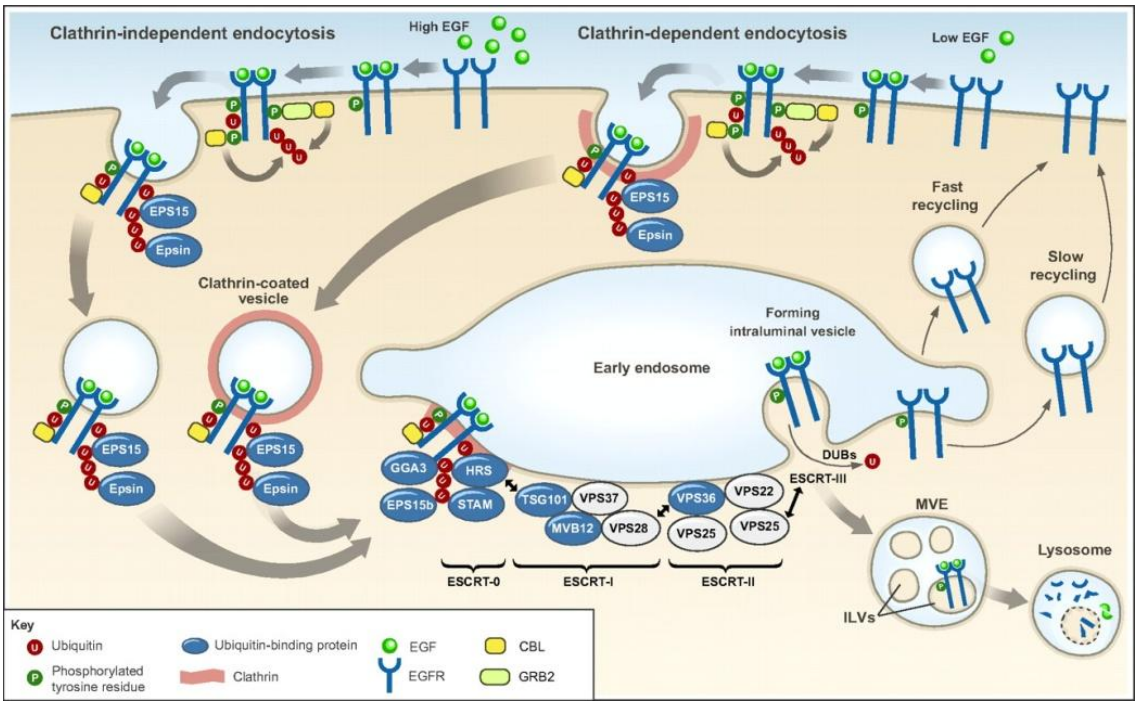

Figure 2.29 - EGR endocytosis and endosomal sorting (Haglund and Dikic, 2012). Upon EGF binding, the receptor undergoes endocytosis, which can occur in a clathrin-indipendent (left) or clathrin-mediated (right) manner. In both cases, after being internalized, the receptor is routed to early endosomes and then sorted to late endosomes (MVE) for lysosomal degradation (ubiquitylated receptors) or recycled to the plasma membrane.

2.11 EGFR ubiquitination is a crucial step for its degradation

In addition to controlling localization, function and stability of target proteins, ubiquitination appears as a crucial event in EGFR endocytosis and degradation. Ubiquitinated EGFR is mainly degraded through lysosomal vesicles (Futter *et al.*, 1996; Marmor and Yarden, 2004) and not by "classical" proteasomal degradation.

2.11.1 EGFR degradation induced by c-CBL

Commonly known as being a negative regulator of various activated receptor tyrosine kinases (RTKs) such as EGFR and c-MET, c-CBL plays a crucial role in EGFR endocytic

trafficking. Notably, c-CBL is a member of the evolutionarily conserved Cbl family of cytoplasmic proteins and because of its crucial role in the attenuation of receptor signalling, c-CBL deregulation can lead to malignant diseases. Accordingly, Zhang J. *et al*. (Zhang *et al.*, 2013) reported that c-CBL inhibition correlates with poor prognosis in glioblastoma patients. Interestingly, it was shown that if c-CBL is unable to correctly regulate EGFR, this receptor does not undergo lysosomal degradation. This block eventually results in extended EGFR-signalling activities (Figure 2.30).

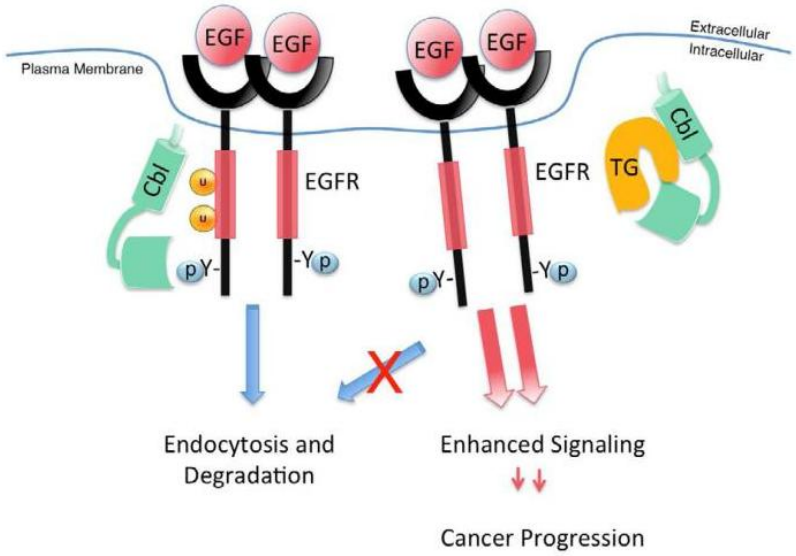

Figure 2.30 - c-CBL-mediated ubiquitination leads to EGFR endocytosis and degradation. Adapted from (Zhang *et al.*, 2013). c-CBL crucially mediates EGFR ubiquitination and degradation. The impairment of c-CBL activity results in enhanced signalling which contributes to cancer progression.

Upon ligand-binding, EGFR undergoes dimerization and autophosphorylation of several tyrosine residues in the cytoplasmic tail. These phosphorylations represent the prerequisite for clathrin-dependent endocytosis. In particular, phosphorylation of tyrosine 1045 (Tyr-1045) is crucial for the direct binding of c-CBL to EGFR (Levkowitz *et al.*, 1999). It has been recently reported that the hypophosphorylation at Tyr1045 allows EGFRvIII to

evade degradation (Grandal *et al.*, 2007). In this setting, c-CBL is not recruited to EGFR, which therefore it is not ubiquitinated correctly (Figure 2.31).

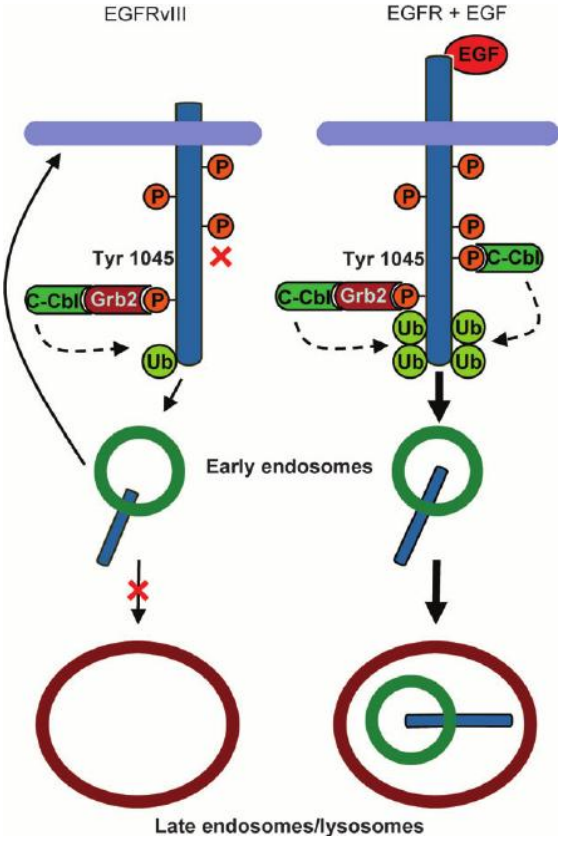

Figure 2.31 - Phosphorylation of Tyr-1045 is crucial for c-CBL-mediated EGFR degradation (Grandal *et al.*, 2007). The binding of c-CBL requires the phosphorylation of EGFR at Tyr-1045. Consequently, the mutant form of EGFR, named EGFRvIII, which is hypophosphorylated at Tyr-1045, avoids the ubiquitination by c-CBL and is less degraded.

2.11.2 RAB family proteins regulate the EGFR endocytic trafficking

Once EGFR is in early endosomes, it can be routed to the late endosome and lysosome for degradation, or recycled to the plasma membrane. If the receptor is targeted for degradation, it is first internalized in multivesicular body (MVB; Stahl and Barbieri, 2002), and subsequently released to the lysosomes. RAB proteins have been identified as key

regulators of EGFR endocytic trafficking and mediate this process. The RAB family consists of small GTPases proteins (Somsel Rodman and Wandinger-Ness, 2000) and is composed by over 60 members that are characterized by similar structure and properties, but exert different functions in the regulation of intracellular vesicles trafficking and fusion reactions. So far, only a few RAB proteins have been described as being regulators of EGFR endocytic trafficking (Ceresa, 2006) namely RAB5, RAB11 and RAB7. RAB5 and 11 are established markers of early (Barbieri *et al.*, 2004; Konstantinopoulos *et al.*, 2007) and recycling endosomes (Cullis *et al.*, 2002), respectively. Conversely, RAB7 is a marker of late endosomes, and therefore drives EGFR to degradation (Ceresa, 2006; Figure 2.32).

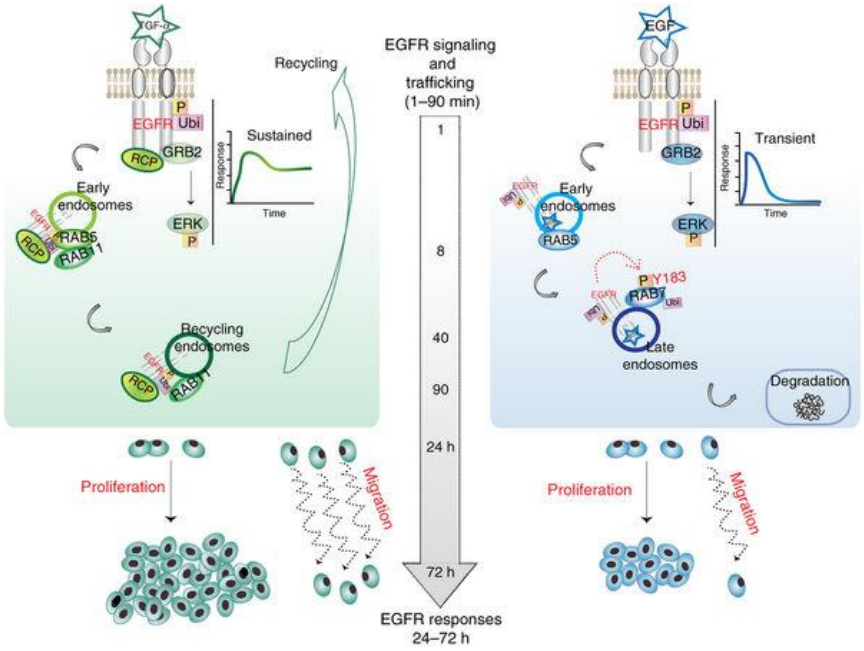

Figure 2.32 - Different RAB family members are responsible for EGFR recycling and degradation (Francavilla *et al.*, 2016). Once in early endosomes, EGFR can be recycled to the cell surface or further routed to late endosomes and lysosomes for degradation. While RAB11 is a marker of the recycling process, RAB7 is a marker of late endosomes and co- localizes with degrading EGFR.

2.12 The role of LRIG1 in EGFR down-regulation

Together with c-CBL, the leucine rich repeat and immunoglobulin-like domain protein-1 (LRIG1) has recently been identified as a negative regulator of c-MET and the ErbB family members (Figure 2.33). Particularly, Gur *et al.* reported the involvement of LRIG1 in increasing EGFR ubiquitination and degradation, which occurs by enhancing the recruitment of c-CBL to the receptor (Gur *et al.*, 2004). However, while LRIG1 mediates EGFR degradation in a c-CBL dependent manner (Gur *et al.*, 2004), c-MET degradation does not require ubiquitination and is mediated by LRIG1 in a c-CBL-independent manner (Shattuck *et al.*, 2007).

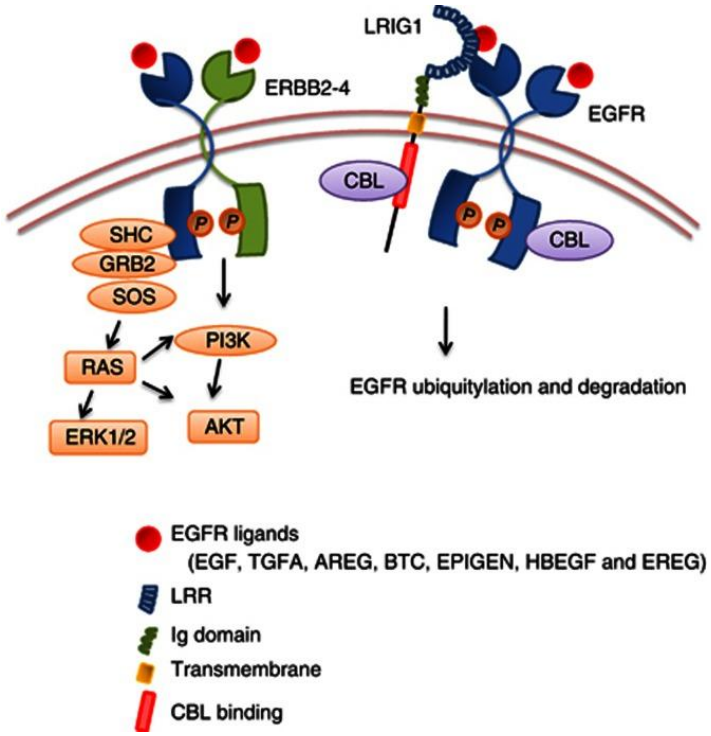

Figure 2.33 - The role of LRIG1 in EGFR degradation (Wang *et al.*, 2013). LRIG1 negatively regulates EGFR via enhancing its interaction with c-CBL. The presence of LRIG1, in fact, favours EGFR degradation by accelerating the recruitment of the E3 ligase c-CBL through a CBL-binding domain in the LRIG1 cytoplasmic tail. This mechanism enhances EGFR ubiquitination and lysosomal degradation.

LRIG1 has been described as a tumour suppressor due to its capability to inhibit cell proliferation and cancer growth (Hedman *et al.*, 2002) and its expression has been analysed in many human cancers. Importantly, gene expression analysis of five cancers, including breast, lung, bladder, glioma and melanoma (Rouam *et al.*, 2010), revealed that LRIG1 decreased expression correlates with poor survival. Being a transcriptional target of estrogen receptor-alpha (ERα), LRIG1 expression is high in Luminal A (ER-positive) breast cancers and low in the basal-like subtype (Wang *et al.*, 2013). Interestingly, LRIG1 low expression contributes to the aggressiveness of basal-like tumours. In fact, a negative correlation has been found between its expression and the presence of mesenchymal markers (Yokdang *et al.*, 2016).

2.13 EGFR and c-MET cross-talk

Together with EGFR, also the activation of c-MET mediated by its ligand, the hepatocyte growth factor (HGF), is known to promote the survival of many cell types. Furthermore, c-MET enhances tumour invasion via increased ERK phosphorylation, and this results in a high metastatic potential of cancer cells. Importantly, the interaction between EGFR and c-MET has been found in tumour but not in normal cells (Jo *et al.*, 2000). This evidence suggests that a tumour-specific cross-talk exists between EGFR and c-MET receptors and promotes the activation of their shared down-stream pathways (Figure 2.34). Many signalling pathways are in common between both receptors and therefore several studies support a possible synergism between EGFR and c-MET, which favours tumour growth and aggressiveness. However, the underlying mechanisms responsible for this functional interaction remain unknown. Furthermore, Engelman and colleagues reported

that patients affected by NSCLC are initially sensitive to treatment with the EGFR inhibitor gefitinib, but later become resistant because of c-MET gene amplification. Emerging evidence shows that about 20 % of acquired resistance to EGFR-targeted therapies derives from the amplification of the c-MET receptor (Corso and Giordano, 2013). Accordingly, breast cancer cells acquire resistance to EGFR TKIs after HGF exposure and the HGF-induced cell survival results abrogated in EGFR-depleted cells, indicating a critical role for EGFR/c-MET cross-talk (Mueller *et al.*, 2012). Intriguingly, this information supports the employment of simultaneous treatment with anti-EGFR and anti-c-MET drugs to restore the sensitivity and efficiency of tumour treatment (Yu *et al.*, 2013).

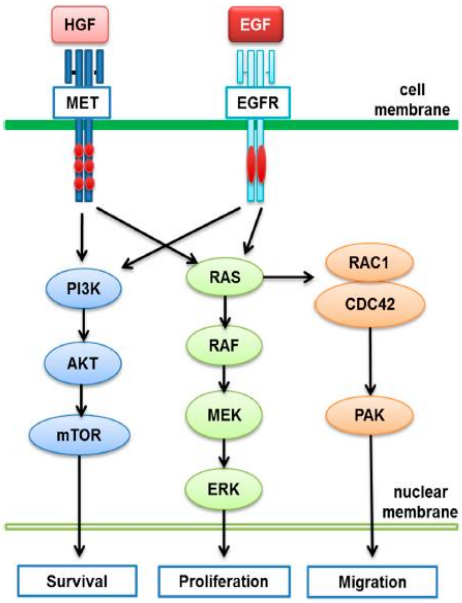

Figure 2.34 - Functional interaction between EGFR and c-MET (Zhang *et al.*, 2015). A cross-talk between EGFR and c-MET down-stream signalling pathways occurs thereby enhancing tumour malignant phenotype. The two receptors elicit similar signal transduction pathways and therefore their synergism increases the strength and duration of shared signalling pathways. EGFR and c-MET are often co-expressed in tumour with a high grade of aggressiveness and their combined activity promotes cell survival, proliferation and migration.

3 AIM OF THE STUDY

Despite the progress in the understanding of the molecular and cellular basis driving to metastasis formation, this process remains the major cause of mortality. The central purpose of this study is therefore to characterize the role of IAPs in the metastatic cascade.

The specific aims of this work are:

- Investigate the effect of SM83-mediated depletion of IAPs on metastasis formation *in vivo*
- Determine the mechanism of SM83-induced down-regulation of SNAI2
- Study the role of IAPs, and in particular of cIAP1, in regulating EGFR-mediated SNAI2 expression
- Investigate the role of cIAP1 in regulating EGFR levels.

4 MATERIALS AND METHODS

4.1 Reagents

4.1.1 Buffers and Solutions

Freezing solution

- 60 % RPMI or DMEM supplemented with
    - 1 % L-Glutamine (LONZA)
    - 1 % NEAA (LONZA)
    - 1 % Sodium pyruvate (LONZA)
    - 1 % Hepes (LONZA)
- 30 % FBS
- 10 % DMSO (Sigma-Aldrich)

SDS lysis buffer

- 5 % SDS
- 125 mM Tris HCl pH 6,8
- Milli-Q water up to volume

Mix of proteases and phosphatases inhibitors

- 200 µg/ml Aprotinin
- 200 µg/ml Leupeptin
- 200 mM EDTA
- 200 mM β-glycerophosphate

- 200 mM sodium fluoride
- 200 mM sodium orthovanadate
- 50 mM sodium pyrophosphate
- Milli-Q water up to volume

Protein loading buffer 10X (ZAP)

- 0.25 M Tris HCl pH 6.8
- 30 % glycerol
- 8 % SDS
- 0.02 % BFB
- 10 % β-mercaptoethanol
- Milli-Q water up to volume

Running Buffers

MES and MOPS were purchased from Thermo Fisher Scientific

Transfer buffer

- NuPAGE Transfer Buffer 1X (Thermo Fisher Scientific)
- 20 % methanol
- Milli-Q water up to volume

PBS-T

- PBS (LONZA, Cat. #17-516F)
- 0.1 % TWEEN 20

Blocking buffer

- 4 % non-fat dry milk (Blotting-Grade Blocker, BIO-RAD)
- 0.01 % Tween-20 (Sigma-Aldrich)
- 1X PBS

ELB buffer

- 150 mM NaCl
- 50 mM Hepes
- 5 mM EDTA
- 0.5 % NP40
- Milli-Q water up to volume
- pH 7.5

Nucleic acid loading dye 6X

- 0.25 % bromophenol blue powder
- 30 % glycerol
- Milli-Q water up to volume

TAE buffer 1X

- 20 mM Tris acetate
- 10 mM EDTA
- 2.85 % acetic acid
- Milli-Q water up to volume

Antibody solution

- 5 % Albumin from Bovine Serum (BSA; Sigma-Aldrich),
- 0.01 % Tween-20,
- 0.01 % Sodium Azide purchased from Sigma-Aldrich,
- 1X PBS

4.2 Cell cultures

The human breast adenocarcinoma MDA-MB231, BT549, MDA-MB157, SkBr3 and HCC1937 cell lines were cultured in Roswell Park Memorial Institute (RPMI)-1640 medium (LONZA Group, Basel, CH) supplemented with 10 % fetal bovine serum (FBS; EuroClone, Milan, IT), 2 mM L-glutamine, sodium pyruvate, non essential amino acids (NEAA) and penicillin (100 U/ml)/streptomycin (100 µg/ml; all from LONZA). SUM149 and SUM159, together with the human hTERT-mammary immortalized epithelial HME and MCF10A cell lines- parental and bearing the EGFR delE746A750 mutation (HME EGFR and MCF10A EGFR hereafter, respectively) -were cultured in Dulbecco's Modified Eagle's medium-F12 (DMEM-F12; Gibco), supplemented with 10 % FBS, 2 mM L-glutamine, 20 ng/ml EGF (Cat. #GRF-10544, Selleck Chemicals, Munich, D), 10 µg/ml insulin (Sigma-Aldrich, St. Louis, MO, USA), 500 µg/ml hydrocortisone (Sigma-Aldrich). BT474, MDA-MB453, T47D and MDA-MB361 cell lines were maintained in DMEM (Gibco-Thermo Fisher Scientific, Massachusetts, USA) supplemented with 10 % FBS and 2 mM L-glutamine. HEK293FT (Thermo Fisher Scientific) highly transfectable cell line were cultured in DMEM with 10 % FBS and used for lentiviral production. All cells were grown at 37 °C in fully humidified atmosphere with 5 % CO2.

MDA-MB231 cell lines were purchased from American Type Culture Collection while all the other breast cancer cell lines employed for this thesis were kindly provided by Dr Elda Tagliabue. The mouse 4T1 mouse mammary carcinoma were a kind gift from Dr Mario Colombo, while human mammary immortalized epithelial HME and MCF10A cell lines were all kindly provided by Prof. Alberto Bardelli. All cell lines have been checked for their identity (STR characterization) and were mycoplasma-free as determined by *Takara* Mycoplasma Detection Kit (Clontech, Mountain View, CA, USA).

4.3 Cell viability assay

Cell viability was established using the CellTiter-Glo (Promega, Madison, USA). According to the manufacturer's instructions, cells were seeded in white optical 96-well plates and treated as indicated. Medium was discarded at the end of the experiments and replaced with 60 µl of reagent diluted 1:4 in phosphate-buffered saline PBS. After 15 min of shaking at RT, luminescence was measured with a Tecan Ultra plate reader. Viability of cells silenced with indicated siRNAs (Table 4.1) was shown as a percentage compared to untreated or mock treated cells.

Pool Catalog Number	Gene Symbol
M-003155-02	MERTK
M-005563-02	GPER
M-017626-00	BDNF
M-012633-02	CTGF
M-009328-02	PTPRU
M-016029-01	OSR1
M-010911-00	KLHL3
M-009900-01	RGS4
M-008705-01	FOXQ1
M-004788-00	HSDL1

M-025119-01	RNF144B
M-017386-00	SNAI2
M-005130-02	PAPPA
D-001206-13	Non-targeting #1

Table 4.1 - List of Dharmacon siRNA pools (GE Healthcare, Lafayette, CO, USA).

4.4 Cell treatments

To deplete cIAPs, cells were treated with 100 nM SM83 whose synthesis has recently been described (Manzoni *et al.*, 2012). The activation of TNF-Rs was achieved by the administration of recombinant TNF (Emmerich *et al.*, 2011) produced by the University of Milan using a plasmid encoding for tagged human TNF kindly provided by Prof. Henning Walczak. To specifically activate the non-canonical NF-κB pathway, the recombinant human TWEAK provided by Prof. Harald Wajant (Salzmann *et al.*, 2013) was employed. In combination therapy with SM83 the necroptosis inhibitor Necrostatin-1 (Enzo Life Sciences, Plymouth Meeting, PA, USA) and Pan-caspase inhibitor z-VAD(OMe)-FMK (BIOMOL) were used. Cells were treated with the PI3K and AKT (LY294002 and Triciribine, Enzo Life Sciences), MEK (U0126, Calbiochem, Merck KGaA, Darmstadt, D) and p38 (SB203580, Selleck Chemicals) inhibitors. EGFR activation was induced through the administration of 20 ng/ml EGF (Cat. #GRF-10544, Selleck Chemicals) or TGFα (#100-16A, Peprotech, London, UK) in cells serum-starved overnight using medium supplemented with 0.1 % FBS. Cetuximab employed to specifically block EGFR was provided by the pharmacy of the Fondazione IRCCS Istituto Nazionale dei Tumori (Milan, IT). When needed, protein levels were stabilised with the lysosomal inhibitor chloroquine (CLQ, #C6628) from Sigma-Aldrich, used at 100 µM and added to the cell growth medium 1 h before EGFR stimulation. The protein synthesis

inhibitor cycloheximide (CHX, #239764, Calbiochem) was added to BT549 cells at 100 µM 30 min before treatments, while half of the dose was employed in MCF10A cells.

4.5 *In vivo* experiments

Experiments were approved by the Ethics Committee for Animal Experimentation of the Fondazione IRCCS Istituto Nazionale dei Tumori (INT) of Milan according to institutional guidelines and by the Italian Minister of Health (Projects INT_12_2011 and INT_02_2015). Mice were maintained in laminar flow rooms keeping temperature and humidity constant. Mice had free access to food and water and were weighted twice a week.

In vivo effect of SM83 was assessed using the breast cancer xenograft models, non-obese diabetic/severe combined immunodeficiency disease (NOD/SCID) mice. Animals were engrafted in the left flank by subcutaneous (sc) injection of 200 µl physiological saline containing $5x10^6$ MDA-MB231. Randomization occurred at the day 13, when mice were treated with ip or iv injections with 5 mg/kg SM83, 5 times/week to a total of 15 injections. Tumour growth was evaluated by biweekly measurements of tumour diameter with a Vernier caliper and tumour volume (TV) was calculated according to the formula: 4/3 x 3.14 x (l/2) x (w/2) x (h/2) where l, w and h are length, width and height, respectively. Biochemical analysis and gene expression analysis of the primary tumour were performed in mice sacrificed 6 h after the last injection. In metastasis studies, NOD/SCID mice were killed 2 weeks after the last SM83 administration and, together with subcutaneous nodules, lungs were collected and formalin-fixed/paraffin-embedded for IHC detection of metastasis with anti-human Vimentin antibody (M0725, DAKO-Agilent, Santa Clara, CA, USA).

The anti-metastasis effect of SM83 was also tested using immuno-competent BALB/c mice injected with 1×10^4 4T1(cl5) cells on day 0 into the mammary fat pad. After 13 days, mice were treated with ip injections of SM83 at a dose of 5 mg/kg body weight, three times/weeks for 2 weeks. The progression of metastasis was assessed 2 days after the last SM83 injection.

4.6 Gene expression profiling and bioinformatics

MDA-MB231 nodules were collected from NOD/SCID xenografts 6 h after the last injection of SM83 and cut in pieces. One piece was lysed for RNA extraction using RNeasy Mini Kit (Qiagen, Hilden, Germany) and then total RNA was retro-transcribed using SuperScript II Reverse Transcriptase kit (Thermo Fisher Scientific) for gene expression profiling (GEP). GEP was performed by the Functional Genomics and Bioinformatic Core Facility of INT using Illumina HumanHT-12 v4 Expression BeadChip arrays (Illumina, San Diego, CA, USA).

Raw data were pre-processed using the R/Bioconductor package "lumi" (Du *et al.*, 2008) that provides statistical methods for analysis of Illumina microarray data. Data were Log2-transformed and normalized using the robust spline normalization method. Probes not annotated to HUGO gene symbols were filtered out. For the remaining probes only those with a detection p-value < 0.01 (a measure of the confidence that a probe is expressed above the background level, defined by negative control probes) in at least one sample were considered. Finally, multiple probes mapping to the same gene were collapsed selecting the probe detected in the highest number of samples.

Differential expression analysis was performed using the "limma" package (Phipson *et al.*, 2016) that combines linear models with moderated t-statistic to identify differentially expressed genes across experimental conditions. The moderated t-statistics has the same interpretation as an ordinary t-statistic except that the standard errors are moderated across genes, i.e., squeezed towards a common value, using a simple Bayesian model. P-values obtained from limma were adjusted for multiple-testing using the Benjamini-Hochberg false discovery rate (FDR) to reduce the number of false positives. Genes showing an absolute fold change ≥ 1.5 and an FDR <0.05 were considered significantly differentially expressed. Expression profiles are deposited in the Gene Expression Omnibus (GEO) repository with accession number GSE98691.

For public gene expression datasets, normalized data for breast cancer cell lines were downloaded from ArrayExpress repository (https://www.ebi.ac.uk/arrayexpress/) with accession number E-MTAB-181 (Heiser *et al.*, 2012). RNA-Seq level-3 expression data for TCGA breast cancer patients were downloaded from Firehose portal (http://gdac.broadinstitute.org/) with accession date 2016-01-28. Data were normalized using the trigger mean of M-value method (Robinson and Oshlack, 2010) and transformed in logarithmic scale (base 2). Correlation between continuous variables was calculated using the Pearson's correlation coefficient.

4.7 Wound healing-based migration assay

Wound healing experiments were performed using Culture-Insert in µ-Dish 35 mm (Ibidi). To assess cell migration, $4x10^4$ MDA-MB231 cells were reverse transfected in the culture inserts in 12-well plates. After 72 h, inserts were removed, cells were washed once to

eliminate detached cells and multi-well plates were put in a Cell-IQ instrument (CM-Technologies) to test cell motility. Images were taken every hour for 24 h and analysed with the provided software to measure the gap area.

Wound healing assay was performed using the same protocol described above, also to compare the migration capability of MDA-MB231, BT549, HCC1937 and T47D cell lines and then to assess the effect of cIAP1 depletion on cell motility in BT549 and MCF10A, either *wt* or bearing mutated EGFR, stably silenced for cIAP1 compared to control. Data obtained by Cell-IQ instrument were analysed and used to draw a sigmoidal curve with GraphPad Prism thus determining the time necessary to close half of the wound area.

4.8 Gene knock-down by silencing (reverse protocol)

To achieve transient knock-down of target genes, cells were transfected with indicated short interfering RNAs (siRNAs, Table 4.2) using a reverse transfection protocol in which siRNAs (Qiagen) and RNAiMAX (Thermo Fisher Scientific) have been employed. A mix containing 3.25 µl of RNAiMAX in 100 µl Optimem (Gibco) and another one with 3.25 µl of siRNA (20 µM) stock were prepared, and after 5 min at RT were combined and left at RT for 30-40 min. In the meantime, cells were trypsinized, counted and about 0.25 x 10^6 cells were cultured in a 6-well plate in a final volume of 2 ml medium without antibiotics. After the incubation, the siRNA/RNAiMAX mix was added on top of the cells in the culturing well. Cells were incubated for 72 h to have an efficient knock-down in all cases. If cells needed to be stimulated, 48 h after transfection cells were serum-starved for the following 24 h. In each experiment, scramble siRNAs (siCtr) were used as control and siRNA targeting an essential gene (ubiquitin, UBB) served to evaluate the transfection efficiency. For transfection in 96-

well plates, mixes were prepared with 0.25 µl siRNAs plus 0.25 µl RNAiMAX and 10^4 cells were seeded in 100 µl final volume.

Name	Sequence	Source
siLUC	5'- CGUACGCGGAAUACUUCGATT-3'	Eurofins

Name	Assay ID	Source
siclAP1	Hs_BIRC2_7 and 8	Qiagen
siclAP2	Hs_BIRC2_8 and 9	Qiagen
siTNF	Hs_TNF_1	Qiagen
siTNF-R1	Hs_TNFRSF1A_5	Qiagen
siTNF-R2	Hs_ TNFRSF1B_1	Qiagen
siERK1	Hs_MAPK3_3 and 7	Qiagen
siERK2	Hs_MAPK1_ 9 and 10	Qiagen
siNFkB2	Hs_NFKB2_1	Qiagen
siNF-kB1	Hs_NFKB1_3	Qiagen
siRELA	Hs_RELA_5	Qiagen
siLRIG1	Hs_LRIG1_5 and 6	Qiagen
siMET	Hs_MET_6	Qiagen
siGENOME SMARTpool for XIAP	M-004098-01	Dharmacon
siGENOME Non-Targeting siRNA Pool #1	NT1; D-001206-13	Dharmacon
siGENOME SMARTpool for SNAI2	M-017386-00	Dharmacon

Table 4.2 - List of siRNAs used in this thesis.

4.9 Lentiviral transduction for stably knock-down

MDA-MB231 cells were engineered to stably knock-down SNAI2 through lentiviral-mediated gene delivery. Lentiviral particles containing the pGFP-C-shLenti SNAI2 (NM_003068) were purchased from OriGene. Target cells (5×10^4 cells) were cultured with medium containing lentiviral particles for 48 h before addition of puromycin (0.5 µg/ml) for selection. After selection, transfection was confirmed by protein expression analyses.

To stably knock-down cIAP1, lentivirus was produced by transfection of HEK293FT packaging cells with the pLKO.1-cIAP1 shRNA (Cat. #44129, Addgene). Lentiviral particles were collected 48 h after transfection and filtered through a 0.45 μm filter.

4.10 Gene over-expression

To ectopically express EGFR and c-CBL, lentiviral plasmids were used to produce lentiviral particles in HEK293FT packaging cells. Viruses were obtained by reverse transfection of HEK293FT cells following manufacturer's protocol. After 24 h, medium was replaced with fresh medium that was collected after further 24 h and used to transduce BT549 and MCF10A cells. The plasmid for human EGFR (Myc/Flag-tagged) ectopic expression was purchased by Origene Company (#RC217384L1; Rockville, MD, USA), while the c-CBL-expressing vector (RRL-CMV-CBL) was kindly provided by Prof. Pier Paolo Di Fiore.

To over-express *wt* and mutated cIAP1, cells were seeded the day before transfection, using a medium without antibiotics, in order to have 80-90 % of confluent cells the following day. BT549 cells were transfected with pcdna3.1 plasmids kindly provided by Jon Ashwell (Addgene plasmid #8311 and #8337, respectively), according to the manufacturer's instructions. Briefly, DNA was complexed with Opti-MEM, as well as Lipofectamine 2000 (ratio DNA : Lipofectamine = 1 : 2). Mixtures were incubated 5 min at RT and then combined to allow the formation of the liposomes-DNA complexes; 30 min later, the solution was added to the cells and the desired protein expression was verified 48 h later.

4.11 Western blot analysis

4.11.1 Preparation of total cell extracts

Cells were trypsinized and harvested by centrifugation at 4500 rpm for 5 min at 4 °C. After washing with PBS supplemented with 0.1 mM Na_3VO_4 to inhibit phosphatase, cells were lysed by boiling in 60-100 µl SDS lysis buffer supplemented with the mix of phosphatases and proteases inhibitors. Samples were then sonicated with 20 % amplitude for 20 sec (Branson Digital Sonifier) to dissolve DNA molecules, and then centrifuged at 13000 rpm for 20 min at room temperature (RT). Cleared supernatants were transferred to a new tube and frozen at -20 °C.

4.11.2 Quantification of total cell extracts

Bicinchonic acid (BCA)-containing protein assay was used to determine the protein content of total cell extracts, according to the manufacturer's instructions (QuantumMicro Protein, EuroClone). Briefly, 2 µl of lysate were incubated with 148 µl water and serial dilutions of bovine serum albumin (BSA) used as standard protein, in a 96-well plate. BCA solution was added in a 1:1 ratio. After incubation at RT, absorbance was measured at 485 nm using Ultra microplate reader (Tecan). Protein concentration was determined by interpolation with the curve obtained with the standard BSA.

4.11.3 SDS-PAGE

Proteins were separated according to their molecular weight using pre-cast 4-12 % Bis-Tris NuPAGE gels (Thermo Fisher Scientific). Cell lysates were mixed with 4 x reducing SDS-Sample buffer and heated for 10 min at 99 °C. Before loading, protein samples were

prepared by adding ZAP solution to 20-50 µg of proteins and samples were denatured for 10 min at 99 °C. As a molecular weight standard, Page Ruler Plus Pre-Stained Protein Ladder (EuroClone) was used. The electrophoretic separation was achieved by applying a constant voltage in MES or MOPS buffer. As suggested by the manufacturer, 500 µl of NuPAGE antioxidant were added to the chamber to protect reduced disulfide bonds and sensitive amino acids from oxidation, thus allowing proper protein migration in reducing conditions. Proteins within the gels were then blotted onto PVDF Immobilon-P Transfer Membrane (Millipore), previously activated with 100 % methanol, rehydrated in Milli-Q water, and equilibrated in transfer buffer. Transfer was carried out using the XCell II blot module (Thermo Fisher Scientific). Transfer sandwich was composed of three sponges; three 3MM wetted papers (Whatman), the gel, PVDF and three additional 3MM wetted papers. The sandwich was put into the XCell SureLock Mini-Cell, the blot module was filled with transfer buffer and the outside chamber with distilled water; transfer of proteins was carried out at 180 mA for 2 h. Membranes were incubated with blocking buffer (4% non-fat milk dissolved in PBS plus tween 0.1 %, PBS-T) for 30 min and then incubated overnight with the indicated primary antibodies. Membranes were then washed 3 times in PBS-T and incubated 1 h with the appropriate horseradish peroxidase-conjugated secondary antibody (Sigma). After washing in PBS-T, proteins were detected by electrochemiluminescence (ECL) reaction, by exposure of films to the membranes after incubation with luminol-based chemiluminescent substrates (Pierce).

4.12 Immunoprecipitation

Immunoprecipitation (IP) was performed in BT549 cells over-expressing FLAG-tagged EGFR for the identification of EGFR binding proteins (co-IP). To this end, cells were collected, washed 1 time with PBS supplemented with Na_3VO_4 and lysed in ice-cold ELB buffer supplemented with the mix of proteases and phosphatases inhibitors (hereafter ELB+), at 4 °C with rotation for 30 min. Samples were then centrifuged at 13000 rpm for 15 min at 4 °C, supernatant was transferred in a new low-retention microcentrifuge tube and 1 mg of total protein extract was incubated at 4°C for 3 h with 30 µl of the 50 % slurry of anti-FLAG M2 Affinity Gel (#A2220, Sigma-Aldrich) previously washed with ELB+ buffer three times. After the incubation time, resins were resuspended in 15 µl of SDS lysis buffer and 5 µl ZAP solution, denatured for 10 min at 99 °C and stored at −20 °C. The bound polypeptides were analysed by SDS-PAGE and immunoblotting with indicated antibodies (Table 4.3).

Target antigen	Cod.	Immunoglobulin type	Host organism	Dilution	Source
cIAP1	#ab108361	polyclonal	rabbit	1:1000	Abcam
cIAP2	#552783	polyclonal	rabbit	1:1000	Cell Signaling
XIAP	#610763	monoclonal	mouse	1:5000	Sigma-Aldrich
Cleaved PARP	#5625	polyclonal	rabbit	1:1000	Cell Signaling
LRIG1	#12752	polyclonal	rabbit	1:1000	Cell Signaling
SNAI2	#9585	polyclonal	rabbit	1:1000	Cell Signaling
Cleaved Caspase-3	#9501	polyclonal	rabbit	1:1000	Cell Signaling
NIK	#4994	polyclonal	rabbit	1:1000	Cell Signaling
NF-kB2 p100/p52	#4882	polyclonal	rabbit	1:1000	Cell Signaling
NF-kB1 p105/p50	#3035	polyclonal	rabbit	1:1000	Cell Signaling
Phospho-ERK1/2	#M8159	polyclonal	rabbit	1:5000	Sigma-Aldrich
Total ERK1/2	#M5670	monoclonal	mouse	1:10000	Sigma-Aldrich
pEGFR (Tyr1068)	#2236	polyclonal	rabbit	1:1000	Cell Signaling

Total-EGFR	#ab30	polyclonal	rabbit	1:1000	Abcam
c-CBL	#2747	polyclonal	rabbit	1:1000	Cell Signaling
Flag-t*ag*	#F1804	monoclonal	mouse	1:1000	Sigma-Aldrich
Clathrin	#4796	polyclonal	rabbit	1:1000	Cell Signaling
Myc-*tag*	#2278	polyclonal	rabbit	1:1000	Cell Signaling
EGFR pTyr-1045	#2237	polyclonal	rabbit	1:1000	Cell Signaling
Sprouty 1	#13013	polyclonal	rabbit	1:1000	Cell Signaling
RelA/p65	#3034	polyclonal	rabbit	1:1000	Cell Signaling
c-MET	#sc10	polyclonal	rabbit	1:1000	Sanza Cruz Biotechnology
E-Cadherin	#3195	polyclonal	rabbit	1:1000	Cell Signaling
COL6A2	#HPA007029	polyclonal	rabbit	1:1000	Sigma-Aldrich
SOX9	#82630	polyclonal	rabbit	1:1000	Cell Signaling
SOX2	#3579	polyclonal	rabbit	1:1000	Cell Signaling
PLEXIN-A1	#GTX62196	polyclonal	rabbit	1:1000	GeneTex
Actin	#A1978	monoclonal	mouse	1:10000	Sigma-Aldrich
Vinculin	#V9131	monoclonal	mouse	1:10000	Sigma-Aldrich

Table 4.3 - List of antibodies employed in this thesis.

4.13 Stripping of western blot membranes

Western blot membranes were incubated with stripping buffer at 37 °C for 30 min and then washed for 3 times with PBS-T, followed by incubation in blocking solution and a new round of probing.

4.14 Immunofluorescence

BT549 cells were trypsinized, resuspended in 3 ml of cold RPMI with 10 % FBS and spotted on glass microscope slides using cytospin (Cytospin 2, Shandon). According to Cytospin protocol, slides and filters were placed into appropriate slots in the cytospin with the cardboard filters facing the center of the cytospin. About 100-200 μl of cell suspension were put into each of the wells and spinned at 500 rpm for 5 min. Then slides were dried

overnight fixed with 4 % paraformaldehyde for 10 min, permeabilized for 10 min at RT with 0.2 % Triton X-100 and blocked in PBS, 3 % BSA, 0.1 % Tween-20. Cover slips were then incubated overnight at 4 °C in a humidified chamber with the primary antibody diluted in PBS 2 % BSA overnight. After three washes in PBS, the appropriate secondary fluorescent Alexa Fluor conjugated antibody (Thermo Fisher Scientific), diluted in PBS 2 % BSA was added to the cells for 1 h and the plate was kept in the dark. After incubation, three washes with PBS were performed and nuclei were counterstained with DAPI (0.5 µg/ml in PBS) for 10 min. Then coverslips were mounted on glass microscope slides with ProLong Gold reagent mounting solution (Thermo Fisher Scientific). Fluorescence images were acquired using a fluorescence microscopy and digital image acquisition on a Nikon Eclipse E1000 equipped with a DSU3 CCD camera.

4.15 *In situ* Proximity Ligation Assay (PLA)

Duo Link in Situ reagents (Duolink In Situ PLA; Sigma-Aldrich) were employed in this thesis following the manufacturer's guidelines. Through the cytospin, BT549 cells were spotted on glass microscope slides and dried before being fixed with 4 % paraformaldehyde, and incubated with two primary antibodies raised in different species specific for the target proteins (Table 4.2). Glasses were incubated with primary antibodies diluted in PBS 3 % BSA in a humidity chamber for 2 h at RT. Then cells were stained with the PLA probes diluted 1:5 in PBS 1 % BSA in a humidified chamber for 1 h at 37 °C. Since a short DNA strand is attached to each PLA probe, when protein targets are in close proximity, an enzymatic ligation and a subsequent rolling circle amplification (at 37 °C for 100 min) occur after the addition of other circle-forming DNA oligonucleotides. At the end of the amplification step, glasses are washed

with the supplied buffers, dried and mounted with cover slips using Duo Link mounting solution containing DAPI. Glasses were stored at -20 °C until analysis, performed with fluorescence microscopy Nikon Eclipse E1000. Protein interactions result easy detectable as a distinct bright spot (Duo Link datasheet).

Antibody	Host organism	Dilution	Source
EGFR	mouse	1:200	Abcam
cIAP1	rabbit	1:150	Cell Signaling
RAB7	rabbit	1:150	Cell Signaling
RAB11	rabbit	1:150	Cell Signaling

Table 4.4 - List of antibodies used for PLA.

4.16 Real-Time PCR

4.16.1 RNA extraction

For Real-time qPCR, total RNA was extracted from cells with the miRNeasy mini columns (Qiagen), following the manufacturer's instructions. Briefly, cells were harvested and washed once with PBS before being lysed in QIAzol and stored at -80 °C. To proceed with the RNA extraction, 140 µl of chloroform were added to each sample and after centrifugation (15 min at 13000 rpm at 4 °C), the aqueous, upper phase, was recovered in a new microcentrifuge tube and mix with 1.5 volumes of 100 % ethanol. Then, samples were loaded into RNeasy Mini columns thus allowing the RNA isolation exploiting the affinity with the column membrane. For this, columns were centrifuged and washed one time with the RWT buffer and, then, further two times with the RPE buffer, before being transferred to a new clean and sterile tube and added with 30 µl of RNase-free water to elute RNA. Following RNA extraction, the obtained RNA was quantified using the spectrophotometer NanoDrop 2000C

(Thermo Fisher Scientific). After quantification, 1 µg of RNA was subjected to electrophoresis (with 1 % agarose gel) to control the quality of the extracted RNA.

4.16.2 RNA reverse transcription

Transcriptor First Strand cDNA Synthesis Kit (Roche, Indianapolis, IN, USA) was used for the RNA reverse transcription to obtain and amplify cDNA in a single step. According to the manufacturer's instructions, a mix containing 1 µg RNA and 60 µM random examers was prepared and denatured at 65 °C for 10 min. After denaturation, a mix consisting in reaction buffer (containing 8 mM $MgCl_2$), protector RNase inhibitor (20 U), dNTPs mix (1 mM each) and Transcriptor Reverse Transcriptase (10 U) was prepared and added to each sample to reach 20 µl final volume.

The PCR program used was:

25 °C 10 min

50 °C 50 min

85 °C 5 min

Based on the RNA used and the volume of the reaction, the PCR products (cDNA) had a concentration of 50 ng/µl. cDNA was then stored at -20 °C until Real-Time PCR analysis.

4.16.3 Quantitative Real-Time PCR

The quantification of target gene mRNA was performed using Taqman standard curve method, which specifically amplified sequences encoding the gene of interest. Probes employed for this assay (Applied Biosystems- Thermo Fisher Scientific) had FAM as fluorescent dye in the 5' position and were conjugated to the quencher TAMRA at the 3'.

During the Real-Time PCR, gene targets are identified by specific probes and therefore amplified. The intensity of light released by the probe during this reaction is measured in real time and reflects the expression levels of the gene in the analysed sample. For each reaction the total volume was 20 µL of a mix containing 10 µl of TaqMan Universal PCR Mastermix (Applied Biosystems #4304437), 1 µl of probe (dual labelled), 4 µl of RNase-free water and 5µl of cDNA which is replaced with 5 µl of RNase-free water as a negative control (NTC). All standards, samples and negative controls were assayed in triplicate to ensure accurate results. PCR reaction was performed in 96-well plates (MicroAmp Fast Optical 96-Well Reaction Plate with Barcode, Applied Biosystems) covered with optical adhesive covers. The instrument used was ViiA™ 7 Real-Time PCR System (Applied Biosystems).

Real time PCR was performed with FAST running method:

Hold stage

Step 1: 95 °C 20 sec

PCR stage (40 cycles)

Step 1: 95 °C 1 sec

Step 2: 60 °C 20 sec

Melting curve stage

Step 1: 95 °C 15 sec

Step 2: 60 °C 60 sec

Step 3: 95 °C 15 sec (dissociation)

The threshold cycle (Ct Value) is the intensity of fluorescence considered statistically significant above the baseline values. Relative expression levels were calculated using the

comparative Ct method and calibrated relative to the reference gene. The probes listed in Table 4.5 were used for Real-Time PCR:

Taqman probe	Assay ID	Source
SNAI2	Hs00161904_m1	Applied Biosystems
NIK	Hs.PT.58.3867615	IDT
LRIG1	Hs01006152_m1	Applied Biosystems
EGFR	Hs01076090_m1	Applied Biosystems
ZEB1	Hs.PT.58.3948500	IDT
TWIST1	Hs.PT.58.18940950	IDT
E-Cadherin	Hs.PT.58.3324071	IDT
Vimentin	Hs.PT.58.38906895	IDT
MMP9	Hs.PT.58.22814824.g	IDT
GAPDH	Hs02786624_g1	Applied Biosystems

Table 4.5 - List of Taqman probes used for Real-Time PCR.

4.17 Statistical and image analysis

Graph and statistical analyses were performed using GraphPad Prism 5.02. For analysis of *in vivo* data two-tailed unpaired Student's t-test was applied. Real-Time PCR data were analysed using two-tailed paired Student's t-test with the date of the experiment as pairing factor. A p-value < 0.05 was considered statistically significant. Western blot densitometric analysis was performed with ImageQuant 5.2. GEP analysis was performed as previously described (Paragraph 4.6).

5 RESULTS

5.1 SM83-mediated cIAP1 depletion reduces the metastatic potential of TNBCs

5.1.1 In vivo activity of SM83 on tumour growth

The overall effect of IAP-depletion on cancer growth was investigated employing NOD/SCID mice subcutaneously engrafted with the TNBC cell line MDA-MB231. As shown in the experimental design (Figure 5.1A), when primary tumours became evident (13 days after the inoculum), animals were treated with intraperitoneal (ip) injections of SM83 (5 mg/Kg) until the end of the experiment (30 days). Notably, MDA-MB231 subcutaneous tumour volumes were reduced more than 50 % (Figure 5.1B) in SM83 treated mice compared to untreated mice, indicating an effective anti-tumour effect of SM83 administration.

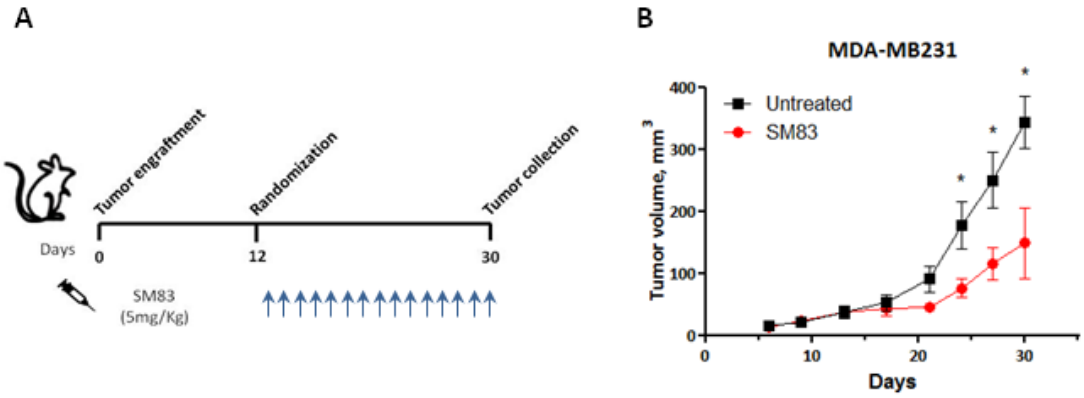

Figure 5. 1 - SM83 inhibits the primary tumour growth of human breast cancers in xenograft models. (A) Experimental design. (B) NOD/SCID mice engrafted subcutaneously with $5x10^6$ MDA-MB231 cells were ip injected with SM83 (5 mg/Kg, 5 times/week for 3 weeks) or left untreated (4 mice/group) until the end of the experiment. (Significant differences in days 24, 27 and 30. P = 0.0476, 0.0391 and 0.0344, respectively. Unpaired two-tailed t test).

Aiming to evaluate the levels of SM83 targets, MDA-MB231 nodules were collected 6 h after the last SM83 injection and protein lysates were tested by western blot. As expected, SM83 administration triggers the self-ubiquitination and proteasomal degradation of cIAP1 and cIAP2, resulting in a strong reduction of cIAP1 and cIAP2 protein levels (Figure 5.2A). The treatment also affected XIAP levels and this effect is likely to be a consequence of cIAP1 down-regulation rather than being a direct effect of SM83 treatment. In fact, the silencing of cIAP1 was sufficient to induce XIAP down-regulation in MDA-MB231 cells (Figure 5.2B). Western blots failed to detect any sign of activated apoptosis (Figure 5.2C).

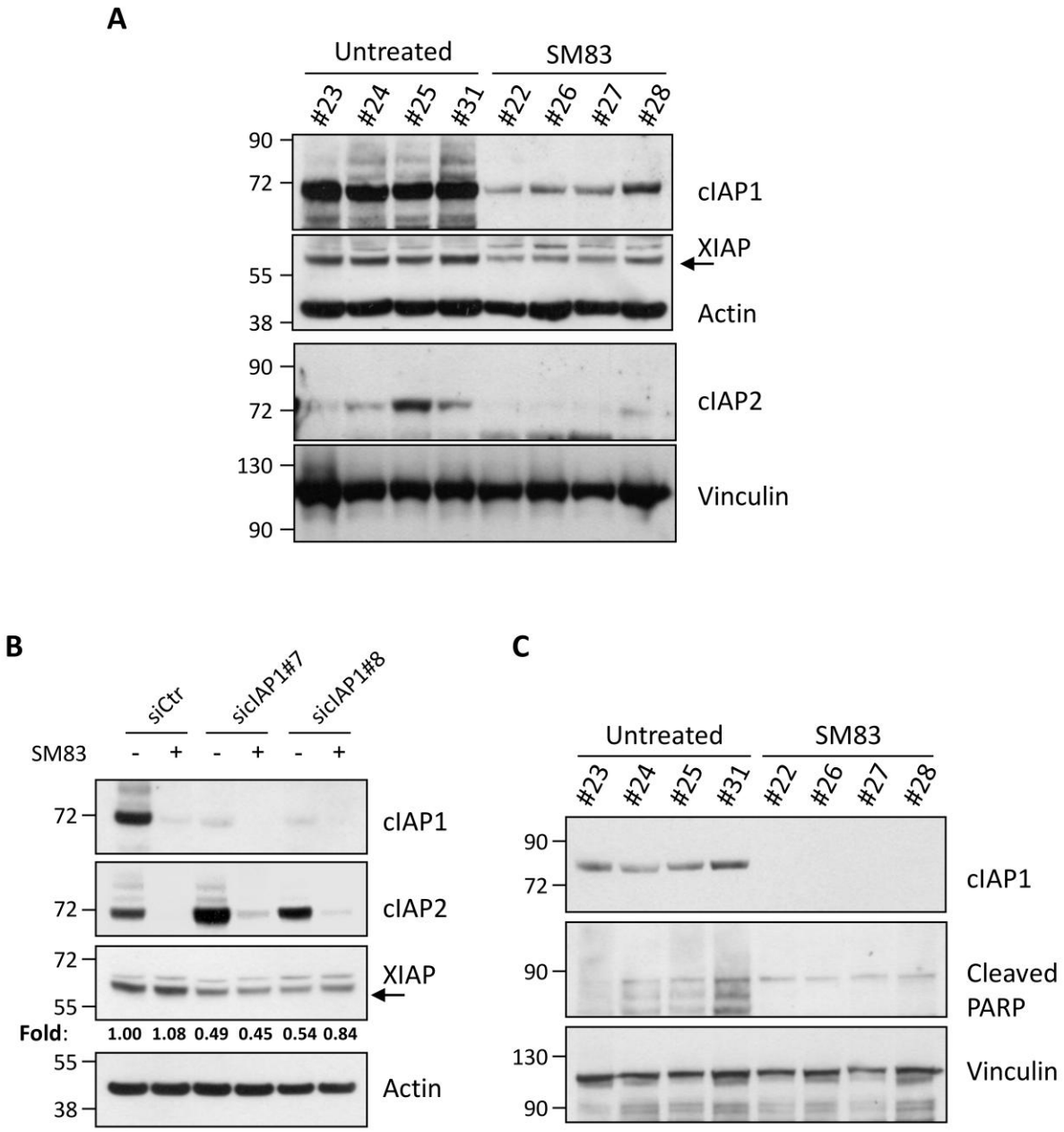

Figure 5.2 - cIAP1, cIAP2 and XIAP are reduced by SM83 treatment. (A) MDA-MB231 nodules were collected 6 h after the last injection and analysed by western blot. (B) MDA-MB231 cells were transfected *in vitro* with two siRNAs specific for cIAP1 and treated with 100 nM SM83 for 1 h. A reduction of cIAP1, cIAP2 and XIAP levels was assessed by western blot performed 72 h after transfection. Values show the fold levels of XIAP. (C) No sign of apoptosis (cleaved PARP) was detectable in MDA-MB231 primary tumours. Actin or Vinculin are shown as loading controls.

5.2 SM83 treatment reduces spontaneous lung metastasis in NOD/SCID mice xenografted with MDA-MB231 cells

Since it has been shown that IAP can play a role in migration and invasion (Fulda, 2014c), I hypothesised that SM83 could affect the metastatic process. In order to answer this question, NOD/SCID mice subcutaneously engrafted with MDA-MB231 cells were treated for three weeks with SM83 and then lungs were collected after further two weeks (Figure 5.3A). To investigate the SM83 effect on tumours and metastatic sites, at the end of the experiment, primary tumours, lymph nodes and lungs were collected and either lysed for RNA extraction and biochemical analysis, or paraffin-embedded for IHC. First, a delay of primary tumour growth was assessed after SM83 injection (Figure 5.3B), in accordance to my previous observation (Figure 5.1B). The inhibitory effect of SM83 on the growth of primary tumours was confirmed also employing intravenous (iv) injections. As shown in Figure 5.3B, the administration route (ip *vs* iv) did not influence drug efficacy and, moreover, the primary tumours of treated mice started growing as well as the untreated ones after the interruption of the injections. Importantly, a significant reduction in the number and size of lung metastasis was found in SM83 treated mice bearing MDA-MB231 tumours, which are known to spontaneously metastasize to lungs in NOD/SCID mice (Minn *et al.*, 2005; Figure 5.3A-B).

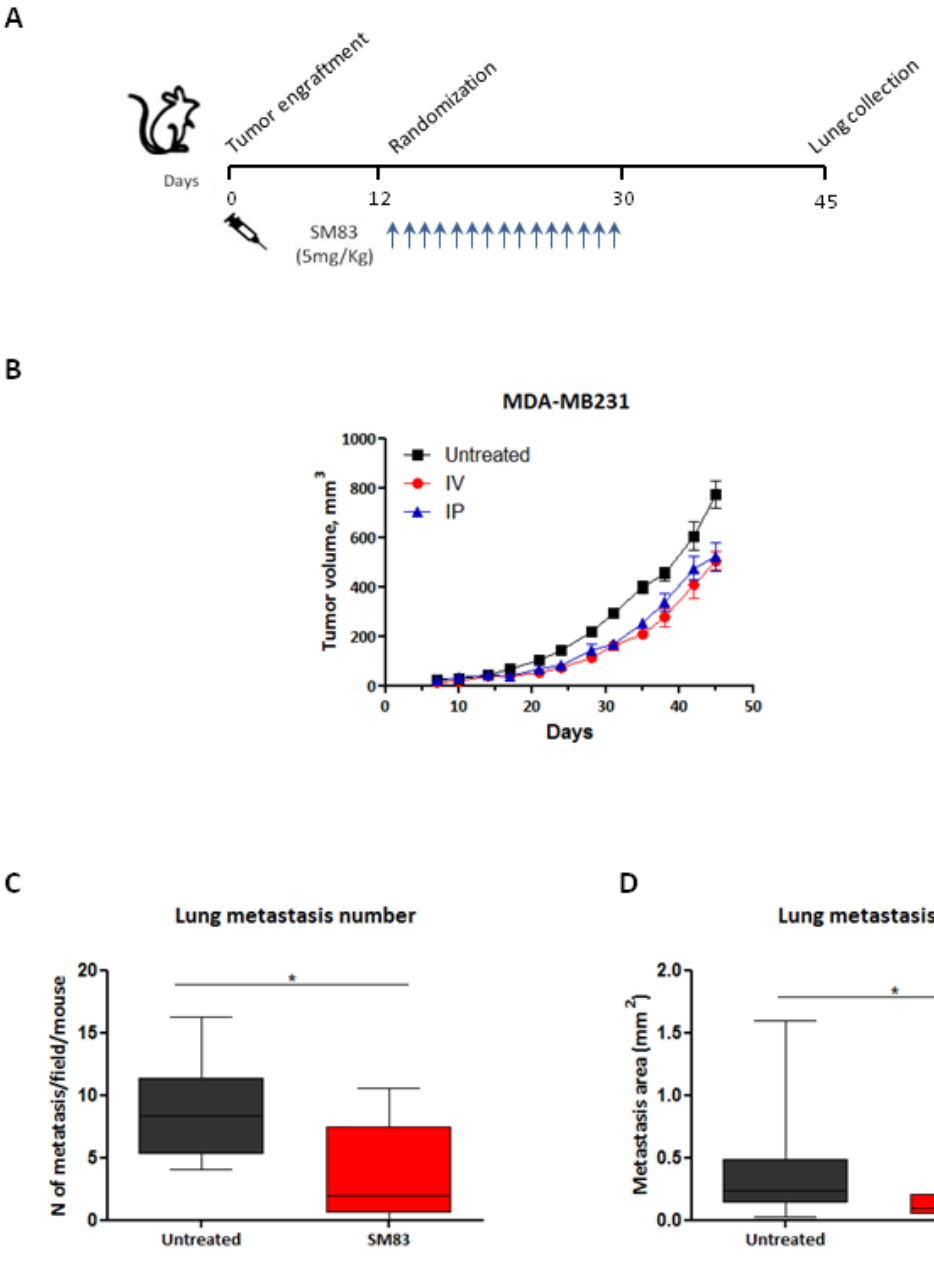

Figure 5.3 - Treatment with SM83 affects metastasis formation in NOD/SCID mice engrafted with the highly metastatic MDA-MB231 cell line. (A) Experimental design. (B) NOD/SCID mice were engrafted subcutaneously with MDA-MB231 cells and, after two weeks, were treated for 3 weeks with ip and iv injections of SM83 (5 mg/Kg, 5 times/week) in two independent experiments. Mice were killed 2 weeks after the last injection. Graph shows tumour volumes. (C) Number (untreated n = 7, SM83-treated mice n = 8; sum of two independent

experiments shown in Figure 5.1B and 5.3B; P = 0.0238. Unpaired two-tailed t test) and (D) size (35 metastases/group; P = 0.0107. Unpaired two-tailed t test) of spontaneous MDA-MB231 lung metastases.

Notably, the anti-metastatic effect was evident independently from the administration routes, i.e. iv and ip injections. Detection of micro- and macro-metastasis was allowed by the high expression of human Vimentin of MDA-MB231 (Figures 5.4A-C).

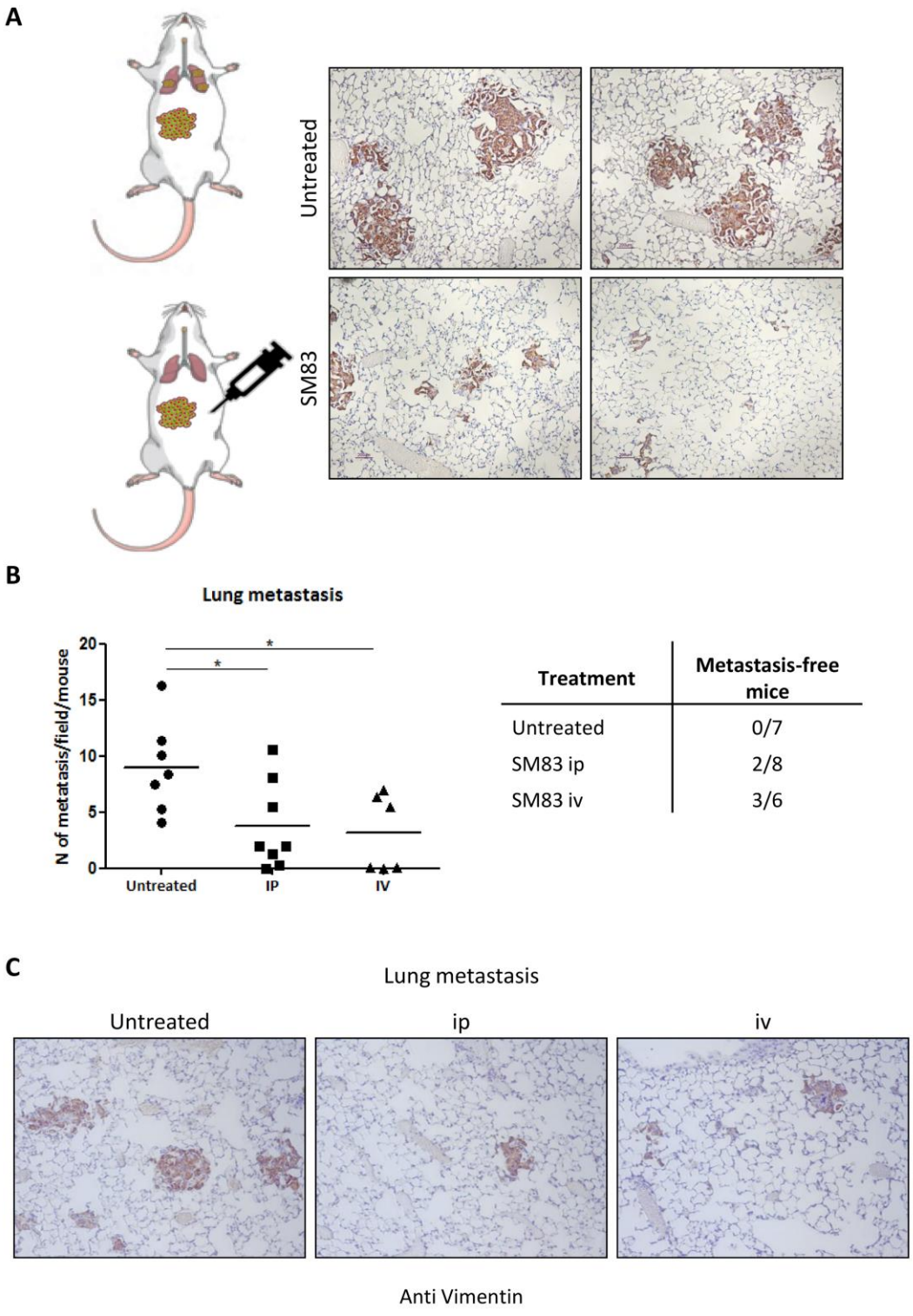

Figure 5.4 - SM83 treatment displays anti-metastasis activity independently from the administration route. (A) Lungs of NOD/SCID mice bearing MDA-MB231 tumours were collected 2 weeks after the last injection with SM83, formalin-fixed and paraffin-embedded. IHC of lungs with anti-human Vimentin antibody. (B) The graph

shows the number of lung metastases (Untreated *vs* ip P = 0.0238, Untreated *vs* iv P = 0.0190, ip *vs* iv not significant; Unpaired two-tailed t test), whereas the table shows the metastasis-free MDA-MB231-bearing mice. (C) SM83 injections (5 mg/Kg, 5 times/week) were performed ip and iv in two independent experiments. Lungs were collected from NOD/SCID mice xenografted with MDA-MB231 cells and metastasis were detected through anti-Vimentin staining in IHC.

5.3 SM83 treatment perturbs gene expression of MDA-MB231 tumours

Having found a significant reduction of MDA-MB231 spontaneous lung metastasis in mice treated with SM83, I hypothesised that IAP targeting could perturb the expression of genes responsible for the metastatic process. To test this hypothesis, MDA-MB231 nodules were collected 6 h after the last SM83 injection and profiled for gene expression (Figure 5.5). Interestingly, 65 genes were significantly modulated by SM83 treatment and, among them, 50 genes resulted up-regulated and 15 down-regulated, as compared to tumours collected from untreated mice. IAPs are known to be apical modulators of several receptor complexes and eventually control MAPK and NF-kB signalling pathways. Accordingly, the expression of a number of genes involved in the NF-kB signalling pathway (e.g. baculoviral IAP repeat containing 3/BIRC3, matrix metallopeptidase-9/MMP9, intercellular adhesion molecule 1/ICAM1) or NF-kB targets (e.g. TRAF1, TRAF2, NFKBIA, NFKB2, RelB) were indeed altered.

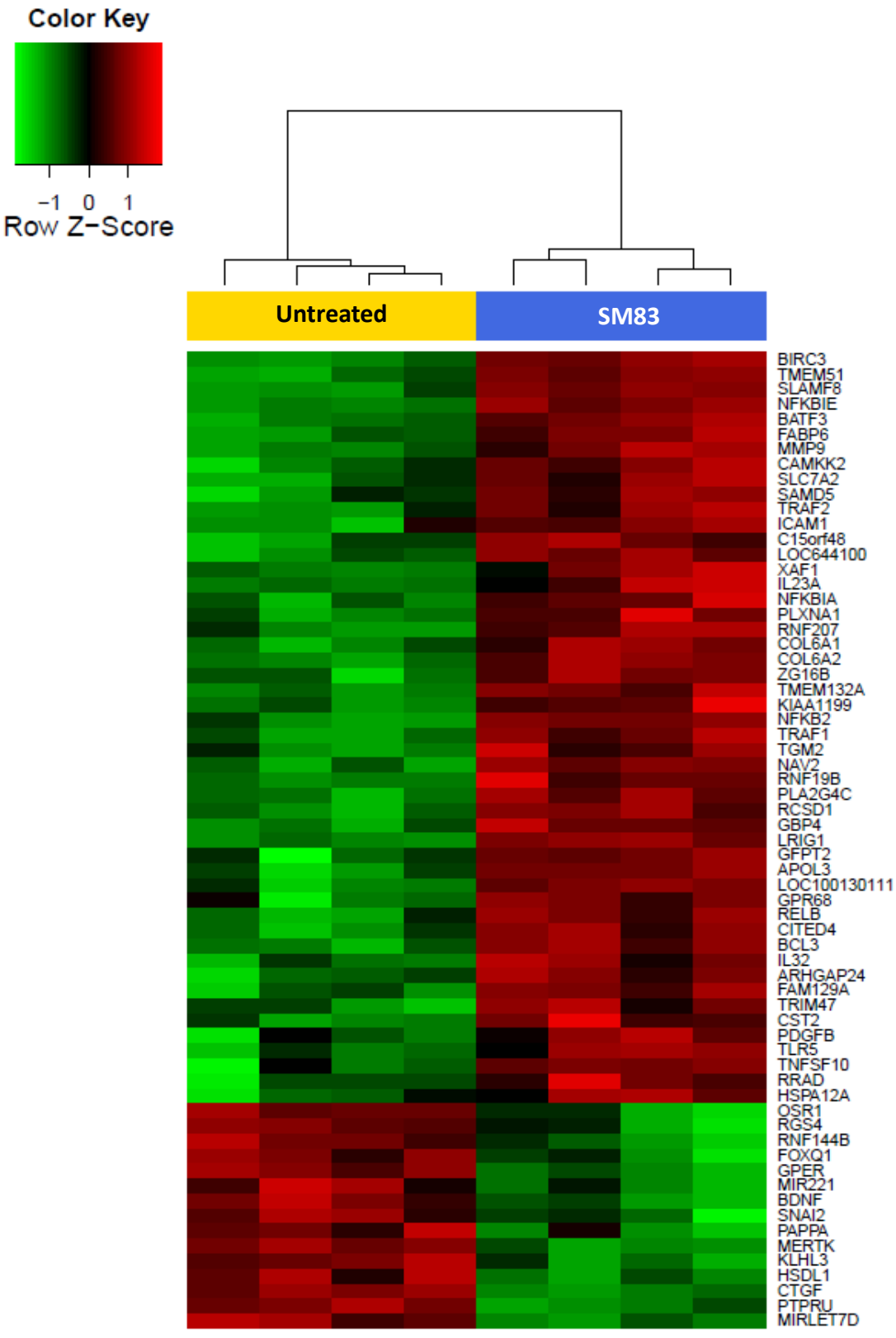
Color Key
−1 0 1
Row Z−Score
Untreated
SM83
BIRC3
TMEM51
SLAMF8
NFKBIE
BATF3
FABP6
MMP9
CAMKK2
SLC7A2
SAMD5
TRAF2
ICAM1
C15orf48
LOC644100
XAF1
IL23A
NFKBIA
PLXNA1
RNF207
COL6A1
COL6A2
ZG16B
TMEM132A
KIAA1199
NFKB2
TRAF1
TGM2
NAV2
RNF19B
PLA2G4C
RCSD1
GBP4
LRIG1
GFPT2
APOL3
LOC100130111
GPR68
RELB
CITED4
BCL3
IL32
ARHGAP24
FAM129A
TRIM47
CST2
PDGFB
TLR5
TNFSF10
RRAD
HSPA12A
OSR1
RGS4
RNF144B
FOXQ1
GPER
MIR221
BDNF
SNAI2
PAPPA
MERTK
KLHL3
HSDL1
CTGF
PTPRU
MIRLET7D

Figure 5.5 - SM83 administration perturbs the gene expression of MDA-MB231 primary tumours. MDA-MB231 primary tumours were subjected to microarray analysis. Heat map shows the expression levels of the 65 genes significantly modulated by SM83 injection compared to the control (expression values are in log2 scale. Red indicates higher expression; green lower expression).

In order to select the genes whose down-regulation could be responsible for the SM83-mediated anti-metastatic effect, each down-regulated gene was individually knocked-down in MDA-MB231 cells and wound healing assay was performed (Figure 5.6A). Importantly, I found that the depletion of SNAI2 was the most effective in reducing the capability of cells to migrate (Figure 5.6B), whereas the viability was only slightly affected (Figure 5.6C).

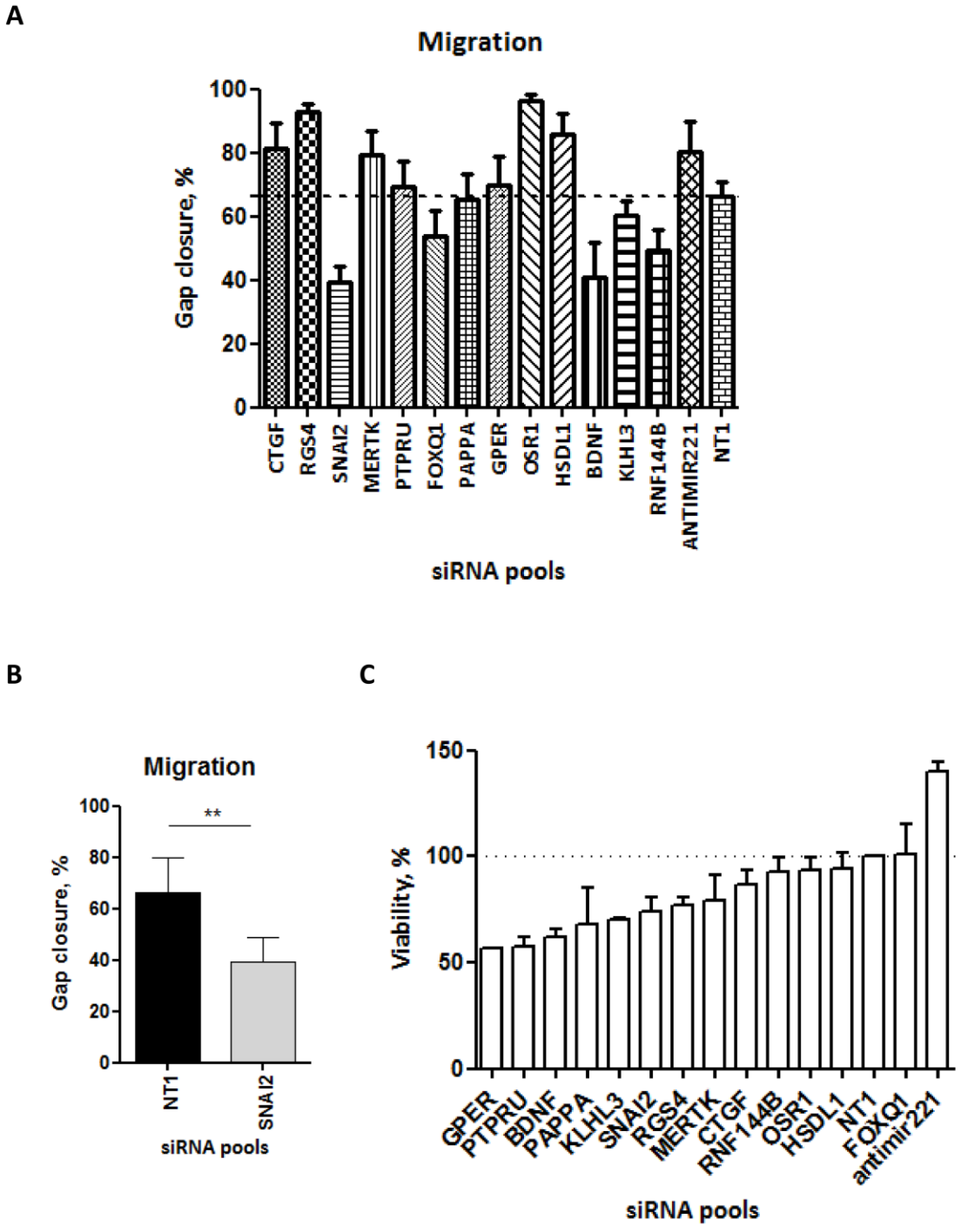

Figure 5.6 - Loss of SNAI2 reduces MDA-MB231 cell motility. (A) The 15 genes down-regulated in subcutaneous MDA-MB231 nodules upon treatment with SM83 were individually silenced in MDA-MB231 cells. To assess cell motility, $4x10^4$ cells were seeded in Ibidi chambers and cultured overnight to perform wound-healing experiments. After the removal of the insert, images were acquired every hour in a Cell-IQ instrument and analysed with the integrated software. Graphs represent the percentage of gap closure after 24 h of migration

and show the average of at least four independent experiments. (B) The graph shows the same experiment illustrated in Figure 5.6A, but focused on the effect of SNAI2 depletion. The percentage of gap closure was calculated after 24 h of migration for MDA-MB231 cells transfected with control (NT1) or SNAI2-specific siRNAs. (n = 4, P = 0.0033, Unpaired two-tailed t test). (C) MDA-MB231 cells transfected in the same way were also seeded in 96-well plates and viability assessed by CellTiter-Glo assay, 5 days after transfection.

Since GEP analysis revealed that SM83 administration down-regulates SNAI2, its protein level was detected in primary tumours collected from mice treated with SM83 or left untreated (Figure 5.7A). Western blot analysis confirmed the strong reduction of SNAI2 protein in primary tumours treated by SM83. Of note, LRIG1, an ubiquitin-ligase which is known to be induced by SM administration and that I found up-regulated in GEP, showed an opposite regulation by SM83 compared to SNAI2 (Figures 5.7A-B).

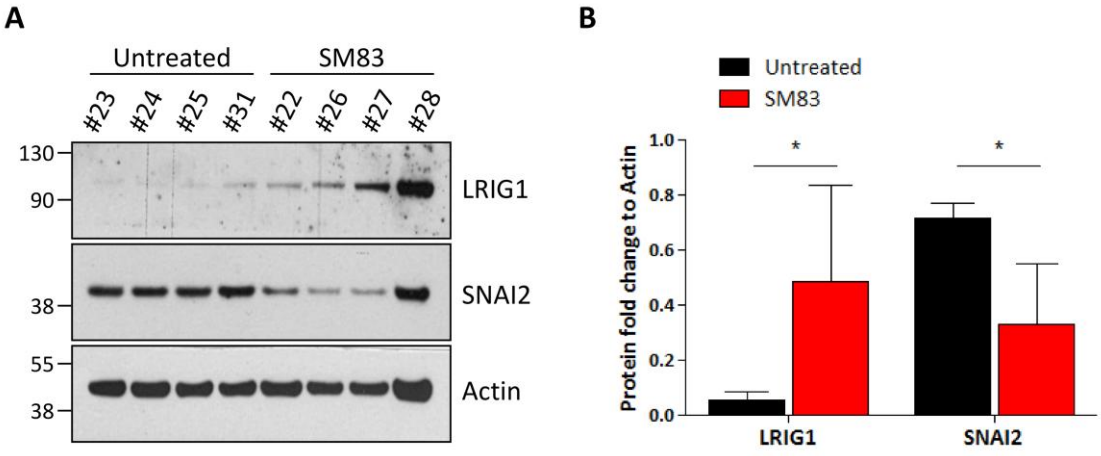

Figure 5.7 - SM83 treatment down-regulates SNAI2 and up-regulates LRIG1 levels *in vivo*. (A) The levels of SNAI2, down-regulated in GEP (Figure 5.5), and the up-regulation of LRIG1, were assessed by western blot performed on MDA-MB231 nodules. (B) The graph shows the fold levels of SNAI2 and LRIG1 measured by densitometric analysis of western blot and normalized to Actin levels. LRIG1: Untreated *vs* SM83 P = 0.046; SNAI2: Untreated *vs* SM83 P = 0.0143; Unpaired two-tailed t test.

5.4 cIAP1, but neither cIAP2 nor XIAP, controls SNAI2 expression

As SM83 targets different IAPs, I studied which one was responsible for SNAI2 down-regulation. To this end, I silenced cIAP1, cIAP2 and XIAP through siRNAs and I found that cIAP1, and not cIAP2 or XIAP depletion, was sufficient to reduce SNAI2 levels both in MDA-MB231 and BT549 cell lines (Figure 5.8A). Then, to further address these results, two different siRNAs targeting cIAP1 were employed in a panel of TNBC cell lines (MDA-MB231, BT549, MDA-MB157 and SUM159) showing a widely valid regulation of SNAI2 mediated by this IAP (Figure 5.8B). Taken together these results show that cIAP1 is responsible for sustaining the expression of the pro-metastastatic gene SNAI2.

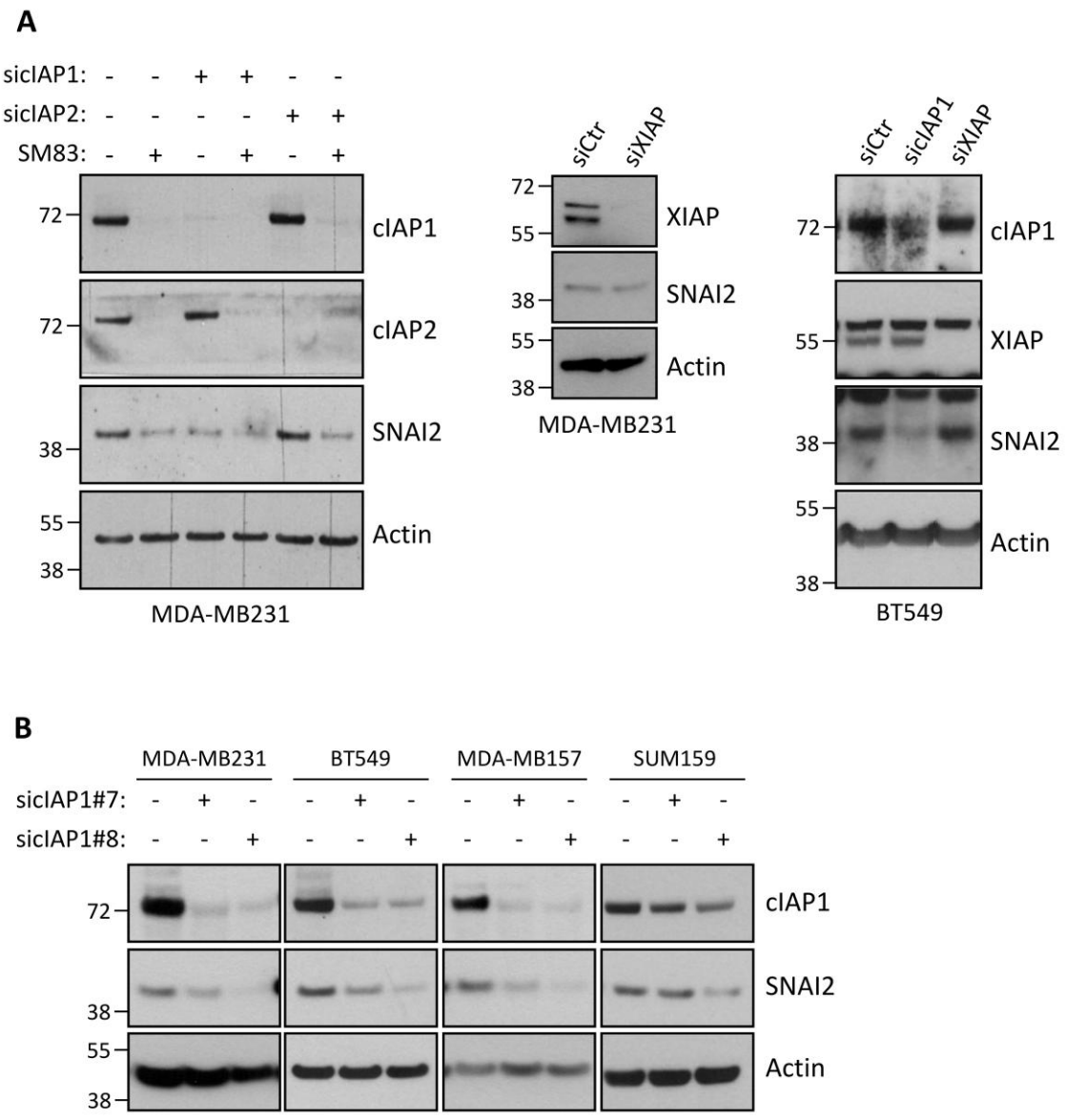

Figure 5.8 - cIAP1 is the sole SM target responsible for supporting SNAI2 expression. (A) SNAI2 levels were detected by western blot in MDA-MB231 cells transfected with siRNAs targeting cIAP1, cIAP2 or XIAP, and in BT549 cells silenced for cIAP1 or XIAP. After 72 h, cells were treated for further 6 h with 100 nM SM83. (B) SNAI2 protein levels were detected in MDA-MB231, BT549, MDA-MB157 and SUM159 cells knocked-down for cIAP1 using two different siRNAs.

Since SM83 killed a small percentage of cancer cells when administered in monotherapy, I checked if SNAI2 down-regulation was a consequence of SM83-related toxicity. Therefore, viability test was performed treating the same panel of TNBC cell lines

described above (Figure 5.8B) with 200 nM SM83, thus finding that MDA-MB231 and BT549 cells were sensitive to the treatment (Figure 5.9A). Nonetheless, SNAI2 down-regulation occurred even when cells were treated with half of the SM83 dose and also after pre-treatment with inhibitors of apoptosis (z-VAD) and necroptosis (Nec-1; Figures 5.9B-C). Accordingly, I concluded that SNAI2 reduction is dependent on cIAP1 targeting and is not a side effect of SM83 toxicity.

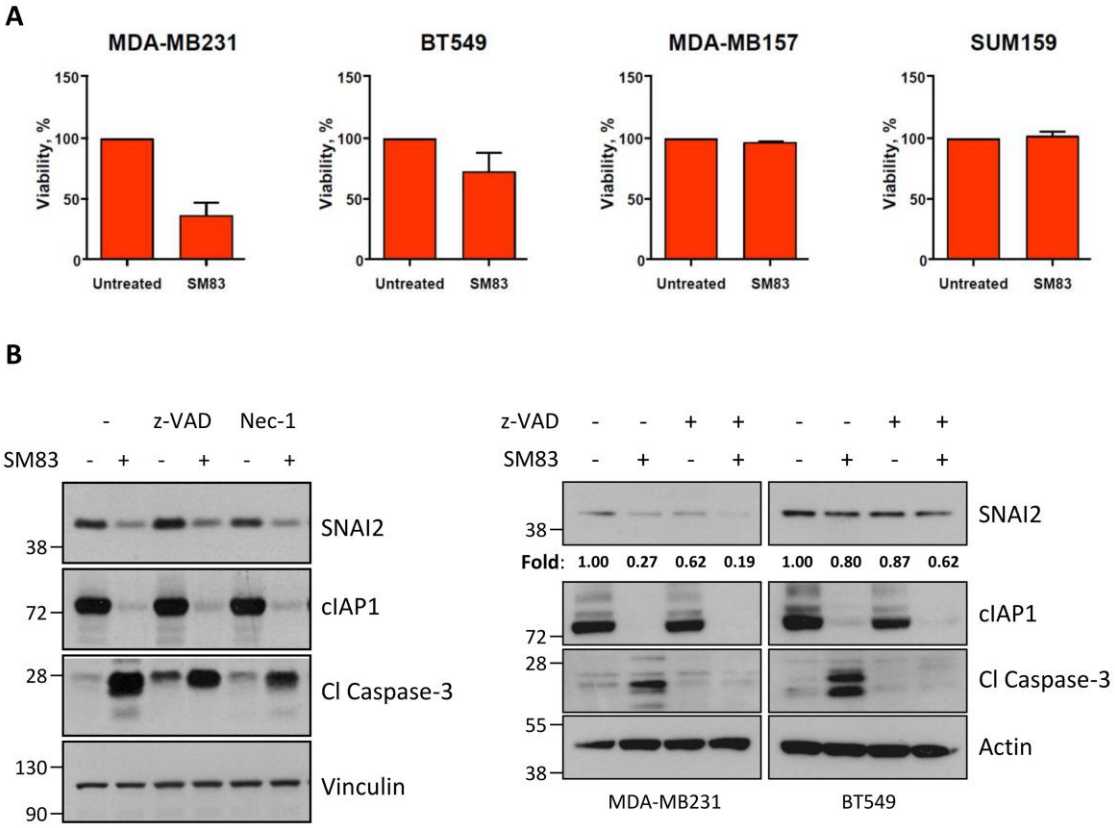

Figure 5.9 - SNAI2 down-regulation is not a side effect of SM83 toxicity. (A) Cell viability was tested by CellTiter-Glo in the same cell lines employed in Figure 5.8B. Cells were treated with 200 nM SM83 and viability was assessed 24 h later. (B) MDA-MB231 cells were treated with half of the dose of SM83 (100 nM) employed in Figure 5.9A and, pre-treated or not for 1 h with caspase inhibitor z-VAD or RIP1 inhibitor Nec-1 (left panel). The treatment with z-VAD was performed also in BT549 cells (right panel). Western blot was performed to

detect the total levels of SNAI2 and cIAP1, and the cleaved form of Caspase-3. Values show the fold levels of SNAI2 relative to untreated cells.

5.5 SM83 dependent activation of the non-canonical NF-kB pathway correlates with SNAI2 down-regulation

These findings suggest that SM83 anti-metastasis effect could occur via the down-regulation of SNAI2. However, specific effectors directly involved in the cIAP1/SNAI2 axis have not been identified yet. Notoriously, cIAPs are components of several receptor complexes as the TNF-R superfamily, and allow the subsequent activation of TNF-R down-stream pathways. Therefore, I investigated the underlying mechanisms through which cIAPs, particularly cIAP1, could promote SNAI2 expression focusing on the TNF-dependent activation of NF-kB and MAPK signalling pathways.

5.5.1 TNF-R2, but not TNF-R1, is responsible for SNAI2 expression

To assess if the activity of TNF-Rs promotes SNAI2 expression, the endogenous ligand TNF and its receptors, TNF-R1 and 2, were knocked-down through specific siRNAs in MDA-MB231 and BT549 cell lines. Western blot analysis revealed that in both cell lines a strong down-regulation of SNAI2 occurred after TNF and TNF-R2 depletion, while TNF-R1 seems to play only a marginal role in SNAI2 expression (Figure 5.10).

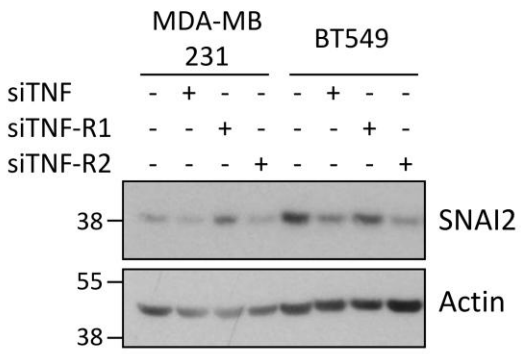

Figure 5.10 - Depletion of TNF-R2 affects SNAI2 expression. MDA-MB231 and BT549 cells were transfected with siRNAs targeting TNF, TNF-R1 and TNF-R2. Cells were harvested 72 h after transfection and western blot was performed to detect SNAI2 levels. Actin is shown as a loading control.

Consequently, to investigate the mechanisms through which cIAP1 promotes SNAI2 expression, I examined the role of the non-canonical NF-kB pathway whose activation is thought to be triggered by SM-mediated IAP depletion (Gyrd-Hansen and Meier, 2010). Therefore, MDA-MB231 cells were treated with SM83 for 6 h after being knocked-down for different NF-kB-related effectors (Figure 5.11A). In accordance to my previous findings, SNAI2 levels were reduced by the treatment, while protein stability was increased by NIK and NF-kB2 depletion upon SM83 treatment, thereby suggesting the non-canonical NF-kB pathway as a possible suppressor of SNAI2. To detail the role of cIAP1 in the regulation of the non-canonical NF-kB pathway, Real-Time PCR was performed in two different TNBC cell lines, MDA-MB231 and BT549. In both cases, cIAP1 depletion enhanced *NIK* mRNA, indicating that this IAP not only reduces the protein stability mediating ubiquitination of NIK (Zarnegar *et al.*, 2008), but also inhibits its expression (Figure 5.11B), thus preventing the activation of the non-canonical NF-kB pathway.

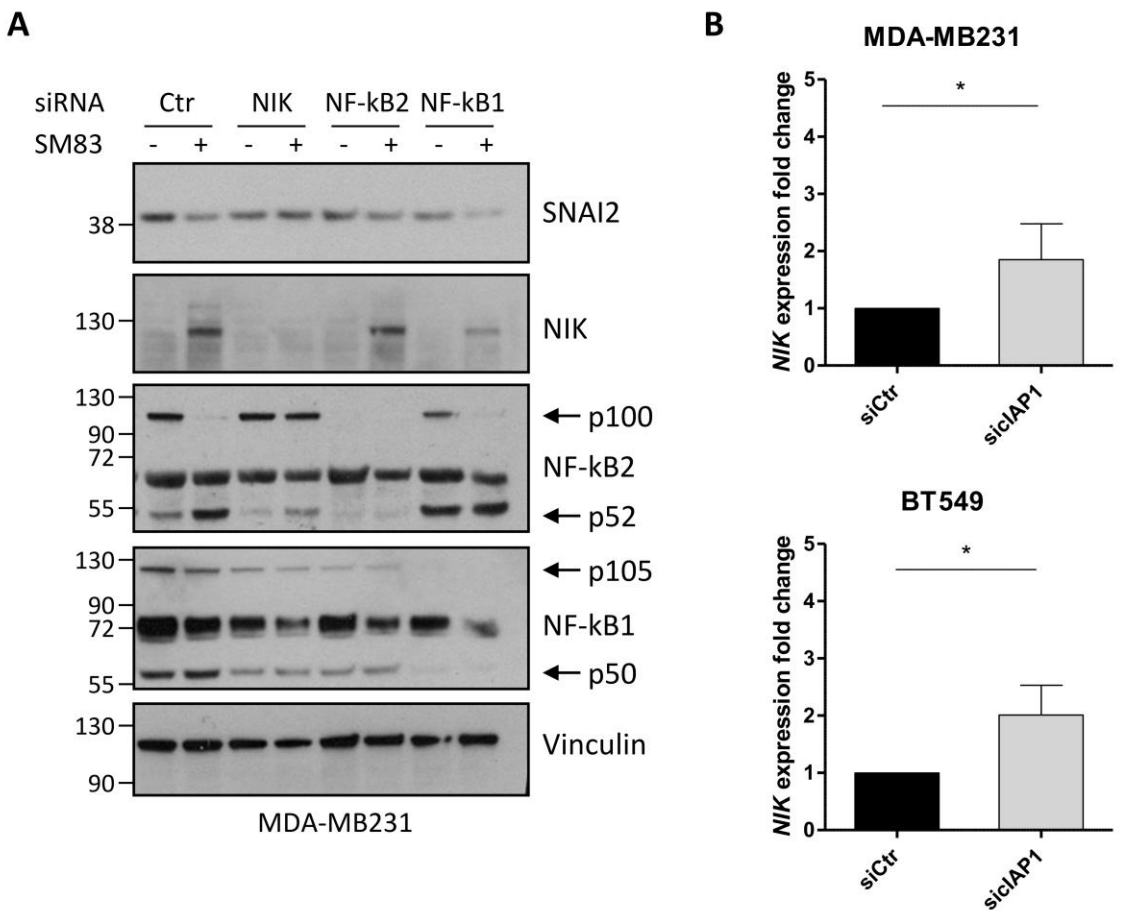

Figure 5.11 - cIAP1 depletion induces NIK and consequently non-canonical NF-kB pathway. (A) Several mediators and regulators of the NF-kB pathway were knocked-down using specific siRNAs in MDA-MB231 cells. After 72 h, cells were treated with 100 nM SM83 for 6 h and harvested. Western blot shows that the depletion of NIK and NF-kB2 prevented the non-canonical NF-kB activation and blocked SM83-mediated SNAI2 down-regulation. Vinculin is shown as a loading control. (B) Real-Time PCR was performed in MDA-MB231 and BT549 cells transiently silenced for cIAP1. *NIK* mRNA was evaluated as fold expression change relative to *GAPDH*, in cells depleted for cIAP1 compared to controls. MDA-MB231 P = 0.0464; n = 4 siCtr *vs* sicIAP1; Paired two-tailed t test. BT549: P = 0.0487; n = 4 siCtr *vs* sicIAP1; Paired two-tailed t test.

Indeed, time-course experiments performed in MDA-MB231 cells treated with SM83 at different time-points confirmed the negative correlation between SNAI2 expression and NF-kB2 activation (Figure 5.12A). This result was also observed in TNBC primary tumours

from The Cancer Genome Atlas (TCGA; Figure 5.12B). MDA-MB231 cells were also stimulated by TWEAK, a ligand of the TNF family, which preferentially activates the non-canonical NF-kB pathway. As shown in Figure 5.12C, the activation of the non-canonical NF-kB pathway seems to be followed by SNAI2 down-regulation, leading me to hypothesise a possible inhibition of SNAI2 mediated by this pathway.

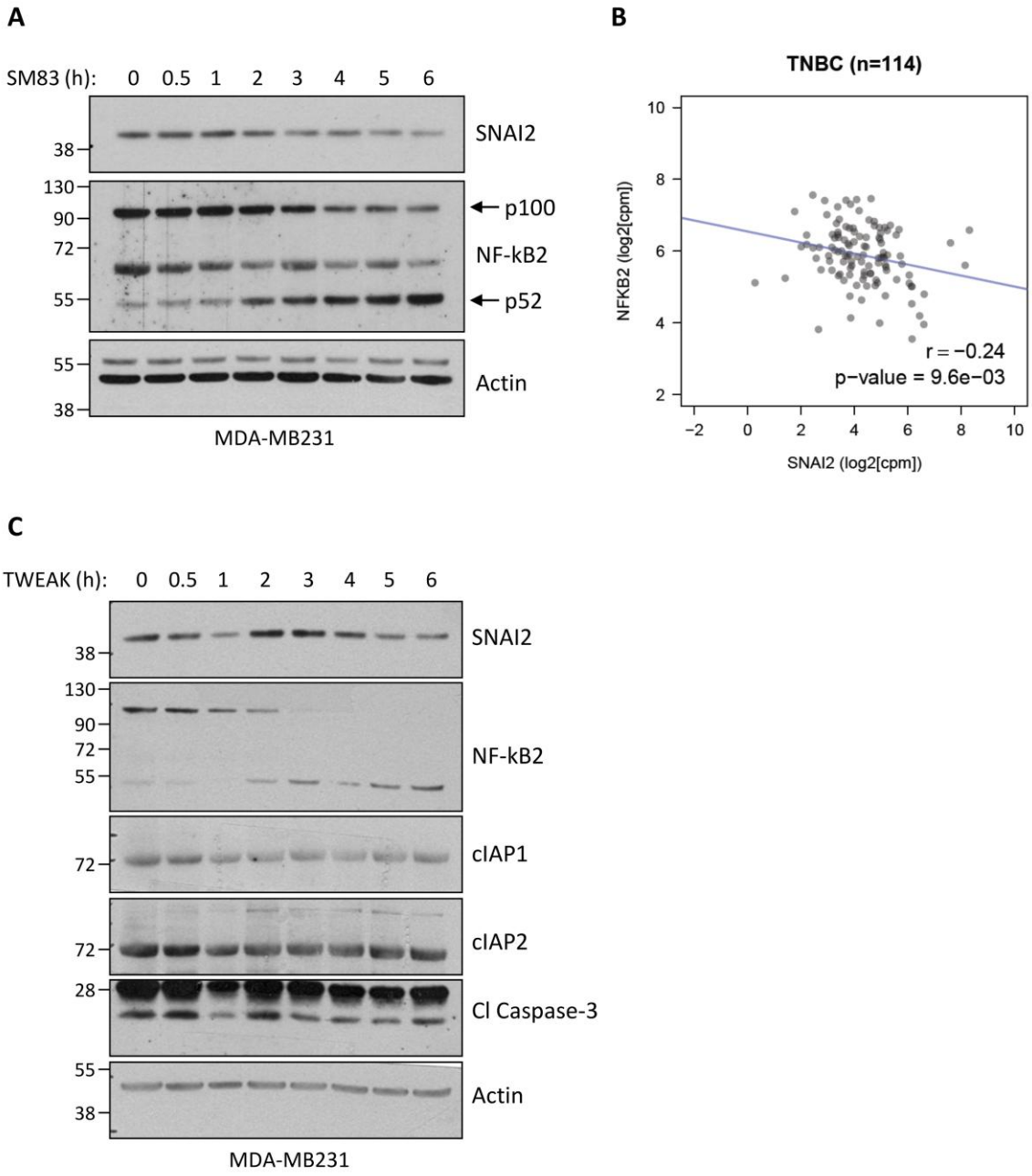

Figure 5.12 - SNAI2 down-regulation correlates with the activation of the non-canonical NF-kB pathway. (A) Time-course experiments performed in MDA-MB231 cells showing the reduction of SNAI2 after 100 nM SM83 administration, along with the activation of the non-canonical NF-kB. Actin is shown as a loading control. (B) NF-kB2, which recapitulates the activation of non-canonical NF-kB pathway, negatively correlates with SNAI2 expression levels in TNBC patients from TCGA dataset (Pearson's correlation: -0.24; p-value: 9.6e-03). Expression values are expressed as log2 counts per million transcripts. (C) Time-course experiment was performed in MDA-MB231 cell line treated with 200 ng/ml TWEAK, a specific ligand for the non-canonical NF-kB pathway activation.

However, the silencing of NF-kB2 (Figures 5.11A-5.13) by itself did not result in the expected increase of SNAI2, leading me to investigate the involvement of other pathways in SNAI2 regulation. Hence, I focused on the role of MAPKs to establish if cIAP1 supports SNAI2 expression mediating the regulation of these signalling pathways.

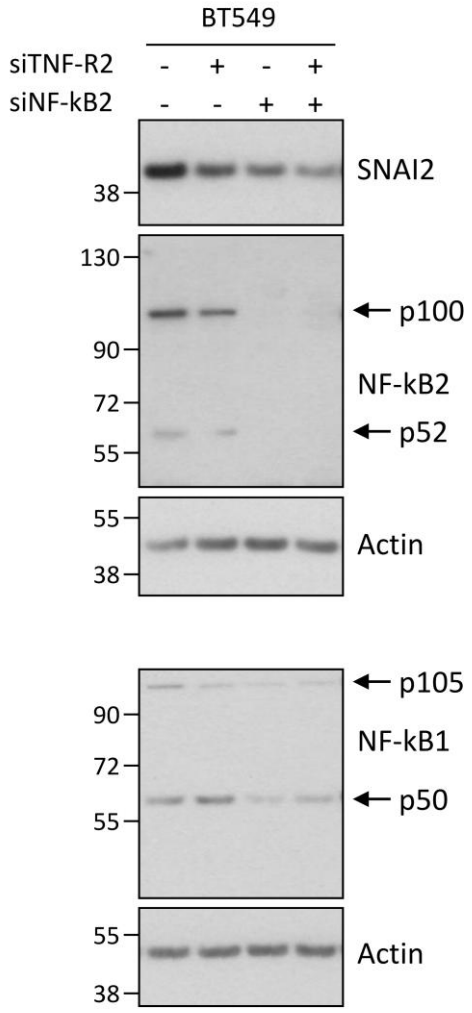

Figure 5.13 - The targeting of NF-kB2 does not increase SNAI2 levels. Western blot was performed to detect SNAI2 levels in BT549 cells transfected with siRNAs targeting TNF-R2 and NF-kB2. Actin is shown as a loading control.

5.6 Loss of cIAP1 prevents SNAI2 accumulation through the inhibition of MEK signalling pathways

To identify which down-stream pathway is responsible for cIAP1-dependent expression of SNAI2, MDA-MB231, BT549 and MDA-MB157 cell lines were pre-treated for 2 h with LY294002, Triciribine, UO126 and SB203580, which target PI3K, AKT, MEK and p38 respectively. As shown in Figure 5.14A, the MEK inhibitor UO126 strongly reduced SNAI2

expression in all cell lines, and the same effect was obtained through the silencing of ERK1 and 2 (Figure 5.14B), thus confirming that MAPK effectors ERK1/2 regulate SNAI2. The Figure 5.14C shows that SM83 treatment decreased SNAI2 levels and also affected ERK phosphorylation. However, ERK activation did not appear to be dependent on TNF stimulation at these time-points.

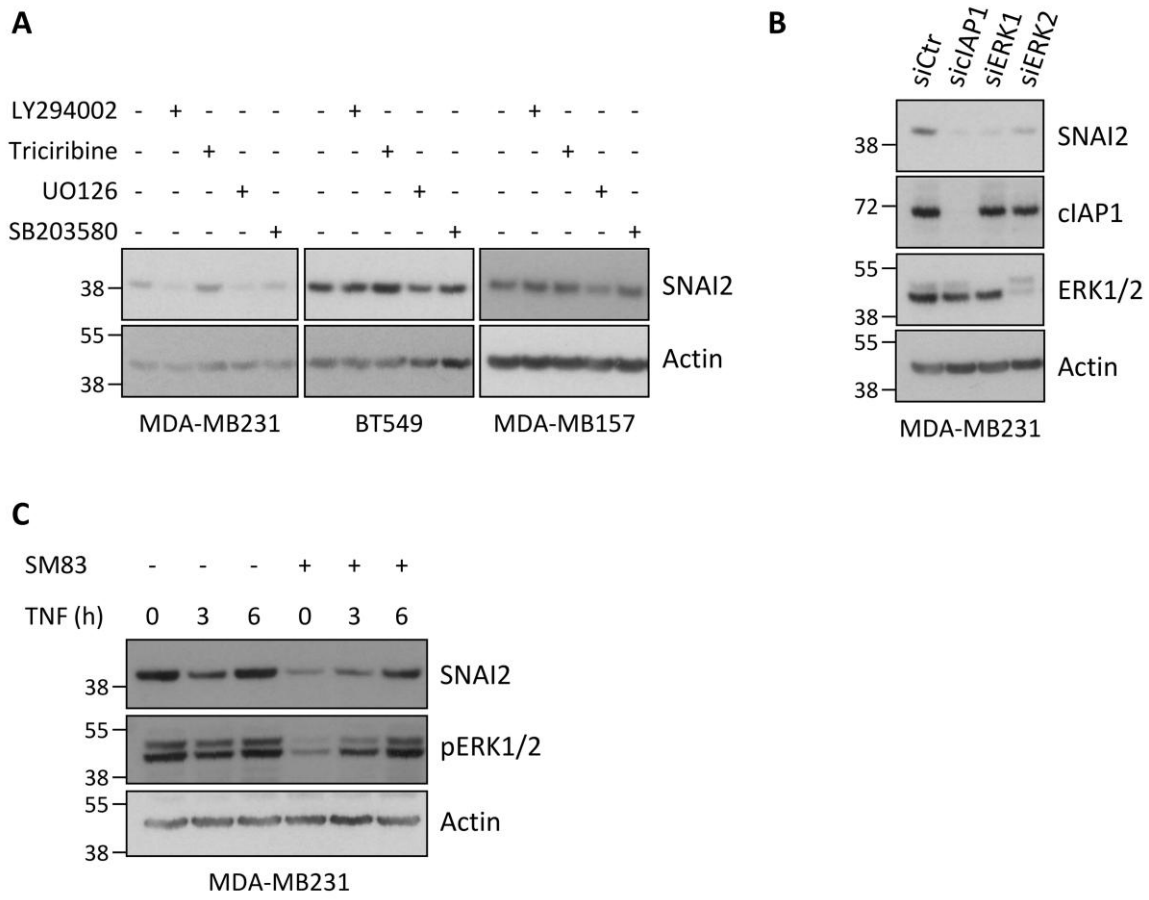

Figure 5.14 - SNAI2 expression is promoted by MAPK signalling pathway. (A) MDA-MB231, BT549 and MDA-MB157 cells were treated for 2 h with 10 µM inhibitor of PI3K (LY294002), AKT (Triciribine), MEK (UO126) and p38 (SB203580). SNAI2 levels were detected by western blot. (B) MDA-MB231 were transfected with siRNAs targeting cIAP1, ERK1 and ERK2 for 72 h. Western blot shows SNAI2 levels. cIAP1 and ERK1/2 are shown as transfection controls. (C) Time-course experiments were performed in MDA-MB231 cells pre-treated with 100

nM SM83 for 1 h and then stimulated with 50 ng/ml TNF, for different time-points. SNAI2 levels were detected together with pERK1/2. Actin is used as a loading control.

Moreover, when MDA-MB231 cells were stimulated with TNF 50 ng/ml for 15 min and 4 h (Figures 5.15A-B), SNAI2 levels did not change. Overall, these data suggest that, in this setting, TNF did not exert any significant effect on SNAI2 expression, which appeared to be induced by ERK activation. Therefore, I speculated that other exogenous stimuli could be involved.

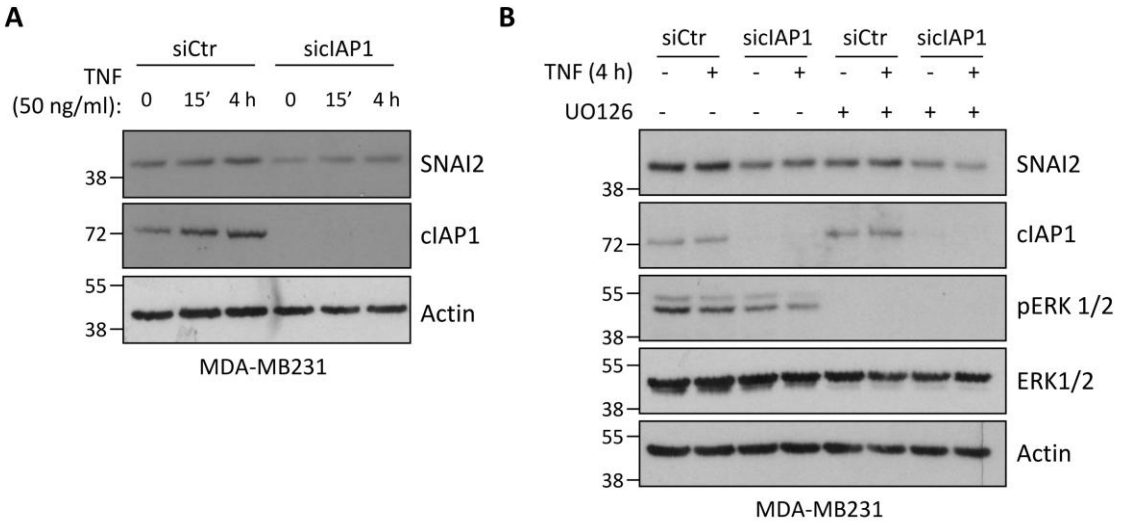

Figure 5.15 - ERK-mediated induction of SNAI2 is not dependent on TNF stimulation. (A) MDA-MB231 cells were transfected with siRNA targeting cIAP1 and, after 72 h, were treated with 50 ng/ml TNF, for 15 min and 4 h, and harvested. Western blot was performed to evaluate SNAI2 levels. (B) The MDA-MB231 cell line was silenced for cIAP1 and, 72 h after transfection, cells were pre-treated for 2 h with 10 µM inhibitor of MEK (UO126) and, then, stimulated with 50 ng/ml TNF for 4 h. Western blot shows the effect of ERK inhibition and/or TNF stimulation on SNAI2. Actin is shown as a loading control.

5.7 Targeting of cIAP1 affects the EGFR down-stream pathways thus inhibiting SNAI2 expression

5.7.1 SNAI2 expression is induced in response to EGFR activation

According to several studies showing that SNAI2 is expressed in an EGF-dependent manner (Lee *et al.*, 2008; Kusewitt *et al.*, 2009), I observed a correlation between EGFR and SNAI2 expression in breast cancer patients from TCGA (Figure 5.16A). Moreover, in a gene expression dataset of breast cancer cell lines (Heiser *et al.*, 2012), I noticed a significant up-regulation of SNAI2 and EGFR in TNBC cells compared to Luminal ones (Figure 5.16B). Based on these observations, SNAI2 levels were detected by western blotting in a panel of breast cancer cell lines and the highest expression of this pro-metastatic factor was found in TNBC cell lines: MDA-MB231, MDA-MB157, SUM159, BT549 and HCC1937 (Figure 5.16C). Finally, wound-healing assay showed that the TNBC cells MDA-MB231, BT549 and HCC1937 migrated faster than the Luminal T47D (Figure 5.16D), thus suggesting that high levels of SNAI2 promotes cell motility and tumour aggressiveness.

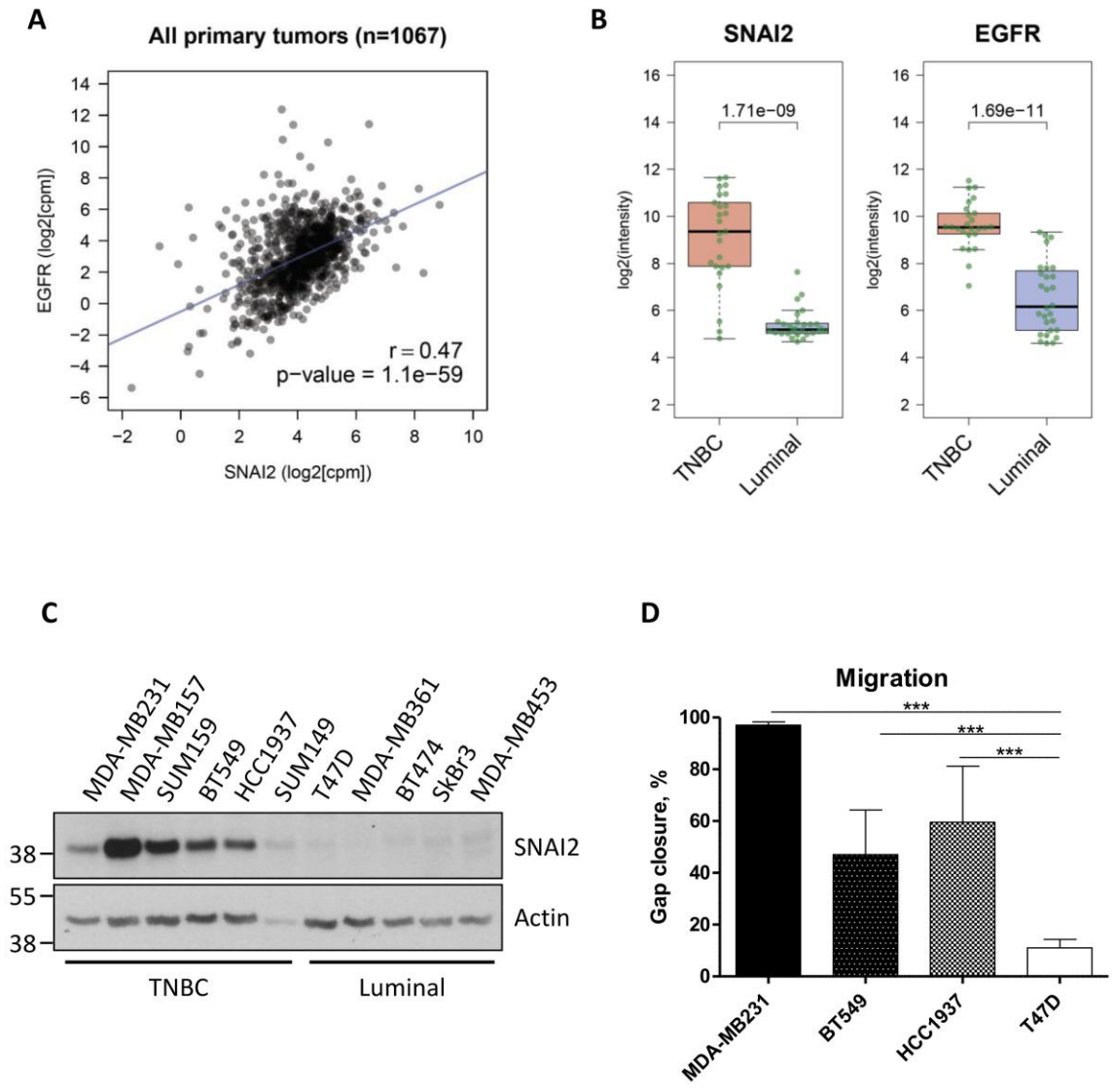

Figure 5.16 - SNAI2 expression correlates with EGFR levels. (A) Scatter plot showing the relationship between SNAI2 and EGFR expression in breast cancer primary tumours from TCGA dataset. A significant correlation was observed (Pearson's correlation coefficient= 0.47, p-value= 1.1e-59). Expression values are expressed as log2 counts per million transcripts. (B) Box plots showing a higher expression of SNAI2 and EGFR in TNBC versus Luminal cell lines from publicly available gene expression data. (C) A panel of breast cancer cell lines was tested to compare the levels of SNAI2. TNBC: MDA-MB231, MDA-MB157, SUM159, BT549, HCC1937, SUM149; Luminal: T47D, MDA-MB361, BT474, SkBr3, MDA-MB453. These cell lines were classified in accordance to Neve et al. classification (Neve *et al.*, 2006). (D) Motility of different cell lines expressing diverse levels of SNAI2 was tested in wound-healing experiments by seeding $4x10^4$ cells in Ibidi chambers. Images were acquired every hour

in a Cell-IQ instrument and analysed with the integrated software. The graph shows the percentage of gap closure after 12 h of migration and represents the average of at least four independent experiments. MDA-MB231 *vs* T47D P<0.0001; BT549 *vs* T47D P=0.0005; HCC1937 *vs* T47D P=0.0003; Unpaired two-tailed t test.

Then, BT549 cells were stimulated with two specific ligands of EGFR (EGF and TGFα) and, as expected, a significant increase of SNAI2 level was observed, in particular after 2-3 h (Figure 5.17A). Furthermore, SNAI2 accumulation was detected in non-malignant epithelial cell lines, MCF10A and HME, upon EGFR stimulation or in the presence of a constitutive activated mutant of EGFR (Figure 5.17B), supporting the EGFR-dependent expression of SNAI2. As shown in Figure 5.17C, TGFα exposure increased ERK phosphorylation, suggesting that ERK activation occurred in response to EGFR stimulation.

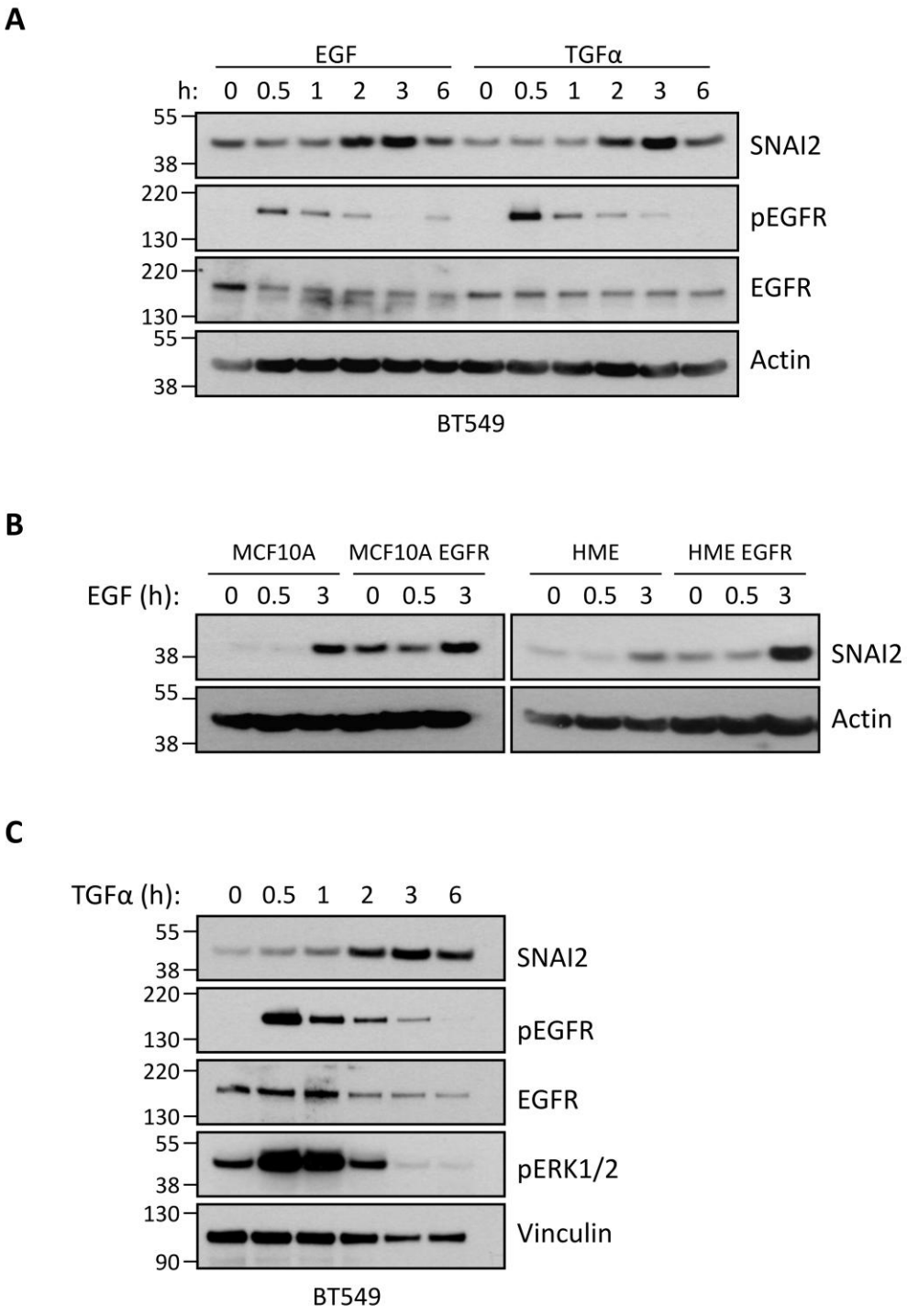

Figure 5.17 - EGFR activation promotes SNAI2 expression. (A) For time-course experiments, BT549 cells were serum-starved overnight and then stimulated with 20 ng/ml EGF and TGFα. SNAI2 levels are shown together with total and activated levels of EGFR. (B) In human mammary epithelial cell lines, both parental and mutated for EGFR, SNAI2 levels were assessed by western blot. After overnight serum starvation, cells were stimulated

with 20 ng/ml EGF for the indicated times. (C) Time-course experiments show SNAI2 levels upon TGFα stimulation. SNAI2 up-regulation is shown together with the total and activated amount of EGFR and, activated ERK. Vinculin is shown as a loading control.

Moreover, to further test that SNAI2 up-regulation resulted from EGFR activation, cells were treated with cetuximab, a monoclonal antibody that targets the EGFR extracellular domain thus impeding the binding with its ligand and consequently preventing EGFR activation. Given that EGFR signalling involves a plethora of effectors among which MAPKs, I focused on ERK pathway since my data supported its crucial role in SNAI2 regulation (Figures 5.14A-B). Western blot analysis revealed that EGFR inhibition mediated by cetuximab abolished SNAI2 accumulation by preventing the activation of ERK signalling pathway (Figures 5.18 A-B) both in MDA-MB231 and BT549 cell lines.

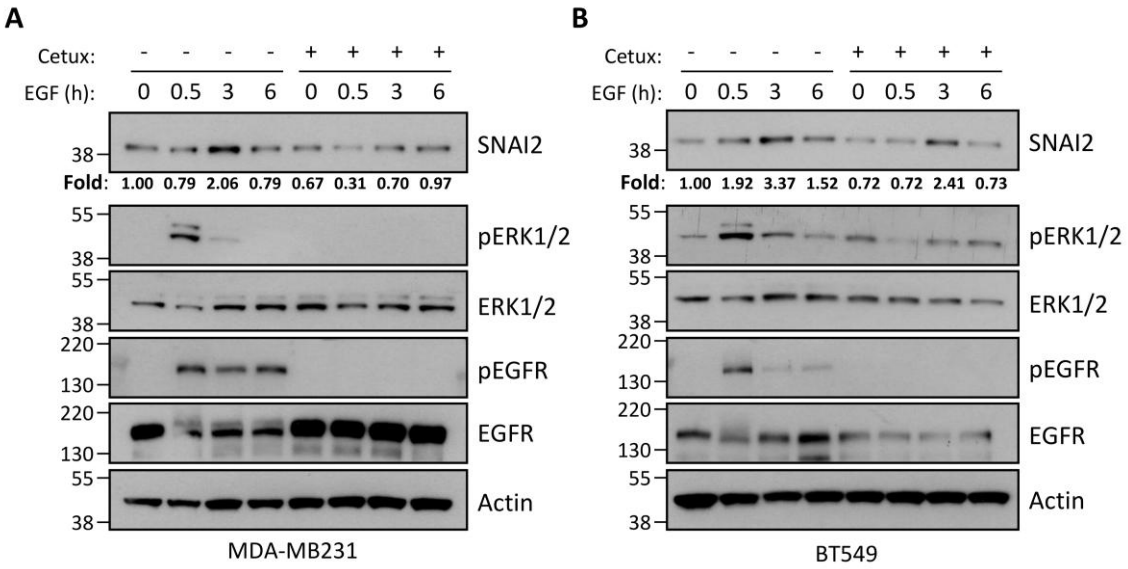

Figure 5.18 - EGFR inhibition prevents SNAI2 up-regulation. (A) MDA-MB231 and (B) BT549 cells were pre-treated with 100 µg/ml cetuximab for 1 h, after being serum-starved for 24 h. Next, cells were stimulated with 20 ng/ml EGF for the indicated time-points and SNAI2 levels were detected by western blot, together with total and phosphorylated ERK1/2 and EGFR. Values show the fold levels of SNAI2 relative to untreated cells.

5.7.2 cIAP1 sustains the EGFR-mediated expression of SNAI2

At this step, I asked whether the loss of cIAP1 affects the EGFR-mediated regulation of ERK signalling pathway. Therefore, MDA-MB231 and BT549 cells were silenced for cIAP1 and western blot analysis was performed after EGF exposure. Notably, a strong reduction of ERK activation could be detectable also at basal conditions in both cell lines (Figures 5.19A-B), and, interestingly, the up-regulation of SNAI2 was impaired even after EGF and TGFα stimulation, in the absence of cIAP1 (Figure 5.19C). Moreover, SNAI2 induction was also abolished in normal mammary epithelial cells either *wt* or bearing mutated EGFR (Figure 5.19D), supporting the idea that cIAP1 enhances the EGFR-dependent expression of SNAI2 by favouring the activation of ERK signalling pathway.

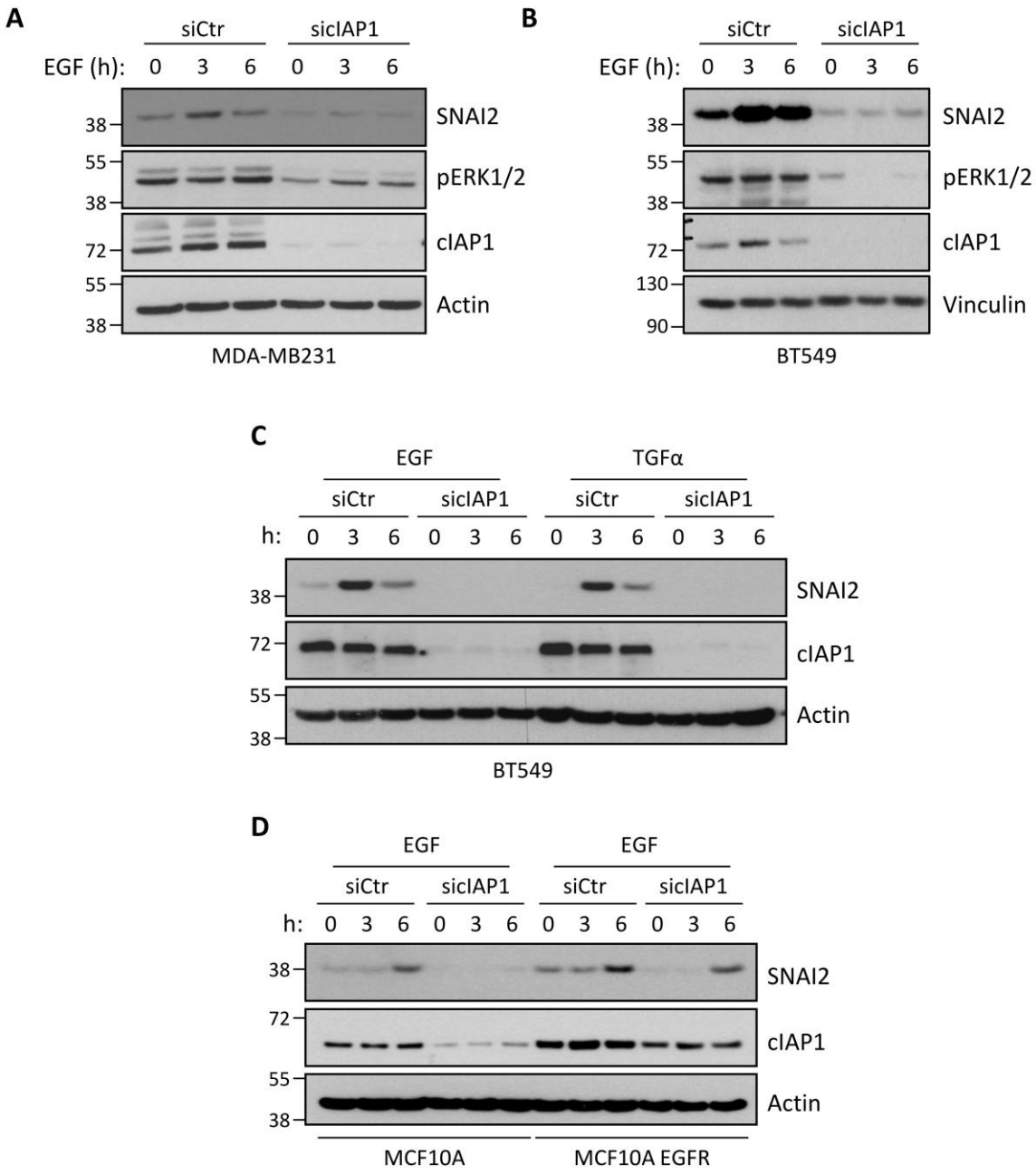

Figure 5.19 - The targeting of cIAP1 hinders EGFR-mediated expression of SNAI2. (A) MDA-MB231 and (B) BT549 cells were knocked-down for cIAP1 through specific siRNAs and, 48 h after transfection, starved overnight. SNAI2 levels were detected by western blot in unstimulated cells or stimulated with 20 ng/ml EGF for the indicated time-points. Detection of ERK1/2 and cIAP1 levels confirms the transfection efficiency. (C) Western blot analysis was performed to evaluate SNAI2 expression in BT549 and (D) MCF10A - *wt* or bearing

mutated EGFR. Cells were transfected as in Figure 5.19A and stimulated with the indicated EGFR ligands (20 ng/ml).

5.7.3 cIAP1 regulates SNAI2 at transcription level

Since cells silenced for cIAP1 showed lower levels of SNAI2 compared to control cells, I investigated whether the absence of cIAP1 causes a decrease of SNAI2 protein stability. To this aim, SNAI2 protein half-life was evaluated in MDA-MB231 cells treated with cycloheximide, an inhibitor of protein synthesis (Figure 5.20A). Although SNAI2 was less expressed in cells knocked-down for cIAP1 (sicIAP1), the protein was found to be more stable in these cells compared to the control (siCtr). Therefore, I evaluated if a transcriptional regulation of SNAI2 is mediated by cIAP1. Real-Time PCR was performed in BT549 and MCF10A cells, and *SNAI2* expression level was evaluated in cIAP1-depleted cells compared to control (Figure 5.20B). Interestingly, the analysis revealed that cIAP1-targeting by specific siRNAs or IAP inhibitors (Figure 5.20B and 5.5, respectively) both resulted in the reduction of *SNAI2* levels. Indeed, cIAP1 depletion not only affected SNAI2 expression at basal levels, but also impaired its up-regulation upon EGFR-stimulation. Hence, these results indicate that cIAP1 promotes SNAI2 expression, resulting in a decrease of its protein levels in the absence of cIAP1 (Figure 5.20C).

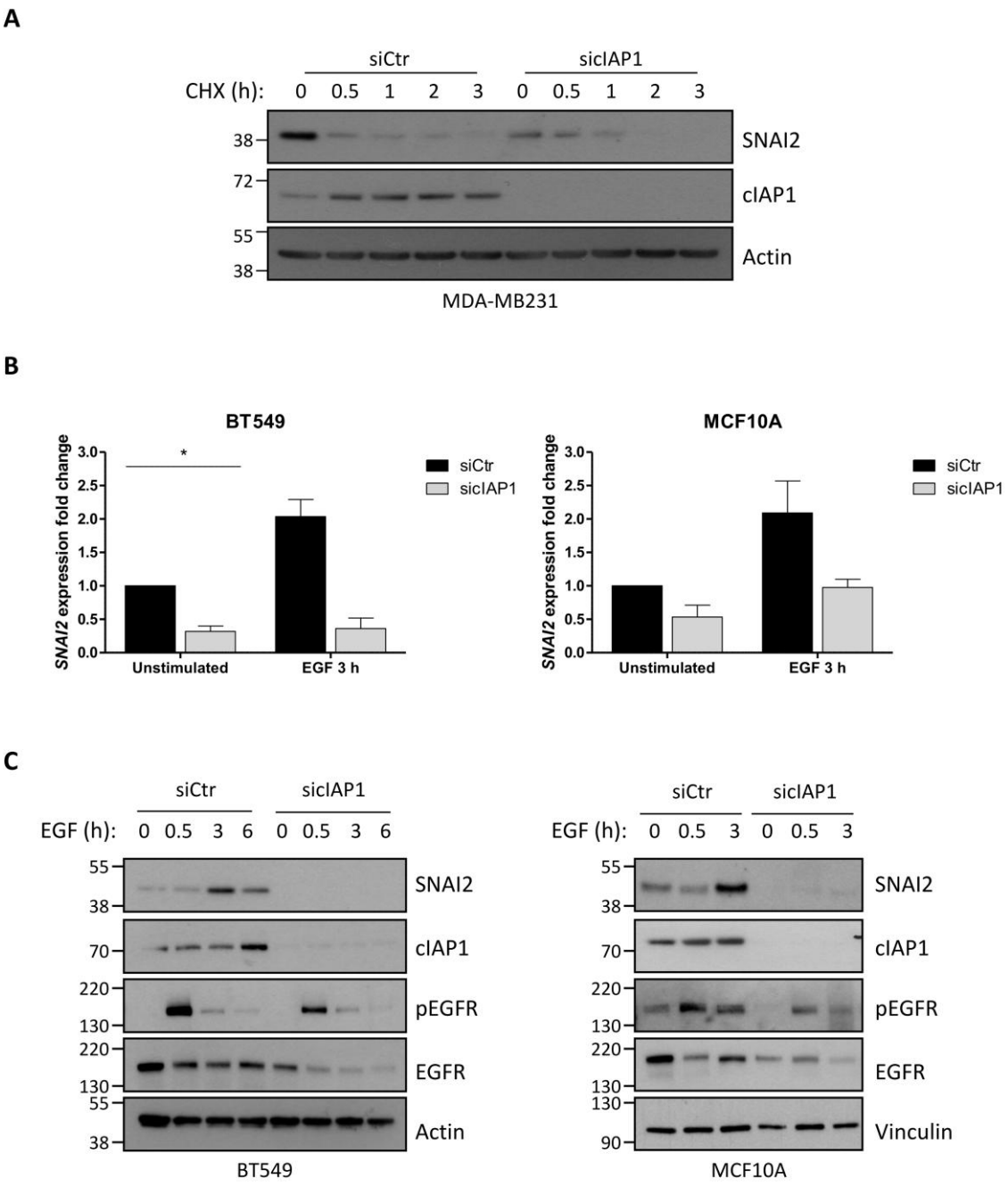

Figure 5.20 - cIAP1 regulates SNAI2 mRNA levels. (A) MDA-MB231 cells were treated with 100 µg/ml cycloheximide in the presence or absence of cIAP1 and harvested at the indicated time points. Western blot was performed to assess SNAI2 levels. cIAP1 was detected as a control of silencing efficacy, while Actin as a loading control. (B) BT549 and MCF10A cells were silenced for cIAP1 as described before. After serum starvation, cells were stimulated for 3 h with 20 ng/ml EGF and lysed to extract RNA. Real-Time PCR was performed to evaluate *SNAI2* fold expression relative to *GAPDH*. BT549: Unstimulated siCtr *vs* siCIAP1 P = 0.0137, EGF 3 h siCtr *vs* siCIAP1 P = 0.0558; n = 3; Paired two-tailed t test. MCF10A: Unstimulated siCtr *vs* siCIAP1

P = 0.0784, EGF 3 h siCtr *vs* sicIAP1 P = 0.0742; n = 4; Paired two-tailed t test. (C) SNAI2 levels were assessed by western blot together with EGFR total and activated levels, in BT549 and MCF10A cell lines. After 48 h from transfection with control siRNA (siCtr) or siRNAs specific for cIAP1 (sicIAP1), cells were serum-starved overnight and then stimulated with 20 ng/ml EGF for the indicated time-points.

Having demonstrated that cIAP1 supports the expression of this pro-metastasis gene, I speculated that the loss of this IAP might be responsible for the SM83 anti-metastasis effect (Figures 5.3-4). Herein, *in vitro* motility assay was performed to test the possible cell motility variation that might occur in the absence of cIAP1 in BT549 and in MCF10A cells, *wt* and carrying EGFR mutation (Figure 5.21).

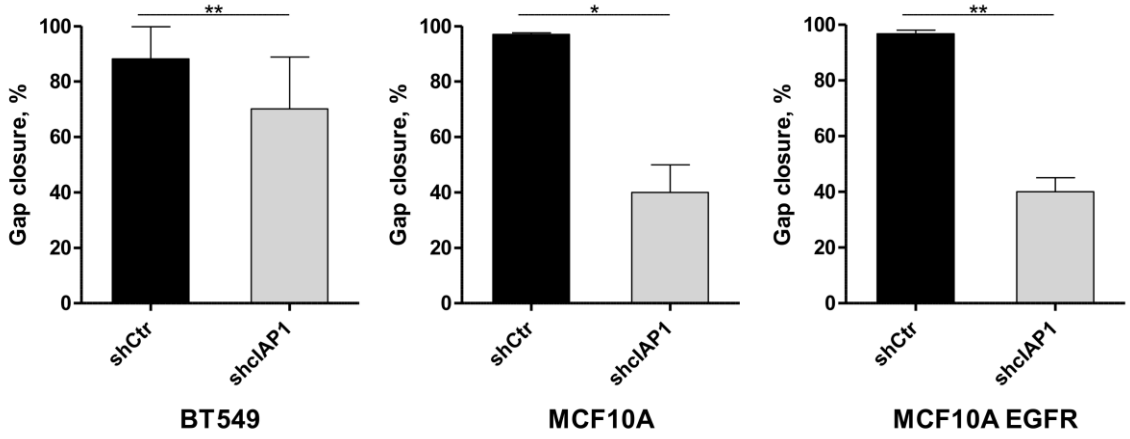

Figure 5.21 - Depletion of cIAP1 reduces cell motility. Wound healing assay was performed as described in Figure 5.6B. Motility assay was carried out using scramble-shRNA and cIAP1-shRNA transduced BT549, MCF10A and MCF10A bearing mutated EGFR cells. Graphs show the percentages of gap closure after 12 h of migration. shCtr *vs* shcIAP1 BT549: P= 0.0043, n=12, Paired two-tailed t test; shCtr *vs* shcIAP1 MCF10A: P= 0.0102, MCF10A EGFR: P= 0.0029, n= 4, Paired two-tailed t test.

Based on the reduction of *in vitro* cell motility (Figure 5.21) and *in vivo* metastasis formation (Figures 5.3-4) mediated by IAP-depletion, the effect of SM83 administration was assessed also by using a syngenic mouse model injecting the highly metastatic 4T1 murine

cells in BALB/c mice (Figure 5.22). In contrast with what I expected, SM83 administration does not affect the metastatic potential of this cell line. This result can be explained by the fact that 4T1 cells express low levels of SNAI2 (Ferrari-Amorotti *et al.*, 2013) and therefore they metastasize in a SNAI2-independent manner. Consequently, SM83-mediated down-regulation of SNAI2 cannot impact on 4T1 metastatic potential.

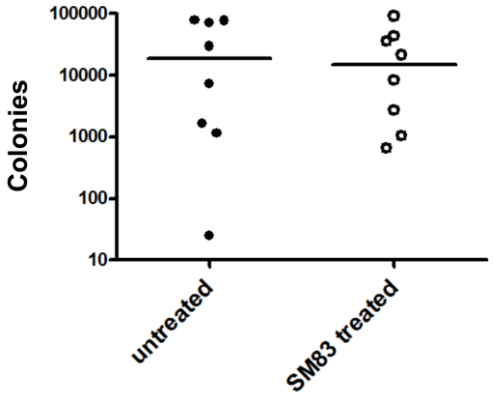

Figure 5.22 - SM administration does not affect 4T1 metastatic potential. 4T1 murine cells were inoculated in syngeneic BALB/c mice that were treated with vehicle or SM83. Graph shows the number of metastatic colonies.

5.8 cIAP1 modulates not only EGFR signalling, but also its protein levels

5.8.1 EGFR levels are affected by cIAP1 depletion

The strong inhibition of ERK1/2 signalling pathway that occurred after targeting cIAP1, led me to investigate whether this IAP only promotes EGFR signalling or also regulates the receptor levels. Intriguingly, I noticed that cIAP1 depletion resulted in a marked reduction of EGFR levels in both cancer and normal mammary epithelial cell lines (Figures 5.20C and 5.23A-B), that further decreased upon EGFR stimulation. Indeed, immunofluorescence

analysis highlighted that the loss of cIAP1 strongly abrogated the number of EGFR foci induced by stimulation with its ligand, suggesting an impaired capability to transduce the receptor signals (Figure 5.23C). Having shown that cIAP1 depletion results in the reduction of EGFR protein levels, I investigated whether this is due to a direct effect of cIAP1 on receptor stability or if it is caused indirectly through the regulation of the EGFR inhibitors LRIG1 and/or c-CBL (Fry *et al.*, 2009).

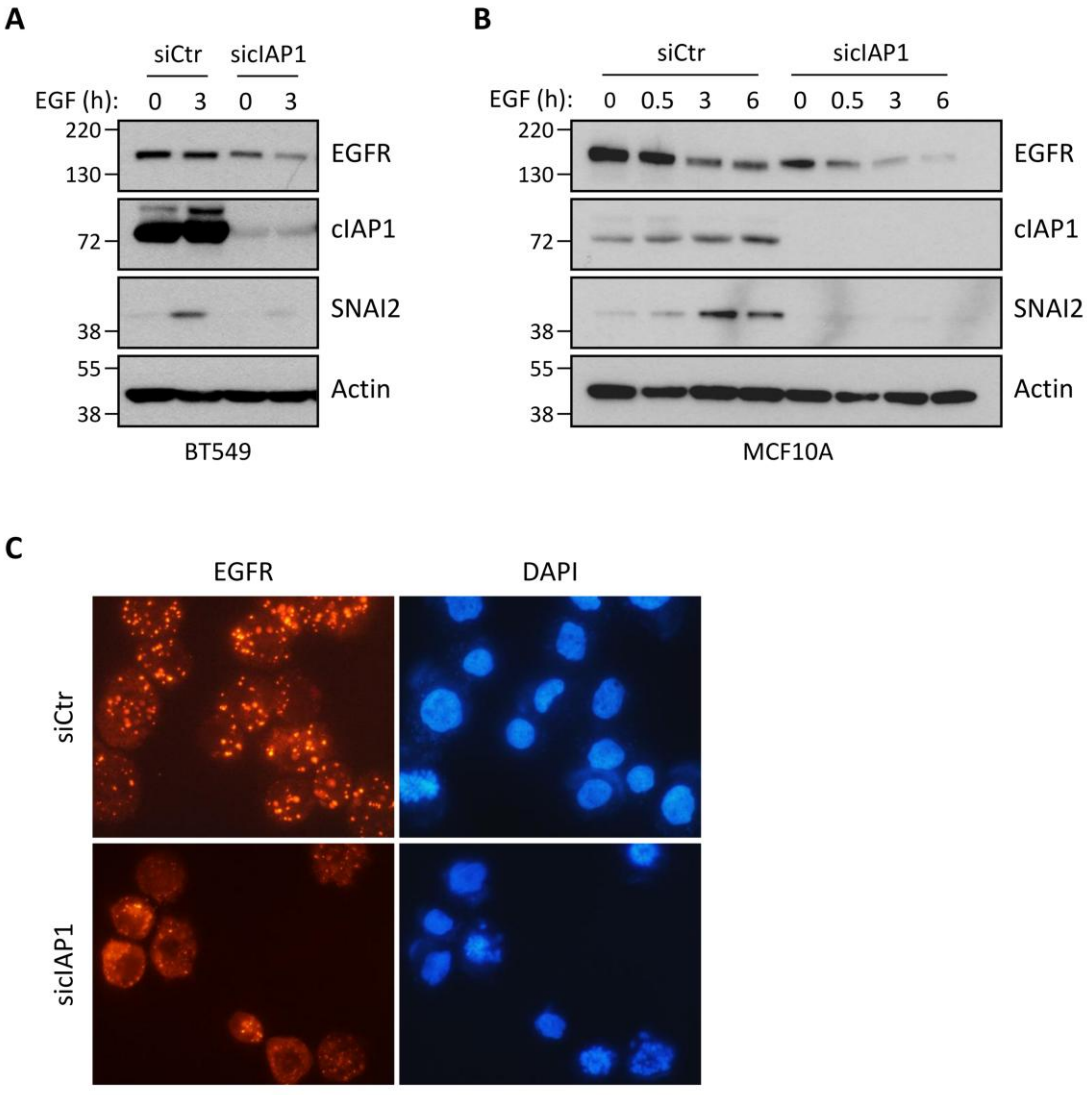

Figure 5.23 - cIAP1 depletion decreases EGFR levels. (A) BT549 and (B) MCF10A cells knocked-down for cIAP1 were stimulated with 20 ng/ml EGF under serum-starved (basal) conditions, and EGFR, cIAP1 and SNAI2 levels

were analyzed by western blot. (C) BT549 cells were transfected with control or cIAP1-specific siRNAs before being overnight serum-starved and stimulated for 30 min with 20 ng/ml EGF. Cells were fixed and incubated with anti-EGFR antibody and nuclei stained with DAPI. Images were obtained with a 60x magnification.

5.8.2 cIAP1 targeting destabilizes endogenous EGFR in an LRIG1-independent manner

It has been shown that LRIG1 up-regulation represents an acquired mechanism for SM resistance (Bai *et al.*, 2012). GEP and western blot analyses confirmed that LRIG1 up-regulation occurred at transcriptional and protein level (Figures 5.5 and 5.7A-B, respectively) in MDA-MB231 subcutaneous tumours treated with SM83. To determine whether LRIG1 increase is a result of cIAP1 depletion, I targeted this IAP through siRNAs and, then, I performed Real-Time PCR and western blot analyses to examine LRIG1 mRNA and protein level, respectively. Although LRIG1 resulted up-regulated both at transcriptional and protein level in the absence of cIAP1 (Figures 5.24A-B), surprisingly, LRIG1 knock-down did not significantly increase EGFR (Figure 5.24C). Furthermore, in sharp contrast with the strong reduction of the receptor levels (Figures 5.20C and 5.23B), the up-regulation of LRIG1 was not evident in MCF10A cells lacking cIAP1 (Figure 5.24D). The latter evidence strongly supports the idea that the observed reduction of EGFR does not stem from LRIG1 up-regulation.

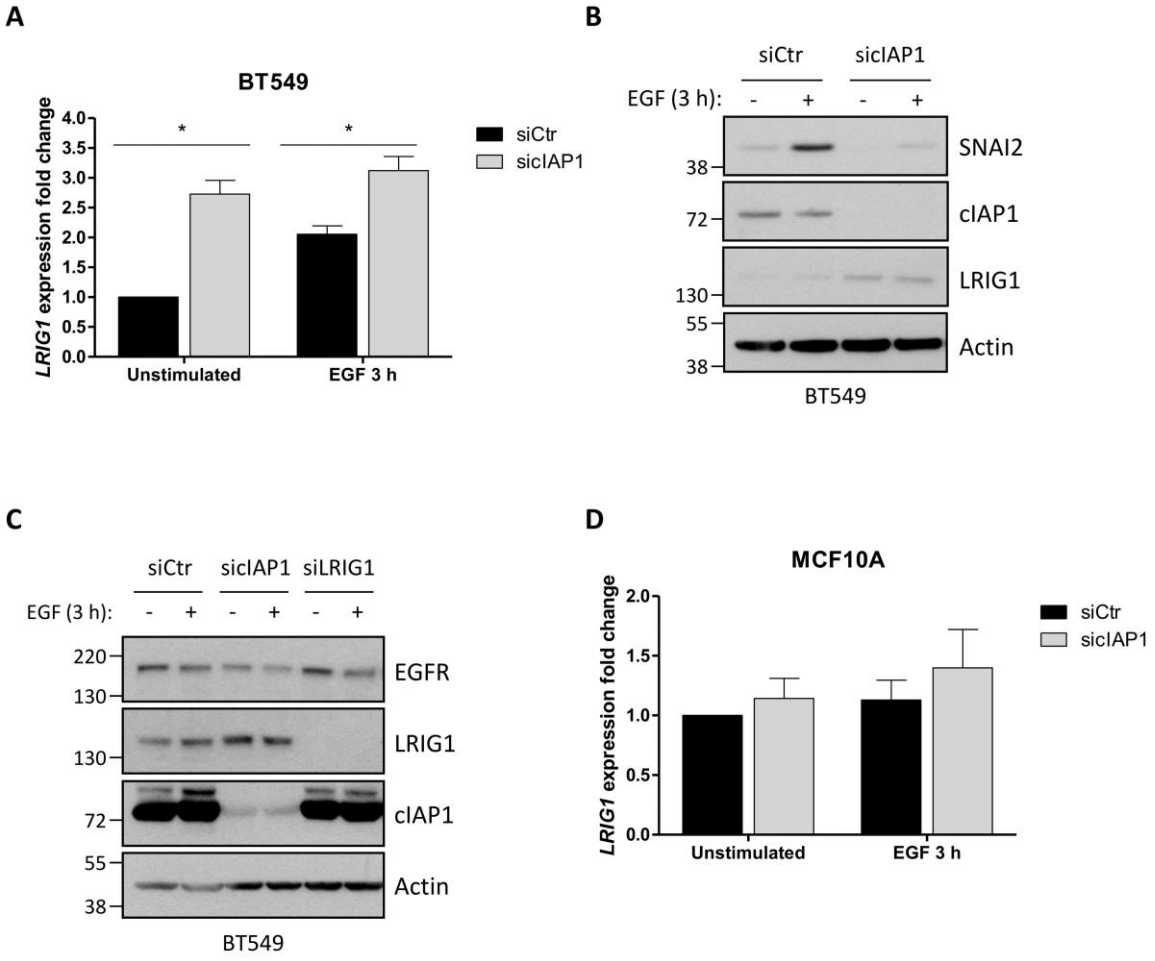

Figure 5.24 - LRIG1 up-regulation mediated by cIAP1 has a limited effect on EGFR levels. (A) Real-Time PCR was performed in BT549 cells transfected with control (siCtr) or cIAP1-targeting (siclAP1) siRNAs to assess *LRIG1* expression levels. After 48 h from transfection, cells were serum-starved overnight and stimulated with 20 ng/ml EGF. Unstimulated siCtr *vs* siclAP1 P = 0.0175, EGF 3 h siCtr *vs* siclAP1 P = 0.0341; n = 3; Paired two-tailed t test. (B) Western blot shows SNAI2 and LRIG1 levels in BT549 cells silenced for cIAP1 and stimulated with 20 ng/ml EGF. cIAP1 was detected as control of the transfection efficiency. (C) EGFR levels were assessed in BT549 cells silenced for cIAP1 and LRIG1, stimulated with 20 ng/ml EGF after overnight serum starvation. (D) *LRIG1* expression levels were evaluated by Real-Time PCR in MCF10A cells under the same conditions described in Figure 5.24A. Unstimulated siCtr *vs* siclAP1 P = 0.4585, EGF 3 h siCtr *vs* siclAP1 P = 0.5052; n = 4; Paired two-tailed t test.

5.8.3 cIAP1 interacts with EGFR and modulates its stability

Having demonstrated that the absence of cIAP1 reduces EGFR levels and that LRIG1 is only partially involved, I investigated other possible mechanisms through which cIAP1 could regulate EGFR stability. I firstly evaluated the interaction between EGFR and cIAP1 using two different approaches: PLA and co-IP. Through PLA endogenous EGFR–cIAP1 protein complexes could be visualized as a single bright spot in BT549 cells (Figure 5.25A). This result was fur/Flagaddressed performing co-IP of ectopically expressed Myc/Flag-*tagged* EGFR and endogenous cIAP1 (Figure 5.25B), confirming the interaction between EGFR and its negative regulator c-CBL, which increased after EGFR stimulation.

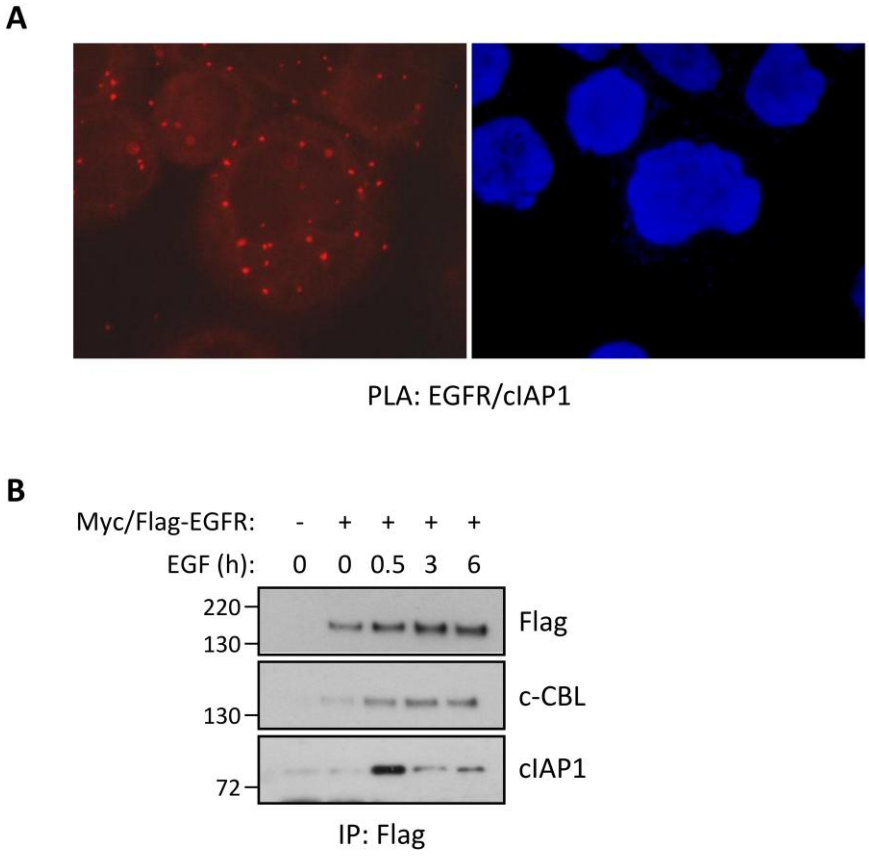

Figure 5.25 - **EGFR physically interacts with cIAP1**. (A) The cIAP1/EGFR interaction was tested in the BT549 cell line by PLA (red spots). DAPI staining was used to label cell nuclei (blue). Images were acquired with a 60x

magnification. (B) Co-IP was performed in BT549 cells stably expressing Myc/Flag-tagged EGFR. Cells were serum-starved overnight and then stimulated with 20 ng/ml EGF at the indicated time-points. Cells were lysed and EGFR was immunoprecipitated with anti-Flag antibody. The interaction of ectopic EGFR with cIAP1 and c-CBL was tested through western blot.

Next, to assess whether cIAP1 plays a role in the EGFR degradation, BT549 cells transfected with siCtr and sicIAP1 were pre-treated with chloroquine, in order to block lysosomal degradation. Chloroquine administration prevented the EGFR down-regulation that occurred in the absence of cIAP1, even after EGF exposure (Figure 5.26), thus suggesting that cIAP1 could affect the receptor lysosomal degradation.

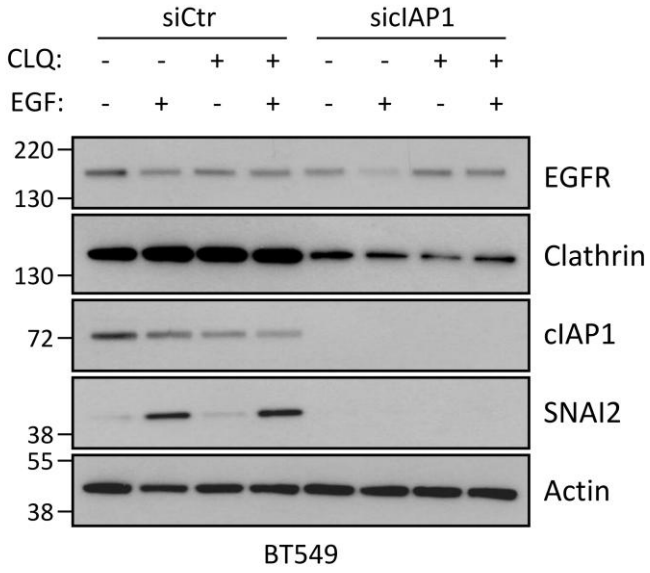

Figure 5.26 - cIAP1 affects the lysosome-dependent degradation of EGFR. BT549 cells were first transfected with control or cIAP1-specific siRNAs. After 48 h from transfection, cells were serum-starved overnight and exposed to 100 µM lysosome inhibitor chloroquine for 1 h and subsequently stimulated with 20 ng/ml EGF for 3 h.

Considering that the main pathway of EGFR internalization is mediated by Clathrin, which drives the receptor to its degradation (Sigismund *et al.*, 2008), I also evaluated if cIAP1

affects Clathrin expression. Unexpectedly, Clathrin levels were reduced, rather than increased, by targeting of cIAP1, as shown in Figure 5.26. In accordance to this result, immunofluorescence analysis (Figure 5.27) highlighted the reduction of EGFR internalization rates caused by cIAP1 silencing. Furthermore, labelling cells with an antibody against Clathrin showed a decreased organization of the endocytic structures in cIAP1-depleted cells, whereas a clear signal resulted visible in siCtr cells before and after EGFR stimulation. Indeed, these observations prompted me to speculate that cIAP1 targeting does not trigger EGFR degradation but, instead increased its stability.

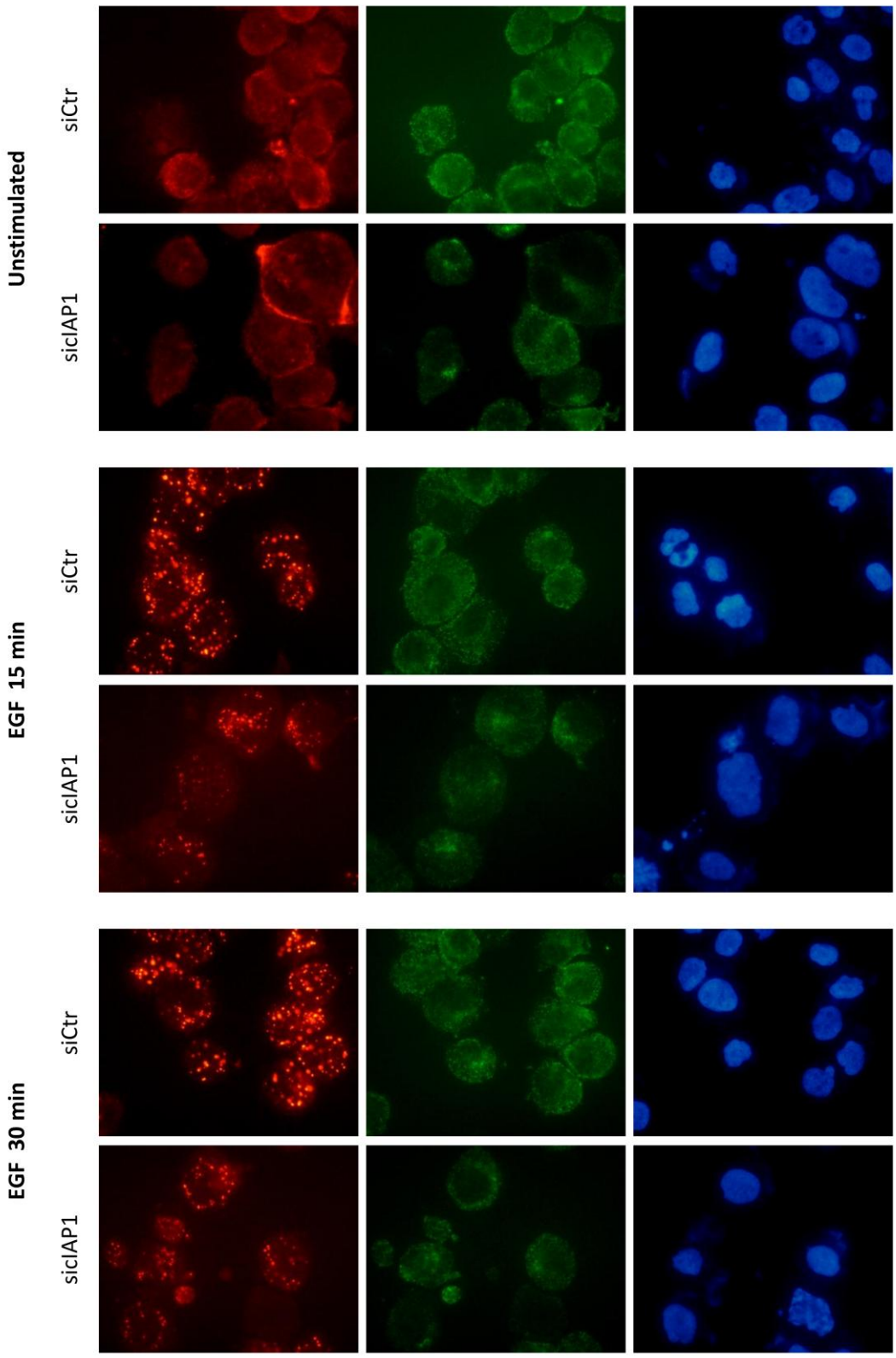

Figure 5.27 - The targeting of cIAP1 reduces Clathrin dependent EGFR endocytosis. BT549 cells treated with control or cIAP1 targeting siRNAs were serum-starved overnight and incubated with 20 ng/ml EGF for 15 or 30

min. After fixation, cells were analyzed for endocytosis and therefore incubated with an antibody against EGFR and Clathrin. Results are representative of at least three independent experiments. Images were acquired with a 60x magnification.

5.8.4 The targeting of cIAP1 increases EGFR protein stability

To substantiate the effect of cIAP1 on EGFR stability, I examined the receptor levels in BT549 and MCF10A cells ectopically expressing Myc-*tagged* EGFR. As shown in Figure 5.28A, cIAP1 depletion did not reduce EGFR protein levels, but rather increased them. Basing on this result, I further investigated the effect of cIAP1 depletion on EGFR stability. To this aim, BT549 and MCF10A cells were pre-treated with cycloheximide and stimulated using EGF for different time-points. Strikingly, cIAP1 depletion promoted the receptors stability upon EGF exposure, thus enhancing its half-life and supporting the idea that cIAP1 promotes EGFR degradation (Figure 5.28B).

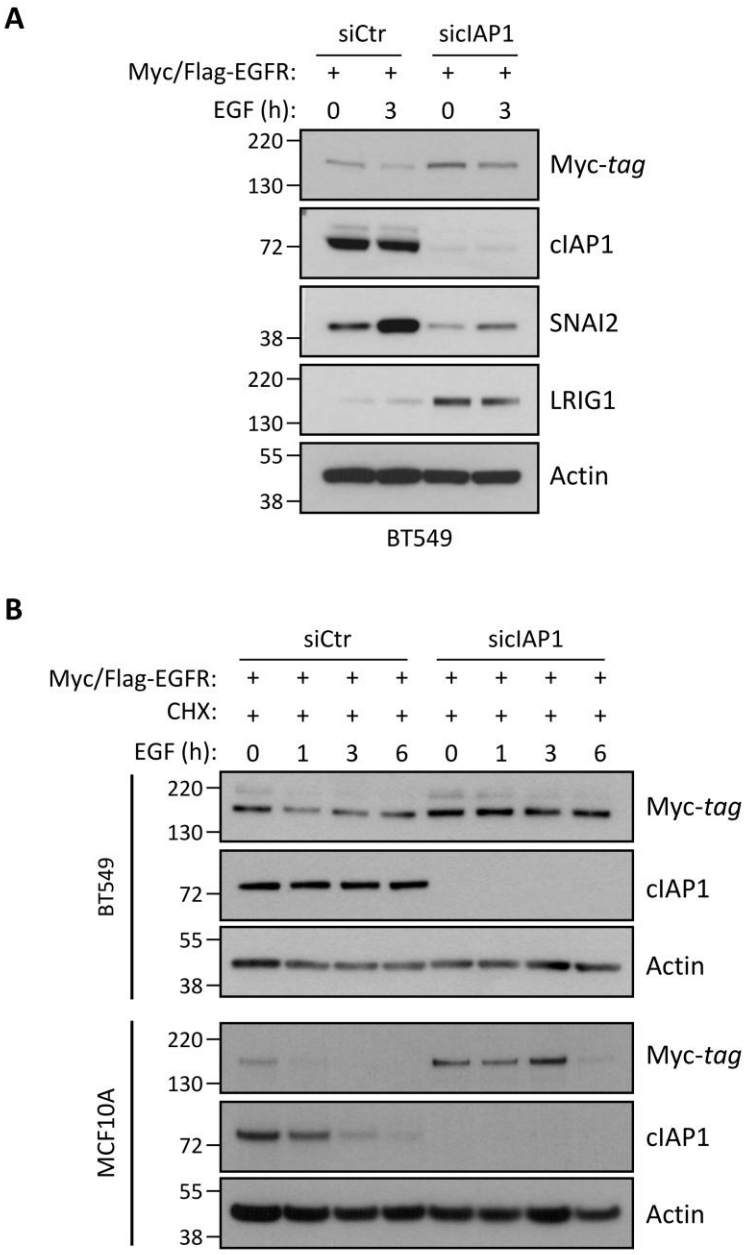

Figure 5.28 - Ectopic EGFR fails to be degraded in the absence of cIAP1. (A) BT549 cells stably expressing Myc/Flag-tagged EGFR were grown in serum starvation for 24 h and then stimulated with 20 ng/ml EGF for 3 h. EGFR, SNAI2 and LRIG1 levels were assessed by western blot. Ectopic EGFR was detected with anti-Myc antibody. (B) Myc/Flag-tagged EGFR was stably expressed in BT549 and MCF10A cell lines. Cells were serum-starved overnight and pre-treated with 100 (BT549) or 50 (MCF10A) µg/ml cycloheximide for 30 min before being stimulated with 20 ng/ml EGF for the indicated times.

The effect of EGFR stabilization exerted by cIAP1 loss was further sustained by the observation obtained over-expressing an ubiquitin-ligase inactive form of cIAP1 which inhibited the degradation of EGFR (Figure 5.29), supporting the notion that the catalytic activity of cIAP1 triggers to receptor degradation.

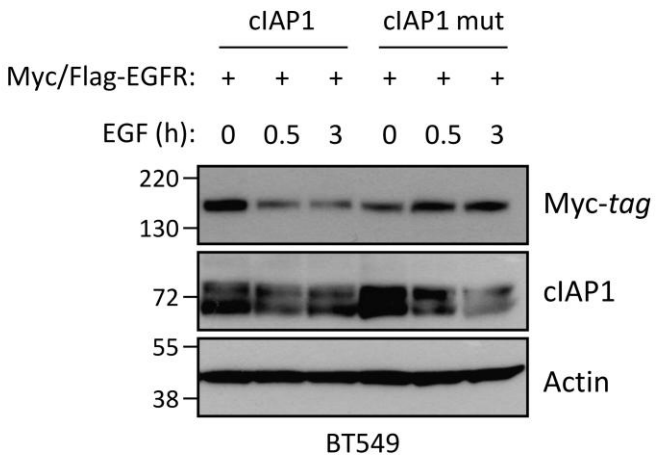

Figure 5.29 - cIAP1 ubiquitin-ligase activity triggers EGFR degradation. BT549 cells transiently transfected with *wt* or mutated cIAP1 were employed to evaluate EGFR ectopic levels by western blot.

5.8.5 c-CBL reduction mediated by the lack of cIAP1 enhances EGFR stability

Since post-translational modifications including phosphorylation and ubiquitination are events that regulate EGFR endocytosis, the effect of cIAP1 on the ubiquitin ligase c-CBL was tested. In fact, I hypothesised that loss of cIAP1 could enhance the receptor stability through the reduction of c-CBL capability to trigger EGFR degradation. To this end, Myc-*tagged* EGFR was co-immunoprecipitated with c-CBL in BT549 cells stimulated with EGF for 30 min, in the presence or absence of cIAP1 (Figure 5.30A). These experiments showed that c-CBL co-immunoprecipitated with EGFR mainly upon EGF stimulation and the interaction between these two proteins was slightly reduced in cells silenced for cIAP1 (Figure 5.30A).

Conversely, c-CBL over-expression limited EGFR stabilization caused by cIAP1 depletion (Figure 5.30B).

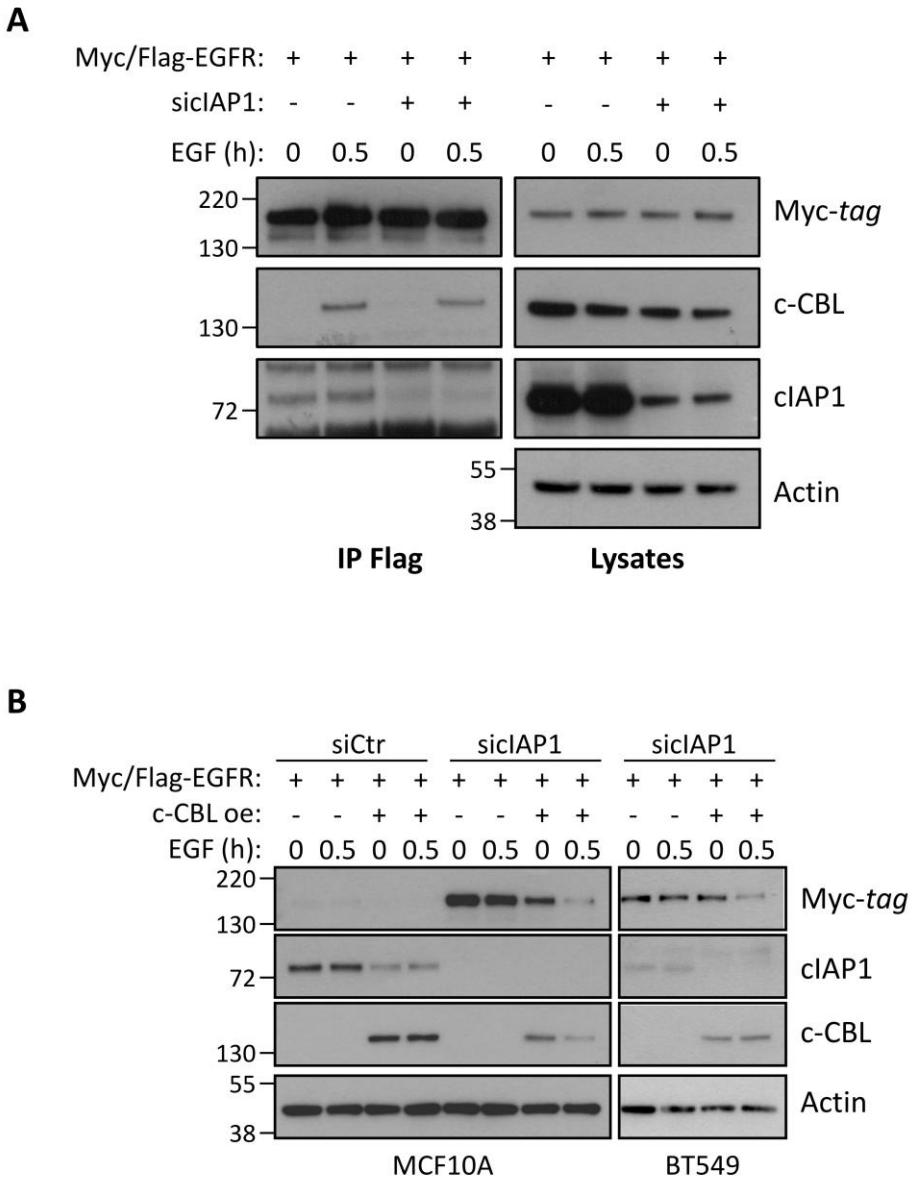

Figure 5.30 - cIAP1 depletion stabilizes EGFR reducing its c-CBL-mediated degradation. (A) Ectopic EGFR was immunoprecipitated as described in Figure 5.24B from BT549 cells transfected with control and cIAP1-specific siRNAs. Total levels of c-CBL and the amount of c-CBL interacting with EGFR were evaluated by western blot. (B) Lentiviral vectors were employed to transduce MCF10A and BT549 to stably express Myc/Flag-tagged EGFR. Then, cells were further transduced to over-express c-CBL or GFP as a control, in cells depleted for cIAP1

employing specific siRNAs. After overnight serum starvation, both cell lines were stimulated with 20 ng/ml EGF and analysed by western blot to evaluate the levels of ectopic EGFR employing a Myc-tagged specific antibody.

I then investigated the phosphorylation of EGFR at the Tyr-1045 residue, which is crucial for c-CBL/EGFR interaction upon EGF stimulation. I observed that, despite the fact that total levels of EGFR were reduced upon cIAP1 silencing (Figure 5.31, upper panel), the ratio of EGFR phosphorylated was increased (Figure 5.31, bottom panel). This suggests that the reduced amount of c-CBL impairs the cell capacity to degrade EGFR.

To further study the mechanisms through which cIAP1 controls EGFR levels, I also assessed the effect of cIAP1 depletion on the expression of another EGFR antagonist, named Sprouty1. Despite its role as an EGFR inhibitor, the suppression of Sprouty1 in TNBC correlates with inhibition of cell growth, invasion and metastasis (He *et al.*, 2016). Notably, immunoblotting analysis performed in BT549 cells showed that Sprouty1 is considerably reduced in cIAP1-silenced cells compared to control cells (Figure 5.31, upper panel).

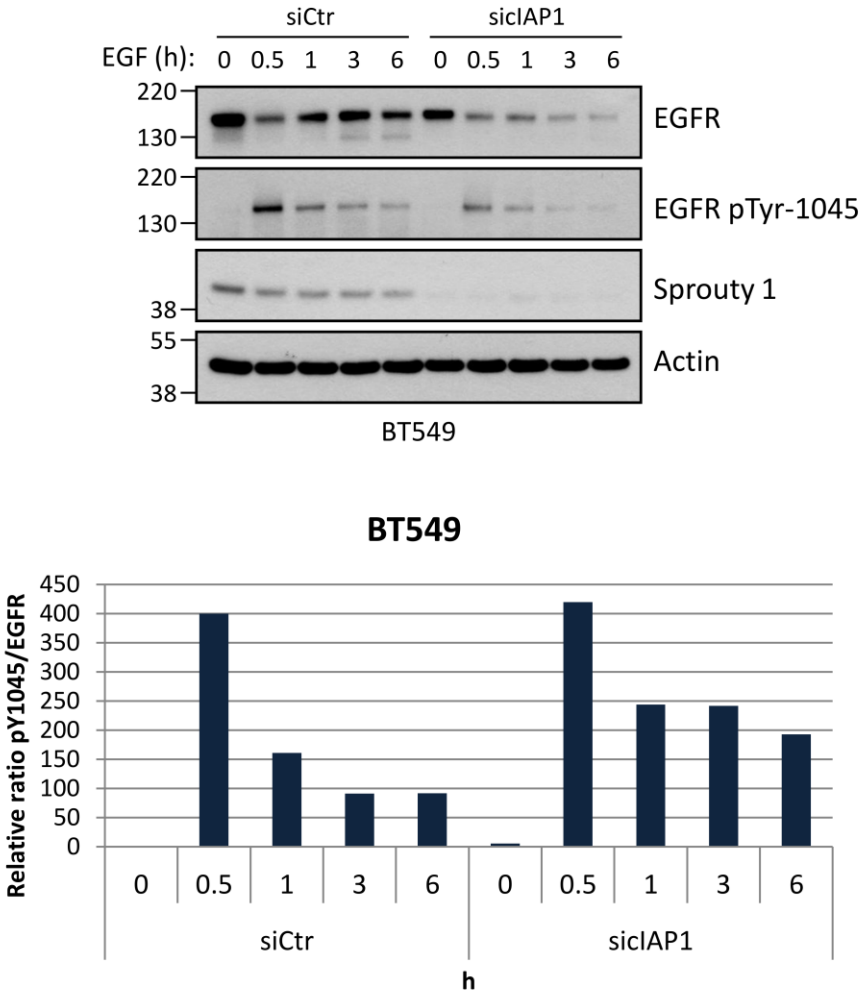

Figure 5.31 - cIAP1 knock-down enhances EGFR phosphorylation at the c-CBL binding site Tyr-1045. BT549 cells were silenced for cIAP1 through specific siRNAs and starved for 24 h before being stimulated with 20 ng/ml EGF for the indicated time-points. Sprouty 1, EGFR total levels and EGFR phosphorylation at the Tyr-1045 were assessed by western blot (upper panel). Densitometric analysis was performed on western blots and graphs (bottom panel) show the levels of EGFR phosphorylated in Tyr-1045 normalized by the total levels of the receptor.

5.8.6 Possible role of cIAP1 in regulating the degradation and the recycling of EGFR

After endocytosis, EGFR is guided to early endosomes where the receptor fate is decided: it is either recycled back to the cell surface or further led to late endosomes and lysosomes for degradation. To determine which endocytic route is affected by cIAP1, I studied the interaction between EGFR and RAB family proteins, with a particular focus on RAB11 and RAB7, which play a role in recycling and late endosomes, respectively (Ceresa, 2006). By PLA assay, I found that cIAP1 silencing slightly increases the interaction between EGFR and RAB11 (Figure 5.32A), while dramatically reducing the interaction of this receptor with RAB7 (Figure 5.32B). Taking into account that cIAP1 silencing reduces the total levels of EGFR (Figures 5.20C and 5.23A-B), these findings support the idea that cIAP1 depletion could promote EGFR recycling rather than its endocytosis in late vesicles. Nonetheless, further experiments are needed to clarify the role of cIAP1 in these processes.

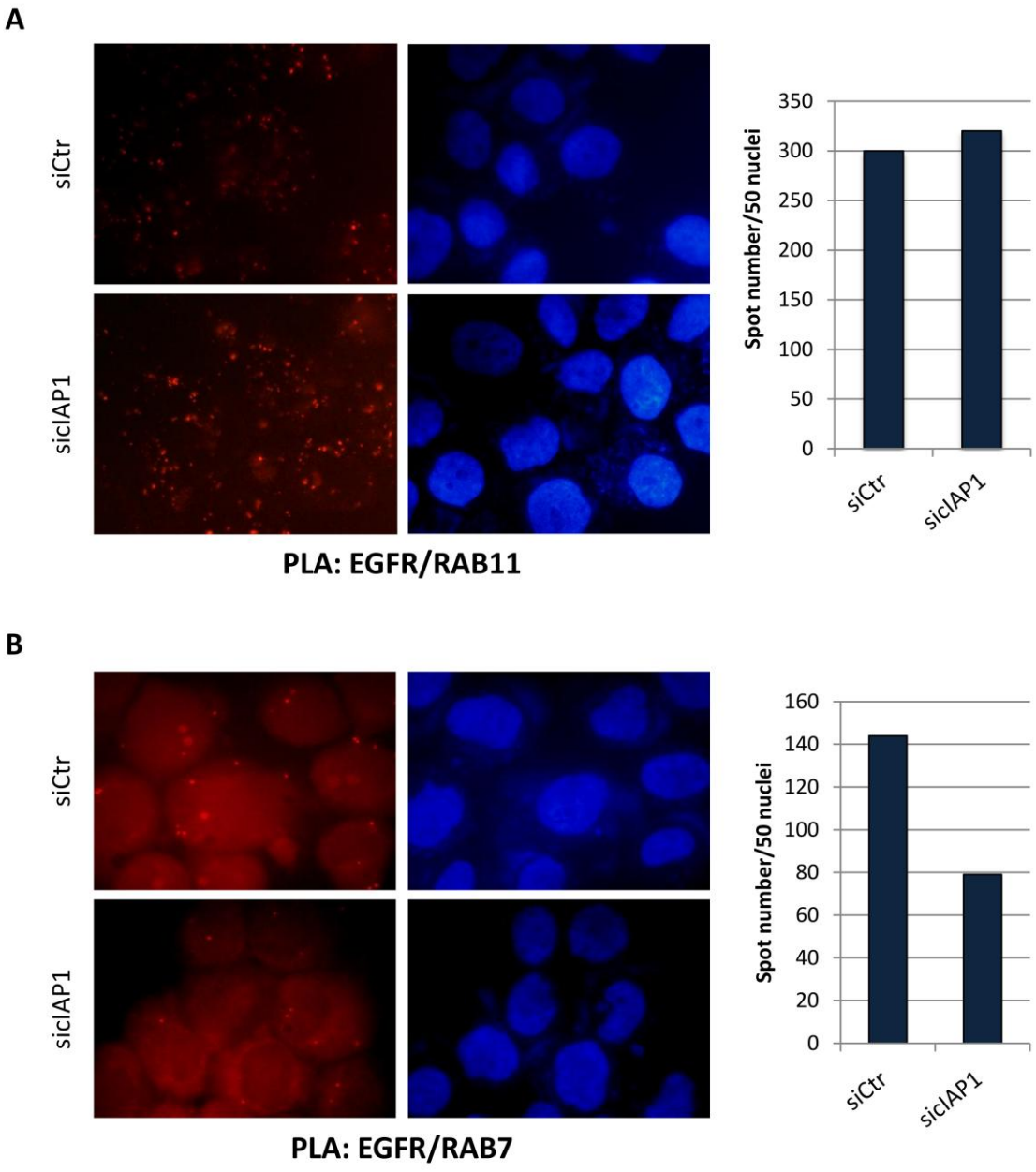

Figure 5.32 - Loss of cIAP1 promotes EGFR recycling. (A) BT549 cells were transfected with control or cIAP1 siRNAs. After 48 h post-transfection, cells were serum-starved overnight and then stimulated with 20 ng/ml EGF. At the indicated time points, fixed cells were tested using PLA to assess interaction between EGFR and RAB11 or (B) RAB7. Images were acquired with a 60x magnification and are representative of three independent experiments. Graphs on the right panels show the number of foci counted in 50 cells.

5.8.7 Depletion of cIAP1 inhibits EGFR transcription

Despite the increased protein stability of EGFR, the overall effect of cIAP1 targeting was a strong reduction of the receptor levels. In light of these findings, I tested whether cIAP1 controls EGFR in a transcriptional manner and, therefore, the receptor expression levels were assessed through Real-Time PCR in BT549 and MCF10A cells, silenced or not for cIAP1. The analysis revealed a significant down-regulation of *EGFR* mRNA in the absence of cIAP1 (Figure 5.33), therefore suggesting that the observed downregulation of EGFR could stem, at least in part, from the reduced expression of EGFR gene.

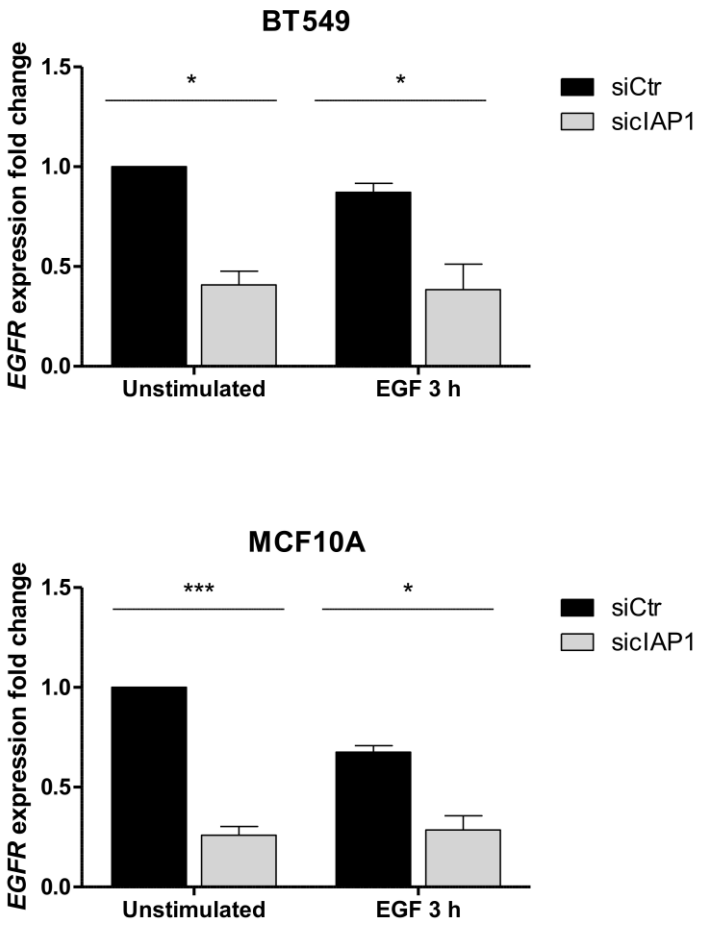

Figure 5.33 - Loss of cIAP1 inhibits EGFR transcription. BT549 (upper panel) and MCF10A (bottom panel) cells were silenced for cIAP1 and stimulated with EGF (20 ng/ml) for 3 h after overnight serum starvation. Real-Time PCR was performed to quantify the levels of *EGFR* expression relative to *GAPDH*. BT549: Unstimulated siCtr *vs* sicIAP1 P = 0.0134, EGF 3 h siCtr *vs* sicIAP1 P = 0.0270; n = 3; Paired two-tailed t test. MCF10A: Unstimulated siCtr *vs* sicIAP1 P = 0.004, EGF 3 h siCtr *vs* sicIAP1 P = 0.0183; n = 4; Paired two-tailed t test.

To further investigate the mechanisms through which cIAP1 transcriptionally induced EGFR, I focused on NF-kB signalling pathway that is regulated by IAPs. I first found that silencing of p65/RelA resulted in a strong reduction of EGFR (Figure 5.34), suggesting that EGFR is expressed in a NF-kB-dependent manner. Therefore, as cIAP1 promotes the NF-kB canonical pathway, and EGFR expression is promoted by NF-kB, it is possible that the

reduced EGFR levels observed upon cIAP1 depletion is a consequence of an impaired activation of NF-kB.

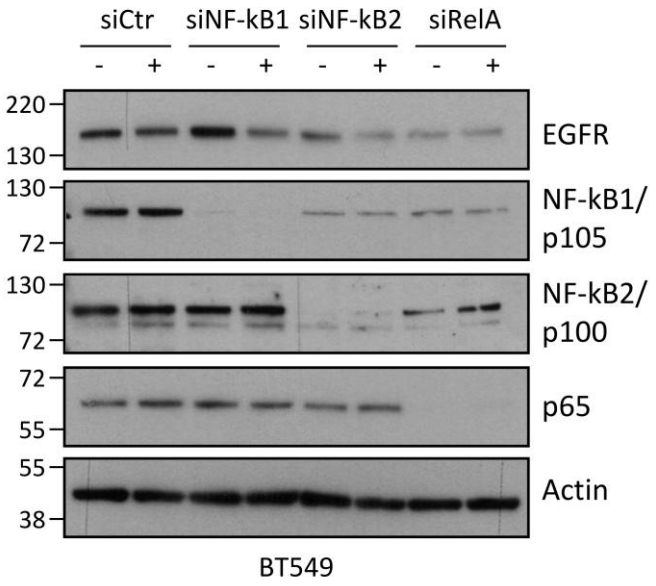

Figure 5.34 - cIAP1 supports EGFR transcriptionally in an NF-kB dependent manner. MDA-MB231 cells were transfected with a control siRNA or siRNAs specific for NF-kB1, NF-kB2 and RelA and analysed by western blot to detect the levels of endogenous EGFR.

5.9 cIAP1 promotes the EGFR/c-MET cross-talk

To understand more deeply the role of cIAP1 in the regulation of EGFR activity, I focused my attention also on c-MET, a receptor which is known to cross-talk with EGFR (Mueller *et al.*, 2010). Importantly, the synergism of EGFR and c-MET pathways is implicated in the development and progression of cancer favouring cell cycle progression, motility and metastasis. In order to examine whether cIAP1 also controls c-MET levels, BT549 were depleted for cIAP1 and stimulated with the c-MET specific ligand, HGF. Compared with

control cells, c-MET levels resulted stabilized by the loss of cIAP1 even after HGF stimulation (Figure 5.35A). Furthermore, in response to c-MET depletion, cIAP1 was significantly reduced (Figure 5.35B). Based on these preliminary data, I concluded that cIAP1 might represent a functional link also between EGFR and c-MET, and that cIAP1 levels are controlled by c-MET.

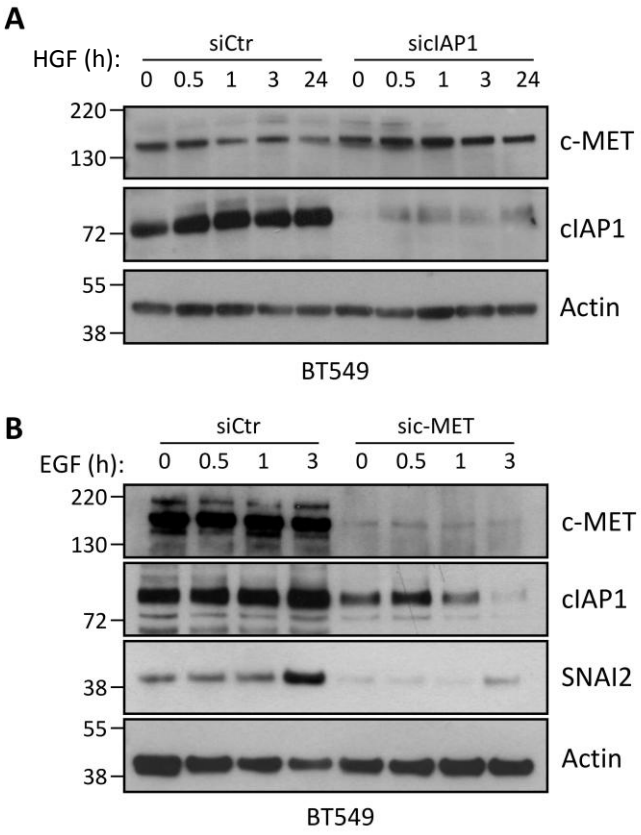

Figure 5.35 - Loss of cIAP1 induces c-MET stabilization. (A) BT549 cells were serum-starved overnight and stimulated with recombinant human HGF 20 ng/ml or with EGF 20 ng/ml (B) for the indicated time-points. Thereafter, cell lysates were collected and loaded for western blot with the indicated antibodies. Actin was used as a loading control.

5.10 Role of cIAP1 in the regulation of EMT-inducing factors

5.10.1 Targeting of cIAP1 increases, rather than inhibiting, ZEB1 expression

Having demonstrated that IAP-depletion perturbs the gene expression of SNAI2, which is an EMT-inducing factor (Phillips and Kuperwasser, 2014), I investigated if cIAP1 also controls the expression of other members involved in this process. Real-Time PCR performed both in MDA-MB231 and BT549 cells silenced for cIAP1 showed that this IAP did not support, but rather inhibited, the expression of another EMT-activator, named *ZEB1* (Lehmann *et al.*, 2016; Figure 5.36A). However, the expression of *TWIST1* (Garg, 2013) was slightly reduced in the absence of cIAP1 in BT549 cells, as shown in Figure 5.36B, and it was not detectable in MDA-MB231 cells, as confirmed by western blot analysis (Figure 5.36C). Therefore, cIAP1 regulates in different manners the diverse EMT mediators: on the one hand this IAP promotes SNAI2 expression, on the other hand is responsible for ZEB1 inhibition.

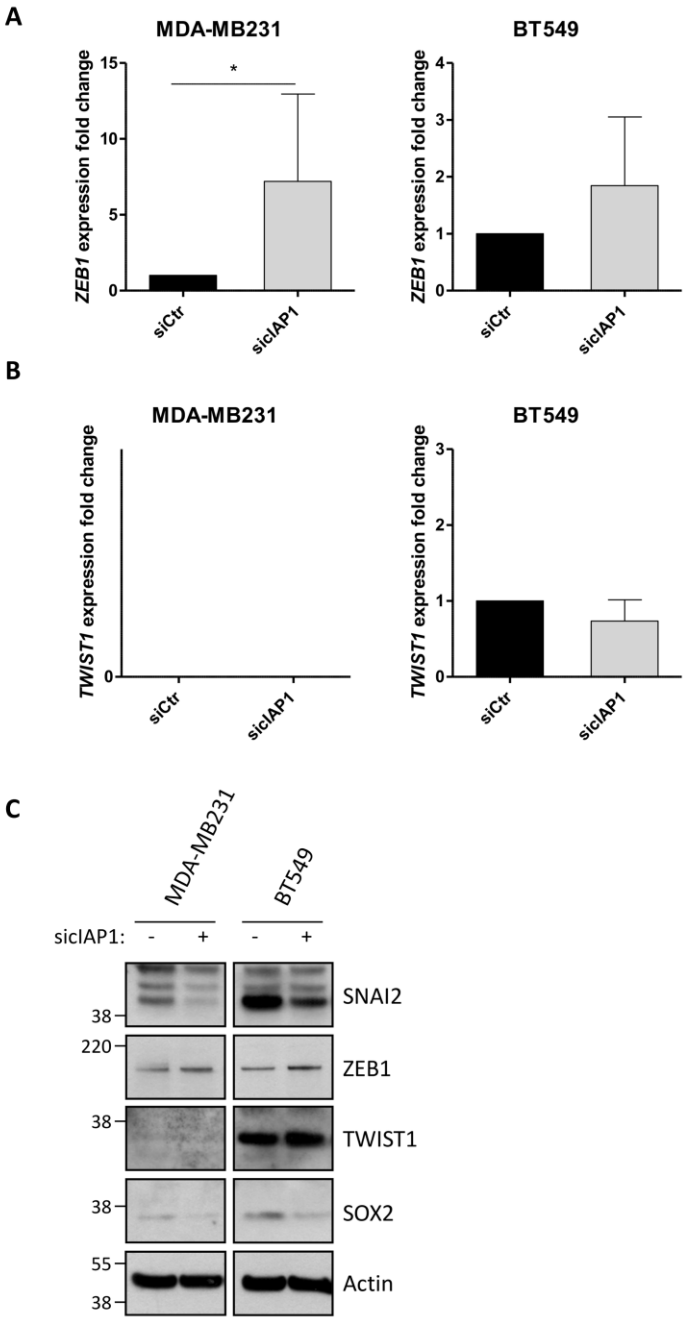

Figure 5.36 - cIAP1 inhibits the expression of ZEB1 EMT-regulator. (A) Real-Time PCR was performed as described in Figure 36 to quantify the levels of ZEB1 in MDA-MB231 and BT549 cells. MDA-MB231: siCtr *vs* sicIAP1 P = 0.0121; BT549: P = 0.0713; n = 5; Paired two-tailed t test. (B) TWIST1 mRNA was evaluated by Real-Time PCR performed in MDA-MB231 and BT549 cells. MDA-MB231 siCtr *vs* sicIAP1: not detectable; BT549 siCtr *vs* sicIAP1: P = 0.1023; n = 5; Paired two-tailed t test. (C) Western blot analysis was performed to detect SNAI2,

ZEB1, TWIST1 and SOX2 protein levels, in BT549 cell knocked-down for cIAP1 compared to Ctr. Actin was employed as a loading control.

5.10.2 SNAI2 down-regulation mediated by targeting of cIAP1 does not affect the epithelial marker E- Cadherin

To clarify whether cIAP1 regulates the capability of breast cancer cells to undergo EMT, MDA-MB231 cells were stably transduced using three specific shRNAs targeting SNAI2. As shown in Figure 5.37, SNAI2 was efficiently knocked-down in cells transduced with sequences B and C. Although SNAI2 expression has been reported to strongly correlate with the loss of E-Cadherin, which is an important EMT mediator (Vergara *et al.*, 2015), my results showed that cells depleted for SNAI2 failed to increase the epithelial marker E-Cadherin, but rather down-regulated it (Figure 5.37).

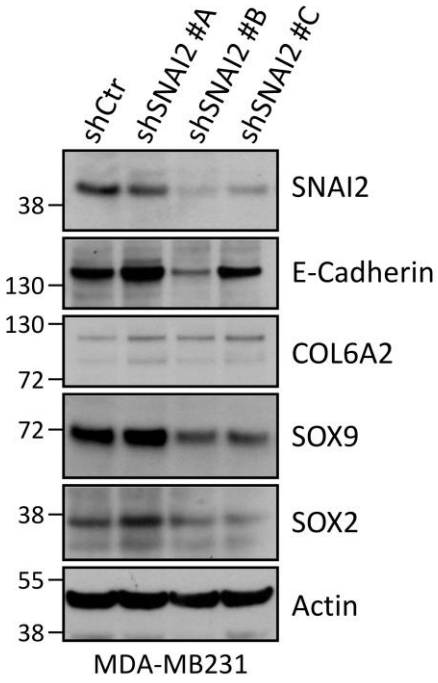

Figure 5.37 - Effect of SNAI2 depletion on different EMT targets. MDA-MB231 cells were stably silenced for SNAI2 employing lentiviral particles. Levels of E-Cadherin, Collagen 6A2 (COL6A2), SOX9 and SOX2 were

detected in shcIAP1 cells compared to the scrambled (shCtr), by western blot. SNAI2 and Actin levels are used as a transduction and loading control, respectively.

To further validate the previous finding, I studied the effect of cIAP1-mediated SNAI2 down-regulation on the expression of E-Cadherin and Vimentin, which is a mesenchymal marker (Figures 5.38A-B). By using the MDA-MB231 and BT549 models, I found that the depletion of cIAP1 inhibits E-Cadherin mRNA (Figure 5.38A), whereas the mesenchymal marker is not significantly modified (Figure 5.38B).

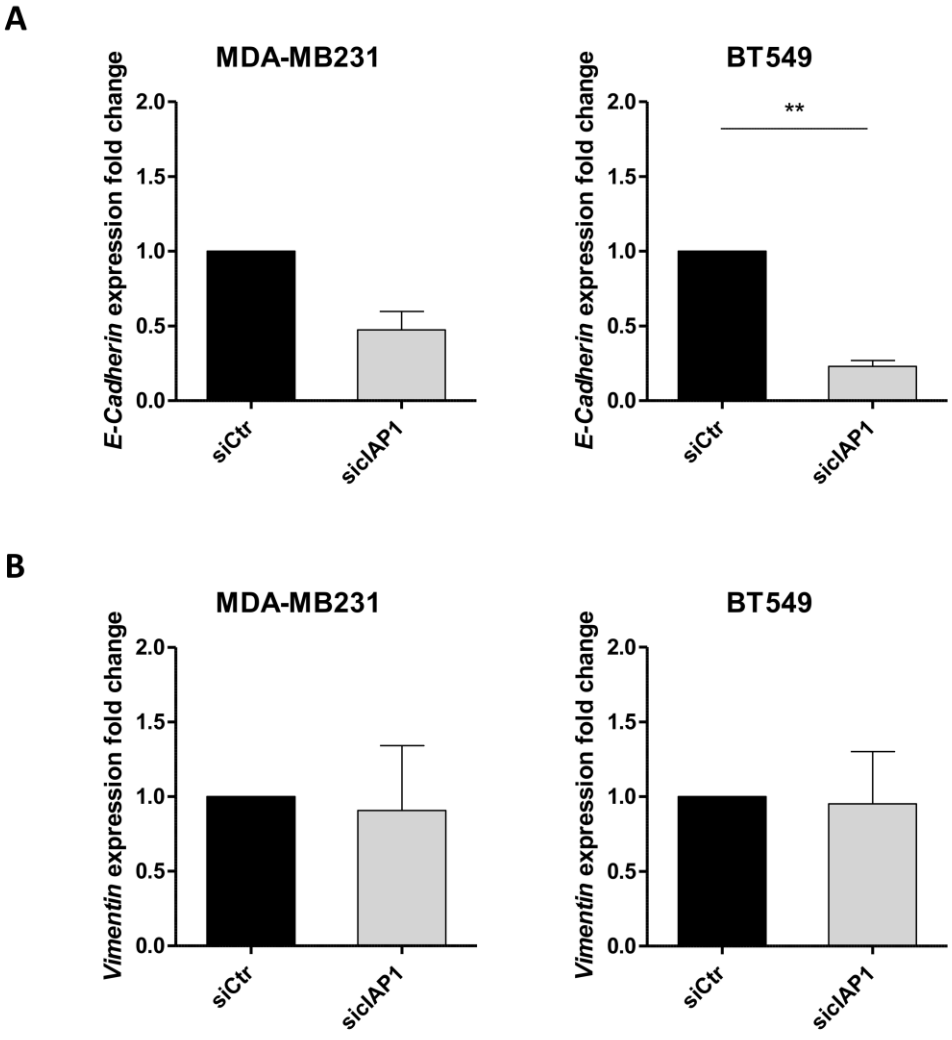

Figure 5.38 - cIAP1 depletion down-regulates rather than increases E-Cadherin expression. (A) Real-Time PCR performed in MDA-MB231 and BT549cells transfected with control or specific-cIAP1 siRNAs to assess E-

Cadherin expression levels. MDA-MB231 siCtr *vs* sicIAP1: P= 0.0688; BT549 siCtr *vs* sicIAP1: P= 0.0052, n = 3; Paired two-tailed t test. (B) Vimentin expression was evaluated as described above. MDA-MB231 siCtr *vs* sicIAP1: P= 0.5694; BT549 siCtr *vs* sicIAP1: P= 0.4219; n = 3; Paired two-tailed t test.

5.11 Targeting of SNAI2 affects the transcriptional regulators of cancer stem cells SOX2 and SOX9

Recently, it has been reported a correlation between SNAI2 and SOX9, which are key determinants of stem cell state (Luanpitpong *et al.*, 2016), supporting the role of SNAI2 as a key regulator of human breast cancer stem cells. In light of these findings, I evaluated the effect of SNAI2 depletion on the expression of two regulators SOX2 and 9, which are both implied in tumour progression and malignancy, thus linking stem/progenitor signalling with oncogenesis in cancer. My data supported the mechanistic relationship between SNAI2 and SOX2/9 that was confirmed employing MDA-MB231 cells stably silenced for SNAI2 (shSNAI2), which showed a strong decrease of both factors in the absence of SNAI2 (Figure 5.37). Furthermore, SOX2 down-regulation occurred also in MDA-MB231 and BT549 cells depleted for cIAP1 (Figure 5.36C), supporting the existence of a regulatory axis consisting of cIAP1/SNAI2/SOX2.

5.12 Effect of cIAP1/SNAI2 axis on SM83-up-regulated genes

Notably, GEP analysis revealed that SM83 treatment up-regulated several genes, including some matrix-remodelling (MMP9) or collagen-encoding (COL6A1 and COL6A2) genes (Figure 5.5), thereby suggesting a possible role of IAPs in the remodelling of tumour extracellular matrix (ECM). Importantly, Real-Time PCR showed that the up-regulation of *MMP9* observed in primary tumours collected from SM83-treated mice also occurred in

MDA-MB231 and BT549 cells depleted for cIAP1 (Figure 5.39A). Then, to identify if a link exists between SM83-mediated IAP depletion and the cIAP1-mediated SNAI2 down-regulation, I evaluated the effect of SNAI2 depletion on some of those genes resulted up-regulated by SM83 treatment. SNAI2 was stably depleted in MDA-MB231 cells using the most efficient shRNA targeting SNAI2 (shSNAI2 #B, Figure 5.37). Importantly, SNAI2 depletion enhances COL6A2 levels supporting the hypothesis that its up-regulation occurred as a result of SM83-mediated SNAI2 down-regulation (Figure 5.39B). Furthermore, shSNAI2 cells also showed an increase of PLEXIN-A1, another gene resulted up-regulated by SM83 administration. Collectively, these data document a possible role of the cIAP1/SNAI2 axis in the regulation of a number of genes found up-regulated in MDA-MB231 primary tumours collected from SM83-treated mice (Figure 5.5).

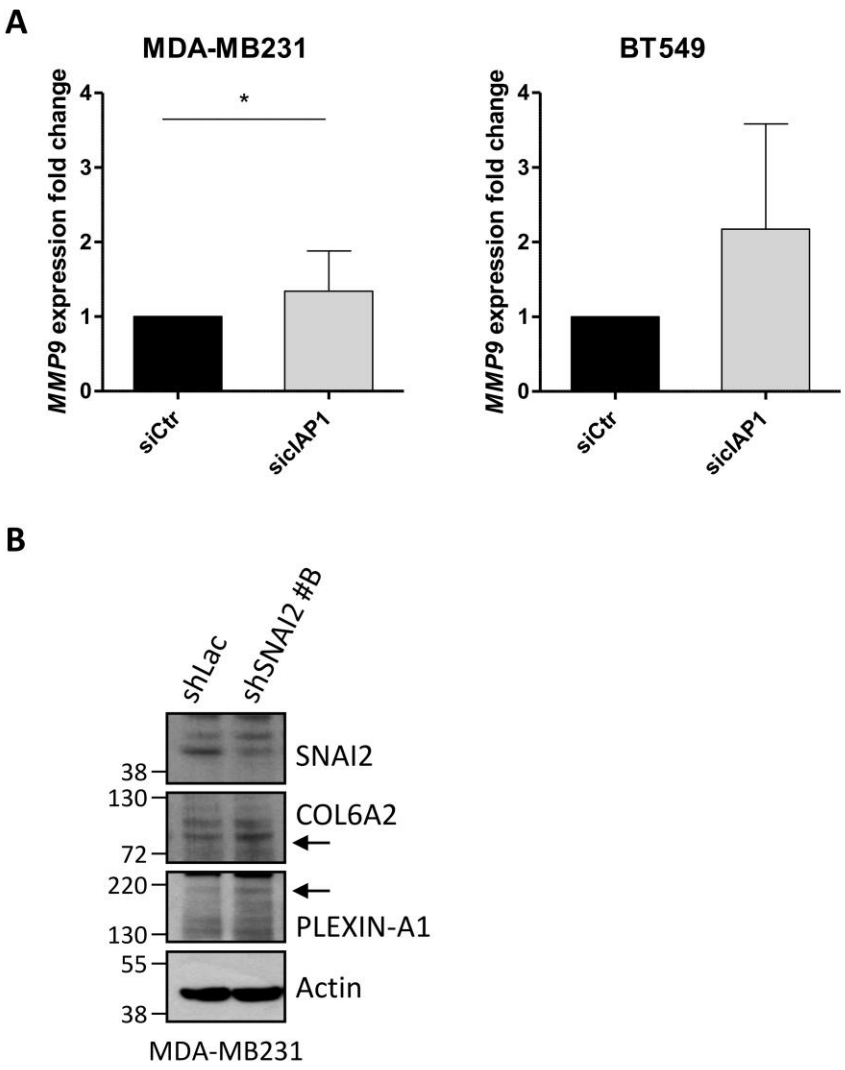

Figure 5.39 - SM83 administration increases the expression of several genes modulated by the cIAP1/SNAI2 axis. (A) Real-Time PCR performed in MDA-MB231 and BT549 cells silenced using Ctr or cIAP1-specific siRNAs to evaluate MMP9 expression. MDA-MB231: siCtr *vs* sicIAP1 P= 0.0312; BT549 siCtr *vs* sicIAP1: P= 0.2750; n = 3; Paired two-tailed t test. (B) Stable knock-down of SNAI2 in MDA-MB231 cells were analysed by western blot to assess the level of COL6A2 and PLEXIN-A1 protein levels.

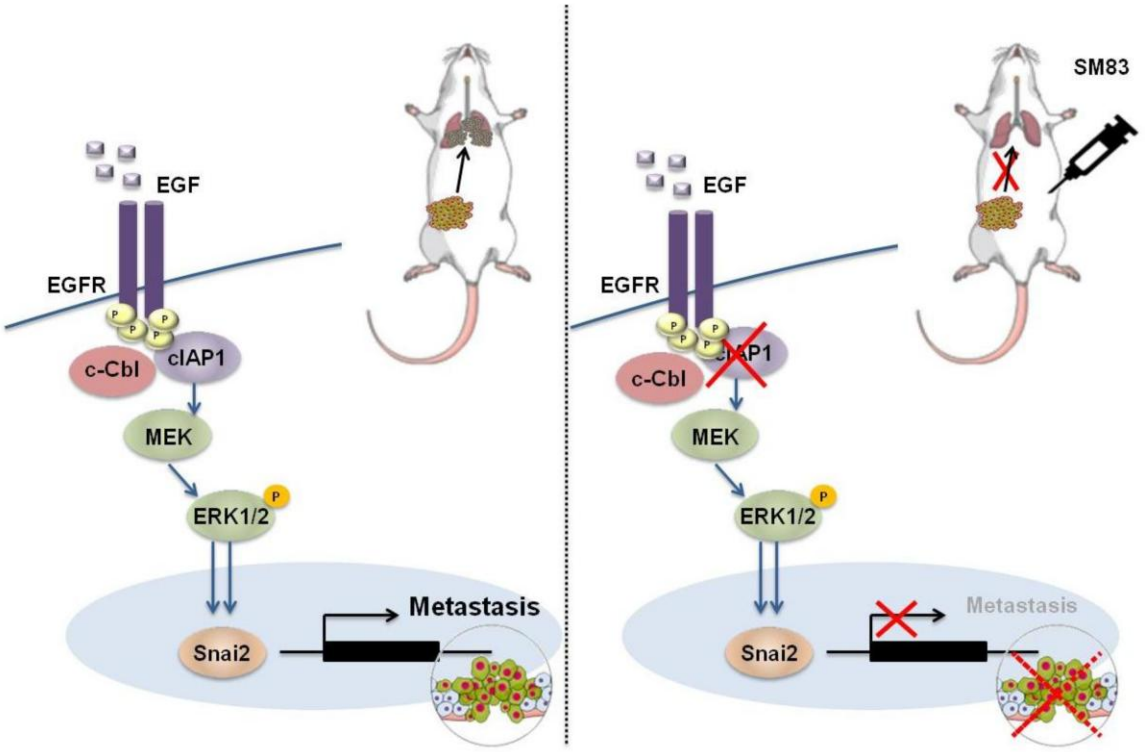

Figure 5.40 - Schematic of the proposed mechanism for SM83 anti-metastatic activity.

6 DISCUSSION

In this thesis, I focused on the comprehension of the role of IAPs in regulating the metastatic process. Beyond their largely described anti-apoptosis activity, IAPs act in the modulation of several receptor signalling pathways as being components of different receptor complexes, such as TNF-R superfamily members (Varfolomeev *et al.*, 2012) and pattern recognition receptors (PRRs; Vandenabeele and Bertrand, 2012). Therefore, IAP depletion not only triggers cancer cell death, but also perturbs numerous signalling pathways including MAPK and NF-kB cascades (Varfolomeev *et al.*, 2012). This eventually results in the modification of the expression of several genes (Chesi *et al.*, 2016; Beug *et al.*, 2017). Since 2007, our laboratory has contributed to the development of a class of compounds designed to inhibit IAPs and named Smac mimetics (SMs). Due to their capability to target well-known inhibitors of apoptosis and increase the cytotoxic activity of traditional chemotherapies, SMs have raised great interest for cancer therapy and their employment is currently tested in clinical trials (Fulda, 2014a). Initially considered as specific XIAP inhibitors (Sun *et al.*, 2007), SMs were later reported to target others members of IAP family, including cIAP1, cIAP2 and ML-IAP (Condon *et al.*, 2014; Cossu *et al.*, 2009a), thereby resulting in diverse activities and treatment outcomes. Nonetheless, the efficacy of SM administration is still limited and there is hence the need to fully understand the mechanisms of SM activity in order to define the right settings for their successful employment and to fully exploit the potential anti-cancer effect of this class of compounds.

In my PhD studies, I decided to investigate the role of IAPs in the metastatic process. To this purpose, I took advantage of a library of about 140 SMs, which has been developed

and characterized by our laboratory in collaboration with the University of Milan. All these compounds have been tested *in vitro* to evaluate their affinity for cIAP1, cIAP2 and XIAP, and to measure their cytotoxic activity in a panel of cancer cell lines. According to its *in vitro* activity and pharmacokinetic profile, I decided to perform my experiments with the compound SM83, also termed 9a in our previous publications (Lecis *et al.*, 2012; Lecis *et al.*, 2013). Notably, SM83 is a dimeric compound able to bind simultaneously with two BIR domains within the same IAP with nanomolar affinities. Indeed, *in vitro* tests have demonstrated a potent cytotoxic effect of SM83 in sensitive cancer cells and highlighted its capability to synergise with other compounds, thus enhancing their effect both *in vitro* and *in vivo* (Lecis *et al.*, 2012). By using our SM, in my PhD work, I provide evidence that the targeting of IAPs could be a possible approach to hinder the formation of metastasis (Figure 5.40).

My data show that SM83 administration reduces MDA-MB231 spontaneous lung metastasis (Minn *et al.*, 2005), in number and size. Although this result confirms that the targeting of IAPs can affect the aggressiveness of cancer cells as already shown by other groups, the underlying mechanism are still largely unknown. In fact, SM83 anti-metastasis effect may derive from many different mechanisms, such as direct killing of cancer cells, effect on tumour microenvironment (Lecis *et al.*, 2013) and the associated blood vessels (Witt *et al.*, 2015), as well as perturbation of gene expression. In my work, I mainly focused on the latter aspect. Indeed, by gene expression profiling of primary tumours collected from mice injected with SM83, I identified the genes whose expression was altered by treatment and suggested new potential insights regarding the role of IAPs in the metastatic process. Bioinformatic analysis showed that the *in vivo* administration of SM83 perturbed 65 genes in

primary MDA-MB231 nodules. Among the modified genes, 50 were up-regulated, whilst 15 down-regulated. In accordance with other studies and confirming the role of IAPs in the regulation of the NF-kB pathway, the majority of the perturbed genes are well-known targets of the NF-kB cascade (e.g. TRAF1, TRAF2, NFKBIA, NFKB2, RelB; Chesi *et al.*, 2016). To identify the genes that could play a role in the pro-metastatic activity of IAPs, I employed an unbiased approach by silencing all the genes down-regulated by SM83 treatment *in vivo* and performing wound-healing migration assays. In this way, I demonstrated that SNAI2 down-regulation, which was a consequence of IAP-targeting, results in the reduction of cell motility and, partially, cell proliferation. In light of this result, I hypothesised that the decrease of SNAI2 levels found in treated tumours could contribute to SM83 anti-metastatic potential. Importantly, among the SM83 targets, I identified cIAP1 as the sole responsible of SNAI2 expression since only its depletion, and not XIAP or cIAP2 targeting, inhibits SNAI2 expression. Wound healing assay performed using different cell lines (BT549, MCF10A *wt* or bearing EGFR mutation) further supported the idea that cIAP1 promotes cell motility in various tumour cell lines therefore suggesting that this is not a cell-type specific phenomenon.

Furthermore, my results suggest a novel role of cIAP1 as a regulator of SNAI2 expression, at least in breast cancer cells. As this transcription factor is a well-known promoter of metastasis and the *in vivo* experiments showed a massive down-regulation of SNAI2 upon SM83 administration, these findings could provide a novel link between IAPs and the metastatic process. In fact, although SM83 administration also reduces the volume of primary tumors, and this could obviously affect the number of circulating cancer cells, this effect is only marginal and it is unlikely to be sufficient to explain the dramatically reduction

of number and size of lung metastasis detected at the end of my experiments. Moreover, the down-regulation of SNAI2 could be itself a consequence of SM83 toxicity and I therefore investigated this point. Nonetheless, several experiments support that SNAI2 is a direct effect of cIAP1 targeting and not a toxicity side effect. In fact, not only SM83 administration, but also cIAP1 silencing (confirmed by using more than one sequence) resulted in SNAI2 reduction. These findings were also confirmed by pre-treating cells with pan-caspase or necroptosis inhibitors and validated in cell lines resistant to SM treatment at any dose.

Importantly, the capability of cIAP1 to induce SNAI2 expression via the modulation of NF-kB and MAPK signalling has been examined. First, I noticed that a negative correlation exists between SNAI2 and NF-kB2, which is a marker of activation of the non-canonical NF-KB pathway. Indeed, the triggering of the non-canonical NF-kB pathway in cells treated with SM83 or TWEAK, which is a specific activator of the non-canonical NF-kB pathway, is paralleled by SNAI2 down-regulation. However, further analyses revealed that the major effect on SNAI2 levels derives from the activation of ERK pathway (Chen *et al.*, 2009). Nevertheless, in our models the activation of ERK by TNF seemed to be only marginal and therefore I tested the effect of other stimuli responsible for activation of ERK.

To this end, a panel of TNBC cell lines has been employed, as these cells are highly aggressive and therefore represent a favourite model for dissecting the metastatic process. Of note, SNAI2 is often highly expressed in invasive tumours, such as aggressive TNBC cells, and it therefore very likely to play an important role in the aggressive phenotype of this tumour subtype. Importantly, the role of the transcription factor SNAI2 in the metastatic process has been widely described by several groups: SNAI2 was shown to promote

metastasis and to be linked to stem features, and its expression was demonstrated to be associated with poor prognosis and cancer relapse (Harney *et al.*, 2009). Interestingly, my work suggests that cIAP1 supports SNAI2 expression in a broadly valid manner, excluding a cell line-specific effect. Based on my results, cIAP1 could support TNBC aggressiveness by allowing the expression of high levels of the metastasis-promoting gene SNAI2. IAPs have been shown to favour the pro-metastatic features of cancer cells independently of their capability to control apoptosis (Mehrotra *et al.*, 2010) and therefore SM treatment could represent a possible approach to reduce SNAI2-mediated metastasis, through the reduction of its apical regulator cIAP1.

To check this hypothesis, I have studied the signalling cascade controlled by cIAP1 and focused on EGFR. In fact, hyper-activation and/or over-expression of EGFR characterize the TNBC subtype, which is also distinguished by high levels of SNAI2. Moreover, EGFR is known to control ERK signalling which promotes SNAI2 expression. Intriguingly, cIAP1 and cIAP2 have recently been shown to interact also with EGFRvIII, an oncogenic mutant expressed in glioblastoma multiforme (GBM; Puliyappadamba *et al.*, 2013), but the biological function of this interaction is still largely unknown. In our settings, I found that loss of cIAP1 inhibits SNAI2 expression upon EGFR stimulation because of prevention of ERK activation. Therefore, my data provide new insights on EGFR regulation and show for the first time the mechanistic role of cIAP1 in mediating the EGFR-dependent expression of SNAI2 via activation of ERK signalling pathway.

Moreover, I provide evidence that the loss of cIAP1 hinders EGFR activity also by reducing its levels. In fact, the silencing of cIAP1 causes a reduction of EGFR transcription.

These findings further support the employment of SMs in cancer treatment, sustaining the idea that SM-mediated IAP depletion may attenuate EGFR signalling also preventing its expression. Importantly, it is well documented that only a small percentage of cancer cell lines are killed by SMs in monotherapy (Petersen *et al.*, 2007), while the vast majority is resistant to these compounds independently of the dose employed. Nonetheless, later works have shown that also intrinsically sensitive cancer cells can acquire resistance and this depends on the up-regulation of LRIG1, which is triggered by SM treatment (Bai *et al.*, 2012). This ubiquitin-ligase is a negative regulator of several receptors, including EGFR (Miller *et al.*, 2008) and c-MET (Shattuck *et al.*, 2007). Therefore, I investigated whether LRIG1 up-regulation could be responsible, together with the reduction of gene expression, for the reduction of EGFR observed in cells depleted for cIAP1. Paradoxically, EGFR protein stability is increased in lack of cIAP1. I then investigated whether this IAP promotes EGFR degradation by direct ubiquitination or by controlling the levels of other EGFR inhibitors, such as c-CBL. In fact, numerous studies have defined the role of c-CBL as a regulator of ligand-induced down-regulation of EGFR (Duan *et al.*, 2003) and proved that c-CBL regulates the cascade of events that trigger EGFR endocytosis and degradation (Haglund and Dikic, 2012). Interestingly, c-CBL physically interacts with EGFR and binds to its phosphorylated Tyr-1045 residue. This event has been shown to be crucial for EGFR degradation. In fact, several works have shown that EGFR degradation is impaired when the Tyr-1045F mutant is ectopically expressed. My data showed that the Tyr-1045 residue is more phosphorylated and this should correlate with increased degradation of EGFR in the absence of cIAP1. As already mentioned, the reduction of cIAP1 was associated with increased stability of this receptor, rather than augmented degradation. Thus, I hypothesised that EGFR, even if correctly phosphorylated on Tyr-1045,

could be degraded less efficiently in the absence of cIAP1 due to a reduction of c-CBL levels or activity. In agreement with this notion, I found that the targeting of cIAP1 causes a slight reduction of both c-CBL total levels and of the portion recruited to the EGFR complex. This evidence could explain at least in part the enhanced stability of EGFR when IAPs are targeted. Altogether these results demonstrated that cIAP1 depletion on the one hand reduces the expression of EGFR gene and on the other increases its protein stability.

In my work, I also studied the role of Sprouty1, which is another negative regulator of EGFR. Despite its role as an EGFR inhibitor, loss of Sprouty1 has been recently reported to affect EGFR-mediated mesenchymal phenotype (He *et al.*, 2016). In particular, high expression of Sprouty1 in TNBCs has been reported to be responsible for their aggressive phenotype and promote cell migration, invasion, and anchorage-dependent and -independent growth. Accordingly, Sprouty1 depletion impairs the induction of SNAIL and SNAI2 expression by EGF, and this effect is associated with increased EGFR degradation in MDA-MB231 cells. Intriguingly, my work reveals a massive down-regulation of Sprouty1 in BT549 TNBC cells in the absence of cIAP1. This evidence may provide a further explanation regarding the mechanisms through which cIAP1 controls SNAI2 expression and the observed increase of EGFR stability in cells depleted for this IAP.

Previous reports support the importance of c-CBL-dependent ubiquitination for Clathrin-mediated endocytosis of EGFR (Jiang and Sorkin, 2003; Stang *et al.*, 2004), which is a mechanism for RTK signal attenuation, by allowing the removal of RTKs from the cell surface (Haglund and Dikic, 2012). Interestingly, by immunofluorescence analyses, I found that the EGFR foci detected in control cells upon stimulation with EGF are abrogated by cIAP1 knock-

down. This event is also accompanied by the reduction of Clathrin expression. Since the covalent addition of ubiquitin to the EGFR receptor represents the major signal which drives to EGFR endocytosis (Haglund *et al.*, 2003), I evaluated the effect of cIAP1 E3-ubiquitin ligase activity. The ectopic expression of an ubiquitin ligase inactive form of cIAP1 resulted in the increase of EGFR levels, supporting the notion that cIAP1 catalytic activity promotes the degradation of EGFR. Moreover, the observation that cIAP1 regulates also the levels of Clathrin suggests that this IAP tightly regulates the internalization process of EGFR.

After endocytosis, EGFR can follow two main trails: it can be recycled back to the cell surface or routed to late endosomes for lysosomal degradation. Although the importance of ubiquitination in targeting activated EGFR for degradation is established, emerging evidence show that EGFR can evade the ubiquitin-mediated degradation through the recycling to the plasma membrane. Hence, my data support the idea that cIAP1 directs EGFR to degradation while preventing its recycling after receptor endocytosis. Accordingly, by PLA, I show that the interaction between EGFR and the recycling endosome marker RAB11 is not affected by the absence of cIAP1. Conversely, loss of this IAP impairs the interaction between EGFR and late endosome marker RAB7, meaning reduced receptor degradation, in this condition.

Altogether, my thesis work supports the idea that SMs could be useful in clinics for the treatment of tumours expressing high levels of EGFR, either in monotherapy or in combination with EGFR-targeted therapy (Nakai *et al.*, 2016). Despite the fact that SNAI2 is a well-known regulator of metastasis and tumour aggressiveness, making it a promising target for anti-cancer treatment, SNAI2-specific therapy is still lacking. In fact, so far, only proof-of-concept molecules (Harney *et al.*, 2009) or compounds targeting SNAI2 interactors have been

described (Ferrari-Amorotti *et al.*, 2013). Therefore, the indirect inhibition of SNAI2 mediated by SM-induced IAP depletion could represent a novel strategy to prevent metastasis formation and resistance to therapy. Accordingly, a large amount of evidence supports the role of SNAI2 in promoting cell migration and dissemination to distal organs by reducing their stem-like properties and EMT features (Kao *et al.*, 2014).

EMT is responsible for several cellular processes, including cell proliferation, programmed cell death and differentiation during early developmental stages and tissue morphogenesis. Furthermore, many works showed a role of EMT, and of its mediator SNAI2, in metastasization even if recent works have questioned the importance of EMT in metastasis formation (Fischer *et al.*, 2015), also proposing a negligible role of SNAI2 in cancer cell metastatic properties (Ye *et al.*, 2015). Although transcription factors such as SNAIL, SNAI2, ZEB1, and ZEB2 are usually considered as being direct inhibitors of E-Cadherin, this point is still under debate (Cano *et al.*, 2000). In my, experiments, I found no correlation between SNAI2 and E-Cadherin, suggesting that SNAI2 does not regulate it in all conditions. This could be due to the different cellular contexts in which the experiments were performed. Intriguingly, in our settings, the depletion of cIAP1 resulted in the up-regulation of another mediator of EMT, i.e. ZEB1 (Lehmann *et al.*, 2016). This further support the notion that IAPs, and in particular cIAP1, play a role in EMT regulation and allows me to speculate that SNAI2 down-regulation is counteracted by the increase of ZEB1. E-Cadherin levels could therefore be determined by the balance between these two opposing effects.

SNAI2 also promotes CSC-like features contributing to the aggressive tumour phenotype (Luanpitpong *et al.*, 2016). In my study, I have confirmed that SNAI2 regulates

SOX2 and SOX9 showing that the knock-down of SNAI2 reduces SOX2 and 9 protein levels. This is consistent with the down-regulation of both SOX proteins that I have found in cIAP1-depleted cells, thus highlighting the importance of cIAP1/SNAI2 axis in the regulation of SOX2 and 9. Since CSCs are critical for dissemination of tumour cells and metastases formation (Luanpitpong *et al.*, 2016), the effect of cIAP1 depletion could result in an anti-metastasic effect mediated by the decrease of SNAI2 dependent effect on CSCs and not on the EMT process. However, further work is necessary to clarify the role of cIAP1/SNAI2 regulatory axis in breast CSCs in order to evaluate whether its targeting could represent a therapeutic opportunity for advanced and recurrent cancers.

Finally, I investigated whether the up-regulation of PLEXIN-A1 and COLA6A2 genes in MDA-MB231 nodules revealed by GEP analysis may be linked to the SM-mediated down-regulation of SNAI2. In agreement with this hypothesis, my results show that cells stably depleted for SNAI2 increase PLEXIN-A1 and COL6A2 protein levels, indicating them as SNAI2 targets. The study of SNAI2 down-stream pathway represents another important field to be explored in order to evaluate the effect of cIAP1 targeting-mediated SNAI2 inhibition. For instance, the up-regulation of COL6A2 could influence tumour matrix remodelling. Conversely, the role of PLEXIN-A1 is poorly studied. It belongs to the PLEXIN receptor family and can form complexes with RTKs, such as ErbB2, VEGFR2 or c-MET, even if the molecular mechanisms controlling these multimeric receptor complexes are poorly understood (Rizzolio and Tamagnone, 2007). These receptor complexes are diversely expressed in different phases of tumour progression and invasive growth, thereby leading to the formation of signalling complexes eliciting differential (and potentially antagonistic)

pathways. Therefore, SMs could represent a new tool to investigate their regulation and activity in tumour cells.

6.1 Conclusions and future research

In my PhD study, cIAP1 has been defined as a crucial determinant of the EGFR/SNAI2 axis, and this finding has been validated in a panel of breast cancer cell lines, even bearing different mutations, and in normal epithelial cells, parental or with active EGFR. Moreover, my study supports the importance of IAPs, particularly of cIAP1, in tumour dissemination and contributes to the knowledge of the mechanisms underlying cancer cell metastatic potential.

The important roles of EGFR in several cancer cell processes suggest that its targeting may provide a strategy to reduce tumour aggressiveness. Therefore, several approaches have been proposed to target EGFR, whose efficacy is frustrated by various mechanisms of resistance both primary and acquired: EGFR mutation, aberrant activation of down-stream molecules, EMT and redundant kinase signalling pathway (Luo and Fu, 2014). In the last case, a well-documented mechanism of resistance to the treatment with EGFR inhibitors is c-MET activation (Boccaccio *et al.*, 2014). Accordingly, several studies provided the proof of principle that the combination of EGFR and c-MET inhibitors could be beneficial for the treatment of those types of cancer characterized by EGFR hyper-activity. In this regard, I have started to evaluate the effect of IAP targeting also on c-MET activity aiming to investigate a possible role of cIAP1 in mediating EGFR and c-MET cross-talk. Of note, my preliminary results indicate a stabilization of c-MET in cells depleted for cIAP1 and this event could be a consequence of decreased EGFR levels. Further experiments should be performed to elucidate the role of cIAP1 in this complex scenario to identify the most efficient

combination treatment capable to reduce the mechanisms of resistance to EGFR-directed treatment and to evaluate the efficacy of SMs in clinics.

Moreover, recent findings show that SMs not only target cancer cells, but also affects a number of immune cell populations including natural killers, myeloid cells and macrophages (Lecis *et al.*, 2013). In my work, the capability of SM83 to perturb the tumour microenvironment has not been investigated, but the comprehension of this phenomenon is of crucial importance. In this regard, my preliminary data support the notion that SM administration could affect tumour microenvironment through the up-regulation of genes encoding for ECM components. For instance, in MDA-MB231 nodules collected from NOD/SCID mice treated with SM83, I found an increase of MMP9 expression along with COL6A2 up-regulation. Of note, matrix degradation is not the only activity of MMP9, which also regulates the availability of pro-inflammatory cytokines, chemokines and other proteins therefore regulating several aspects of inflammation and immunity. Therefore, the investigation of how IAPs influence the cross-talk between tumour cells and tumour microenviroment, including stromal cells, ECM and immune cells, is crucial to develop new therapeutic approaches.

7 LIST OF ABBREVIATIONS

ANK	Ankyrin repeats motif
APAF-1	Apoptotic protease activating factor 1
ATP	Adenosine triphosphate
AVPI	Alanine-Valine-Proline-Isoleucine
BAFFR	B-cell activation factor
BAK	Bcl-2 homologous antagonist/killer
BAX	Bcl-2-associated X protein
BCA	Bicinchoninic acid
BCL-2	B-cell lymphoma-2
BH3	Bcl-2 homology domain 3
BID	BH3 interacting-domain death agonist
BIR	Baculoviral IAP repeat
BMP	Bone morphogenetic protein
BRCA	Breast cancer susceptibility genes
BSA	Bovine serum albumin
CARD	Caspase recruitment domain
Caspases	Cysteine-dependent aspartate-directed proteases
cDNA	Complementary DNA
CHX	Cycloheximide
cIAP	Cellular IAP
CIE	Clathrin-independent endocytosis
CK	Cytokeratin
CLQ	Chloroquine
CME	Clathrin-mediated endocytosis
CSC	Cancer stem-like cell
DAPI	4',6-Diamidino-2-phenylindole dihydrochloride
DED	Death effector domain
DD	Death domains
DISC	Death inducing signaling complex
DMEM	Dulbecco's Modified Eagle's medium
DMSO	Dimethylsulfoxide
DNA	Deoxyribonucleic acid
DNTPs	Deoxynucleotide triphosphates
DR	Death receptor
ECL	Enhanced chemiluminescence
EDTA	Ethylenediaminetetraacetic acid
EGF	Epidermal growth factor
EGFR	Epidermal growth factor receptor
EMA	European Medicines Agency
EMT	Epithelial to mesenchymal transition
ER	Estrogen Receptor
ERK	Extracellular signal-regulated kinase
FADD	Fas-associated protein with death domain
FBS	Fetal bovine serum
FDA	Food and Drug Administration
FDR	False Discovery Rate
FGF	Fibroblast growth factor
GEP	Gene expression profiling
HER2	Human epidermal growth factor receptor 2
HEPES	N'-2-hydroxyethylpiperazine-N'-2 ethanesulphonic acid
HGF	Hepatocyte growth factor

HME	Human mammary epithelial
IAP	Inhibitor of apoptosis protein
IBM	IAP binding motif
ICAD	Inhibitor of caspase activated DNase
ICAM1	Intercellular adhesion molecule 1
IF	Immunofluorescence
IHC	Immunohistochemistry
IkB	Inhibitor of NF-kB
IKK	Inhibitor of NF-kB kinase
IL	Interleukin
IL-1R	Interleukin-1 receptor
ip	Intraperitoneal
iv	Intravenous
JNK/SAPK	c-Jun N-terminal kinase/stress-activated protein kinase
LPS	Lipopolysaccharides
LRIG1	Leucine-rich repeats and immunoglobulin-like domains protein 1
LTβR	Lymphtoxin β-receptor
LZ	Leucin-zipper-like domain
MAPK	Mitogen-activated protein kinases
MCL-1	Induced myeloid leukemia cell differentiation protein
mCRC	Metastatic colorectal cancer
MEK	MAPK/ERK kinase
ML	Mesenchymal-like
ML-IAP	Melanoma-IAP
MMP9	Matrix metallopeptidase-9
MOMP	Mitochondrial outer membrane permeabilization
MSL	Mesenchymal stem–like
mRNA	Messenger RNA
mTNF	Membrane TNF
NAIP	Neuronal-IAP
NEAA	Non essential amino acids
NEMO	NF-kB essential modulator
NF-kB	Nuclear factor kappa-light-chain-enhancer of activated B cells
NIK	NF-kB inducing kinase
NOD	Nucleotide-binding oligomerization
NOD/SCID	Non-obese diabetic/severe combined immunodeficiency disease
NSCLC	Non-small cell lung cancer
PARP	Poly-ADP ribose polymerase
Pen/Strep	Penicillin, Streptomycin
PBS	Phosphate-buffered saline
PBS-T	PBS-Tween
PCR	Polymerase chain reaction
PI3K	Phosphatidylinositol 4,5-bisphosphate 3-kinase
PLA	Proximity ligation assay
PRRs	Pattern recognition receptors
PR	Progesterone receptor
PVDF	Polyvinylidene difluoride
Rac1	Ras related C3 botulinum toxin substrate
RANK	Receptor activator for nuclear factor kappa B
RING	Really interesting new gene
RHD	Rel homology domain
RIP1	Receptor interacting protein 1
RNA	Ribonucleic acid
rpm	Revolution per minute
RPMI-1640	Roswell Park Memorial Institute-1640

RT	Room temperature
RTK	Receptor tyrosine kinases
sc	Subcutaneous
SDS	Sodium dodecyl sulfate
siRNA	Short interfering (siRNA)
Smac/DIABLO	Second mitochondria-derived activator of caspase/direct inhibitor of apoptosis-binding protein with low pI
SM	Smac mimetic
sTNF	Soluble TNF
TA	Transcription activation domain
TAB	TGF-beta-activated kinase 1-binding protein 3
TAK	TNF-associated kinase
TCGA	The Cancer Genome Atlas
TGF	Transforming growth factor
TIM	TRAF-interacting motif
TLR	Toll-like receptors
TNBC	Triple negative breast cancer
TNF	Tumour necrosis factor
TNF-R	TNF-receptor
TNF-RS	TNF-R superfamily
TRADD	TNF-R1-associated death domain
TRAF	TNF-receptor-associating factors
TRAIL	TNF-related apoptosis-inducing ligand
TV	Tumour volume
TWEAK	TNF-related weak inducer of apoptosis
UBA	Ubiquitin-associated domain
XIAP	X-linked IAP
wt	Wild-type
ZEB	Zinc-finger E box-binding homeobox

8 LIST OF FIGURES

9 LIST OF TABLES

10 REFERENCES

Acloque, H., Thiery, J. P. and Nieto, M. A. (2008). The physiology and pathology of the EMT. Meeting on the epithelial-mesenchymal transition. EMBO Rep. *4*, 322-326.

Adeyinka, A., Nui, Y., Cherlet, T., Snell, L., Watson, P. H. and Murphy, L. C. (2002). Activated mitogen-activated protein kinase expression during human breast tumorigenesis and breast cancer progression. Clin. Cancer Res. *6*, 1747-1753.

Ahn, S. G., Kim, S. J., Kim, C. and Jeong, J. (2016). Molecular Classification of Triple-Negative Breast Cancer. J. Breast Cancer. *3*, 223-230.

Allensworth, J. L., Sauer, S. J., Lyerly, H. K., Morse, M. A. and Devi, G. R. (2013). Smac mimetic Birinapant induces apoptosis and enhances TRAIL potency in inflammatory breast cancer cells in an IAP-dependent and TNF-alpha-independent mechanism. Breast Cancer Res. Treat. *2*, 359-371.

Alluri, P. and Newman, L. A. (2014). Basal-like and triple-negative breast cancers: searching for positives among many negatives. Surg. Oncol. Clin. N. Am. *3*, 567-577.

Amaravadi, R., Schilder, R., Dy, G., Ma, W., Fetterly, G., Weng, D., Graham, A., Burns, J., Chunduru, S. and Condon, S. (2011). Phase 1 study of the Smac mimetic TL32711 in adult subjects with advanced solid tumors and lymphoma to evaluate safety, pharmacokinetics, pharmacodynamics and antitumor activity. Cancer Res. 71(8 Suppl):Abstract nr LB-406.

Ashkenazi, A. and Dixit, V. M. (1998). Death receptors: signaling and modulation. Science *5381*, 1305-1308.

Ashkenazi, A., Fairbrother, W. J., Leverson, J. D. and Souers, A. J. (2017). From basic apoptosis discoveries to advanced selective BCL-2 family inhibitors. Nat. Rev. Drug Discov. *4*, 273-284.

Bae, G. Y., Choi, S. J., Lee, J. S., Jo, J., Lee, J., Kim, J. and Cha, H. J. (2013). Loss of E-cadherin activates EGFR-MEK/ERK signaling, which promotes invasion via the ZEB1/MMP2 axis in non-small cell lung cancer. Oncotarget *12*, 2512-2522.

Bai, L., McEachern, D., Yang, C. Y., Lu, J., Sun, H. and Wang, S. (2012). LRIG1 modulates cancer cell sensitivity to Smac mimetics by regulating TNFalpha expression and receptor tyrosine kinase signaling. Cancer Res. *5*, 1229-38.

Bai, L., Smith, D. C. and Wang, S. (2014). Small-molecule SMAC mimetics as new cancer therapeutics. Pharmacol. Ther. *1*, 82-95.

Bailey, C. K., Mittal, M. K., Misra, S. and Chaudhuri, G. (2012). High motility of triple-negative breast cancer cells is due to repression of plakoglobin gene by metastasis modulator protein SLUG. J. Biol. Chem. *23*, 19472-19486.

Barbieri, M. A., Fernandez-Pol, S., Hunker, C., Horazdovsky, B. H. and Stahl, P. D. (2004). Role of rab5 in EGF receptor-mediated signal transduction. Eur. J. Cell Biol. *6*, 305-314.

Barnhart, B. C., Alappat, E. C. and Peter, M. E. (2003). The CD95 type I/type II model. Semin. Immunol. *3*, 185-193.

Barrallo-Gimeno, A. and Nieto, M. A. (2005). The Snail genes as inducers of cell movement and survival: implications in development and cancer. Development *14*, 3151-3161.

Bartholomeusz, C., Gonzalez-Angulo, A. M., Liu, P., Hayashi, N., Lluch, A., Ferrer-Lozano, J. and Hortobagyi, G. N. (2012). High ERK protein expression levels correlate with shorter survival in triple-negative breast cancer patients. Oncologist *6*, 766-774.

Batlle, E., Sancho, E., Franci, C., Dominguez, D., Monfar, M., Baulida, J. and Garcia De Herreros, A. (2000). The transcription factor snail is a repressor of E-cadherin gene expression in epithelial tumour cells. Nat. Cell Biol. *2*, 84-89.

Beug, S. T., Beauregard, C. E., Healy, C., Sanda, T., St-Jean, M., Chabot, J., Walker, D. E., Mohan, A., Earl, N., Lun, X., Senger, D. L., Robbins, S. M., Staeheli, P., Forsyth, P. A., Alain, T., LaCasse, E. C. and Korneluk, R. G. (2017). Smac mimetics synergize with immune checkpoint inhibitors to promote tumour immunity against glioblastoma. Nat. Commun., 10.1038/ncomms14278.

Birnbaum, M. J., Clem, R. J. and Miller, L. K. (1994). An apoptosis-inhibiting gene from a nuclear polyhedrosis virus encoding a polypeptide with Cys/His sequence motifs. J. Virol. *4*, 2521-2528.

Boccaccio, C., Luraghi, P. and Comoglio, P. M. (2014). MET-mediated resistance to EGFR inhibitors: an old liaison rooted in colorectal cancer stem cells. Cancer Res. *14*, 3647-3651.

Bocker, W., Docheva, D., Prall, W. C., Egea, V., Pappou, E., Rossmann, O., Popov, C., Mutschler, W., Ries, C. and Schieker, M. (2008). IKK-2 is required for TNF-alpha-induced invasion and proliferation of human mesenchymal stem cells. J. Mol. Med. (Berl) *10*, 1183-1192.

Borghi, A., Verstrepen, L. and Beyaert, R. (2016). TRAF2 multitasking in TNF receptor-induced signaling to NF-kappaB, MAP kinases and cell death. Biochem. Pharmacol., 1-10.

Cabal-Hierro, L. and Lazo, P. S. (2012). Signal transduction by tumor necrosis factor receptors. Cell. Signal. *6*, 1297-1305.

Cano, A., Perez-Moreno, M. A., Rodrigo, I., Locascio, A., Blanco, M. J., del Barrio, M. G., Portillo, F. and Nieto, M. A. (2000). The transcription factor snail controls epithelial-mesenchymal transitions by repressing E-cadherin expression. Nat. Cell Biol. *2*, 76-83.

Ceresa, B. P. (2006). Regulation of EGFR endocytic trafficking by rab proteins. Histol. Histopathol. *9*, 987-993.

Chaffer, C. L. and Weinberg, R. A. (2011). A perspective on cancer cell metastasis. Science *6024*, 1559-1564.

Chai, J., Shiozaki, E., Srinivasula, S. M., Wu, Q., Dataa, P., Alnemri, E. S. and Shi, Y. (2001). Structural Basis of Caspase-7 Inhibition by XIAP *5*, 769-780.

Chang, T. H., Tsai, M. F., Su, K. Y., Wu, S. G., Huang, C. P., Yu, S. L., Yu, Y. L., Lan, C. C., Yang, C. H., Lin, S. B., Wu, C. P., Shih, J. Y. and Yang, P. C. (2011). Slug confers resistance to the epidermal growth factor receptor tyrosine kinase inhibitor. Am. J. Respir. Crit. Care Med. *8*, 1071-1079.

Che, X., Yang, D., Zong, H., Wang, J., Li, X., Chen, F., Chen, X. and Song, X. (2012). Nuclear cIAP1 overexpression is a tumor stage- and grade-independent predictor of poor prognosis in human bladder cancer patients. Urol. Oncol. *4*, 450-456.

Chen, H., Zhu, G., Li, Y., Padia, R. N., Dong, Z., Pan, Z. K., Liu, K. and Huang, S. (2009). Extracellular signal-regulated kinase signaling pathway regulates breast cancer cell migration by maintaining slug expression. Cancer Res. *24*, 9228-9235.

Chen, Y. Q., Sengchanthalangsy, L. L., Hackett, A. and Ghosh, G. (2000). NF-kappaB p65 (RelA) homodimer uses distinct mechanisms to recognize DNA targets. Structure *4*, 419-428.

Chen, Z. J. (2012). Ubiquitination in signaling to and activation of IKK. Immunol. Rev. *1*, 95-106.

Chesi, M., Mirza, N. N., Garbitt, V. M., Sharik, M. E., Dueck, A. C., Asmann, Y. W., Akhmetzyanova, I., Kosiorek, H. E., Calcinotto, A., Riggs, D. L., Keane, N., Ahmann, G. J., Morrison, K. M., Fonseca, R., Lacy, M. Q., Dingli, D., Kumar, S.K., Ailawadhi, S., Dispenzieri, A., Buadi, F., Gertz, M.A., Reeder, C. B., Lin, Y., Chanan-Khan, A. A., Stewart, A.K., Fooksman, D. and Bergsagel, P. L. (2016). IAP antagonists induce anti-tumor immunity in multiple myeloma. Nat. Med. *12*, 1411-1420.

Chimge, N. O. and Frenkel, B. (2013). The RUNX family in breast cancer: relationships with estrogen signaling. Oncogene *17*, 2121-2130.

Choi, Y. E., Butterworth, M., Malladi, S., Duckett, C. S., Cohen, G. M. and Bratton, S. B. (2009). The E3 ubiquitin ligase cIAP1 binds and ubiquitinates caspase-3 and -7 via unique mechanisms at distinct steps in their processing. J. Biol. Chem. *19*, 12772-12782.

Cildir, G., Low, K. C. and Tergaonkar, V. (2016). Noncanonical NF-kappaB Signaling in Health and Disease. Trends Mol. Med. *5*, 414-429.

Condon, S. M. *et al.* (2014). Birinapant, a smac-mimetic with improved tolerability for the treatment of solid tumors and hematological malignancies. J. Med. Chem. *9*, 3666-3677.

Corso, S. and Giordano, S. (2013). Cell-autonomous and non-cell-autonomous mechanisms of HGF/MET-driven resistance to targeted therapies: from basic research to a clinical perspective. Cancer. Discov. *9*, 978-992.

Cossu, F., Mastrangelo, E., Milani, M., Sorrentino, G., Lecis, D., Delia, D., Manzoni, L., Seneci, P., Scolastico, C. and Bolognesi, M. (2009a). Designing Smac-mimetics as antagonists of XIAP, cIAP1, and cIAP2. Biochem. Biophys. Res. Commun. *2*, 162-167.

Cossu, F., Milani, M., Mastrangelo, E., Vachette, P., Servida, F., Lecis, D., Canevari, G., Delia, D., Drago, C., Rizzo, V., Manzoni, L., Seneci, P., Scolastico, C. and Bolognesi, M. (2009b). Structural Basis for Bivalent Smac-Mimetics Recognition in the IAP Protein Family. J. Mol. Biol. *3*, 630-644.

Cossu, F., Milani, M., Vachette, P., Malvezzi, F., Grassi, S., Lecis, D., Delia, D., Drago, C., Seneci, P., Bolognesi, M. and Mastrangelo, E. (2012). Structural insight into inhibitor of apoptosis proteins recognition by a potent divalent smac-mimetic. PLoS One *11*, e49527.

Cullis, D. N., Philip, B., Baleja, J. D. and Feig, L. A. (2002). Rab11-FIP2, an adaptor protein connecting cellular components involved in internalization and recycling of epidermal growth factor receptors. J. Biol. Chem. *51*, 49158-49166.

Damgaard, R. B. and Gyrd-Hansen, M. (2011). Inhibitor of apoptosis (IAP) proteins in regulation of inflammation and innate immunity. Discov. Med. *58*, 221-231.

Danial, N. N. and Korsmeyer, S. J. (2004). Cell death: critical control points. Cell *2*, 205-219.

Darding, M., Feltham, R., Tenev, T., Bianchi, K., Benetatos, C., Silke, J. and Meier, P. (2011). Molecular determinants of Smac mimetic induced degradation of cIAP1 and cIAP2. Cell Death Differ. *8*, 1376-1386.

Datta, R., Oki, E., Endo, K., Biedermann, V., Ren, J. and Kufe, D. (2000). XIAP Regulates DNA Damage-induced Apoptosis Downstream of Caspase-9 Cleavage. J. Biol. Chem. ; J. Biol. Chem. *41*, 31733-31738.

de Almagro, M. C. and Vucic, D. (2012). The inhibitor of apoptosis (IAP) proteins are critical regulators of signaling pathways and targets for anti-cancer therapy. Exp. Oncol. *3*, 200-211.

Degterev, A. and Yuan, J. (2008). Expansion and evolution of cell death programmes. Nat. Rev. Mol. Cell Biol. *5*, 378-390.

Dempsey, P. W., Doyle, S. E., He, J. Q. and Cheng, G. (2003). The signaling adaptors and pathways activated by TNF superfamily. Cytokine Growth Factor Rev. *3-4*, 193-209.

Dhillon, A. S., Hagan, S., Rath, O. and Kolch, W. (2007). MAP kinase signalling pathways in cancer. Oncogene *22*, 3279-3290.

Dickens, L. S., Boyd, R. S., Jukes-Jones, R., Hughes, M. A., Robinson, G. L., Fairall, L., Schwabe, J. W., Cain, K. and Macfarlane, M. (2012). A death effector domain chain DISC model reveals a crucial role for caspase-8 chain assembly in mediating apoptotic cell death. Mol. Cell *2*, 291-305.

Du, P., Kibbe, W. A. and Lin, S. M. (2008). lumi: a pipeline for processing Illumina microarray. Bioinformatics *13*, 1547-1548.

Duan, L., Miura, Y., Dimri, M., Majumder, B., Dodge, I. L., Reddi, A. L., Ghosh, A., Fernandes, N., Zhou, P., Mullane-Robinson, K., Rao, N., Donoghue, S., Rogers, R. A., Bowtell, D., Naramura, M., Gu, H., Band, V. and Band, H. (2003). Cbl-mediated ubiquitinylation is required for lysosomal sorting of epidermal growth factor receptor but is dispensable for endocytosis. J. Biol. Chem. *31*, 28950-28960.

Dunn, K. L., Espino, P. S., Drobic, B., He, S. and Davie, J. R. (2005). The Ras-MAPK signal transduction pathway, cancer and chromatin remodeling. Biochem. Cell Biol. *1*, 1-14.

Eckelman, B. P., Drag, M., Snipas, S. J. and Salvesen, G. S. (2008). The mechanism of peptide-binding specificity of IAP BIR domains. Cell Death Differ. *5*, 920-928.

Eckelman, B. P., Salvesen, G. S. and Scott, F. L. (2006). Human inhibitor of apoptosis proteins: why XIAP is the black sheep of the family. EMBO Rep. *10*, 988-994.

Emmerich, C. H., Schmukle, A. C., Haas, T. L., Gerlach, B., Cordier, S. M., Rieser, E. and Walczak, H. (2011). The linear ubiquitin chain assembly complex forms part of the TNF-R1 signalling complex and is required for effective TNF-induced gene induction and prevents TNF-induced apoptosis. Adv. Exp. Med. Biol., 115-126.

Eralp, Y., Derin, D., Ozluk, Y., Yavuz, E., Guney, N., Saip, P., Muslumanoglu, M., Igci, A., Kücücük S., Dincer, M., Aydiner, A. and Topuz E. (2008). MAPK overexpression is associated with anthracycline resistance and increased risk for recurrence in patients with triple-negative breast cancer. Ann. Oncol. *4*, 669-674.

Favaloro, B., Allocati, N., Graziano, V., Di Ilio, C. and De Laurenzi, V. (2012). Role of apoptosis in disease. Aging (Albany NY) *5*, 330-349.

Feltham, R., Bettjeman, B., Budhidarmo, R., Mace, P. D., Shirley, S., Condon, S. M., Chunduru, S. K., McKinlay, M. A., Vaux, D. L., Silke, J. and Day, C. L. (2011). SMAC-mimetics activate the E3 ligase activity of cIAP1 by promoting RING dimerisation. J. Biol. Chem. *19*, 17015-17028.

Ferrari-Amorotti, G., Chiodoni, C., Shen, F., Cattelani, S., Soliera, A.R., Manzotti. G., Grisendi, G., Dominici, M., Rivasi, F., Colombo, M. P., Fatatis, A. and Calabretta, B. (2014). Suppression of invasion and metastasis of triple-negative breast cancer lines by pharmacological or genetic inhibition of slug activity. Neoplasia *12*, 1047-1058.

Ferrari-Amorotti, G., Fragliasso, V., Esteki, R., Prudente, Z., Soliera, A.R., Cattelani, S., Manzotti, G., Grisendi, G., Dominici, M., Pieraccioli, M., Raschellà, G., Chiodoni, C., Colombo, M. P. and Calabretta, B. (2013). Inhibiting interactions of lysine demethylase LSD1 with snail/slug blocks cancer cell invasion. Cancer Res. *1*, 235-245.

Ferraro, D. A., Gaborit, N., Maron, R., Cohen-Dvashi, H., Porat, Z., Pareja, F., Lavi, S., Lindzen, M., Ben-Chetrit, N., Sela, M. and Yarden, Y. (2013). Inhibition of triple-negative breast cancer models by combinations of antibodies to EGFR. Proc. Natl. Acad. Sci. U. S. A. *5*, 1815-1820.

Fischer, K. R., Durrans, A., Lee, S., Sheng, J., Li, F., Wong, S. T., Choi, H., El Rayes, T., Ryu, S., Troeger, J., Schwabe, R., Vahdat, L. T., Altorki, N. K., Mittal, V. and Gao, D. (2015). Epithelial-to-mesenchymal transition is not required for lung metastasis but contributes to chemoresistance. Nature *7579*, 472-476.

Fischer, U., Janicke, R. U. and Schulze-Osthoff, K. (2003). Many cuts to ruin: a comprehensive update of caspase substrates. Cell Death Differ. *1*, 76-100.

Fischer-Colbrie, J., Witt, A., Heinzl, H., Speiser, P., Czerwenka, K., Sevelda, P. and Zeillinger, R. (1997). EGFR and steroid receptors in ovarian carcinoma: comparison with prognostic parameters and outcome of patients. Anticancer Res. *1B*, 613-619.

Francavilla, C., Papetti, M., Rigbolt, K. T., Pedersen, A. K., Sigurdsson, J. O., Cazzamali, G., Karemore, G., Blagoev, B. and Olsen, J. V. (2016). Multilayered proteomics reveals molecular switches dictating ligand-dependent EGFR trafficking. Nat. Struct. Mol. Biol. *6*, 608-618.

Friedl, P. and Gilmour, D. (2009). Collective cell migration in morphogenesis, regeneration and cancer. Nat. Rev. Mol. Cell Biol. *7*, 445-457.

Fry, W. H., Kotelawala, L., Sweeney, C. and Carraway, K. L.,3rd (2009). Mechanisms of ErbB receptor negative regulation and relevance in cancer. Exp. Cell Res. *4*, 697-706.

Fulda, S. (2015). Promises and Challenges of Smac Mimetics as Cancer Therapeutics. Clin. Cancer Res. *22*, 5030-5036.

Fulda, S. (2014a). Inhibitor of Apoptosis (IAP) proteins in hematological malignancies: molecular mechanisms and therapeutic opportunities. Leukemia *7*, 1414-1422.

Fulda, S. (2014b). Molecular pathways: targeting inhibitor of apoptosis proteins in cancer--from molecular mechanism to therapeutic application. Clin. Cancer Res. *2*, 289-295.

Fulda, S. (2014c). Regulation of cell migration, invasion and metastasis by IAP proteins and their antagonists. Oncogene *6*, 671-676.

Fulda, S. and Debatin, K. M. (2006). Extrinsic versus intrinsic apoptosis pathways in anticancer chemotherapy. Oncogene *34*, 4798-4811.

Fulda, S. and Vucic, D. (2012). Targeting IAP proteins for therapeutic intervention in cancer. Nat. Rev. Drug Discov. *2*, 109-124.

Futter, C. E., Pearse, A., Hewlett, L. J. and Hopkins, C. R. (1996). Multivesicular endosomes containing internalized EGF-EGF receptor complexes mature and then fuse directly with lysosomes. J. Cell Biol. *6*, 1011-1023.

Galluzzi, L., Bravo-San Pedro, J. M., Vitale, I., Aaronson, S. A., Abrams, J. M., Adam, D., Alnemri, E.S., Altucci, L., Andrews, D., Annicchiarico-Petruzzelli, M., Baehrecke, E. H., Bazan, N. G., Bertrand, M. J., Bianchi, K., Blagosklonny, M. V., Blomgren, K., Borner, C., Bredesen, D. E., Brenner, C., Campanella, M., Candi, E., Cecconi, F., Chan, F. K., Chandel, N. S., Cheng, E. H., Chipuk J. E., Cidlowski, J. A., Ciechanover, A., Dawson, T. M., Dawson, V. L., De Laurenzi, V., De Maria, R., Debatin, K. M., Di Daniele, N., Dixit, V. M., Dynlacht, B. D., El-Deiry, W. S., Fimia, G. M., Flavell, R. A., Fulda, S., Garrido, C., Gougeon, M. L., Green, D. R., Gronemeyer, H., Hajnoczky, G., Hardwick, J. M., Hengartner, M. O., Ichijo, H., Joseph, B., Jost, P. J., Kaufmann, T., Kepp, O., Klionsky, D. J., Knight, R. A., Kumar, S., Lemasters, J. J., Levine, B., Linkermann, A., Lipton, S. A., Lockshin, R. A., López-Otín, C., Lugli, E., Madeo, F., Malorni, W., Marine, J.C., Martin, S. J., Martinou, J. C., Medema, J. P., Meier, P., Melino, S., Mizushima, N., Moll, U., Muñoz-Pinedo, C., Nuñez, G., Oberst, A., Panaretakis, T., Penninger, J. M., Peter, M. E., Piacentini, M., Pinton, P., Prehn, J. H., Puthalakath, H., Rabinovich, G. A., Ravichandran, K. S., Rizzuto, R., Rodrigues, C. M., Rubinsztein, D. C., Rudel, T., Shi, Y., Simon, H. U., Stockwell, B. R., Szabadkai, G., Tait, S. W., Tang, H. L., Tavernarakis, N., Tsujimoto, Y., Vanden Berghe, T., Vandenabeele, P., Villunger, A., Wagner E. F., Walczak, H., White, E., Wood, W.G., Yuan, J., Zakeri, Z., Zhivotovsky, B., Melino, G. and Kroemer, G. (2015). Essential versus accessory aspects of cell death: recommendations of the NCCD 2015. Cell Death Differ. *1*, 58-73.

Galluzzi, L., Kepp, O. and Kroemer, G. (2012). Mitochondria: master regulators of danger signalling. Nat. Rev. Mol. Cell Biol. *12*, 780-788.

Ganten, T. M., Haas, T. L., Sykora, J., Stahl, H., Sprick, M. R., Fas, S. C., Krueger, A., Weigand, M. A., Grosse-Wilde, A., Stremmel, W., Krammer, P. H and Walczak, H. (2004). Enhanced caspase-8 recruitment to and activation at the DISC is critical for sensitisation

of human hepatocellular carcinoma cells to TRAIL-induced apoptosis by chemotherapeutic drugs. Cell Death Differ., S86-S96.

Gardam, S., Turner, V. M., Anderton, H., Limaye, S., Basten, A., Koentgen, F., Vaux, D. L., Silke, J. and Brink, R. (2011). Deletion of cIAP1 and cIAP2 in murine B lymphocytes constitutively activates cell survival pathways and inactivates the germinal center response. Blood *15*, 4041-4051.

Garg, M. (2013). Epithelial-mesenchymal transition - activating transcription factors - multifunctional regulators in cancer. World J. Stem Cells *4*, 188-195.

Ghosh, S. and Hayden, M. S. (2008). New regulators of NF-kappaB in inflammation. Nat. Rev. Immunol. *11*, 837-848.

Giampieri, S., Manning, C., Hooper, S., Jones, L., Hill, C. S. and Sahai, E. (2009). Localized and reversible TGFbeta signalling switches breast cancer cells from cohesive to single cell motility. Nat. Cell Biol. *11*, 1287-1296.

Giehl, K. (2005). Oncogenic Ras in tumour progression and metastasis. Biol. Chem. *3*, 193-205.

Gimenez-Bonafe, P., Tortosa, A. and Perez-Tomas, R. (2009). Overcoming drug resistance by enhancing apoptosis of tumor cells. Curr. Cancer. Drug Targets *3*, 320-340.

Graham, J., Muhsin, M. and Kirkpatrick, P. (2004). Cetuximab. Nat. Rev. Drug Discov. *7*, 549-550.

Grandal, M. V., Zandi, R., Pedersen, M. W., Willumsen, B. M., van Deurs, B. and Poulsen, H. S. (2007). EGFRvIII escapes down-regulation due to impaired internalization and sorting to lysosomes. Carcinogenesis *7*, 1408-1417.

Greer, R. M. *et al.* (2011). SMAC mimetic (JP1201) sensitizes non-small cell lung cancers to multiple chemotherapy agents in an IAP-dependent but TNF-alpha-independent manner. Cancer Res. *24*, 7640-7648.

Grilli, M., Chen-Tran, A. and Lenardo, M. J. (1993). Tumor necrosis factor alpha mediates a T cell receptor-independent induction of the gene regulatory factor NF-kappa B in T lymphocytes. Mol. Immunol. *14*, 1287-1294.

Gur, G., Rubin, C., Katz, M., Amit, I., Citri, A., Nilsson, J., Amariglio, N., Henriksson, R., Rechavi, G., Hedman, H., Wides, R. and Yarden, Y. (2004). LRIG1 restricts growth factor signaling by enhancing receptor ubiquitylation and degradation. EMBO J. *16*, 3270-3281.

Gyrd-Hansen, M. and Meier, P. (2010). IAPs: from caspase inhibitors to modulators of NF-kappaB, inflammation and cancer. Nat. Rev. Cancer. *8*, 561-574.

Haglund, K. and Dikic, I. (2012). The role of ubiquitylation in receptor endocytosis and endosomal sorting. J. Cell. Sci. *Pt 2*, 265-275.

Haglund, K., Sigismund, S., Polo, S., Szymkiewicz, I., Di Fiore, P. P. and Dikic, I. (2003). Multiple monoubiquitination of RTKs is sufficient for their endocytosis and degradation. Nat. Cell Biol. *5*, 461-466.

Hanahan, D. and Weinberg, R. A. (2011). Hallmarks of cancer: the next generation. Cell *5*, 646-674.

Harney, A. S., Lee, J., Manus, L. M., Wang, P., Ballweg, D. M., LaBonne, C. and Meade, T. J. (2009). Targeted inhibition of Snail family zinc finger transcription factors by oligonucleotide-Co(III) Schiff base conjugate. Proc. Natl. Acad. Sci. U. S. A. *33*, 13667-13672.

Hayden, M. S. and Ghosh, S. (2004). Signaling to NF-kappaB. Genes Dev. *18*, 2195-2224.

He, Q., Jing, H., Liaw, L., Gower, L., Vary, C., Hua, S. and Yang, X. (2016). Suppression of Spry1 inhibits triple-negative breast cancer malignancy by decreasing EGF/EGFR mediated mesenchymal phenotype. Sci. Rep., 23216.

Hedman, H., Nilsson, J., Guo, D. and Henriksson, R. (2002). Is LRIG1 a tumour suppressor gene at chromosome 3p14.3?. Acta Oncol. *4*, 352-354.

Hehlgans, T. and Pfeffer, K. (2005). The intriguing biology of the tumour necrosis factor/tumour necrosis factor receptor superfamily: players, rules and the games. Immunology *1*, 1-20.

Heiser, L. M., Sadanandam, A., Kuo, W.L., Benz, S.C., Goldstein, T.C., Ng, S., Gibb, W.J., Wang, N.J., Ziyad, S., Tong, F., Bayani, N., Hu, Z., Billig, J.I., Dueregger, A., Lewis, S., Jakkula, L., Korkola, J.E., Durinck, S., Pepin, F., Guan, Y., Purdom, E., Neuvial, P., Bengtsson, H., Wood, K.W., Smith, P.G., Vassilev, L.T., Hennessy, B.T., Greshock, J., Bachman, K.E., Hardwicke, M.A., Park, J.W., Marton, L.J., Wolf, D.M., Collisson, E.A., Neve, R.M., Mills, G.B., Speed, T.P., Feiler, H.S., Wooster, R.F., Haussler, D., Stuart, J.M., Gray, J.W. and Spellman, P.T. (2012). Subtype and pathway specific responses to anticancer compounds in breast cancer. Proc. Natl. Acad. Sci. U. S. A. *8*, 2724-2729.

Hoesel, B. and Schmid, J. A. (2013). The complexity of NF-kappaB signaling in inflammation and cancer. Mol. Cancer., 86-4598-12-86.

Huang, C., Jacobson, K. and Schaller, M. D. (2004). MAP kinases and cell migration. J. Cell. Sci. *Pt 20*, 4619-4628.

Hundsdoerfer, P., Dietrich, I., Schmelz, K., Eckert, C. and Henze, G. (2010). XIAP expression is post-transcriptionally upregulated in childhood ALL and is associated with glucocorticoid response in T-cell ALL. Pediatr. Blood Cancer. *2*, 260-266.

Infante, J. R., Dees, E. C., Olszanski, A. J., Dhuria, S. V., Sen, S., Cameron, S. and Cohen, R. B. (2014). Phase I dose-escalation study of LCL161, an oral inhibitor of apoptosis proteins inhibitor, in patients with advanced solid tumors. J. Clin. Oncol. *28*, 3103-3110.

Irwin, M. W., Mak, S., Mann, D. L., Qu, R., Penninger, J. M., Yan, A., Dawood, F., Wen, W. H., Shou, Z. and Liu, P. (1999). Tissue expression and immunolocalization of tumor necrosis factor-alpha in postinfarction dysfunctional myocardium. Circulation *11*, 1492-1498.

Ishitoya, J., Toriyama, M., Oguchi, N., Kitamura, K., Ohshima, M., Asano, K. and Yamamoto, T. (1989). Gene amplification and overexpression of EGF receptor in squamous cell carcinomas of the head and neck. Br. J. Cancer *4*, 559-562.

Jang, M. H., Kim, H. J., Kim, E. J., Chung, Y. R. and Park, S. Y. (2015). Expression of epithelial-mesenchymal transition-related markers in triple-negative breast cancer: ZEB1 as a potential biomarker for poor clinical outcome. Hum. Pathol. *9*, 1267-1274.

Janmaat, M. L. and Giaccone, G. (2003). Small-molecule epidermal growth factor receptor tyrosine kinase inhibitors. Oncologist *6*, 576-586.

Jiang, X. and Sorkin, A. (2003). Epidermal growth factor receptor internalization through clathrin-coated pits requires Cbl RING finger and proline-rich domains but not receptor polyubiquitylation. Traffic *8*, 529-543.

Jo, M., Stolz, D. B., Esplen, J. E., Dorko, K., Michalopoulos, G. K. and Strom, S. C. (2000). Cross-talk between epidermal growth factor receptor and c-Met signal pathways in transformed cells. J. Biol. Chem. *12*, 8806-8811.

Kantari, C. and Walczak, H. (2011). Caspase-8 and bid: caught in the act between death receptors and mitochondria. Biochim. Biophys. Acta *4*, 558-563.

Kao, S. H., Wang, W. L., Chen, C. Y., Chang, Y. L., Wu, Y. Y., Wang, Y. T., Wang, S. P., Nesvizhskii, A. I., Chen, Y. J., Hong, T. M. and Yang, P. C. (2014). GSK3beta controls epithelial-mesenchymal transition and tumor metastasis by CHIP-mediated degradation of Slug. Oncogene *24*, 3172-3182.

Karin, M. and Gallagher, E. (2009). TNFR signaling: ubiquitin-conjugated TRAFfic signals control stop-and-go for MAPK signaling complexes. Immunol. Rev. *1*, 225-240.

Kolch, W., Halasz, M., Granovskaya, M. and Kholodenko, B. N. (2015). The dynamic control of signal transduction networks in cancer cells. Nat. Rev. Cancer. *9*, 515-527.

Konstantinopoulos, P. A., Karamouzis, M. V. and Papavassiliou, A. G. (2007). Post-translational modifications and regulation of the RAS superfamily of GTPases as anticancer targets. Nat. Rev. Drug Discov. *7*, 541-555.

Krepler, C., Chunduru, S.K., Halloran, M.B., He, X., Xiao, M., Vultur, A., Villanueva, J., Mitsuuchi, Y., Neiman, E.M., Benetatos, C., Nathanson, K.L., Amaravadi, R.K., Pehamberger, H., McKinlay, M. and Herlyn, M. (2013). The novel SMAC mimetic birinapant exhibits potent activity against human melanoma cells. Clin. Cancer Res. *7*, 1784-1794.

Kusewitt, D. F., Choi, C., Newkirk, K. M., Leroy, P., Li, Y., Chavez, M. G. and Hudson, L. G. (2009). Slug/Snai2 is a downstream mediator of epidermal growth factor receptor-stimulated reepithelialization. J. Invest. Dermatol. *2*, 491-495.

LaCasse, E. C., Mahoney, D. J., Cheung, H. H., Plenchette, S., Baird, S. and Korneluk, R. G. (2008). IAP-targeted therapies for cancer. Oncogene *48*, 6252-6275.

Lamkanfi, M. (2011). Emerging inflammasome effector mechanisms. Nat. Rev. Immunol. *3*, 213-220.

Lecis, D., De Cesare, M., Perego, P., Conti, A., Corna, E., Drago, C., Seneci, P., Walczak, H., Colombo, M. P., Delia, D. and Sangaletti, S. (2013). Smac mimetics induce inflammation and necrotic tumour cell death by modulating macrophage activity. Cell. Death Dis., e920.

Lecis, D., Drago, C., Manzoni, L., Seneci, P., Scolastico, C., Mastrangelo, E., Bolognesi, M., Anichini, A., Kashkar, H., Walczak, H. and Delia, D. (2010). Novel SMAC-mimetics synergistically stimulate melanoma cell death in combination with TRAIL and Bortezomib. Br. J. Cancer *12*, 1707-1716.

Lecis, D., Mastrangelo, E., Belvisi, L., Bolognesi, M., Civera, M., Cossu, F., De Cesare, M., Delia, D., Drago, C., Manenti, G., Manzoni, L., Milani, M., Moroni, E., Perego, P., Potenza, D., Rizzo, V., Scavullo, C., Scolastico, C., Servida, F., Vasile, F. and Seneci, P. (2012). Dimeric Smac mimetics/IAP inhibitors as in vivo-active pro-apoptotic agents. Part II: Structural and biological characterization. Bioorg. Med. Chem. *22*, 6709-6723.

Lee, M. Y., Chou, C. Y., Tang, M. J. and Shen, M. R. (2008). Epithelial-mesenchymal transition in cervical cancer: correlation with tumor progression, epidermal growth factor receptor overexpression, and snail up-regulation. Clin. Cancer Res. *15*, 4743-4750.

Lehmann, B. D., Bauer, J. A., Chen, X., Sanders, M. E., Chakravarthy, A. B., Shyr, Y. and Pietenpol, J. A. (2011). Identification of human triple-negative breast cancer subtypes and preclinical models for selection of targeted therapies. J. Clin. Invest. *7*, 2750-2767.

Lehmann, B. D. and Pietenpol, J. A. (2015). Clinical implications of molecular heterogeneity in triple negative breast cancer. Breast, S36-40.

Lehmann, W., Mossmann, D., Kleemann, J., Mock, K., Meisinger, C., Brummer, T., Herr, R., Brabletz, S., Stemmler, M. P. and Brabletz, T. (2016). ZEB1 turns into a transcriptional activator by interacting with YAP1 in aggressive cancer types. Nat. Commun., 10498.

Levkowitz, G., Waterman, H., Ettenberg, S.A., Katz, M., Tsygankov, A.Y., Alroy, I., Lavi, S., Iwai, K., Reiss, Y., Ciechanover, A., Lipkowitz, S. and Yarden, Y. (1999). Ubiquitin ligase activity and tyrosine phosphorylation underlie suppression of growth factor signaling by c-Cbl/Sli-1. Mol. Cell *6*, 1029-1040.

Lindsey, S. and Langhans, S. A. (2015). Epidermal growth factor signaling in transformed cells. Int. Rev. Cell. Mol. Biol., 1-41.

Lopez, J., John, S. W., Tenev, T., Rautureau, G. J., Hinds, M. G., Francalanci, F., Wilson, R., Broemer, M., Santoro, M. M., Day, C. L. and Meier, P. (2011). CARD-mediated autoinhibition of cIAP1's E3 ligase activity suppresses cell proliferation and migration. Mol. Cell *5*, 569-583.

Luanpitpong, S., Li, J., Manke, A., Brundage, K., Ellis, E., McLaughlin, S. L., Angsutararux, P., Chanthra, N., Voronkova, M., Chen, Y. C., Wang, L., Chanvorachote, P., Pei, M., Issaragrisil, S. and Rojanasakul, Y. (2016). SLUG is required for SOX9 stabilization and functions to promote cancer stem cells and metastasis in human lung carcinoma. Oncogene *22*, 2824-2833.

Luo, M. and Fu, L. W. (2014). Redundant kinase activation and resistance of EGFR-tyrosine kinase inhibitors. Am. J. Cancer. Res. *6*, 608-628.

MacEwan, D. J. (2002). TNF ligands and receptors--a matter of life and death. Br. J. Pharmacol. *4*, 855-875.

Manzoni, L., Belvisi, L., Bianchi, A., Conti, A., Drago, C., de Matteo, M., Ferrante, L., Mastrangelo, E., Perego, P., Potenza, D., Scolastico, C., Servida, F., Timpano, G,. Vasile, F., Rizzo, V. and Seneci, P. (2012). Homo- and heterodimeric Smac mimetics/IAP inhibitors as in vivo-active pro-apoptotic agents. Part I: Synthesis. Bioorg. Med. Chem. *22*, 6687-6708.

Marmor, M. D. and Yarden, Y. (2004). Role of protein ubiquitylation in regulating endocytosis of receptor tyrosine kinases. Oncogene *11*, 2057-2070.

Martinelli, E., De Palma, R., Orditura, M., De Vita, F. and Ciardiello, F. (2009). Anti-epidermal growth factor receptor monoclonal antibodies in cancer therapy. Clin. Exp. Immunol. *1*, 1-9.

Mattson, M. P. (2000). Apoptosis in neurodegenerative disorders. Nat. Rev. Mol. Cell Biol. *2*, 120-129.

McCoy, M. K. and Tansey, M. G. (2008). TNF signaling inhibition in the CNS: implications for normal brain function and neurodegenerative disease. J. Neuroinflammation, 45-2094-5-45.

McIlwain, D. R., Berger, T. and Mak, T. W. (2013). Caspase functions in cell death and disease. Cold Spring Harb Perspect. Biol. *4*, a008656.

Mehrotra, S., Languino, L. R., Raskett, C. M., Mercurio, A. M., Dohi, T. and Altieri, D. C. (2010). IAP regulation of metastasis. Cancer. Cell. *1*, 53-64.

Micheau, O. and Tschopp, J. (2003). Induction of TNF receptor I-mediated apoptosis via two sequential signaling complexes. Cell *2*, 181-190.

Miller, J. K., Shattuck, D. L., Ingalla, E. Q., Yen, L., Borowsky, A. D., Young, L. J., Cardiff, R. D., Carraway, K. L.,3rd and Sweeney, C. (2008). Suppression of the negative regulator LRIG1 contributes to ErbB2 overexpression in breast cancer. Cancer Res. *20*, 8286-8294.

Minn, A. J., Gupta, G. P., Siegel, P. M., Bos, P. D., Shu, W., Giri, D. D., Viale, A., Olshen, A. B., Gerald, W. L. and Massague, J. (2005). Genes that mediate breast cancer metastasis to lung. Nature *7050*, 518-524.

Moller, Y., Siegemund, M., Beyes, S., Herr, R., Lecis, D., Delia, D., Kontermann, R., Brummer, T., Pfizenmaier, K. and Olayioye, M. A. (2014). EGFR-Targeted TRAIL and a Smac Mimetic Synergize to Overcome Apoptosis Resistance in KRAS Mutant Colorectal Cancer Cells. PLoS One *9*, e107165.

Mueller, K. L., Madden, J. M., Zoratti, G. L., Kuperwasser, C., List, K. and Boerner, J. L. (2012). Fibroblast-secreted hepatocyte growth factor mediates epidermal growth factor receptor tyrosine kinase inhibitor resistance in triple-negative breast cancers through paracrine activation of Met. Breast Cancer Res. *4*, R104.

Mueller, K. L., Yang, Z. Q., Haddad, R., Ethier, S. P. and Boerner, J. L. (2010). EGFR/Met association regulates EGFR TKI resistance in breast cancer. J. Mol. Signal., 8-2187-5-8.

Nagata, S. (2010). Apoptosis and autoimmune diseases. Ann. N. Y. Acad. Sci., 10-16.

Nakai, K., Hung, M. C. and Yamaguchi, H. (2016). A perspective on anti-EGFR therapies targeting triple-negative breast cancer. Am. J. Cancer. Res. *8*, 1609-1623.

Neve, R. M., Chin, K., Fridlyand, J., Yeh, J., Baehner, F. L., Fevr, T., Clark, L., Bayani, N., Coppe, J. P., Tong, F., Speed, T., Spellman, P. T., DeVries, S., Lapuk, A., Wang, N. J., Kuo, W. L., Stilwell, J. L., Pinkel, D., Albertson, D. G., Waldman, F. M., McCormick, F., Dickson, R. B., Johnson, M. D., Lippman, M., Ethier, S., Gazdar, A. and Gray, J. W. (2006). A collection of breast cancer cell lines for the study of functionally distinct cancer subtypes. Cancer. Cell. *6*, 515-527.

Nieto, M. A. (2002). The snail superfamily of zinc-finger transcription factors. Nat. Rev. Mol. Cell Biol. *3*, 155-166.

Nosseri, C., Coppola, S. and Ghibelli, L. (1994). Possible involvement of poly(ADP-ribosyl) polymerase in triggering stress-induced apoptosis. Exp. Cell Res. *2*, 367-373.

Oberoi-Khanuja, T. K., Murali, A. and Rajalingam, K. (2013). IAPs on the move: role of inhibitors of apoptosis proteins in cell migration. Cell. Death Dis., e784.

Oberst, A. (2016). Death in the fast lane: what's next for necroptosis?. FEBS J. *14*, 2616-2625.

Obexer, P. and Ausserlechner, M. J. (2014). X-linked inhibitor of apoptosis protein - a critical death resistance regulator and therapeutic target for personalized cancer therapy. Front. Oncol., 197.

O'Dea, E. and Hoffmann, A. (2010). The regulatory logic of the NF-kappaB signaling system. Cold Spring Harb Perspect. Biol. *1*, a000216.

Ofengeim, D. and Yuan, J. (2013). Regulation of RIP1 kinase signalling at the crossroads of inflammation and cell death. Nat. Rev. Mol. Cell Biol. *11*, 727-736.

Ozoren, N. and El-Deiry, W. S. (2002). Defining characteristics of Types I and II apoptotic cells in response to TRAIL. Neoplasia *6*, 551-557.

Pachmayr, E., Treese, C. and Stein, U. (2017). Underlying Mechanisms for Distant Metastasis - Molecular Biology. Visc Med. *1*, 11-20.

Pahl, H. L. (1999). Activators and target genes of Rel/NF-kappaB transcription factors. Oncogene *49*, 6853-6866.

Perkins, N. D. (2007). Integrating cell-signalling pathways with NF-kappaB and IKK function. Nat. Rev. Mol. Cell Biol. *1*, 49-62.

Peschard, P. and Park, M. (2003). Escape from Cbl-mediated downregulation: a recurrent theme for oncogenic deregulation of receptor tyrosine kinases. Cancer. Cell. *6*, 519-523.

Petersen, S. L., Wang, L., Yalcin-Chin, A., Li, L., Peyton, M., Minna, J., Harran, P. and Wang, X. (2007). Autocrine TNFα Signaling Renders Human Cancer Cells Susceptible to Smac-Mimetic-Induced Apoptosis. Cancer Cell *5*, 445-456.

Phillips, S. and Kuperwasser, C. (2014). SLUG: Critical regulator of epithelial cell identity in breast development and cancer. Cell. Adh Migr. *6*, 578-587.

Phipson, B., Lee, S., Majewski, I. J., Alexander, W. S. and Smyth, G. K. (2016). Robust Hyperparameter Estimation Protects Against Hypervariable Genes and Improves Power to Detect Differential Expression. Ann. Appl. Stat. *2*, 946-963.

Prat, A. and Perou, C. M. (2011). Deconstructing the molecular portraits of breast cancer. Mol. Oncol. *1*, 5-23.

Puliyappadamba, V. T., Chakraborty, S., Chauncey, S. S., Li, L., Hatanpaa, K. J., Mickey, B., Noorani, S., Shu, H. K., Burma, S., Boothman, D. A. and Habib, A. A. (2013). Opposing effect of EGFRWT on EGFRvIII-mediated NF-kappaB activation with RIP1 as a cell death switch. Cell. Rep. *4*, 764-775.

Purba, E. R., Saita, E. I. and Maruyama, I. N. (2017). Activation of the EGF Receptor by Ligand Binding and Oncogenic Mutations: The "Rotation Model". Cells *2*, 10.3390/cells6020013.

Razani, B., Reichardt, A. D. and Cheng, G. (2011). Non-canonical NF-kappaB signaling activation and regulation: principles and perspectives. Immunol. Rev. *1*, 44-54.

Reddy, K. B., Nabha, S. M. and Atanaskova, N. (2003). Role of MAP kinase in tumor progression and invasion. Cancer Metastasis Rev. *4*, 395-403.

Reubold, T. F. and Eschenburg, S. (2012). A molecular view on signal transduction by the apoptosome. Cell. Signal. *7*, 1420-1425.

Richter, C. Richter, C., Messerschmidt, S., Holeiter, G., Tepperink, J., Osswald, S., Zappe, A., Branschädel, M., Boschert, V., Mann, D.A., Scheurich, P. and Krippner-Heidenreich, A. (2012). The tumor necrosis factor receptor stalk regions define responsiveness to soluble versus membrane-bound ligand. Mol. Cell. Biol. *13*, 2515-2529.

Riedl, S. J., Renatus, M., Schwarzenbacher, R., Zhou, Q., Sun, C., Fesik, S. W., Liddington, R. C. and Salvesen, G. S. (2001). Structural Basis for the Inhibition of Caspase-3 by XIAP. Cell *5*, 791-800.

Rizzolio, S. and Tamagnone, L. (2007). Semaphorin signals on the road to cancer invasion and metastasis. Cell. Adh Migr. *2*, 62-68.

Robinson, M. D. and Oshlack, A. (2010). A scaling normalization method for differential expression analysis of RNA-seq data. Genome Biol. *3*, R25-2010-11-3-r25.

Rosebeck, S., Madden, L., Jin, X., Gu, S., Apel, I. J., Appert, A., Hamoudi, R. A., Noels, H., Sagaert, X., Van Loo, P., Baens, M., Du, M. Q., Lucas, P. C. and McAllister-Lucas, L. M. (2011). Cleavage of NIK by the API2-MALT1 fusion oncoprotein leads to noncanonical NF-kappaB activation. Science *6016*, 468-472.

Rothe, M., Pan, M. G., Henzel, W. J., Ayres, T. M. and Goeddel, D. V. (1995). The TNFR2-TRAF signaling complex contains two novel proteins related to baculoviral inhibitor of apoptosis proteins. Cell *7*, 1243-1252.

Rouam, S., Moreau, T. and Broet, P. (2010). Identifying common prognostic factors in genomic cancer studies: a novel index for censored outcomes. BMC Bioinformatics, 150-2105-11-150.

Ruland, J. (2011). Return to homeostasis: downregulation of NF-kappaB responses. Nat. Immunol. *8*, 709-714.

Salzmann, S., Lang, I., Rosenthal, A., Schafer, V., Weisenberger, D., Carmona Arana, J. A., Trebing, J., Siegmund, D., Neumann, M. and Wajant, H. (2013). TWEAK inhibits TRAF2-mediated CD40 signaling by destabilization of CD40 signaling complexes. J. Immunol. *5*, 2308-2318.

Samanta, S., Sun, H., Goel, H. L., Pursell, B., Chang, C., Khan, A., Greiner, D. L., Cao, S., Lim, E., Shultz, L. D. and Mercurio, A. M. (2016). IMP3 promotes stem-like properties in triple-negative breast cancer by regulating SLUG. Oncogene *9*, 1111-1121.

Sarkar, A. and Hochedlinger, K. (2013). The sox family of transcription factors: versatile regulators of stem and progenitor cell fate. Cell. Stem Cell. *1*, 15-30.

Scaffidi, C., Fulda, S., Srinivasan, A., Friesen, C., Li, F., Tomaselli, K. J., Debatin, K. M., Krammer, P. H. and Peter, M. E. (1998). Two CD95 (APO-1/Fas) signaling pathways. EMBO J. *6*, 1675-1687.

Schlessinger, J. (2000). Cell signaling by receptor tyrosine kinases. Cell *2*, 211-225.

Sebastian, S., Settleman, J., Reshkin, S. J., Azzariti, A., Bellizzi, A. and Paradiso, A. (2006). The complexity of targeting EGFR signalling in cancer: from expression to turnover. Biochim. Biophys. Acta *1*, 120-139.

Shattuck, D. L., Miller, J. K., Laederich, M., Funes, M., Petersen, H., Carraway, K. L.,3rd and Sweeney, C. (2007). LRIG1 is a novel negative regulator of the Met receptor and opposes Met and Her2 synergy. Mol. Cell. Biol. *5*, 1934-1946.

Shih, J. Y. and Yang, P. C. (2011). The EMT regulator slug and lung carcinogenesis. Carcinogenesis *9*, 1299-1304.

Sigismund, S., Argenzio, E., Tosoni, D., Cavallaro, E., Polo, S. and Di Fiore, P. P. (2008). Clathrin-mediated internalization is essential for sustained EGFR signaling but dispensable for degradation. Dev. Cell. *2*, 209-219.

Sigismund, S., Woelk, T., Puri, C., Maspero, E., Tacchetti, C., Transidico, P., Di Fiore, P. P. and Polo, S. (2005). Clathrin-independent endocytosis of ubiquitinated cargos. Proc. Natl. Acad. Sci. U. S. A. *8*, 2760-2765.

Sikic, B., Eckhardt, S., Gallant, G., Burris, H., Camidge, D. and Covelas, A. (2011). Safety, pharmocokinetics (PK), and pharmacodynamics (PD) of HGS1029, an inhibitor of apoptosis protein (IAP), in patients (Pts.) with advanced solid tumors: Results of a Phase I study. J Clin Oncol. 29. . 10.1200/jco.2011.29.15_suppl.3008.

Sirkisoon, S. R., Carpenter, R. L., Rimkus, T., Miller, L., Metheny-Barlow, L. and Lo, H. W. (2016). EGFR and HER2 signaling in breast cancer brain metastasis. Front. Biosci. (Elite Ed), 245-263.

Somsel Rodman, J. and Wandinger-Ness, A. (2000). Rab GTPases coordinate endocytosis. J. Cell. Sci., 183-192.

Stahl, P. D. and Barbieri, M. A. (2002). Multivesicular bodies and multivesicular endosomes: the "ins and outs" of endosomal traffic. Sci. STKE *141*, pe32.

Stang, E., Blystad, F. D., Kazazic, M., Bertelsen, V., Brodahl, T., Raiborg, C., Stenmark, H. and Madshus, I. H. (2004). Cbl-dependent ubiquitination is required for progression of EGF receptors into clathrin-coated pits. Mol. Biol. Cell *8*, 3591-3604.

Sun, H., Nikolovska-Coleska, Z., Lu, J., Meagher, J. L., Yang, C. Y., Qiu, S., Tomita, Y., Ueda, Y., Jiang, S., Krajewski, K., Roller, P.P., Stuckey, J. A. and Wang, S. (2007). Design, synthesis, and characterization of a potent, nonpeptide, cell-permeable, bivalent Smac mimetic that concurrently targets both the BIR2 and BIR3 domains in XIAP. J. Am. Chem. Soc. *49*, 15279-15294.

Sun, S. C. (2011). Non-canonical NF-kappaB signaling pathway. Cell Res. *1*, 71-85.

Tait, S. W. and Green, D. R. (2010). Mitochondria and cell death: outer membrane permeabilization and beyond. Nat. Rev. Mol. Cell Biol. *9*, 621-632.

Tchoghandjian, A., Jennewein, C., Eckhardt, I., Rajalingam, K. and Fulda, S. (2013). Identification of non-canonical NF-kappaB signaling as a critical mediator of Smac mimetic-stimulated migration and invasion of glioblastoma cells. Cell. Death Dis., e564.

Thiery, J. P. (2002). Epithelial-mesenchymal transitions in tumour progression. Nat. Rev. Cancer. *6*, 442-454.

Thornberry, N. A. and Lazebnik, Y. (1998). Caspases: enemies within. Science *5381*, 1312-1316.

Vandenabeele, P. and Bertrand, M. J. (2012). The role of the IAP E3 ubiquitin ligases in regulating pattern-recognition receptor signalling. Nat. Rev. Immunol. *12*, 833-844.

Vandewalle, C., Comijn, J., De Craene, B., Vermassen, P., Bruyneel, E., Andersen, H., Tulchinsky, E., Van Roy, F. and Berx, G. (2005). SIP1/ZEB2 induces EMT by repressing genes of different epithelial cell-cell junctions. Nucleic Acids Res. *20*, 6566-6578.

Varfolomeev, E., Goncharov, T., Maecker, H., Zobel, K., Komuves, L. G., Deshayes, K. and Vucic, D. (2012). Cellular Inhibitors of Apoptosis Are Global Regulators of NF-kappaB and MAPK Activation by Members of the TNF Family of Receptors. Sci. Signal. *216*, ra22.

Varfolomeev, E. E. and Ashkenazi, A. (2004). Tumor necrosis factor: an apoptosis JuNKie?. Cell *4*, 491-497.

Varfolomeev, E., Blankenship, J. W., Wayson, S. M., Fedorova, A. V., Kayagaki, N., Garg, P., Zobel, K., Dynek, J. N., Elliott, L. O., Wallweber, H. J., Flygare, J. A., Fairbrother, W. J., Deshayes, K., Dixit, V. M. and Vucic, D. (2007). IAP Antagonists Induce Autoubiquitination of c-IAPs, NF-κB Activation, and TNFα-Dependent Apoptosis. Cell *4*, 669-681.

Vaux, D. L. and Silke, J. (2005). IAPs, RINGs and ubiquitylation. Nat. Rev. Mol. Cell Biol. *4*, 287-297.

Vergara, D., Simeone, P., Latorre, D., Cascione, F., Leporatti, S., Trerotola, M., Giudetti, A. M., Capobianco, L., Lunetti, P., Rizzello, A., Rinaldi, R., Alberti, S. and Maffia, M. (2015). Proteomics analysis of E-cadherin knockdown in epithelial breast cancer cells. J. Biotechnol., 3-11.

Vince, J. E., Wong, W. W., Khan, N., Feltham, R., Chau, D., Ahmed, A. U., Benetatos, C. A., Chunduru, S. K., Condon, S. M., McKinlay, M., Brink, R., Leverkus, M., Tergaonkar, V., Schneider, P., Callus, B. A., Koentgen, F., Vaux, D. L. and Silke, J. (2007). IAP Antagonists Target cIAP1 to Induce TNFα-Dependent Apoptosis. Cell *4*, 682-693.

Wajant, H., Pfizenmaier, K. and Scheurich, P. (2003). Tumor necrosis factor signaling. Cell Death Differ. *1*, 45-65.

Wajant, H. and Scheurich, P. (2011). TNFR1-induced activation of the classical NF-kappaB pathway. FEBS J. *6*, 862-876.

Walczak, H. (2013). Death receptor-ligand systems in cancer, cell death, and inflammation. Cold Spring Harb Perspect. Biol. *5*, a008698.

Wan, F. and Lenardo, M. J. (2009). Specification of DNA binding activity of NF-kappaB proteins. Cold Spring Harb Perspect. Biol. *4*, a000067.

Wang, Y., Poulin, E. J. and Coffey, R. J. (2013). LRIG1 is a triple threat: ERBB negative regulator, intestinal stem cell marker and tumour suppressor. Br. J. Cancer *9*, 1765-1770.

Ware, C. F., Crowe, P. D., Vanarsdale, T. L., Andrews, J. L., Grayson, M. H., Jerzy, R., Smith, C. A. and Goodwin, R. G. (1991). Tumor necrosis factor (TNF) receptor expression in T lymphocytes. Differential regulation of the type I TNF receptor during activation of resting and effector T cells. J. Immunol. *12*, 4229-4238.

Wieduwilt, M. J. and Moasser, M. M. (2008). The epidermal growth factor receptor family: biology driving targeted therapeutics. Cell Mol. Life Sci. *10*, 1566-1584.

Witt, A., Seeger, J. M., Coutelle, O., Zigrino, P., Broxtermann, P., Andree, M., Brinkmann, K., Jüngst, C., Schauss, A. C., Schüll, S., Wohlleber, D., Knolle, P. A., Krönke, M., Mauch, C.

and Kashkar, H. (2015). IAP antagonization promotes inflammatory destruction of vascular endothelium. EMBO Rep. *6*, 719-727.

Wong, W. W., Gentle, I. E., Nachbur, U., Anderton, H., Vaux, D. L. and Silke, J. (2010). RIPK1 is not essential for TNFR1-induced activation of NF-kappaB. Cell Death Differ. *3*, 482-487.

Woodburn, J. R. (1999). The epidermal growth factor receptor and its inhibition in cancer therapy. Pharmacol. Ther. *2-3*, 241-250.

Wu, G., Chai, J., Suber, T. L., Wu, J. W., Du, C., Wang, X. and Shi, Y. (2000). Structural basis of IAP recognition by Smac/DIABLO. Nature *6815*, 1008-1012.

Xie, L., Law, B. K., Chytil, A. M., Brown, K. A., Aakre, M. E. and Moses, H. L. (2004). Activation of the Erk pathway is required for TGF-beta1-induced EMT in vitro. Neoplasia *5*, 603-610.

Yang, J., Mani, S. A., Donaher, J. L., Ramaswamy, S., Itzykson, R. A., Come, C., Savagner, P., Gitelman, I., Richardson, A. and Weinberg, R. A. (2004). Twist, a master regulator of morphogenesis, plays an essential role in tumor metastasis. Cell *7*, 927-939.

Ye, X., Tam, W. L., Shibue, T., Kaygusuz, Y., Reinhardt, F., Ng Eaton, E. and Weinberg, R. A. (2015). Distinct EMT programs control normal mammary stem cells and tumour-initiating cells. Nature *7568*, 256-260.

Yokdang, N., Hatakeyama, J., Wald, J. H., Simion, C., Tellez, J. D., Chang, D. Z., Swamynathan, M. M., Chen, M., Murphy, W. J., Carraway Iii, K. L. and Sweeney, C. (2016). LRIG1 opposes epithelial-to-mesenchymal transition and inhibits invasion of basal-like breast cancer cells. Oncogene *22*, 2932-2947.

Yoon, S. and Seger, R. (2006). The extracellular signal-regulated kinase: multiple substrates regulate diverse cellular functions. Growth Factors *1*, 21-44.

Yu, H. A., Arcila, M. E., Rekhtman, N., Sima, C. S., Zakowski, M. F., Pao, W., Kris, M. G., Miller, V. A., Ladanyi, M. and Riely, G. J. (2013). Analysis of tumor specimens at the time of acquired resistance to EGFR-TKI therapy in 155 patients with EGFR-mutant lung cancers. Clin. Cancer Res. *8*, 2240-2247.

Yun, C. H., Boggon, T. J., Li, Y., Woo, M. S., Greulich, H., Meyerson, M. and Eck, M. J. (2007). Structures of lung cancer-derived EGFR mutants and inhibitor complexes: mechanism of activation and insights into differential inhibitor sensitivity. Cancer. Cell. *3*, 217-227.

Zarnegar, B. J., Wang, Y., Mahoney, D. J., Dempsey, P. W., Cheung, H. H., He, J., Shiba, T., Yang, X., Yeh, W. C., Mak, T. W., Korneluk, R. G. and Cheng, G. (2008). Noncanonical NF-

kappaB activation requires coordinated assembly of a regulatory complex of the adaptors cIAP1, cIAP2, TRAF2 and TRAF3 and the kinase NIK. Nat. Immunol. *12*, 1371-1378.

Zeichner, S. B., Terawaki, H. and Gogineni, K. (2016). A Review of Systemic Treatment in Metastatic Triple-Negative Breast Cancer. Breast Cancer. (Auckl), 25-36.

Zhang, J., Antonyak, M. A., Singh, G. and Cerione, R. A. (2013). A mechanism for the upregulation of EGF receptor levels in glioblastomas. Cell. Rep. *6*, 2008-2020.

Zhang, X., Gureasko, J., Shen, K., Cole, P. A. and Kuriyan, J. (2006). An allosteric mechanism for activation of the kinase domain of epidermal growth factor receptor. Cell *6*, 1137-1149.

Zhang, Y., Jain, R. K. and Zhu, M. (2015). Recent Progress and Advances in HGF/MET-Targeted Therapeutic Agents for Cancer Treatment. Biomedicines *1*, 149-181.

11 PUBLICATIONS

Conti A*, **Majorini MT***, Fontanella E, Bardelli A, Giacca M, Delia D, Mano M, Lecis D. Lemur tyrosine kinase 2 (LMTK2) is a determinant of cell sensitivity to apoptosis by regulating the levels of the BCL2 family members. Cancer Lett. 2017 Mar 28;389:59-69. doi: 10.1016/j.canlet.2016.12.025. Epub 2016 Dec 29. PubMed PMID: 28040547. * *co–first authors*

Conti A, **Majorini MT**, Elliott R, Ashworth A, Lord CJ, Cancelliere C, Bardelli A, Seneci P, Walczak H, Delia D, Lecis D. Oncogenic KRAS sensitizes premalignant, but not malignant cells, to Noxa-dependent apoptosis through the activation of the MEK/ERK pathway. Oncotarget. 2015 May 10;6(13):10994-1008. PubMed PMID: 26028667; PubMed Central PMCID: PMC4484434.

12 APPENDIX

Cancer Letters 389 (2017) 59–69

Contents lists available at ScienceDirect

Cancer Letters

journal homepage: www.elsevier.com/locate/canlet

Original Article

Lemur tyrosine kinase 2 (LMTK2) is a determinant of cell sensitivity to apoptosis by regulating the levels of the BCL2 family members

Annalisa Conti [a, 1, 2], Maria Teresa Majorini [a, 2], Enrico Fontanella [a], Alberto Bardelli [b, c, d], Mauro Giacca [e], Domenico Delia [a], Miguel Mano [e], Daniele Lecis [a, *]

[a] Department of Experimental Oncology and Molecular Medicine, Fondazione IRCCS Istituto Nazionale dei Tumori, Milan, Italy
[b] Department of Oncology, University of Torino, Candiolo, Torino, Italy
[c] Candiolo Cancer Institute – FPO, IRCCS, Candiolo, Torino, Italy
[d] FIRC Institute of Molecular Oncology (IFOM), Milano, Italy
[e] International Centre for Genetic Engineering and Biotechnology (ICGEB), Trieste, Italy

ARTICLE INFO

Article history:
Received 21 July 2016
Received in revised form
20 October 2016
Accepted 20 December 2016

Keywords:
LMTK2
TRAIL
Cytotoxic compounds
Cancer cell death
Apoptosis regulation

ABSTRACT

Using a high-throughput approach, we identified lemur tyrosine kinase 2 (LMTK2) as a novel determinant of cell sensitivity to TRAIL. LMTK2 is a poorly characterized serine/threonine kinase believed to play a role in endosomal membrane trafficking and neuronal physiology, and recently found to be mutated in diverse tumor types. We show that LMTK2 silencing sensitizes immortalized epithelial cells and cancer cells to TRAIL, and this phenomenon is accompanied by changes in the expression of BCL2 family members. In epithelial cells, LMTK2 targeting causes the down-regulation of the BCL2 and BCL-xL anti-apoptotic proteins and the reciprocal up-regulation of the pro-apoptotic protein BIM, while, in cancer cells, LMTK2 knock-down reduces BCL2 without increasing BIM levels. We provide evidence that both BIM and BCL2 proteins are regulated by LMTK2 in a GSK3β- and PP1A-dependent manner and that their perturbation, together with BCL-xL reduction, determines an increased sensitivity not only to TRAIL, but also to other compounds. Overall, our findings suggest a broad function of LMTK2 in the regulation of the apoptotic pathway and highlight LMTK2 as a novel candidate target to increase the cytotoxic activity of chemotherapeutic compounds.

Introduction

Among the several approaches and molecules that have been proposed in anti-cancer treatment, tumor necrosis factor-related apoptosis inducing ligand (TRAIL) has raised great expectations owing to its *in vitro* and *in vivo* cytotoxic activity towards cancer cells [1,2], while sparing normal tissues [3]. Unfortunately, later studies demonstrated that cancer cells develop resistance to TRAIL-induced apoptosis through several mechanisms, thus limiting its therapeutic efficacy [2]. Indeed, high levels of the caspase-8 and caspase-3/-7/-9 inhibitors FLIP and XIAP, hyper-activation of many pro-survival pathways (e.g. NF-kB) and aberrant expression of the BCL2 family members BCL2, BCL-xL and MCL-1, prevent TRAIL-mediated apoptosis [2]. In pathological settings, TRAIL administration could even paradoxically sustain cancer cell aggressiveness and promote invasion and metastasis formation [4,5]. Hence, cancer cells need to be primed to death with combination therapy and, to this end, several approaches have been pursued [6–8].

Lemur Tyrosine Kinase 2 (LMTK2) is a poorly characterized serine/threonine kinase initially identified as an interactor of PP1A [9], one of the four PP1 catalytic isoforms [10]. Little is known about the physiological function of LMTK2, except for its role in the maturation of germ cells [11] and in endosomal membrane trafficking through the interaction with myosin VI [12,13]. LMTK2 is a target of CDK5 [14] and has been shown to control Smad2 signaling by regulating PP1A and GSK3β [15]. The latter kinase is constitutively active in unstimulated cells [16], but can undergo a rapid and reversible repression in response to extracellular signals. The regulation of GSK3β is mainly posttranslational and, in particular, dependent on inhibitory phosphorylation. Among the

* Corresponding author. Department of Experimental Oncology and Molecular Medicine, Fondazione IRCCS Istituto Nazionale dei Tumori, Via Amadeo 42, 20133 Milan, Italy. Fax: +39 02 2390 3073.
E-mail address: daniele.lecis@istitutotumori.mi.it (D. Lecis).
[1] Current address: Center for Genomic Science of IIT@SEMM, Fondazione Istituto Italiano di Tecnologia (IIT), Milan, Italy.
[2] These authors contributed equally to this work.

http://dx.doi.org/10.1016/j.canlet.2016.12.025
0304-3835/

phosphorylated residues identified, Ser9 is a known target of AKT [17] while Thr43 of ERK [18].

Due to the interaction of LMTK2 with two proteins involved in numerous processes within the nervous system, i.e. PP1A and CDK5, it is conceivable that LMTK2 may play a role in neurodegeneration [14]. Nonetheless, several LMTK2 mutations have recently been identified also in cancer, and in particular in pulmonary sarcomatoid carcinomas [19], lung adenocarcinomas [20] and prostate cancer [21,22]. Of note, in *in vitro* models of prostate cancer, LMTK2 was shown to regulate the androgen receptor (AR) [23], prostate specific antigen (PSA) and vascular endothelial growth factor (VEGF) secretion [24], and transforming growth factor beta (TGFβ) signaling [15], and could therefore contribute to cancer susceptibility and progression [21].

In this study, we performed a siRNA-based high-throughput screening, targeting 714 kinases and 598 ubiquitin-related proteins, with the ultimate goal of identifying new modulators of TRAIL sensitivity. We found that LMTK2 is a determinant of TRAIL sensitivity and described for the first time its role in the regulation of the BCL-2 family proteins and the underlying mechanisms. Finally, we investigated the effect of LMTK2 silencing in a panel of premalignant and cancer cell lines, confirming a broad effect of LMTK2 in the regulation of the apoptotic pathway triggered not only by TRAIL, but also by other cytotoxic compounds.

Materials and methods

Cell culture and chemicals

Human mammary epithelial HME and MCF10A cell lines parental or bearing the EGFR delE746A750 mutation (HME EGFR and MCF10A EGFR, respectively), and colorectal HCT116 and DLD-1 cell lines were cultured as already described [25]. MDA-MB231 and BT549 cells were cultured in RPMI 1640 medium (Lonza Group, Basel, CH) supplemented with 10% fetal bovine serum (FBS; EuroClone, Milan, IT) at 37 °C and 5% CO_2 in fully humidified atmosphere. Cells were treated with the NF-kB (BAY117082; Selleck Chemicals, Munich, D), the AKT, MEK and GSK3β inhibitors (Triciribine, U0126 and AR-A014418; Enzo Life Sciences, Plymouth Meeting, PA, USA), ABT737 (Calbiochem, Merck KGaA, Darmstadt, D) and staurosporine (Sigma–Aldrich, St Louis, MO, USA).

High-throughput screening and viability assay

On day 0, HME cells bearing the EGFR delE746A750 mutation (named HME EGFR hereafter) were transfected with siRNAs, arrayed on 384-well plates, using a reverse transfection protocol at a final siRNA concentration of 50 nM. The siRNA pools used for the screening corresponded to the human protein kinases and ubiquitin conjugation subsets (1, 2 and 3) sub-libraries (total 1312 gene targets, 4 siRNAs per gene target; siGENOME SMARTPool technology, GE Healthcare Dharmacon, Lafayette, CO, USA). siRNA transfection was performed with Lipofectamine RNAiMAX Transfection Reagent (Thermo Fisher Scientific, Waltham, MA, USA), according to the manufacturer's instructions. After 48 h, cells were treated with Smac mimetic (SM83) [26,27] in combination with isoleucine-zipper TRAIL (izTRAIL) [28] at a final concentration of 100 nM and 0.5 ng/ml, respectively; a parallel set of transfected cells was left untreated. After further 48 h, cell viability was evaluated by measuring cellular ATP content, with CellTiter-Glo (Promega, Madison, WI, USA), according to manufacturer's protocol. Two independent experiments were performed. Luminescence values were normalized to the sample median, on a per plate basis, and untreated:treated ratios were calculated for each knock-down.

Validation experiments of the 20 candidate genes indentified in the screening were performed by transfecting the HME EGFR cells with the 4 individual siRNAs that composed the corresponding siRNA pools (siGENOME, Dharmacon). Experiments were performed in 96 well plates and viability tested using the conditions applied in the screening.

Silencing and ectopic expression

Silencing experiments were performed by reverse transfection using Lipofectamine RNAiMAX Transfection Reagent and siRNAs dissolved in Opti-MEM (Thermo Fisher Scientific). The final siRNA concentration was 50 nM. When a single knock-down was compared to a double knock-down, 25 nM non-targeting siRNA was added to the single targeting siRNA to reach the same final concentration in all the reactions. The individual siRNAs employed were purchased from Dharmacon (NT#1 siGENOME Non-Targeting siRNA Pool #1 D-001206-13, NT#5 siGENOME Non-Targeting siRNA #5 D-001210-05; LMTK2 D-003149-06 and D-003149-21; ERN1 D-004951-02 and 004951-03; CDK5 D-003239-07 and D-003239-08) and QIAGEN (siRelA/p65 Hs_RELA_5; siGSK3β Hs_GSK3B_5; siPP1A Hs_PPP1CA_9; siPP1R2 Hs_PPP1R2_6; siPP1C Hs_PPP1CC_5; siBIM#5 Hs_BCL2L11_5 and siBIM#15 Hs_BCL2L11_15; QIAGEN, Hilden, DE). The control siRNAs (siCtr) used in western blots and viability tests were synthesized by Eurofins Genomics (sequence 5′-CGUACGCGGAAUACUUCGATT-3′).

To ectopically express BCL2 and BCL-xL in combination with LMTK2 silencing, HME EGFR cells were seeded (2×10^4 cells/well in 96 wells) and left adhere overnight. The day after, a mix containing 0.25 μl siRNA 20 μM (control or LMTK2 specific), plus 0.2 μg plasmid (pcDNA-GFP, pCMV6-Entry-BCL2-Myc; Origene #RC204498 and pCMV6-Entry-BCL-xL-Myc; Origene #RC201314) and 0.35 μl Lipofectamine2000 Transfection Reagent was added to each well. After 48 h, cells were treated with 500 ng/mL izTRAIL for 24 h and then viability assessed by CellTiter-Glo. For western blots, cells were seeded in 12-well plates and reagents scaled-up according to well surface (13×).

Caspase activity

Apoptosis induction was measured by CellEvent Caspase-3/7 Green Detection Reagent (Thermo Fisher Scientific) which was dissolved in the culturing medium 1 h before administration of izTRAIL. Caspase activity was detected in time-course experiments by fluorescence and phase contrast image acquisition using a Cell-IQ SLF instrument (CM Technology Oy, Tampere, Finland). Green fluorescence-positive cells were identified and counted using the integrated Cell-IQ Imagen software.

Western blot

To detect protein levels, cells were trypsinized, washed in 1× PBS and boiled in lysis buffer (125 mM Tris HCl pH 6.8, 5% sodium dodecyl sulfate/SDS) for 10 min. Protease and phosphatase inhibitors were added to samples, which were then sonicated and centrifuged at 11,000 rpm for 15 min at RT. Cleared supernatants were separated by SDS-PAGE on precast 4–12% Bis–Tris NuPAGE gels (Thermo Fisher Scientific) and blotted onto PVDF membranes (Merck Millipore, Darmstadt, Germany) using the XCell II blot module (Thermo Fisher Scientific). Membranes were saturated in Tris-buffered saline (TBS) with 4% BSA for 30 min and then incubated overnight with the following primary antibodies: ERN1 #3294, BAX #2772, BAD #9292, XBP-1s #12782, PUMA #4976, BID #2002, p-p65 #3031, GSK3β, #12456, pGSK3β #5558, pPP1A #2581, PP1A #2582, Cleaved PARP #9541, Cleaved Caspase3 #9664, phospho-Akt Ser473 #9271, Akt #2920, Phospho-MEK1/2 #9121, MEK1/2 #4694, Myc-Tag #2278 (Cell Signaling Technology, Danvers, MA, USA), MCL1 sc-819 (Santa Cruz Biotechnology; Dallas, TX 75220, USA), NOXA #OP180 (Merck Millipore; Darmstadt, DE), BIM #559685 (BD Biosciences; 9320 Erembodegem, Belgium), phospho-ERK1/2 #M8159, ERK1/2 #M5670, LMTK2 SAB4500900, Actin #A1978, Vinculin #V9131 (Sigma–Aldrich). Antibodies specific for BCL2 [29] and BCL-xL [30] have been described previously. After 1 h incubation with the appropriate horseradish peroxidase-conjugated secondary antibody (Sigma–Aldrich), proteins were detected by electrochemiluminescence (ECL) reaction (EuroClone). Band density has been calculated by ImageQuant 5.2 and normalized to Actin. An arbitrary value of 1 has been assigned to the appropriate control sample and the others have been expressed as fold values.

Statistical analysis

Statistical analysis and graphs were performed using GraphPad Prism 5.02. P values were calculated by paired two-tailed t-test. A value of $P < 0.05$ was considered statistically significant.

Results

Identification of new modulators of cell sensitivity to TRAIL using a high-throughput RNAi screening approach

To identify genes whose knock-down increases the cytotoxicity of TRAIL, we performed a siRNA-based high-throughput screening using the HME EGFR cell line. Cells were transfected with a library of human siRNAs (pools of 4 siRNAs per target gene) targeting 714 kinases and 598 ubiquitin-related proteins, and then were either left untreated or treated with SM83 in combination with izTRAIL at sub-toxic concentrations. Cell viability was determined 48 h later by measuring cellular ATP content, using a luciferase-based assay (Fig. 1a). For each target gene, sensitivity to izTRAIL/SM83 treatment was assessed by comparing the viability of untreated cells with that of cells treated with izTRAIL/SM83 (Fig. 1b). Genes leading to at least 3-fold reduction of viability in the presence of izTRAIL/SM83 (untreated:izTRAIL/SM83 ratio >3) were selected. The siRNA pools which resulted in cell viability <80% in untreated conditions were considered toxic and excluded from further analysis. Using these criteria, we selected 20 candidate genes (Fig. 1a and c, and

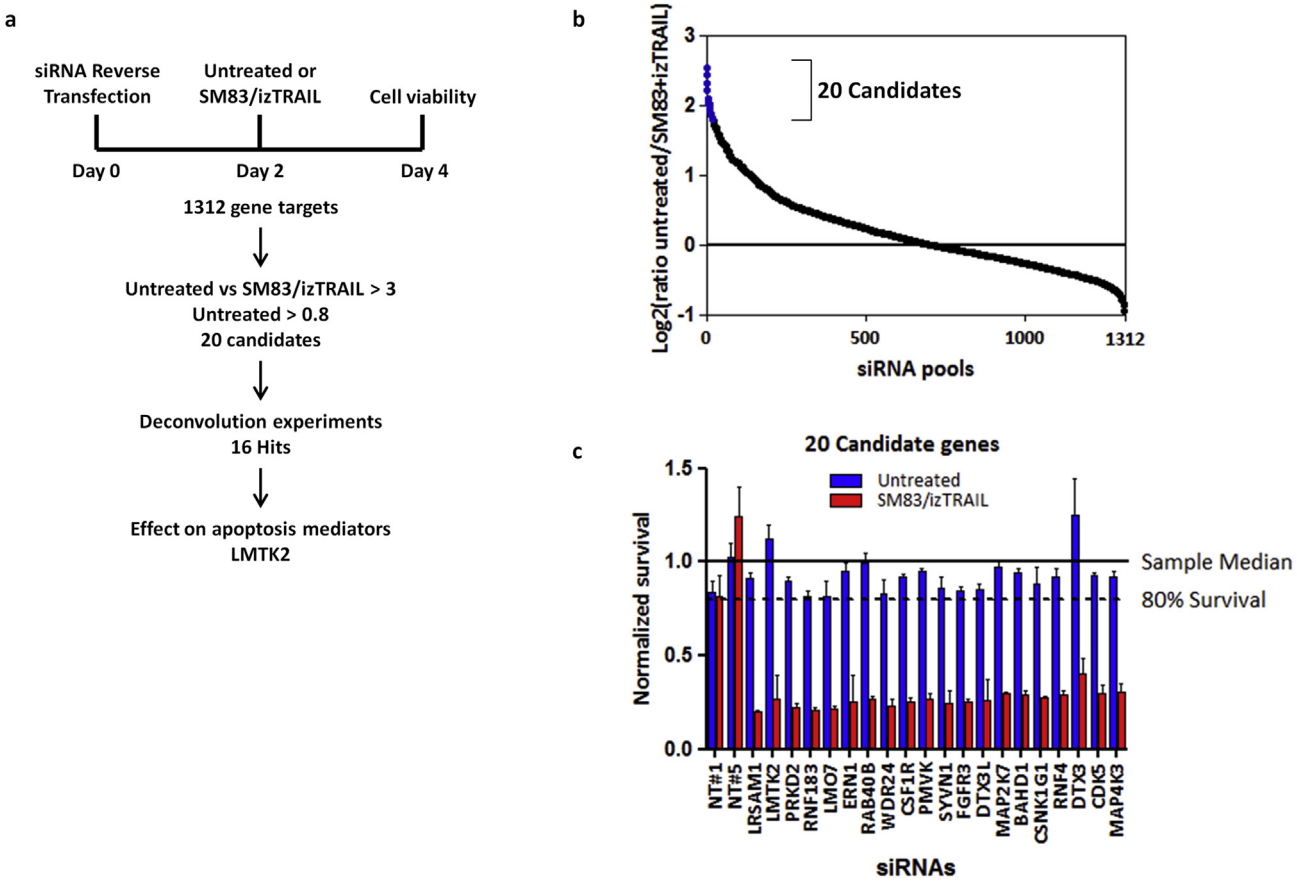

Fig. 1. *High-throughput screening to identify novel determinants of cell sensitivity to TRAIL.* (**a**) Schematic of the RNAi screening to identify determinants of TRAIL sensitivity. On day 0, HME EGFR cells were transfected with siRNA pools targeting human protein kinases and ubiquitin-related enzymes. On day 2, cells were treated with SM83 and izTRAIL and, on day 4, cell viability was evaluated. (**b**) Distribution of the ratio between the viability of cells silenced for each specific siRNA untreated and treated with izTRAIL/SM83. (**c**) Viability of HME EGFR cells transfected with the siRNAs against the 20 candidate genes identified in the primary screening and treated with SM83/izTRAIL; results of untreated (blue) and cells treated with izTRAIL/SM83 (red) are shown; NT#1 and NT#5 indicate two non-targeting siRNAs which were used as controls. (For interpretation of the references to colour in this figure legend, the reader is referred to the web version of this article.)

Table 1), which were further validated in deconvolution experiments using the 4 independent siRNAs that composed the siRNA pools tested initially (Supplementary Fig. S1). Genes were validated and considered true hits only if 2 or more individual siRNAs reproduced the effect observed by the siRNA pools, i.e. the ratio treated:untreated was <0.33 (16 genes out of 20 genes were validated, green in Supplementary Fig. S1): LRSAM1, LMTK2, PRKD2, RNF183, ERN1, RAB40B, WDR24, PMVK, SYVN1, FGFR3, DTX3L,

Table 1
List of the top scoring siRNA pools increasing the sensitivity of HME EGFR cells to treatment. HME EGFR cells were transfected with a library of siRNAs targeting kinases and ubiquitin-related enzymes (total 1312 gene targets; pools of 4 siRNAs per gene target) and treated with izTRAIL and SM83 combination.

Gene ID	Entrez ID	Gene name	Untreated	SM83/TRAIL	Untreated vs SM83/TRAIL
LRSAM1	90678	Leucine rich repeat and sterile alpha motif containing 1	0,914	0,197	4,640
LMTK2	22853	Lemur tyrosine kinase 2	1,122	0,265	4,242
PRKD2	25865	Protein kinase D2	0,900	0,224	4,018
RNF183	138065	Ring finger protein 183	0,814	0,206	3,959
LMO7	4008	LIM domain 7	0,812	0,212	3,830
ERN1	2081	Endoplasmic reticulum to nucleus signaling 1	0,953	0,254	3,752
RAB40B	10966	RAB40B, member RAS oncogene family	0,995	0,270	3,683
WDR24	84219	WD repeat domain 24	0,827	0,230	3,603
CSF1R	1436	Colony stimulating factor 1 receptor	0,921	0,256	3,598
PMVK	10654	Phosphomevalonate kinase	0,950	0,270	3,517
SYVN1	84447	Synovial apoptosis inhibitor 1, synoviolin	0,860	0,248	3,466
FGFR3	2261	Fibroblast growth factor receptor 3	0,849	0,250	3,394
DTX3L	151636	Deltex 3-like (Drosophila)	0,855	0,259	3,301
MAP2K7	5609	Mitogen-activated protein kinase kinase 7	0,972	0,297	3,273
BAHD1	22893	Bromo adjacent homology domain containing 1	0,940	0,288	3,268
CSNK1G1	53944	Casein kinase 1, gamma 1	0,885	0,272	3,252
RNF4	6047	Ring finger protein 4	0,920	0,287	3,211
DTX3	196403	Deltex homolog 3 (Drosophila)	1,248	0,402	3,104
CDK5	1020	Cyclin-dependent kinase 5	0,929	0,300	3,102
MAP4K3	8491	Mitogen-activated protein kinase kinase kinase kinase 3	0,918	0,304	3,020

MAP2K7, CSNK1G1, DTX3, CDK5 and MAP4K3. On the contrary, LM07, CSF1R, BAHD1, and RNF4 were excluded at this stage (red in Supplementary Fig. S1).

LMTK2 affects the expression of BIM, BCL2 and BCL-xL

Next, we checked the effect of the silencing of the validated 16 hits on several mediators of the apoptotic pathway to infer a potential mechanism for the observed sensitization. We focused mainly on LMTK2 and CDK5, which are known to interact with each other and to play a role in some common pathways [14], and ERN1, already known to affect sensitivity to TRAIL (Fig. 2a) by causing DR5 mRNA decay. Accordingly, the silencing of ERN1 was shown to result in increased levels of TRAIL receptor [31]. As no major differences were observed upon CDK5 silencing which could explain the increased sensitivity to TRAIL, following this analysis, we selected LMTK2, a still poorly characterized kinase. In fact, the down-regulation of LMTK2 caused the reduction of the anti-apoptotic BCL2 and BCL-xL proteins, and the up-regulation of the pro-apoptotic protein BIM. The HME EGFR cells were also characterized by FACS analysis for the expression of the TRAIL receptors (R1, R2 and decoy R3 and R4), since their modulation could affect the sensitivity to TRAIL. However, only TRAIL-R2 was detectable in HME cells and its levels were not increased by LMTK2 silencing (data not shown).

As TRAIL is known to activate the NF-kB pathway [4], we checked whether this occurs also in HME EGFR cells and found that TRAIL-dependent phosphorylation of the NF-kB component p65 (Fig. 2b) was more pronounced upon LMTK2 silencing. We therefore questioned whether NF-kB could be responsible for the modulation of BIM levels, as suggested in other settings [32], but neither the treatment with an inhibitor of the NF-kB pathway (BAY117082; Fig. 2c), nor p65 knock-down (Fig. 2d), prevented the LMTK2 silencing-dependent up-regulation of BIM. Therefore, the silencing of LMTK2 results in the modulation of diverse members of the BCL2 family, causing the down-regulation of the anti-apoptotic proteins BCL2 and BCL-xL, and the accumulation of BIM in a NF-kB-independent manner.

The sensitization effect to TRAIL upon LMTK2 targeting is independent of EGFR status and is valid also in cancer cells

As the screening was performed by employing normal epithelial HME cells bearing oncogenic EGFR, we asked whether our observations could be validated in other cell lines and were dependent on mutated EGFR. For this purpose, LMTK2 was silenced both in the HME and MCF10A cell lines, expressing wild type or mutated EGFR, and viability was evaluated in dose–response experiments (Fig. 3a–d). In both human mammary epithelial cell lines, the depletion of LMTK2 enhanced the killing activity of TRAIL in an equivalent manner (compare Fig. 3a *vs* 3c, and 3b *vs* 3d). Moreover, the sensitization effect was independent of EGFR status as both the parental cell lines and those bearing oncogenic EGFR were killed to a similar extent upon TRAIL administration (compare Fig. 3a *vs* 3b, and 3c *vs* 3d). The finding that LMTK2 silencing enhances the sensitivity to TRAIL in immortalized mammary epithelial cell lines led us to investigate whether this effect could also be observed in fully transformed cancer cells. To this end, we selected a panel of cancer cell lines, such as triple negative breast cancers (MDA-MB231 and BT549) and colon cancers (HCT116 and DLD-1), which, together with prostate and cervical tumors, often express high levels of LMTK2. We silenced LMTK2 in all these cancer cell lines and tested their sensitivity to TRAIL. Although differing in their intrinsic sensitivity to izTRAIL, all the cell lines became more sensitive to the treatment upon LMTK2 knock-down (Fig. 3e–h), suggesting that LMTK2 is a determinant of TRAIL sensitivity in multiple

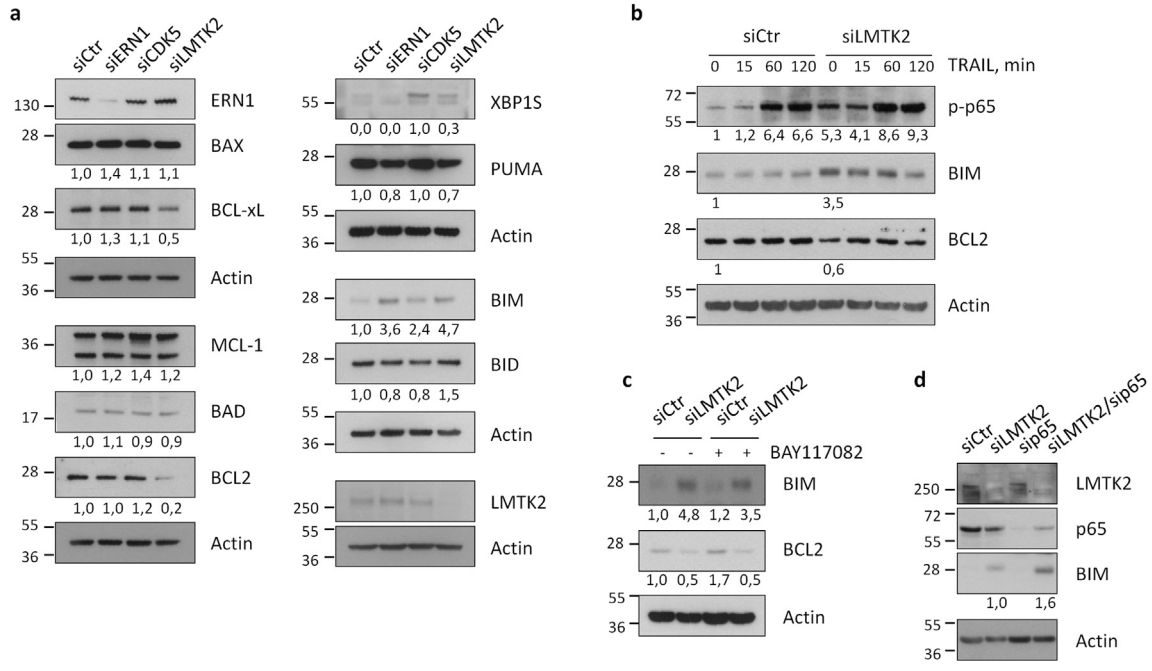

Fig. 2. *LMTK2 controls the levels of several regulators of the apoptotic pathway in an NF-kB-independent manner.* (**a**) HME EGFR cells were transfected with siRNAs targeting ERN1, CDK5 and LMTK2 (two siRNAs per gene, 50 nM final concentration). After 72 h, cells were tested in western blots to evaluate the levels of several mediators of the apoptotic pathway. (**b**) The phosphorylation status of the NF-kB member p65 and the total levels of BIM and BCL2 proteins were evaluated after silencing of LMTK2 in the HME EGFR cell line and treatment with izTRAIL (500 ng/ml) at the indicated time points. The levels of BIM and BCL2 were evaluated also after (**c**) treatment with the NF-kB inhibitor BAY117082 (25 μM) and (**d**) silencing of p65 in the presence o**r** absence of LMTK2 silencing. Actin was used as loading control.

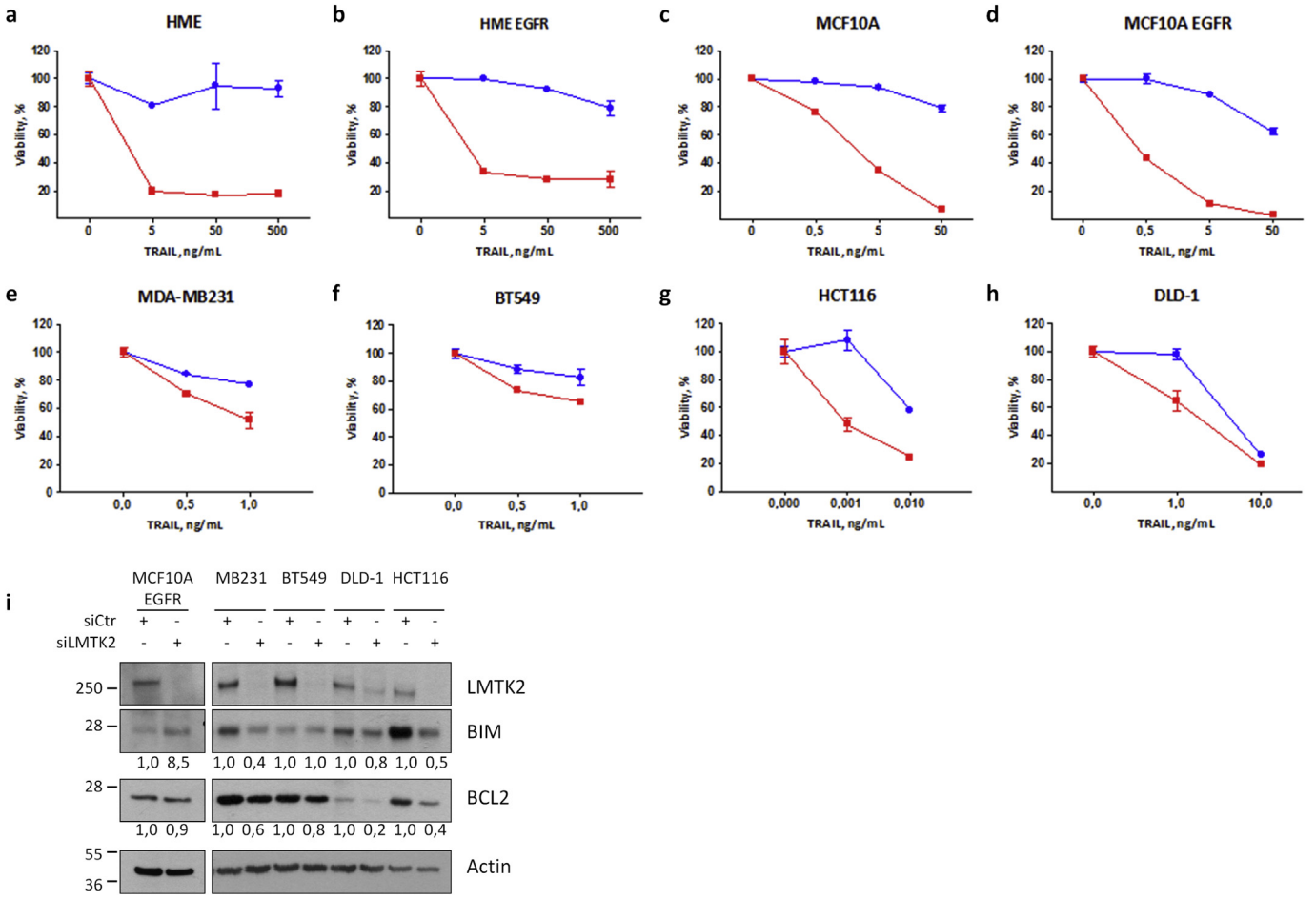

Fig. 3. *Sensitization to TRAIL treatment by LMTK2 silencing is independent of EGFR mutational status and is not cell-line specific.* (**a**–**d**) The capability of LMTK2 silencing to enhance the cytotoxic activity of izTRAIL was tested in the parental (**a**–**c**) and EGFR mutated (**b**–**d**) HME and MCF10A cells. Cells were transfected with non-targeting siRNAs (blue) and siRNAs specific for LMTK2 (red) and, 48 h later, treated with the indicated concentrations of izTRAIL. Viability was assessed after further 24 h (**e**–**f**) Breast and (**g**–**h**) colorectal cancer cell lines were transfected either with non-targeting or LMTK2-specific siRNAs and, after 48 h, treated with the indicated concentrations of izTRAIL. Viability was measured 24 h later. Results are representative of two independent experiments. (**i**) BIM and BCL2 levels in MCF10A EGFR, MDA-MB231, BT549, DLD-1 and HCT116 cells were detected by western blot 72 h after silencing of LMTK2. Actin is shown as loading control. (For interpretation of the references to colour in this figure legend, the reader is referred to the web version of this article.)

cell types. Therefore, the down-regulation of LMTK2 enhances the cytotoxic effect of izTRAIL independently of EGFR mutation and is not cell-line specific.

As BIM up-regulation was observed in HME EGFR cells upon LMTK2 silencing, we checked whether this was true also in MCF10A EGFR. Interestingly, BIM was up-regulated also in these cells, while expression of BCL2 did not vary significantly (Fig. 3i). Then, we checked the effect of LMTK2 silencing in the cancer cells lines described above. In clear contrast to what was observed in HME and MCF10A EGFR cells, LMTK2 knock-down decreased the levels of BIM in MDA-MB231, HCT116 and DLD-1 cells, while in the BT549 cell line it had no effect (Fig. 3i). Nonetheless, BCL2 expression was reduced upon LMTK2 silencing in all the four cell lines tested in accordance to HME EGFR cells. Overall, LMTK2-dependent regulation of BIM is more evident in non-cancer cell lines, while other members of the BCL2 family, such as BCL2 and BCL-xL (Figs. 2a and 3i), could be regulated by LMTK2 mainly in fully transformed cancer cells.

Silencing of LMTK2 affects AKT and ERK signaling

In an attempt to understand the mechanisms by which LMTK2 regulates the above described BCL2 family members and the sensitivity to TRAIL, we investigated the activation of AKT and ERK1/2, known to be induced by TRAIL [4], in control and LMTK2-silenced cells, treated with izTRAIL alone. In fact, we observed that LMTK2 silencing enhances the cytotoxic activity of TRAIL even in the absence of SM83 and therefore we studied the function of this kinase employing TRAIL in monotherapy. LMTK2 silencing resulted in a reduction of AKT and ERK1/2 phosphorylation (Fig. 4a–b) compatible with a decrease of their activity in unstimulated conditions. To understand whether the modulation of these pathways was responsible for BIM regulation, we treated the cells with inhibitors of AKT (Triciribine) or compounds that prevent ERK activation (U0126). All of these treatments increased BIM expression upon LMTK2 silencing (Fig. 4a–b) in untreated conditions. Therefore, LMTK2 silencing reduces the activation of AKT and ERK1/2 and this correlates to increased levels of BIM. Moreover, the chemical inhibition of these kinases further contributes to the increase of BIM levels.

As LMTK2 was shown to regulate GSK3β [15] and this kinase is inhibited by AKT and ERK [17,18], we checked whether GSK3β could play a role in the regulation of BIM. Therefore, cells silenced or not for LMTK2 were treated with the GSK3β inhibitor AR-A014418 and analyzed in time-course experiments for BIM expression. In control cells, the low basal expression of BIM was weakly affected by GSK3β

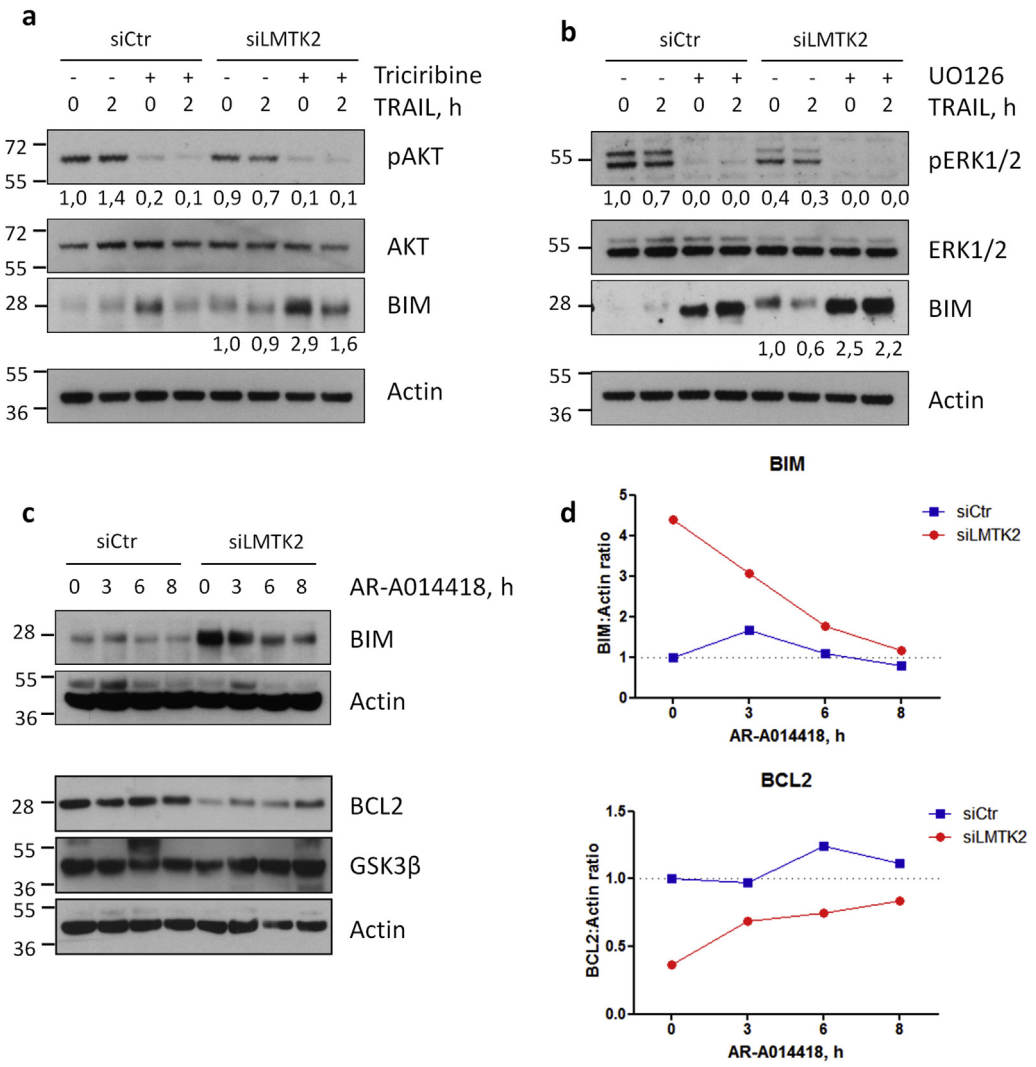

Fig. 4. *Effect of LMTK2 silencing on AKT, ERK and GSK3β signaling.* (**a**–**b**) HME EGFR cells silenced with control siRNAs and siLMTK2 for 72 h were pre-treated with the AKT (20 μM Triciribine) and MEK (25 μM U0126) inhibitors for 1 h and then treated with izTRAIL for an additional 2 h to detect the activation of AKT and ERK1/2, and its correlation with BIM levels. (**c**) HME EGFR cells were transfected with siRNAs targeting LMTK2 for 72 h and then treated with 50 μM GSK3β inhibitor AR-A014418 for the indicated periods. Western blot was performed to evaluate the levels of BIM (upper panel), and BCL2 and GSK3β (lower panel). Actin was used as loading control. (**d**) BIM (upper graph) and BCL2 (lower graph) levels calculated by densitometric analysis of western blot shown in Fig. 4c. Levels of BIM and BCL2 in cells not treated with AR-A014418 and trasfected with control siRNA were arbitrarily set as 1.

inhibition with AR-A014418, but BIM expression was markedly reduced in LMTK2-silenced cells (Fig. 4c–d) which expressed higher levels of BIM (Figs. 2a and 4). Importantly, the down-regulation of BIM caused by GSK3β inhibition was paralleled by the up-regulation of BCL2 (Fig. 4c–d). Altogether, our findings support the notion that the depletion of LMTK2 results in the inhibition of the AKT and ERK pathways and promotes the accumulation of BIM and the reduction of BCL2 and BCL-xL in a GSK3β-dependent fashion.

LMTK2 controls BIM levels through the engagement of GSK3β and PP1A

Then, we investigated the role of PP1A, which is known to interact with LMTK2 and mediate its effect on GSK3β [15], and found that LMTK2 silencing decreases the phosphorylation of PP1A (Fig. 5a, right panel, and 5b) and this correlated with a reduction of GSK3β phosphorylation (Fig. 5a, right panel, and 5b). The latter effect of LMTK2 silencing was more pronounced after the administration of izTRAIL (Fig. 5b), which resulted in less phosphorylation of GSK3β on Ser9 (i.e. increased activation). Interestingly, the silencing of PP1A slightly augmented GSK3β phosphorylation in untreated conditions (Fig. 5a–b), but profoundly after TRAIL treatment. This suggests that PP1A promotes GSK3β activity by reducing its inhibitory phosphorylation, but also counteracts its effect on BIM. Accordingly, BIM was regulated in a positive manner by GSK3β, but negatively by LMTK2 and PP1A (Fig. 5a–b).

PP1A is not the only phosphatase that regulates BIM, since the knock-down of PP1C and PP1R2, both known to interact with LMTK2 [9,33,34], also increased BIM expression (Fig. 5c). Interestingly, PP1A silencing sensitized cells to TRAIL to the same extent as LMTK2 silencing and the double knock-down showed no additive or synergistic effect on TRAIL toxicity (Fig. 5d) suggesting that these proteins play a role in the same pathway. Altogether, our findings indicate that LMTK2 promotes the inhibitory phosphorylation of PP1A which in turn is not able to dephosphorylate GSK3β at Ser9. When LMTK2 is silenced, this results in increased activity of GSK3β,

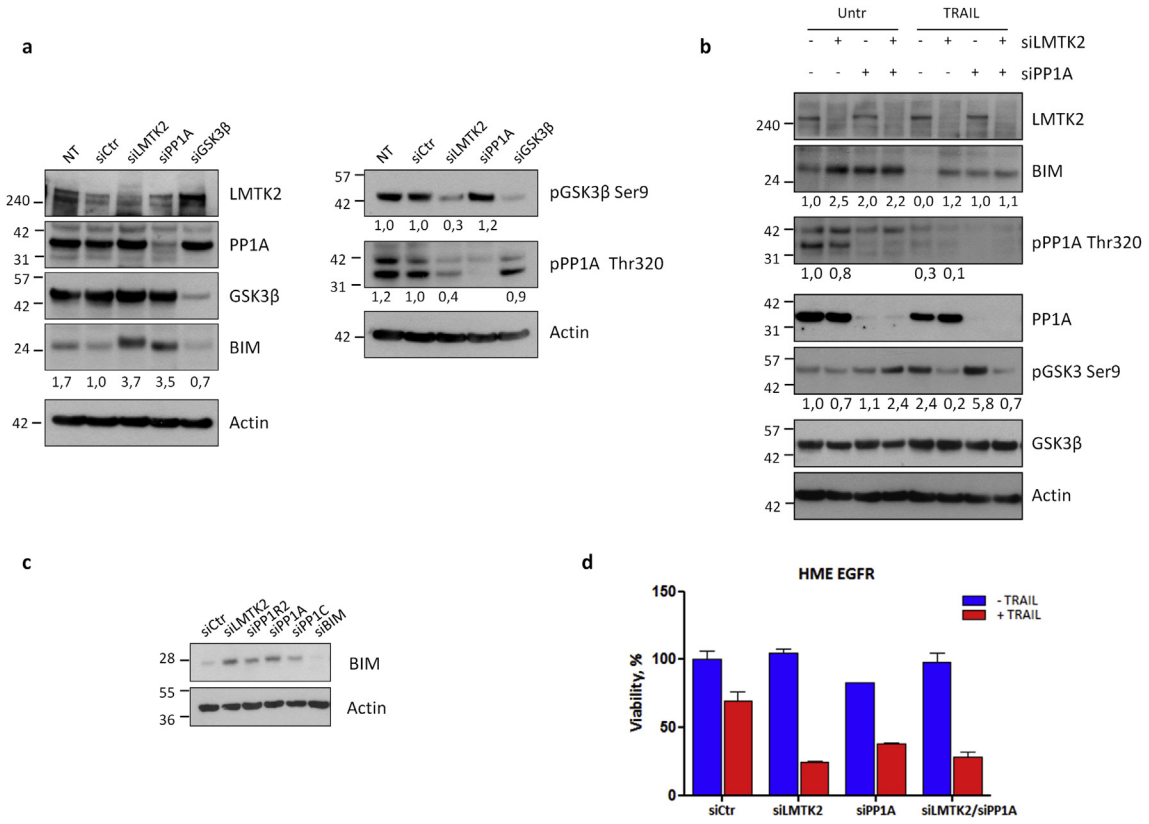

Fig. 5. *LMTK2 regulates BIM levels in a GSK3β- and PP1-dependent manner.* (**a**) LMTK2, PP1A and GSK3β were silenced in HME EGFR cells and, after 72 h, the levels of BIM, the inhibitory phosphorylation status of PP1A and GSK3β, and their total levels, were investigated by western blot. NT: non-transfected control. (**b**) HME EGFR cells were transfected with siRNAs targeting LMTK2, PP1A, and the combination of them. After 72 h, cells were treated with 500 ng/ml izTRAIL for 4 h and tested in western blot to evaluate the levels of LMTK2, BIM, PP1A, GSK3β and the phosphorylation of PP1A and GSK3β. (**c**) The levels of BIM were evaluated 72 h after transfection with siRNAs targeting LMTK2, PP1A and its interactors PP1R2 and PP1C. The silencing of BIM is shown as control of antibody specificity and actin was used as loading control. (**d**) HME EGFR cells were transfected with siRNAs targeting LMTK2, PP1A and their combination. After 48 h, cells were treated with 500 ng/ml izTRAIL for 24 h and cell viability was measured. Results are representative of two independent experiments.

which favors the accumulation of BIM. GSK3β and PP1A mutually regulate each other, but the former is a promoter of BIM accumulation, whereas the latter had an opposite effect.

The perturbation of the BCL2 family members caused by LMTK2 silencing contributes to the increased sensitivity to TRAIL

The observation that LMTK2 silencing causes BIM accumulation and increases the sensitivity to TRAIL, prompted us to investigate the existence of a causal relationship between these events. To this end, BIM was silenced using two different siRNAs (Fig. 6a) alone or in combination with LMTK2 silencing. Interestingly, while LMTK2 knock-down, as expected, sensitized cells to izTRAIL, LMTK2/BIM double knock-down partially, but significantly, protected cells from the treatment. The increased cell viability (Fig. 6a) correlated with a reduced accumulation of cleaved PARP and caspase-3 proteins (Fig. 6b), and lower activity of caspases-3 and -7, as measured by fluorometric assay (Fig. 6c). Therefore, the accumulation of BIM contributes to the observed increased sensitivity to TRAIL, but the regulation of other proteins such as the BCL2 family members (Fig. 2a) could also affect the sensitization.

For this reason, we also investigated the effect of BCL2 and BCL-xL, which are both reduced by siLMTK2. BCL2 and BCL-xL were ectopically expressed in HME EGFR cells silenced for LMTK2 or with control siRNAs (Fig. 6d) and treated with TRAIL. In agreement with our hypothesis, the ectopic expression of both BCL2 and BCL-xL partially protected from TRAIL treatment (Fig. 6d), suggesting that their reduction upon LMTK2 targeting contributes, together with BIM up-regulation, to the increased sensitivity.

Therefore, the partial rescue effect obtained by the ectopic expression of BCL2 and BCL-xL suggests that both proteins, together with BIM, play a role in the increased sensitivity to the treatment. Nonetheless, their role could be underestimated in our experimental conditions as the transfection efficiency for over-expression was approximately 30–40% (Fig. 6e).

The sensitizing effect of LMTK2 is not limited to TRAIL

As the members of the BCL2 family are general regulators of the apoptotic pathway and are not specifically appointed to sensitivity to TRAIL, we tested whether LMTK2 silencing could affect the cytotoxic effect of other chemotherapeutic compounds. First, we treated the HME EGFR cells and two cancer cell lines with the BCL2 and BCL-xL inhibitor ABT737, and found that the down-regulation of LMTK2 increases the cytotoxic effect of the treatment in at least 2 out of the 3 tested cell lines (Fig. 7a–c and Table 2). Moreover, we tested if these observations were valid also for other cytotoxic agents such as staurosporine, cisplatin and etoposide. We found that in all cases LMTK2 silencing led to increased sensitivity to treatments and reduced cell viability, with the exception of MDA-MB231 cells treated with etoposide, which were not affected by LMTK2 silencing (Table 2). Thus, LMTK2 targeting affects the cell response to several cytotoxic agents and therefore this kinase could be considered as a new determinant of sensitivity to cell death.

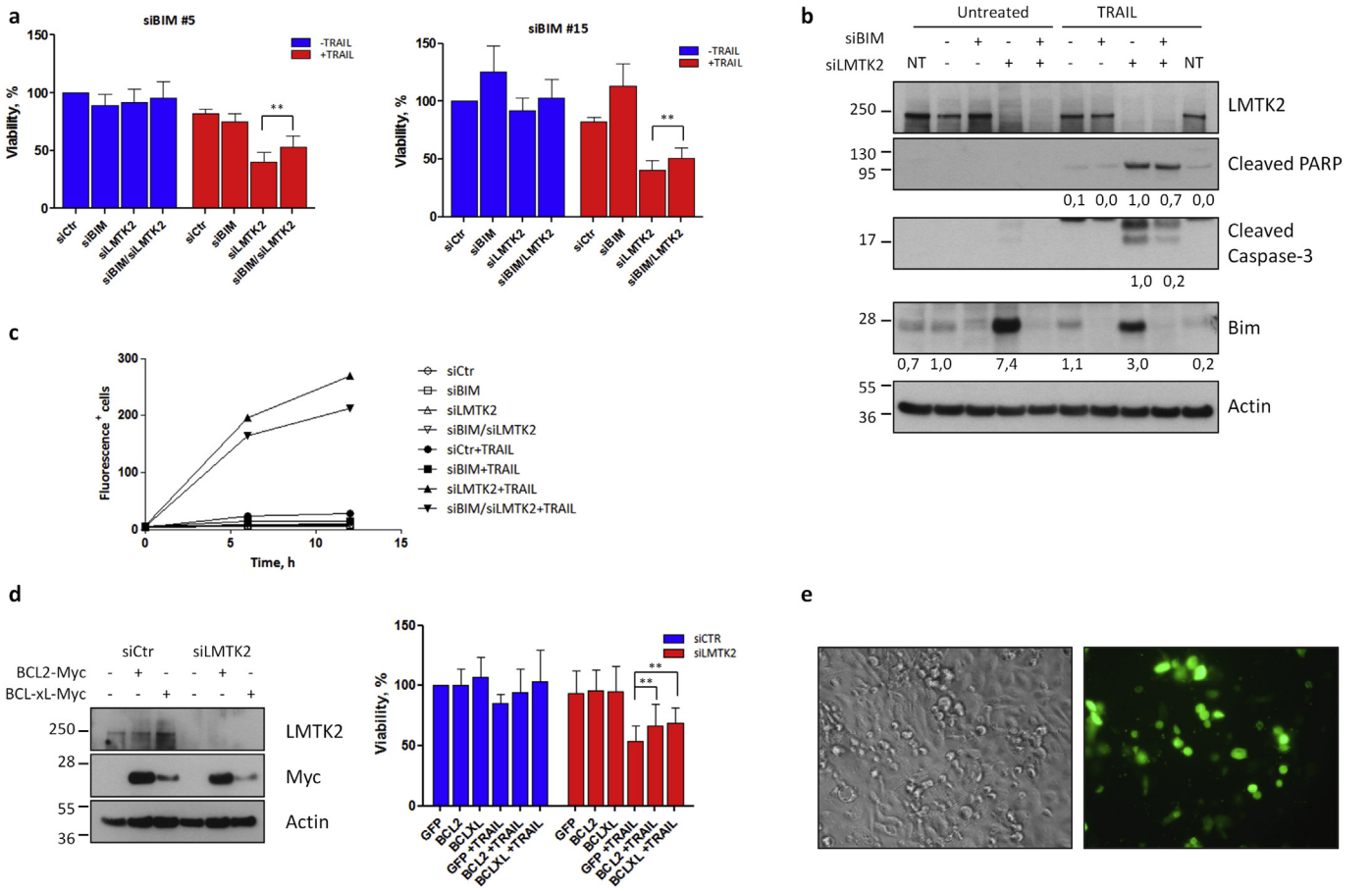

Fig. 6. *The increased sensitivity to TRAIL stemming from LMTK2 silencing is mediated by BIM, BCL2 and BCL-xL.* (**a**) HME EGFR cells were transfected with two different siRNAs targeting BIM and LMTK2 for 48 h and then treated with 500 ng/ml izTRAIL to test cell viability after a further 24 h. Both viability graphs represent the average of 3 independent experiments performed in technical triplicates. The mean of differences between siLMTK2 vs siLMTK2/siBIM #5 and si LMTK2 vs siLMTK2/siBIM #15, treated with izTRAIL, was 12.7% ($P = 0.0169$) and 10.3% ($P = 0.0072$), respectively. P values were obtained by paired two-tailed t-test. (**b**) HME EGFR cells were transfected with siRNAs targeting BIM and LMTK2 alone or in combination; after 72 h, cells were treated with 500 ng/ml izTRAIL for 4 h and subjected to western blot to detect the activation of pro-apoptotic factors. NT: non-transfected control. (**c**) Caspase-3/-7 activity was measured with a fluorescent substrate of Caspase-3/7 upon treatment with 500 ng/ml izTRAIL administered 48 h after the transfection with the indicated siRNAs. (**d**) HME EGFR cells were silenced for LMTK2 and simultaneously transfected to ectopically express BCL2 and BCL-xL, both fused to a Myc-Tag. Control cells were transfected with a GFP-expressing vector. After 48 h, cells were treated with 500 ng/ml izTRAIL and viability assessed after 24 h. Left panel: control of silencing and over-expression showing the levels of LMTK2 and Myc-tagged BCL2 and BCL-xL 72 h after the transfection. Right panel: viability determined in 6 independent experiments: the mean of differences between GFP- vs BCL2-transfected cells and GFP- vs BCL-xL-transfected cells, silenced for LMTK2 and treated with izTRAIL, was 13.2% ($P = 0.0081$) and 15.5% ($P = 0.0039$), respectively. (**e**) Phase contrast and fluorescent microscopy image taken in a representative field to evaluate the transfection efficiency.

Discussion

In this study, we show that LMTK2 represents a novel determinant of sensitivity to TRAIL both in cancer cells and in premalignant models, and its silencing results in enhanced cytotoxic activity of different compounds. This effect is paralleled by the modulation of the BCL2 family proteins, especially BCL2 and BIM. Mechanistically, the down-regulation of LMTK2 causes the reduction of AKT and ERK1/2 activation, a decrease in the inhibitory phosphorylation of GSK3β on Ser9 and consequently an increase of its activity. Moreover, it causes the reduction of PP1A (inhibitory) phosphorylation and this event further contributes to GSK3β activation [15], allowing the phosphatase to reduce the phosphorylation state of GSK3β. Nonetheless, as PP1A is a negative regulator of BIM, its activation counterbalances the GSK3β-dependent accumulation of BIM (Reviewed in the schematic Fig. 7d). Interestingly, BIM up-regulation is observed only in premalignant models, while LMTK2 silencing does not trigger BIM accumulation in cancer cell lines, where however BCL2 is still down-regulated. This observation supports the notion that the outcome of LMTK2 targeting on BIM and BCL2 levels is the result of different effects arising from more than one pathway. This is not surprising as the BIM level, for example, strictly relies not only on its gene transcription, but also on protein stability, which is caused by both phosphorylation and de-phosphorylation events [35]. Therefore, all these mechanisms could be differently regulated in normal, premalignant and fully transformed cells. Nonetheless, the anti-apoptotic effect of LMTK2 is valid for all the cell lines tested and its silencing results in increased sensitivity to TRAIL.

Thus far, the precise physiological function of LMTK2 is unknown. Knock-out mice are viable even if infertile due to defective germ cell maturation [11]. LMTK2 is highly expressed in other tissues, such as skeletal muscle [9,11] and brain [36,37]. Notably, two LMTK2 validated interactors, CDK5 [14·37], and PP1A [9], control neuronal differentiation, synaptic plasticity and axonal transport. The interaction between LMTK2 and the catalytic and regulatory subunits of PP1 has been demonstrated by independent groups [9] and shown to result in GSK3β regulation [15]. Accordingly, we observe that PP1A de-phosphorylates and therefore activates GSK3β [15,38]. Interestingly, both PP1A and LMTK2 were shown to

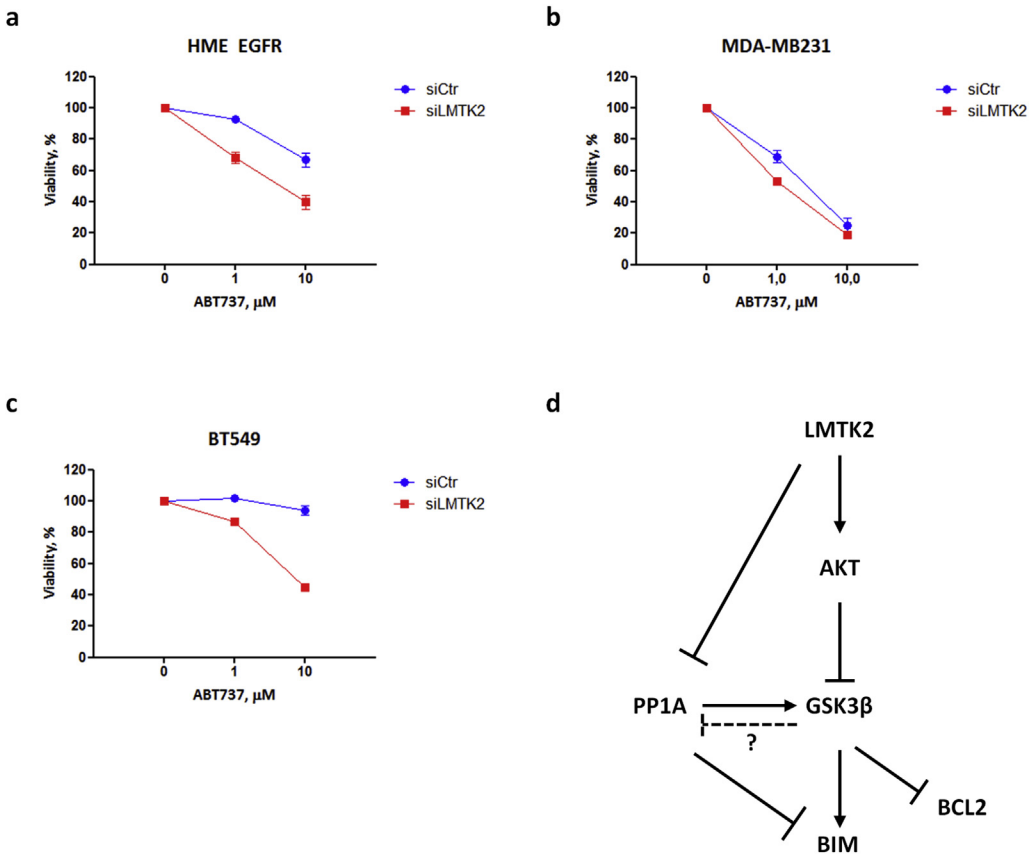

Fig. 7. *LMTK2 silencing enhances the cytotoxic activity of BCL2-directed compounds.* HME EGFR (**a**), MDA-MB231 (**b**) and BT549 (**c**) were silenced for LMTK2 and then treated with 10 μM ABT737. Viability was evaluated by Cell-TiterGlo. (**d**) According to our model, the silencing of LMTK2 causes the reduction of AKT activity, a kinase known to phosphorylate, and therefore inhibit GSK3β. Simultaneously, LMTK2 silencing reduces the inhibitory phosphorylation of PP1A, and this in turn contributes to GSK3β activation. Accordingly, LMTK2 down-regulation correlates to an increased activation of GSK3β observable by the reduction of the inhibitory phosphorylation of Ser9. Then, GSK3β favors the accumulation of BIM and likely promotes the inhibitory phosphorylation of PP1A on Thr320. As PP1A is a negative regulator of BIM, it counterbalances the GSK3β-dependent accumulation of BIM.

Table 2
Effect of LMTK2 silencing on the cytotoxic activity of different compounds. HME EGFR, MDA-MB231 and BT549 cells were transfected with control siRNAs and siRNAs targeting LMTK2 and treated with serial dilutions of the indicated compounds. Viability was evaluated 24 h after the treatment and IC_{50} calculated by Graphpad Prism on the basis of at least of 3 independent experiments.

Cell line	Cisplatin IC_{50} μM		Etoposide IC_{50} μM		Staurosporine IC_{50} μM		ABT737 IC_{50} μM	
	siCtr	siLMTK2	siCtr	siLMTK2	siCtr	siLMTK2	siCtr	siLMTK2
HME EGFR	24,4	9,10	218	129	0,840	0336	19,8	4,33
MDA-MB231	586	186	228	240	4,92	0,975	2,64	1,30
BT549	154	17,6	151	69,9	1,47	0,120	165	7,94

be phosphorylated by CDK5 [37,38]. Also this kinase (CDK5) was found by us among the 16 hits confirmed in validation experiments and therefore represents, together with other CDKs [6,39,40], a potential target for combination therapy with TRAIL, even if the precise mechanism by which CDK5 affects TRAIL sensitivity still needs to be established.

Besides the role of LMTK2 in the neural system, recent findings have suggested a function also in cancer cells. In fact, several mutations have been identified in patients bearing pulmonary sarcomatoid carcinomas [19], lung adenocarcinomas [20] and prostate cancer [21,22], but their biological effect is still unknown. Our findings suggest that LMTK2 could promote cancer survival by hindering the apoptotic cascade. In fact, we show that LMTK2 targeting promotes the expression of the pro-apoptotic factor BIM and the down-regulation of the anti-apoptosis BCL2 family members, BCL-xL and BCL2. As these proteins are universal regulators of the apoptotic pathway, not tightly related to TRAIL-mediated apoptosis, it is conceivable that LMTK2 is a broad regulator of cell death, rather than that selectively triggered by TRAIL or other death ligands. In agreement to this idea, the silencing of LMTK2 resulted in an increased cytotoxic effect of staurosporine, etoposide, cisplatin and especially ABT737, a well characterized inhibitor of BCL2 and BCL-xL. Nonetheless, LMTK2 does not regulate the cell sensitivity to every compound, as the treatment with gemcitabine, for example, was not affected by LMTK2 silencing (data not shown). We have found that different members of the BCL2 family are controlled by LMTK2 in a cell-type dependent manner and all of them contribute to the final sensitivity. Accordingly, the up-regulation of BIM following LMTK2 knock-down is indeed responsible for the increased sensitivity to TRAIL, even if not sufficient to trigger cell death without an apoptotic stimulus, in agreement with other works [35,41]. Moreover, BIM is not the only determinant and the

silencing of BIM only partially rescues the viability of cells depleted for LMTK2 and treated with izTRAIL. Our evidences support the notion that also the down-regulation of BCL2 and BCL2-xL triggered by LMTK2 silencing, contributes to the overall increased sensitivity to treatment. Of note, also the rescue effect of ectopic BCL2 and BCL-xL expression is only partial, as in the case of BIM, suggesting that the overall sensitizing effect of LMTK2 silencing is ascribable to the sum of the effects of BIM up-regulation and BCL2 and BCL-xL down-regulation. Nonetheless, the role of BCL2 and BCL-xL could be more substantial than shown by our results as the transfection efficiency was less than 50% and therefore, their effect could be underestimated as many cells did not express the ectopic proteins.

Notably, LMTK2 silencing sensitizes not only premalignant cells but also cancer cells to TRAIL cytotoxicity, as in the case of breast and colorectal cancers. Interestingly, in these cancer cells BIM appears not involved in the increased sensitivity as its levels do not change, but rather decline, upon LMTK2 silencing. Therefore, other mechanisms are responsible for the increased sensitivity, and BCL2 reduction could play a role in this. More work is indeed necessary to understand the different mechanisms of regulation of BIM and BCL2 in different models, but, in our work, we show that both proteins are regulated in an opposite manner by GSK3β. This observation, together with the finding that LMTK2 silencing reduces the phosphorylation, and therefore, the activation of AKT, supports the existence of a still uncharacterized survival pathway involving LMTK2, AKT and GSK3β, which affect cell viability by regulating the levels of the BCL2 family members.

In conclusion, our work supports the notion that LMTK2 could represent a new potential target for therapy and lay the basis for the development of a new class of small molecules targeting this kinase. These compounds could be exploitable both in clinic and as tool for the comprehension of the physiological role of LMTK2. Nonetheless, the observation that LMTK2 targeting sensitizes both non-cancer, even if immortalized, and cancer cells to death highlights the need of further investigation to evaluate the toxicity of a LMTK2-directed therapy in primary cells and normal tissues. Therefore, more work is necessary to understand the biological role of LMTK2 and to determine whether its inhibition could be exploited as a new approach in anti-cancer therapy.

Acknowledgments

We are grateful to Elda Tagliabue for providing us with the BT549 and MDA-MB231 cells, Henning Walczak for izTRAIL, Pierfausto Seneci for SM83, Christofer Borner and Florian Haun for data discussion. This study was supported by the Italian Association for Cancer Research (AIRC, MCO − 9998, D.D.). M.M. was supported by the FIRB RBAP11Z4Z9 project from the Italian Ministry of Education, University and Research.

Conflict of interest

The authors declare no conflict of interest.

Appendix A. Supplementary data

Supplementary data related to this article can be found at http://dx.doi.org/10.1016/j.canlet.2016.12.025.

References

[1] A. Ashkenazi, R.S. Herbst, To kill a tumor cell: the potential of proapoptotic receptor agonists, J. Clin. Investig. 118 (6) (2008) 1979–1990.
[2] J. Lemke, S. von Karstedt, J. Zinngrebe, H. Walczak, Getting TRAIL back on track for cancer therapy, Cell Death Differ. 21 (9) (2014 Sep) 1350–1364.
[3] H. Walczak, M.A. Degli-Esposti, R.S. Johnson, P.J. Smolak, J.Y. Waugh, N. Boiani, et al., TRAIL-R2: a novel apoptosis-mediating receptor for TRAIL, EMBO J. 16 (17) (1997) 5386–5397.
[4] S. von Karstedt, A. Conti, M. Nobis, A. Montinaro, T. Hartwig, J. Lemke, et al., Cancer cell-autonomous TRAIL-R signaling promotes KRAS-driven cancer progression, invasion, and metastasis, Cancer Cell 27 (4) (2015 Apr 13) 561–573.
[5] C.D. Fingas, B.R. Blechacz, R.L. Smoot, M.E. Guicciardi, J. Mott, S.F. Bronk, et al., A smac mimetic reduces TNF related apoptosis inducing ligand (TRAIL)-induced invasion and metastasis of cholangiocarcinoma cells, Hepatology 52 (2) (2010 Aug) 550–561.
[6] J. Lemke, S. von Karstedt, M. Abd El Hay, A. Conti, F. Arce, A. Montinaro, et al., Selective CDK9 inhibition overcomes TRAIL resistance by concomitant suppression of cFlip and Mcl-1, Cell Death Differ. 21 (3) (2014 Mar) 491–502.
[7] D. Lecis, C. Drago, L. Manzoni, P. Seneci, C. Scolastico, E. Mastrangelo, et al., Novel SMAC-mimetics synergistically stimulate melanoma cell death in combination with TRAIL and Bortezomib, Br. J. Cancer 102 (12) (2010) 1707–1716, 06/08.
[8] M.H. Tuthill, A. Montinaro, J. Zinngrebe, K. Prieske, P. Draber, S. Prieske, et al., TRAIL-R2-specific antibodies and recombinant TRAIL can synergise to kill cancer cells, Oncogene 34 (16) (2015 Apr 16) 2138–2144.
[9] H. Wang, D.L. Brautigan, A novel transmembrane Ser/Thr kinase complexes with protein phosphatase-1 and inhibitor-2, J. Biol. Chem. 277 (51) (2002 Dec 20) 49605–49612.
[10] S. Rebelo, M. Santos, F. Martins, E.F. da Cruz E Silva, O.A. da Cruz E Silva, Protein phosphatase 1 is a key player in nuclear events, Cell Signal 27 (12) (2015 Dec) 2589–2598.
[11] S. Kawa, C. Ito, Y. Toyama, M. Maekawa, T. Tezuka, T. Nakamura, et al., Azoospermia in mice with targeted disruption of the Brek/Lmtk2 (brain-enriched kinase/lemur tyrosine kinase 2) gene, Proc. Natl. Acad. Sci. U. S. A. 103 (51) (2006 Dec 19) 19344–19349.
[12] M.V. Chibalina, M.N. Seaman, C.C. Miller, J. Kendrick-Jones, F. Buss, Myosin VI and its interacting protein LMTK2 regulate tubule formation and transport to the endocytic recycling compartment, J. Cell Sci. 120 (Pt 24) (2007 Dec 15) 4278–4288.
[13] T. Inoue, T. Kon, R. Ohkura, H. Yamakawa, O. Ohara, J. Yokota, et al., BREK/LMTK2 is a myosin VI-binding protein involved in endosomal membrane trafficking, Genes Cells 13 (5) (2008 May) 483–495.
[14] C. Manser, A. Vagnoni, F. Guillot, J. Davies, C.C. Miller, Cdk5/p35 phosphorylates lemur tyrosine kinase-2 to regulate protein phosphatase-1C phosphorylation and activity, J. Neurochem. 121 (3) (2012 May) 343–348.
[15] C. Manser, F. Guillot, A. Vagnoni, J. Davies, K.F. Lau, D.M. McLoughlin, et al., Lemur tyrosine kinase-2 signalling regulates kinesin-1 light chain-2 phosphorylation and binding of Smad2 cargo, Oncogene 31 (22) (2012 May 31) 2773–2782.
[16] M. Medina, F. Wandosell, Deconstructing GSK-3: the fine regulation of its activity, Int. J. Alzheimers Dis. 2011 (2011) 479249.
[17] M. Delcommenne, C. Tan, V. Gray, L. Rue, J. Woodgett, S. Dedhar, Phosphoinositide-3-OH kinase-dependent regulation of glycogen synthase kinase 3 and protein kinase B/AKT by the integrin-linked kinase, Proc. Natl. Acad. Sci. U. S. A. 95 (19) (1998 Sep 15) 11211–11216.
[18] Q. Ding, W. Xia, J.C. Liu, J.Y. Yang, D.F. Lee, J. Xia, et al., Erk associates with and primes GSK-3beta for its inactivation resulting in upregulation of beta-catenin, Mol. Cell 19 (2) (2005 Jul 22) 159–170.
[19] X. Liu, Y. Jia, M.B. Stoopler, Y. Shen, H. Cheng, J. Chen, et al., Next-generation sequencing of pulmonary sarcomatoid carcinoma reveals high frequency of actionable MET gene mutations, J. Clin. Oncol. (2015 Jul 27).
[20] J.S. Seo, Y.S. Ju, W.C. Lee, J.Y. Shin, J.K. Lee, T. Bleazard, et al., The transcriptional landscape and mutational profile of lung adenocarcinoma, Genome Res. 22 (11) (2012 Nov) 2109–2119.
[21] R.A. Eeles, Z. Kote-Jarai, G.G. Giles, A.A. Olama, M. Guy, S.K. Jugurnauth, et al., Multiple newly identified loci associated with prostate cancer susceptibility, Nat. Genet. 40 (3) (2008 Mar) 316–321.
[22] L.W. Harries, J.R. Perry, P. McCullagh, M. Crundwell, Alterations in LMTK2, MSMB and HNF1B gene expression are associated with the development of prostate cancer, BMC Cancer 10 (2010 Jun 22), 315-2407-10-315.
[23] K. Shah, N.A. Bradbury, Lemur Tyrosine Kinase 2, a novel target in prostate cancer therapy, Oncotarget 6 (16) (2015 Jun 10) 14233–14246.
[24] C. Puri, M.V. Chibalina, S.D. Arden, A.J. Kruppa, J. Kendrick-Jones, F. Buss, Overexpression of myosin VI in prostate cancer cells enhances PSA and VEGF secretion, but has no effect on endocytosis, Oncogene 29 (2) (2010 Jan 14) 188–200.
[25] A. Conti, M.T. Majorini, R. Elliott, A. Ashworth, C.J. Lord, C. Cancelliere, et al., Oncogenic KRAS sensitizes premalignant, but not malignant cells, to Noxa-dependent apoptosis through the activation of the MEK/ERK pathway, Oncotarget 6 (13) (2015 May 10) 10994–11008.
[26] D. Lecis, E. Mastrangelo, L. Belvisi, M. Bolognesi, M. Civera, F. Cossu, et al., Dimeric Smac mimetics/IAP inhibitors as in vivo-active pro-apoptotic agents. Part II: structural and biological characterization, Bioorg. Med. Chem. 20 (22) (2012 Nov 15) 6709–6723.
[27] D. Lecis, M. De Cesare, P. Perego, A. Conti, E. Corna, C. Drago, et al., Smac mimetics induce inflammation and necrotic tumour cell death by modulating macrophage activity, Cell Death Dis. 4 (2013 Nov 14) e920.
[28] T.M. Ganten, R. Koschny, J. Sykora, H. Schulze-Bergkamen, P. Buchler, T.L. Haas, et al., Preclinical differentiation between apparently safe and

potentially hepatotoxic applications of TRAIL either alone or in combination with chemotherapeutic drugs, Clin. Cancer Res. 12 (8) (2006 April 15) 2640–2646.
[29] D. Delia, A. Aiello, D. Soligo, E. Fontanella, C. Melani, F. Pezzella, et al., Bcl-2 proto-oncogene expression in normal and neoplastic human myeloid cells, Blood 79 (5) (1992 Mar 1) 1291–1298.
[30] S. Krajewski, M. Krajewska, A. Shabaik, H.G. Wang, S. Irie, L. Fong, et al., Immunohistochemical analysis of in vivo patterns of Bcl-X expression, Cancer Res. 54 (21) (1994 Nov 1) 5501–5507.
[31] M. Lu, D.A. Lawrence, S. Marsters, D. Acosta-Alvear, P. Kimmig, A.S. Mendez, et al., Opposing unfolded-protein-response signals converge on death receptor 5 to control apoptosis, Science 345 (6192) (2014 Jul 4) 98–101.
[32] I. Inta, S. Paxian, I. Maegele, W. Zhang, M. Pizzi, P. Spano, et al., Bim and Noxa are candidates to mediate the deleterious effect of the NF-kappa B subunit RelA in cerebral ischemia, J. Neurosci. 26 (50) (2006 Dec 13) 12896–12903.
[33] M. Fardilha, S.L. Esteves, L. Korrodi-Gregorio, A.P. Vintem, S.C. Domingues, S. Rebelo, et al., Identification of the human testis protein phosphatase 1 interactome, Biochem. Pharmacol. 82 (10) (2011 Nov 15) 1403–1415.
[34] S.L. Esteves, L. Korrodi-Gregorio, C.Z. Cotrim, P.J. van Kleeff, S.C. Domingues, O.A. da Cruz e Silva, et al., Protein phosphatase 1gamma isoforms linked interactions in the brain, J. Mol. Neurosci. 50 (1) (2013 May) 179–197.
[35] A.S. Gillings, K. Balmanno, C.M. Wiggins, M. Johnson, S.J. Cook, Apoptosis and autophagy: BIM as a mediator of tumour cell death in response to oncogene-targeted therapeutics, FEBS J. 276 (21) (2009 Nov) 6050–6062.
[36] S. Kawa, J. Fujimoto, T. Tezuka, T. Nakazawa, T. Yamamoto, Involvement of BREK, a serine/threonine kinase enriched in brain, in NGF signalling, Genes Cells 9 (3) (2004 Mar) 219–232.
[37] S. Kesavapany, K.F. Lau, S. Ackerley, S.J. Banner, S.J. Shemilt, J.D. Cooper, et al., Identification of a novel, membrane-associated neuronal kinase, cyclin-dependent kinase 5/p35-regulated kinase, J. Neurosci. 23 (12) (2003 Jun 15) 4975–4983.
[38] G. Morfini, G. Szebenyi, H. Brown, H.C. Pant, G. Pigino, S. DeBoer, et al., A novel CDK5-dependent pathway for regulating GSK3 activity and kinesin-driven motility in neurons, EMBO J. 23 (11) (2004 Jun 2) 2235–2245.
[39] E.H. Kim, S.U. Kim, D.Y. Shin, K.S. Choi, Roscovitine sensitizes glioma cells to TRAIL-mediated apoptosis by downregulation of survivin and XIAP, Oncogene 23 (2) (2004 Jan 15) 446–456.
[40] A.C. Murphy, B. Weyhenmeyer, J. Noonan, S.M. Kilbride, S. Schimansky, K.P. Loh, et al., Modulation of Mcl-1 sensitizes glioblastoma to TRAIL-induced apoptosis, Apoptosis 19 (4) (2014 Apr) 629–642.
[41] A.C. Faber, R.B. Corcoran, H. Ebi, L.V. Sequist, B.A. Waltman, E. Chung, et al., BIM expression in treatment-naive cancers predicts responsiveness to kinase inhibitors, Cancer Discov. 1 (4) (2011 Sep) 352–365.

Oncogenic KRAS sensitizes premalignant, but not malignant cells, to Noxa-dependent apoptosis through the activation of the MEK/ERK pathway

Annalisa Conti[1], Maria Teresa Majorini[1], Richard Elliott[2], Alan Ashworth[2,8], Christopher J. Lord[2], Carlotta Cancelliere[3,4,5], Alberto Bardelli[3,4,5], Pierfausto Seneci[6], Henning Walczak[7], Domenico Delia[1] and Daniele Lecis[1]

[1] Department of Experimental Oncology and Molecular Medicine, Fondazione IRCCS Istituto Nazionale dei Tumori, Milan, Italy

[2] The Breakthrough Breast Cancer Research Centre and CRUK Gene Function Laboratory, The Institute of Cancer Research, London, UK

[3] Department of Oncology, University of Torino, Candiolo, Torino, Italy

[4] Candiolo Cancer Institute - FPO, IRCCS, Candiolo, Torino, Italy

[5] FIRC Institute of Molecular Oncology (IFOM), Milano, Italy

[6] Università Degli Studi di Milano, Dipartimento di Chimica, Milan, Italy

[7] Centre for Cell Death, Cancer, and Inflammation, University College London, London, UK

[8] Current Address: UCSF Helen Diller Family Comprehensive Cancer Centre, San Francisco, California, USA

***Correspondence to**: Daniele Lecis, **email**: daniele.lecis@istitutotumori.mi.it*

Keywords: KRAS, Smac mimetics, colorectal cancer, camptothecin

***Received**: January 23, 2015* ***Accepted**: February 21, 2015* ***Published**: March 12, 2015*

ABSTRACT

KRAS is mutated in about 20-25% of all human cancers and especially in pancreatic, lung and colorectal tumors. Oncogenic KRAS stimulates several pro-survival pathways, but it also triggers the trans-activation of pro-apoptotic genes. In our work, we show that G13D mutations of KRAS activate the MAPK pathway, and ERK2, but not ERK1, up-regulates Noxa basal levels. Accordingly, premalignant epithelial cells are sensitized to various cytotoxic compounds in a Noxa-dependent manner. In contrast to these findings, colorectal cancer cell sensitivity to treatment is independent of KRAS status and Noxa levels are not up-regulated in the presence of mutated KRAS despite the fact that ERK2 still promotes Noxa expression. We therefore speculated that other survival pathways are counteracting the pro-apoptotic effect of mutated KRAS and found that the inhibition of AKT restores sensitivity to treatment, especially in presence of oncogenic KRAS. In conclusion, our work suggests that the pharmacological inhibition of the pathways triggered by mutated KRAS could also switch off its oncogene-activated pro-apoptotic stimulation. On the contrary, the combination of chemotherapy to inhibitors of specific pro-survival pathways, such as the one controlled by AKT, could enhance treatment efficacy by exploiting the pro-death stimulation derived by oncogene activation.

INTRODUCTION

KRAS is a 21 KDa protein involved in cell signal transduction belonging to the RAS subfamily, which comprises several other small GTPases endowed with GTP-hydrolyzing activity. In unstimulated conditions, GTPases are bound to GDP and display low activity, unable to trigger the down-stream signaling processes. RAS proteins require GTP to be activated and undergo rapid cycles of activation and inactivation crucial for physiological signaling [1]. Because these cascades stimulate cell growth and division, aberrant RAS signaling

can also lead to cancer. The 3 human RAS genes (HRAS, KRAS, and NRAS) are among the most prevalent drivers of human cancer, with KRAS being mutated in 20-25% of all human tumors and up to 90% in certain cancer types, e.g. pancreatic cancer [2]. In these settings, KRAS activates several down-stream effectors leading to the stimulation of the RAF/mitogen-activated protein kinase kinase/extracellular signal-regulated kinase (RAF/MEK/ERK) and phosphatidylinositol-3-kinase (PI3K) pathways.

Colorectal cancer (CRC), one of the most widespread cancer types, displays in 40% of cases KRAS activating mutations, primarily involving codon 12 or 13. Several drug combinations are currently used for CRC treatment, including oxaliplatin, 5-FU and the camptothecin (CPT) analogue irinotecan [3]. Moreover, the epidermal growth factor receptor (EGFR)-blocking antibodies cetuximab and panitumumab are approved for treatment of metastatic CRC in combination with chemotherapy and as maintenance therapy in chemorefractory tumors. Receptor tyrosine kinases such as EGFR, through the activation of the downstream GTPases, regulate MAPK and PI3K pathways. Importantly, mutations or amplification of KRAS is often associated to unresponsiveness and acquired resistance to cetuximab [4].

Even though oncogenic KRAS is often associated with poorer prognosis, its mutations have also been considered for targeted therapy taking advantage of combinations that produce a synthetic lethal effect [5, 6]. In fact, the presence of constitutively active KRAS sensitizes cancer cells to MEK and BCL-XL [7] or RAF [8] inhibition, TRAIL [9], 5-FU and oxaliplatin [10]. Nonetheless, KRAS activation is usually associated with reduced proneness to apoptosis and increased resistance to chemotherapy owing to the activation of pro-survival pathways [11-13] and resulting in the up-regulation of anti-apoptotic factors such as the members of the inhibitor of apoptosis proteins (IAP) family [14, 15].

IAPs are characterized by the presence of a conserved baculoviral IAP repeat (BIR) domain [16] important for protein-protein interactions. Despite the 8 members of the IAP family had initially been considered essentially apoptosis negative regulators, only X-linked IAP (XIAP) is known to physically interact with caspases and prevent their activity [17]. Later studies have shown that IAPs regulate cell life aspects other than apoptosis. Cellular IAP1 (cIAP1) and cIAP2, for example, modulate the signaling of pro-survival pathways, such as the ones regulated by NF-kB transcription factors and MAPKs [16]. Interestingly, IAPs are often deregulated in cancer cells and associated to unfavorable prognosis [18]. An opportunity to target IAPs, and especially cIAP1, cIAP2 and XIAP, both for therapeutic purposes and as tools in pre-clinic research is represented by second mitochondria-derived activator of caspases (SMAC) mimetic (SM) small compounds [19]. SMs were designed to mimic the activity of SMAC [20], a natural antagonist of XIAP, which, by interacting with its BIR domains, displaces caspases and promotes their activity with consequent apoptosis induction. SMs also target cIAP1 and cIAP2, causing their degradation [21, 22], modulating several pathways and overcoming cancer cell resistance to therapy [23] and especially to tumor necrosis factor-related apoptosis inducing ligand (TRAIL) [20, 24].

Here we report that SM83, a SM recently described by us [25, 26], greatly enhances the cytotoxic activity of the topoisomerase I inhibitor CPT in premalignant models in which KRAS G13D is endogenously or ectopically expressed in human epithelial cells. The increased sensitivity of oncogenic KRAS-expressing cells stems at least in part from the basal up-regulation of the pro-apoptotic protein Noxa, which is stimulated in an ERK2-dependent manner. In clear contrast to the premalignant models, a panel of CRC lines with knock-in (KI) and knock-out (KO) mutations of KRAS G13D showed that the sensitivity to treatment is independent of KRAS status. Accordingly, Noxa levels are unaffected by oncogenic KRAS expression and other pathways, such as the ones controlled by PI3K/AKT, protect cancer cells from the potentially pro-apoptotic stimulus of mutated KRAS.

RESULTS

The combination of SMs and CPT selectively kills premalignant epithelial cells bearing oncogenic *KRAS*

As SMs are rarely effective in monotherapy, but sensitize cancer cells to other compounds, we searched for drugs whose cytotoxicity can be efficiently enhanced by SM83 using a high-throughput cell based screening approach. HeLa cells were exposed *in vitro* to SM83 and izTRAIL in addition to a combined library of about 3000 FDA-approved small molecule inhibitors and cell viability assessed (see Materials and Methods). Of the 3000 small molecule inhibitors assessed, we found that the topoisomerase I inhibitor camptothecin (CPT) most profoundly enhanced the cytotoxic effect of SM83 (Table 1). In addition to the enhancing effect of CPT, we also found that different formulations of CPT such as 10-hydroxycamptothecin also enhanced the effects of SM83, further confirming that CPT can be effectively combined with SMs and TRAIL. We then asked whether this combination is more cytotoxic in a specific genetic background and treated a panel of premalignant and cancer cell lines with izTRAIL, SM83 and CPT alone or in combination (data not shown). Viability tests showed that the immortalized human epithelial (HME) cell line bearing a KI G13D mutation in the KRAS gene (D13/+) is far more sensitive to SM83 plus CPT treatment compared to

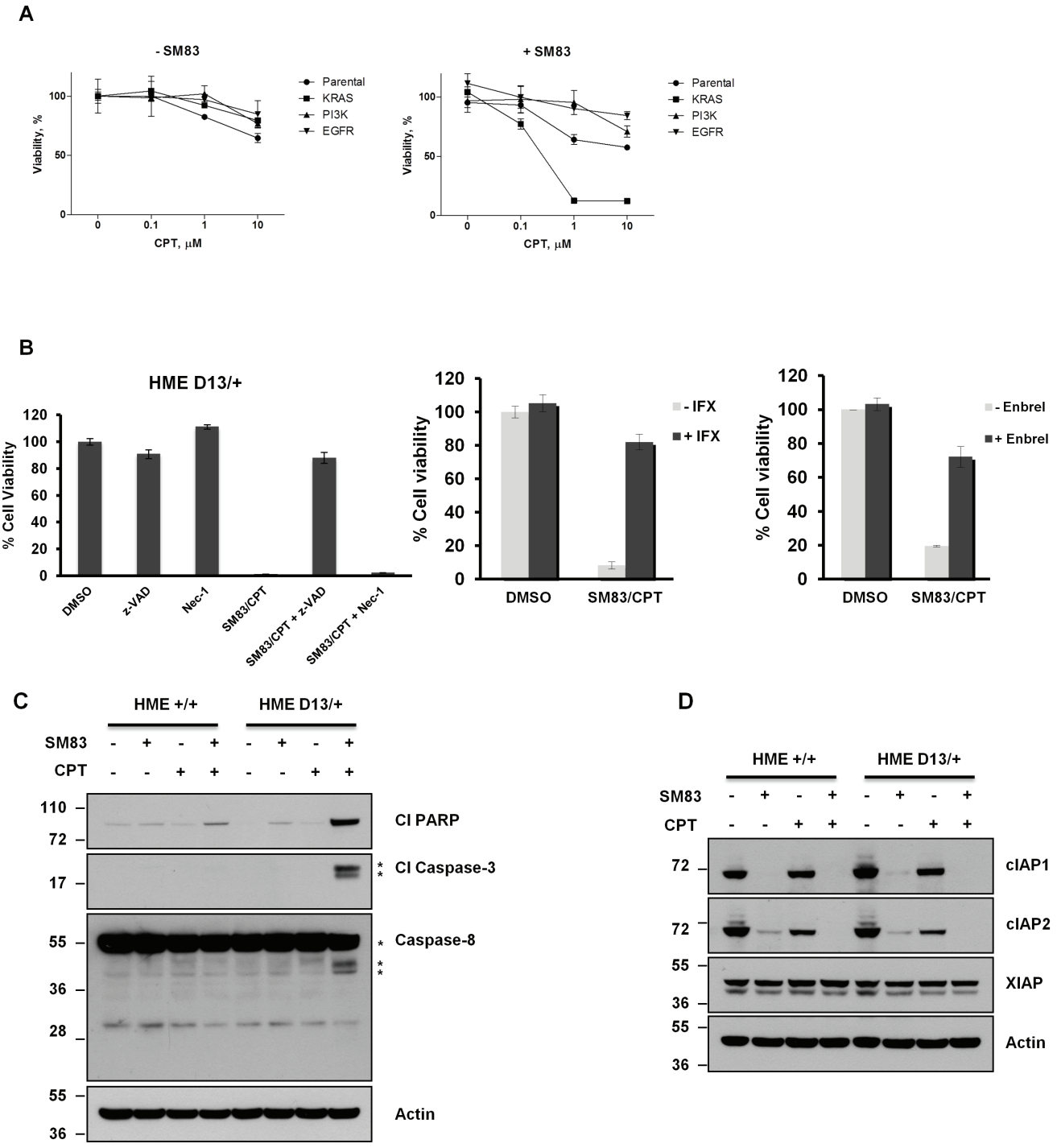

Figure 1: Oncogenic *KRAS* increases sensitivity of HME cells to DNA-damaging agents and TRAIL. (A) The parental human epithelial (HME) cell line and the isogenic cell lines with knock-in mutations in KRAS (G13D), PI3K (H1047R) and EGFR (delE746A750) were treated with varying doses of CPT alone (left panel) or in combination with 100 nM SM83 (right panel). Viabilities are shown after 24 h of treatment. (B) HME D13/+ cells were pre-incubated with DMSO, 50 μM z-VAD, 20 μM Nec-1 (left panel), 10 μg/ml Infliximab (IFX, middle panel) and 10 μg/ml Enbrel (right panel) for 1 h and subsequently treated with 100 nM SM83 and 1 μM CPT. Cell viability was determined after 24 h. (C, D) HME +/+ and HME D13/+ cells were mock treated and treated with 100 nM SM83, 1 μM CPT and with their combination for 6 h. Cells were lysed and subjected to western blot to detect the apoptosis markers cleaved PARP, caspase-3 and caspase-8 (C) and the SM targets cIAP1, cIAP2 and XIAP (D). Actin is the loading control, asterisks show the cleaved forms p17/p19 of caspase-3 and the pro-caspase p55/p57 forms of caspase-8, together with its cleaved forms p41/p43. One representative of two independent experiments is shown.

Table 1: Best hits from the high-throughput screening. HeLa cells were treated with FDA-approved drugs in combination with SM83 and izTRAIL. The most effective 10 compounds enhancers of the cytotoxic effect are listed.

Compound	P-value
10-hydroxycamptothecin	0,000103319
Camptothecin	0,000040974
Camptothecine (S,+)	0,001697753
AMSACRINE	0,000274229
FLUOROURACIL	0,000537959
Aminacrine hydrochloride	0,015471379
Decitabine	0,000022640
MEFLOQUINE	0,000168791
Sutent	0,000444038
NETILMICIN SULFATE	0,005887782

the parental HME or to HME carrying mutations activating PI3K and EGFR (Figure 1A). Moreover, HME D13/+ cells were more sensitive to izTRAIL alone or in combination with SM83 (Figure S1 upper panels), to the topoisomerase II inhibitor etoposide (ETO) and to neocarzinostatin (NCS), a DNA double strand break inducer (Figure S1 lower panel), suggesting a general enhanced sensitivity to cell death more than a specific mechanism favoring CPT-mediated death. Pre-treatment with pan-caspase inhibitor z-VAD strongly supports the idea that SM83/CPT treatment kills HME D13/+ cells through an apoptotic mechanism (Figure 1B left panel). In fact, the blocking of caspases resulted in almost complete protection from the treatment, while necroptosis inhibitor Necrostatin-1 (Nec-1) showed only a negligible effect. Importantly, as TNF is known to be a pivotal player in SM-mediated cell death, HME D13/+ were also pre-treated with the TNF-specific blockers Infliximab (Figure 1B middle panel) and Enbrel (Figure 1B right panel) which both remarkably rescued cells from the treatment, confirming the involvement of TNF in the SM83/CPT cell killing. Finally, by biochemical analysis we further confirmed that SM83 strongly increases the pro-apoptotic effect of CPT, as is evident from the substantial accumulation of cleaved PARP, caspase-8 and -3 (Figure 1C). Importantly, the altered sensitivity to treatment in cells with wild type or mutated *KRAS* did not stem from a diverse expression of the SM known targets cIAP1, cIAP2 and XIAP (Figure 1D), which are also depleted at the same level by SM83.

Endogenous and ectopic oncogenic *KRAS* sensitizes human epithelial cells to SM83 and CPT treatment

To further investigate the role of mutated KRAS in the increased sensitivity of HME, the cytotoxic response to CPT and SM83 was assessed following total KRAS knockdown. The results showed that reduced KRAS decreased the toxicity by about 50% (Figure 2A), thus confirming the involvement of KRAS in the enhanced sensitivity. Unfortunately, the lack of an antibody specific for mutant KRAS did not allow us to determine the efficiency of G13D down-regulation (Figure S2). Furthermore, the silencing also affected wild type KRAS, which might also have a protective role to the treatment. To overcome this limit, KRAS G13D was inducibly expressed in HME cells using doxycycline. Augmented levels of phosphorylated ERK1/2 (Figure 2B), a down-stream effector of KRAS, and GST-RBD pull-down experiments confirmed the increased expression of activated KRAS (Figure 2C) paralleled by an hypersensitivity to SM83/CPT co-treatment (Figure 2D). We then repeated the experiments with another human epithelial cell line to exclude a possible cell line-specificity of our observation. MCF10A transduced with the KRAS G13D inducible vector confirmed that expression of mutant KRAS causes the phosphorylation of ERK1/2 (Figure 2E) and hypersensitivity to cell death (Figure 2F).

Oncogenic KRAS-mediated up-regulation of Noxa sensitizes cells to SM83/CPT co-treatment

To determine the mechanisms by which oncogenic KRAS sensitizes non-tumoral cells to treatment, several cell lines expressing endogenous and ectopic KRAS G13D were analyzed by western blot for the levels of pro- and anti-apoptotic proteins of the Bcl-2 family (data not shown). In accordance to other works, we found that the presence of oncogenic KRAS considerably increases the basal levels of Noxa in untreated cells. Accordingly, HME bearing the KI G13D mutation displayed higher levels of Noxa compared to the parental cell line (Figure 3A left panel), while the basal levels of the Noxa natural antagonist Mcl-1 were not affected by oncogenic KRAS expression, but markedly dropped after CPT treatment in a SM83-independent manner. Moreover, transient induction of ectopic KRAS G13D in HME and MCF10A parental cell lines concurred to a marked increase of Noxa levels in both cell lines (Figure 3A right panels, upper and lower panel respectively). In line with these data, KRAS silencing reduced the levels of Noxa in HME KRAS G13D cells (Figure S2). Furthermore, since Mcl1 levels were reduced concurrently to Noxa up-regulation in HME cells (Figure 3A left panel), we checked whether Noxa increase was responsible for Mcl1 down-regulation. Mcl1 levels were therefore detected in KRAS G13D-induced HME cells which showed that the sole Noxa up-regulation in not sufficient to affect Mcl1 levels in untreated cells. We then analyzed by western blot HME KI D13/+ cells silenced with control or Noxa-specific siRNAs and treated with increasing concentrations of CPT (Figure 3B). Also in this case Mcl-1 stability was independent of Noxa presence, suggesting that Mcl-1 down-regulation stems from the treatment and not from Noxa up-regulation. To determine

whether the oncogenic KRAS-dependent accumulation of Noxa is responsible for the hypersensitivity to SM83/CPT, viability tests were performed after Noxa depletion (Figure S2). The results showed that Noxa silencing confers resistance to treatment in HME D13/+ cells (Figure 3C).

KRAS-induced up-regulation of Noxa is mediated by ERK2

We next investigated the mechanisms responsible for the acquired sensitivity of KRAS-mutated HME to treatment. Both parental and D13/+ HME cell lines were treated with CPT and SM83 in the presence of various inhibitors of the MAPK, AKT and PI3K pathways which can be stimulated by activated RAS. In parental cells, the administration of MEK1/2 inhibitors PD98059 and UO126, AKT inhibitor Triciribine or PI3K inhibitor LY294002 did not affect significantly the toxicity of SM83/CPT treatment (Figure 4A). In contrast, both MEK1/2 inhibitors partially protected D13/+ HME cells from SM83/CPT treatment and conferred resistance at the same degree as parental cells (Figure 4A). Having found that Noxa is a pivotal mediator of KRAS-dependent increased sensitivity to the combination (Figure 3C), we evaluated whether the MAPK pathway was responsible for the increased levels of Noxa. We found that both MEK inhibitors reduced, as expected, the levels of phosphorylated ERK1 and ERK2, and concurrently reduced the levels of Noxa (Figure 4B). Interestingly, also Mcl1 levels were slightly reduced by the MEK inhibitors, suggesting that both Noxa and Mcl1 expression is regulated by the MEK/ERK pathway. Importantly, MEK inhibition slightly reduced Noxa basal levels also in parental HME (left panel) suggesting that the MAPK

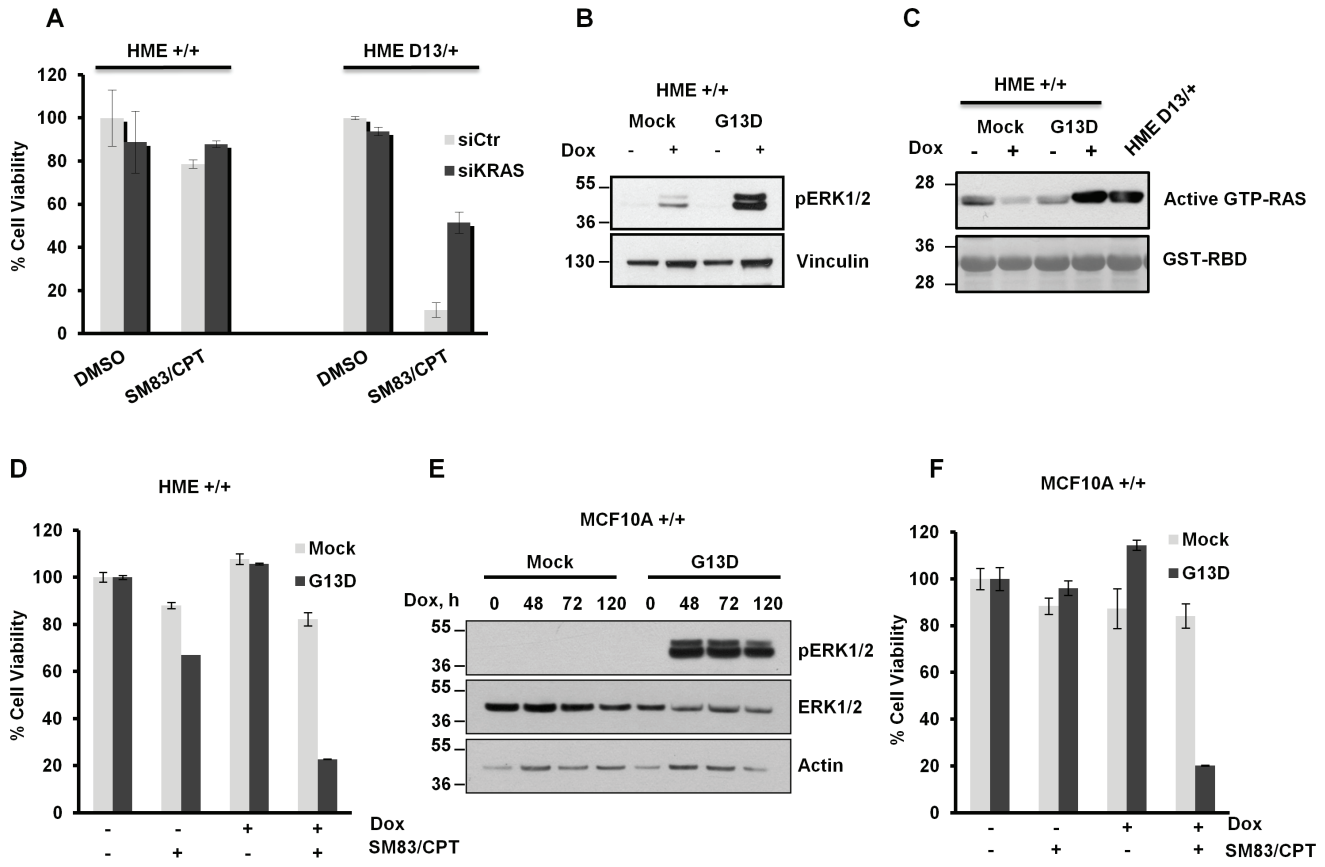

Figure 2: Endogenous and ectopic mutated *KRAS* confers sensitivity to SM83 and CPT co-treatment. (A) HME +/+ and HME D13/+ were transfected with siRNA targeting KRAS for 48 h and subsequently treated with 100 nM SM83 and 1 μM CPT. Cell viability was determined after 24 h of treatment. (B) HME pINDUCER20-Mock (Mock) and HME pINDUCER20-KRAS G13D (G13D) were incubated with doxycycline (Dox, 250 ng/ml) for 48 h, lysed and a western blot was performed. The presence of activated KRAS was determined by detection of phosphorylated ERK1/2. (C) Active GTP-RAS was purified in cells stimulated as in (B) by pull-down assay using the recombinant RBD domain of RAF1; HME D13/+ are shown as positive control for activated KRAS. (D) HME Mock and KRAS G13D were incubated with Dox (250 ng/ml) for 48 h and treated with 100 nM SM83 and 1 μM CPT. Cell viability was determined after 24 h. (E) MCF10A Mock and KRAS G13D were incubated with Dox (250 ng/ml) for the indicated time, lysed and analyzed by western blot for the detection of ERK1/2 and phosphorylated ERK1/2. Actin is shown as a loading control. (F) MCF10A Mock and KRAS G13D were incubated with Dox (250 ng/ml) for 48 h and treated with 100 nM SM83 and 0.1 μM CPT. Cell viability was determined after 24 h. One representative of two independent experiments is shown.

pathway stimulates Noxa also in physiological conditions. To understand whether MEK targets ERK1 and ERK2 both contribute to Noxa regulation, we silenced each of them in D13/+ HME cells and found that only ERK2 down-regulation reduced Noxa levels, while ERK1 silencing marginally increased accumulation of Noxa (Figure 4C right panel). Again, Mcl1 was not down-regulated by Noxa accumulation, further confirming that the treatment with CPT, and not Noxa up-regulation, was responsible for Mcl1 reduction in HME cells (Figure 3A). In line with the regulation of Noxa observed in figure 4C, ERK1 silencing slightly, but significantly, enhanced the sensitivity of D13/+ HME cells to SM83/CPT treatment, while ERK2 silencing resulted in the opposite effect (Figure 4D).

Sensitivity to SM83/CPT is independent of KRAS status in a panel of colorectal cancer cell lines

Our findings support the notion that oncogenic KRAS can sensitize premalignant cells to SM83/CPT treatment. We then considered whether this also occurs in malignant cells, and for this reason we employed a panel of isogenic CRC cell lines where mutated KRAS is either KI (+/+ and D13/+, SW48 and Lim1215) or KO (D13/- and +/-, HCT-116 and DLD1). Surprisingly and in

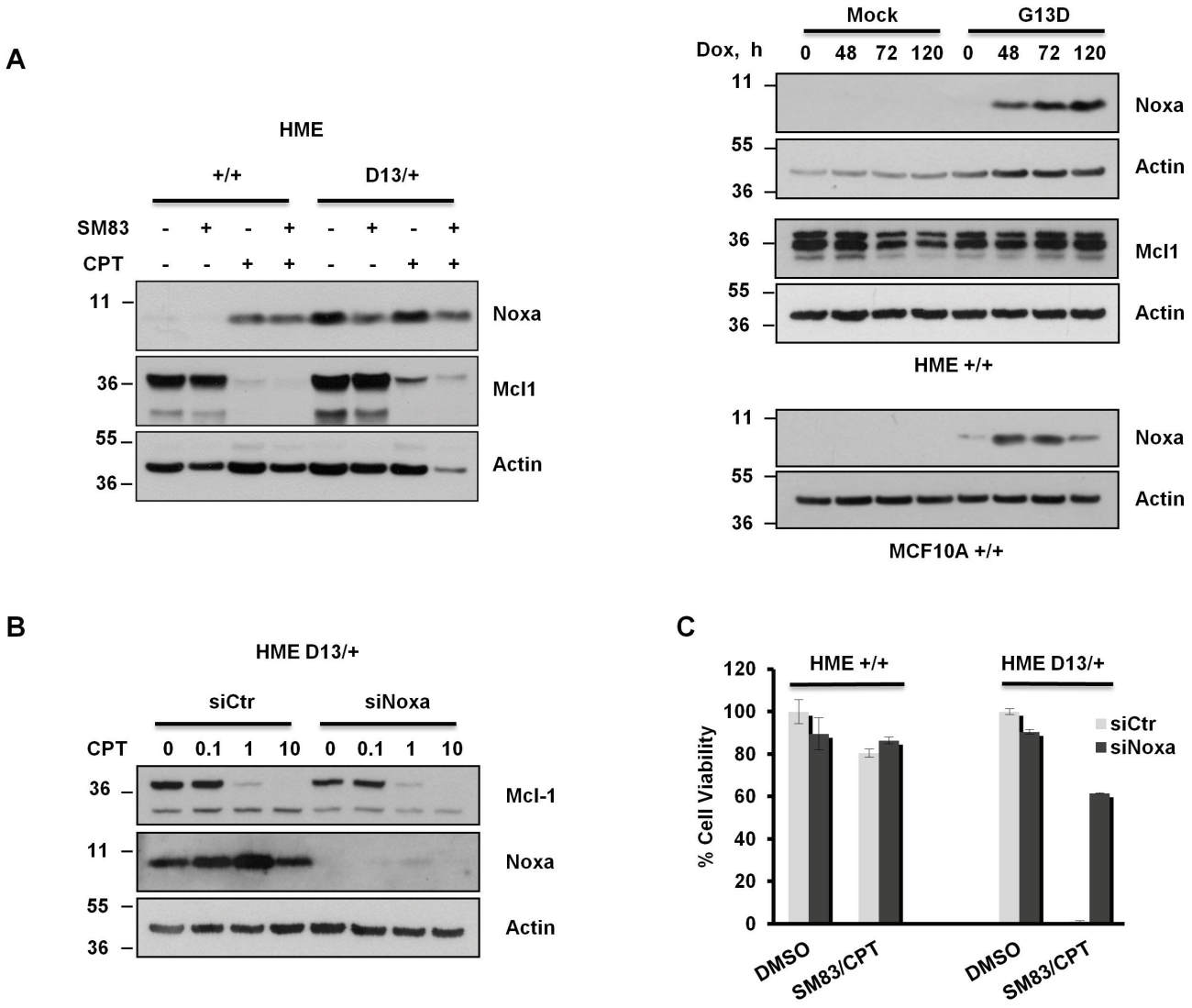

Figure 3: Increased Noxa expression in *KRAS*-mutated HME favours SM83/CPT-induced cell death. (A, left panel) HME +/+ and HME D13/+ cells were treated with 100 nM SM83 and 1 μM CPT for 6 h, lysed and subjected to western blot to detect Noxa and Mcl1 levels. (A, right panel) HME/MCF10A Mock and KRAS G13D were incubated with Dox (250 ng/ml) for the indicated time and subjected to western blot to detect Noxa and Mcl1 levels. Actin is shown as the loading control. (B) HME D13/+ cells were trasfected with control and Noxa-targeting siRNAs and, after 48 h, were treated with the indicated concentration of CPT (μM) for 6 h. Cells were then lysed and analyzed by western blot to evaluate Mcl1 levels. Noxa is shown to check the silencing efficiency and actin as the loading control. (C) HME +/+ and HME D13/+ were transiently transfected with siRNA targeting Noxa for 48 h and subsequently treated with 100 nM SM83 and 1 μM CPT. Cell viability was determined after 24 h. One representative of two independent experiments is shown.

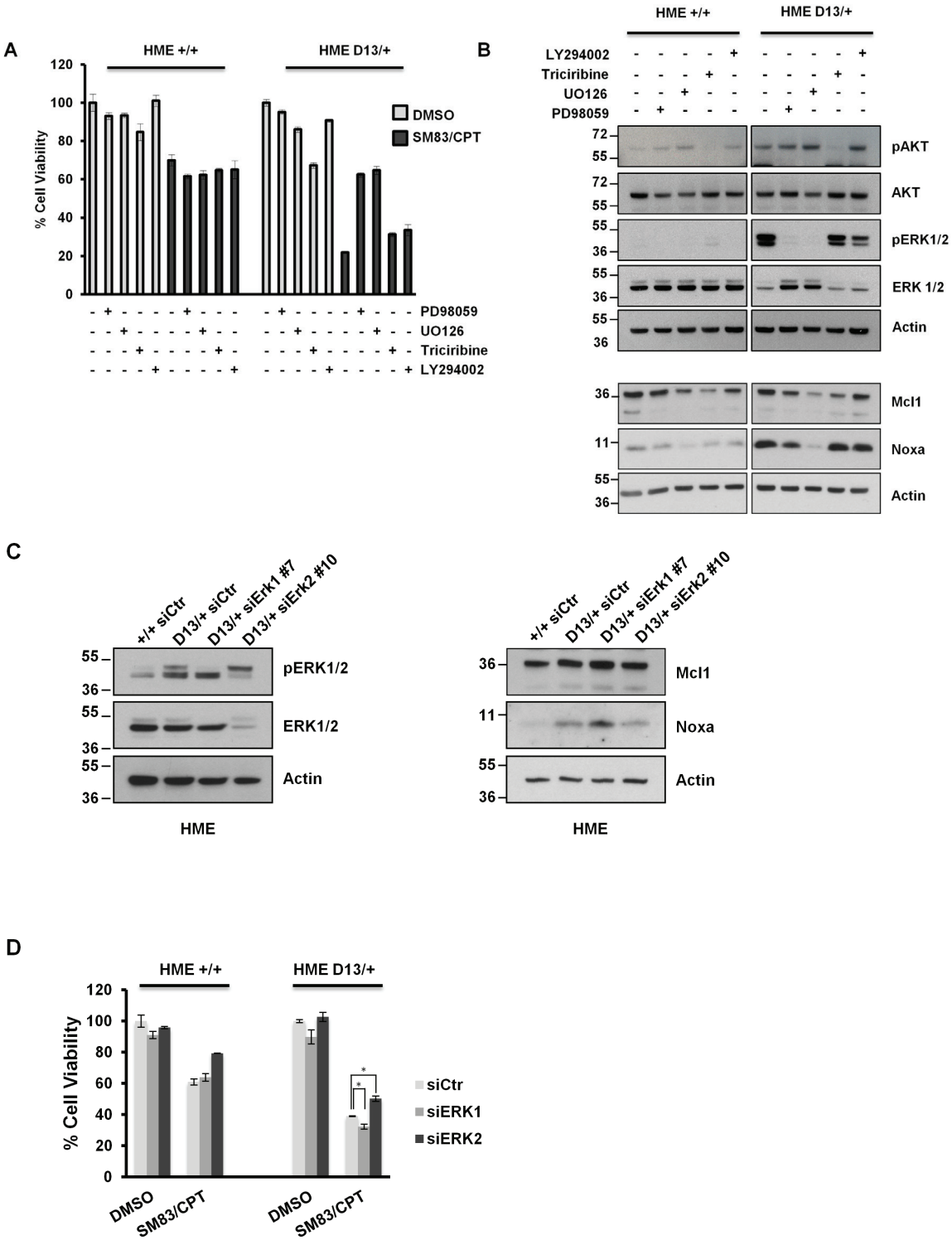

Figure 4: ERK2, but not ERK1 is responsible for KRAS-dependent Noxa-induction. (A) HME +/+ and HME D13/+ cell lines were pre-incubated with 50 μM PD98059, 25 μM UO126, 20 μM Triciribine and 20 μM LY294002 for 2 h, and then treated with 100 nM SM83 and 1 μM CPT. Cell viability was quantified after 24 h. One representative of three independent experiments is shown. (B) HME +/+ (left panel) and HME D13/+ (right panel) cell lines were treated with 50 μM PD98059, 25 nM UO126, 20 μM Triciribine and 20 μM LY294002 for 2 h, and subsequently analyzed by western blot to detect the phosphorylated forms of AKT, ERK1 and ERK2, their total levels (upper panels) or Noxa and Mcl1 (lower panels). Actin is shown as loading control. (C) HME +/+ and HME D13/+ were transiently transfected with the indicated siRNAs for 72 hours and subsequently analyzed by western blot to detect total and phosphorylated ERK1 and ERK2, and their total levels (left panel), Noxa and Mcl1 (right panel). Actin is shown as loading control. (D) Parental HME +/+ and HME D13/+ cells were silenced for 48 h and then treated with DMSO and 100 nM SM83 plus 1 μM CPT for further 24 h. One representative of three independent experiments is shown. * $P < 0.05$ vs siCtr.

contrast to the premalignant settings, the sensitivity of the CRC cell lines to SM83/CPT treatment was independent of the KRAS status (Figure 5A-D). We then investigated the Noxa status, which was responsible for the increased sensitivity of normal epithelial cells bearing oncogenic KRAS, and found that its levels were unaffected by the presence of mutated KRAS (Figure 5E-H). Likewise, the levels of Noxa-antagonist Mcl1 were not repressed by the treatment with CPT and/or SM83, and further experiments confirmed an increased stability of Mcl1 in colorectal cancer compared to HME cells (Figure S3). Noxa basal levels were however higher in CRC than in HME cell lines (data not shown), suggesting that pro-apoptotic mediators can even be up-regulated in tumor cells, but there are likely other activated pathways that counterbalance the potential pro-apoptotic stimuli.

Aberrant activation of AKT counterbalances KRAS-mediated pro-apoptotic scenario in colorectal cancer cells

Despite the presence of mutant KRAS, our findings suggest that cancer cells are not sensitized to SM83/CPT treatment. Therefore, we hypothesized that malignant progression might have caused the deregulation of other pathways that can counterbalance the potential apoptotic effect of oncogenic KRAS. Interestingly, HCT116 and DLD1 cells bear mutated PI3K, which results in hyper-activation of the PI3K/AKT pathway, a signaling cascade known to promote cell survival. For this reason, we treated HCT116 and DLD1 cells bearing mutated and wild type KRAS with SM83/CPT after pre-treatment with inhibitors of MEK1/2, AKT and PI3K. Interestingly, and concordant to our hypothesis, AKT inhibition restored sensitivity to the treatment only in the presence of mutant KRAS (Figure 6A and 6B). Noxa levels were lowered by MAPK blocking (Figure 6C and 6D) as already observed in HME cells (Figure 4B), but were not affected by AKT inhibition, suggesting that the AKT pathway blocks the pro-death effect triggered by oncogenic KRAS in an independent fashion. Importantly, AKT inhibition sensitized to SM83/CPT treatment also CRC cell lines bearing wild type PI3K (Figure S4), further supporting the idea that AKT counteracts the pro-death stimulus deriving from oncogenic KRAS. Surprisingly, LY294002 treatment, which reduced AKT activation, did not sensitize to SM83/CPT treatment (Figure 6C and 6D). We speculate that this stems from the fact that the LY294002 inhibitor did not completely abolish AKT phosphorylation and therefore we tested the GDC-0941 PI3K inhibitor. This compound reduced the AKT activation more efficiently (Figure 6E left panel) and sensitized the HCT116 D13/- in the same way as Triciribine (Figure 6E right panel). Finally, we investigated the mechanisms by which Noxa levels are controlled in HCT116 cells and demonstrated that the findings described for HME are true also in this cancer cell line. In fact, the targeting of ERK1 by silencing enhanced the levels of Noxa, while a specific siRNA targeting ERK2 slightly reduced its expression (Figure 6F).

DISCUSSION

In our work, we searched for FDA-approved drugs that increase the cytotoxic activity of IAP-antagonizing compounds and death ligands. For this purpose, using a high-throughput approach, we combined SM83 [25] and izTRAIL [29] to a library of about 3000 compounds. CPT was identified several times among the best hits and validated, alone or in combination with SM83 and/or izTRAIL, in a panel of normal and cancer cell lines bearing KI and KO mutations in genes frequently mutated in cancer. The employment of isogenic cell lines with distinct point mutations is a powerful tool to comprehend the effect of oncogene activation [31] and addiction [32], and synthetic lethal interactions [27, 33] in cancer cells. With this approach, we found that the endogenous and ectopic expression of KRAS bearing the G13D mutation sensitizes normal, but not cancer cells, to CPT plus SM83 or TRAIL treatment, and to other DNA-damaging agents.

Since oncogenic KRAS stimulates the up-regulation of the pro-apoptotic protein Noxa [10, 34], we checked the occurrence of this event in premalignant cells and whether it was associated with the increased sensitivity to treatment. In both human epithelial cells HME and MCF10A, the expression of oncogenic KRAS was indeed responsible for the up-regulation of Noxa in a MEK/ERK-dependent manner and for the augmented death upon SM83/CPT treatment. Accordingly, chemical inhibition of the MEK1/2 kinases that results in prevention of ERK1/2 phosphorylation and silencing of ERK2, but not ERK1, down-regulated Noxa in HME D13/+ to levels comparable to parental HME (+/+) cells. Of note, ERK2 silencing slightly, but reproducibly, protected HME D13/+ cells, while ERK1 silencing even sensitized to SM83/CPT treatment and simultaneously increased Noxa basal levels especially in CRC cell lines. The observation that ERK1 and ERK2 display opposite effects in regulating Noxa levels and mediating chemotherapy responsiveness was also described in hepatocellular carcinoma cells [35]. In this case, ERK2 knockdown was responsible for increased Noxa levels after cisplatin treatment. Although we investigated Noxa basal levels in our experiments, these contrasting results strongly support that ERK1 and ERK2 mutually regulate each other [36] in a cell type-dependent manner. Surprisingly, MEK inhibitors strongly prevented treatment cytotoxicity, while siRNA targeting ERK1 and ERK2 only have a modest effect, despite siERK2 efficiently down-regulated Noxa levels. This suggests that other unknown regulatory mechanisms between the two ERK proteins eventually impact on the treatment outcome.

We then asked whether our findings are true not only

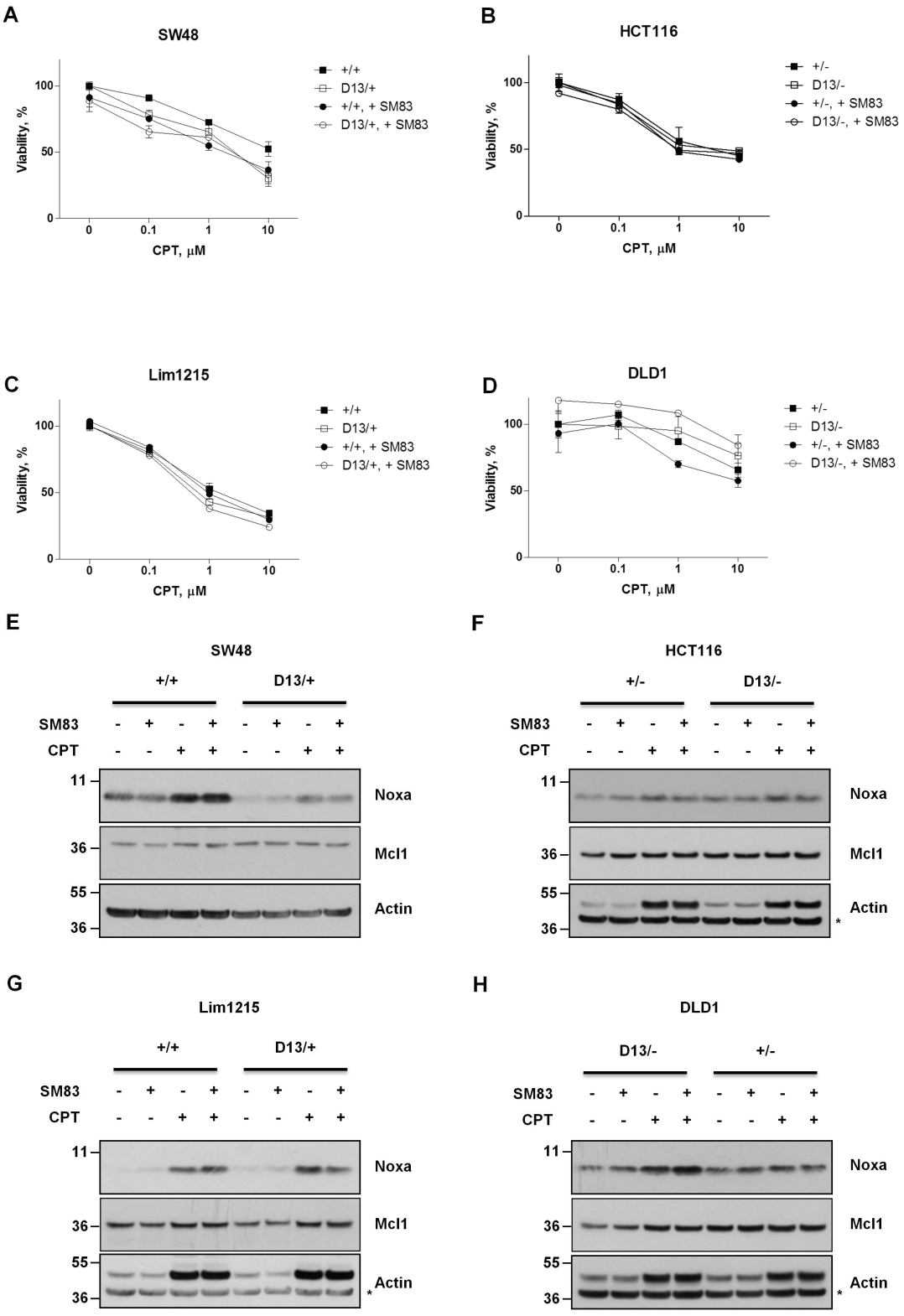

Figure 5: Oncogenic mutation of *KRAS* does not confer sensitivity to combined SM83/CPT nor stimulates Noxa levels. SW48 +/+ and SW48 D13/+ (A), HCT116 +/- and HCT116 D13/- (B), Lim1215 +/+ and Lim1215 D13/+ (C), DLD1 D13/- and DLD1 +/- (D) cell lines were treated with DMSO and the combination of SM83 and CPT at varying concentrations. Cell viability was evaluated after 24 h. One representative of three independent experiments is shown. SW48 +/+ and SW48 D13/+ (E), HCT116 +/- and HCT116 D13/- (F), Lim1215 +/+ and Lim1215 D13/+ (G), DLD1 D13/- and DLD1 +/- (H) cell lines were treated with DMSO and 100 nM SM83, 0.1 μM CPT either alone or in combination for 6 h. Cells were lysed and analyzed by western blotting to determine Noxa and Mcl1 levels. One representative of two independent experiments is shown. Asterisk indicates the specific band of Actin shown as loading control.

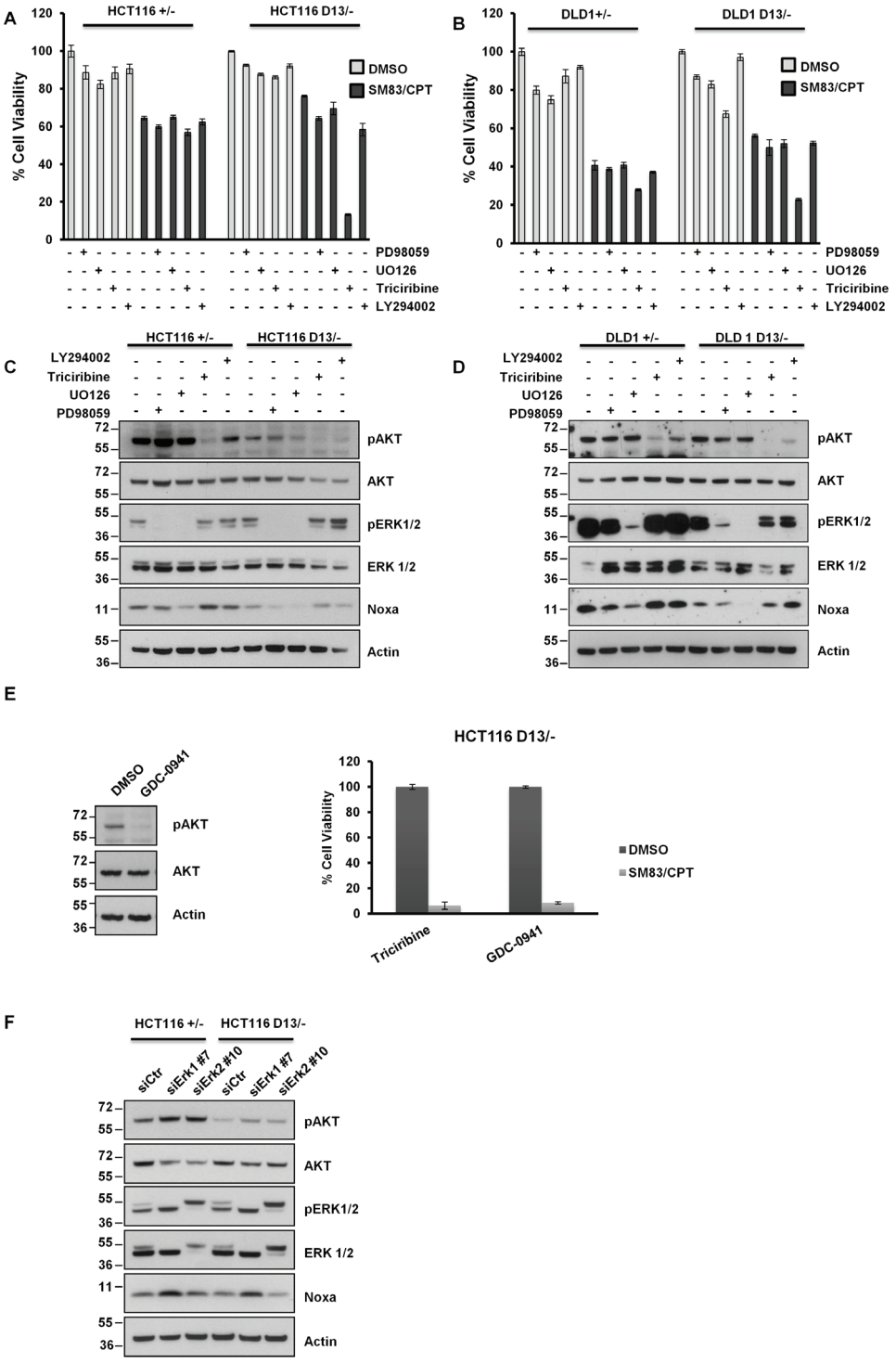

Figure 6: Aberrant AKT activation protects HCT116 and DLD1 cells from the pro-death effect of oncogenic *KRAS*. (A) HCT116 and (B) DLD1 cells were pre-incubated with 50 μM PD98059, 25 μM UO126, 20 μM Triciribine and 20 μM LY294002 for 2 h, and then mock-treated or treated with 100 nM SM83 and 1 μM CPT. Cell viability was quantified after 24 h. (C) HCT116 and (D) DLD1 cells were treated for 2 h with the indicated inhibitors as in (A) and then analyzed by western blot to detect Noxa levels and total and phosphorylated AKT and ERK levels. Actin is shown as loading control. (E, left panel) HCT116 D13/- cells were treated with 1 μM GDC-0941 for 2 h and analyzed by western blot to detect total and phosphorylated levels of AKT. Actin is shown as the loading control. (Right panel) Viability of HCT116 D13/- pre-treated with 1 μM GDC-0941 for 2 h and then treated with 100 nM SM83 and 1 μM CPT. Cell viability was quantified after 24 h and expressed as viability percentage to inhibitor alone. (F) HCT116 cells were transfected with siRNAs targeting ERK1 and ERK2, cells were collected after 72 h and analyzed by western blot to detect Noxa and total and phosphorylated levels of AKT and ERK. Actin is shown as loading control.

in premalignant cells, but also in cancer cells. To this end, a panel of isogenic colon cancer cell lines with KI and KO mutations of KRAS was tested. In clear contrast to HME and MCF10A cells, Noxa levels did not depend on KRAS status in cancer cells and in line with this observation cell sensitivity was almost identical in each pair of isogenic cells. Basal levels of Noxa in cancer cells were higher than in epithelial cells (data not shown), suggesting that tumor cells constitutively express some pro-apoptotic proteins at high level, but could also activate parallel pro-survival pathways to counteract the pro-death signals supported by the MEK/ERK axis. Considerable evidence shows that mutations in the RAS/MEK/ERK cascade are associated to aberrant activation of PI3K/AKT signaling [37] and therefore both pathways should be targeted simultaneously for effective responsiveness to treatment [11, 38]. In accordance to this hypothesis, HCT116 cells and DLD1, which bear PI3K activating mutations, are sensitized to SM83/CPT treatment when pre-treated with AKT inhibitors only in the presence of oncogenic KRAS, supporting the notion that AKT is protecting from oncogenic KRAS-dependent cancer cell sensitization (Figure 7). It is important to note that this protective role was demonstrated also in cells bearing wild type PI3K (Figure S4), confirming the general pivotal role of AKT in counterbalancing the pro-death effect of oncogenic KRAS.

In conclusion, our work has two main implications. First, targeting down-stream effectors of oncogenes might result in an immediate and transient anti-proliferative effect often achieved by conventional therapies, but, more importantly, could also shut-down the pro-death signals derived from oncogene activation. Secondly, for a successful treatment, targeting of the EGFR/MAPK pathway alone is not sufficient [39], as it results in emerging protecting mutations [4, 40], feedbacks [41] and incomplete responses. It is therefore imperative to characterize and inhibit also the aberrantly activated survival pathways in a combination treatment, in order to overcome the anti-apoptotic effect of PI3K/AKT activation and simultaneously to exploit the pro-death signal stemming from oncogenic activation.

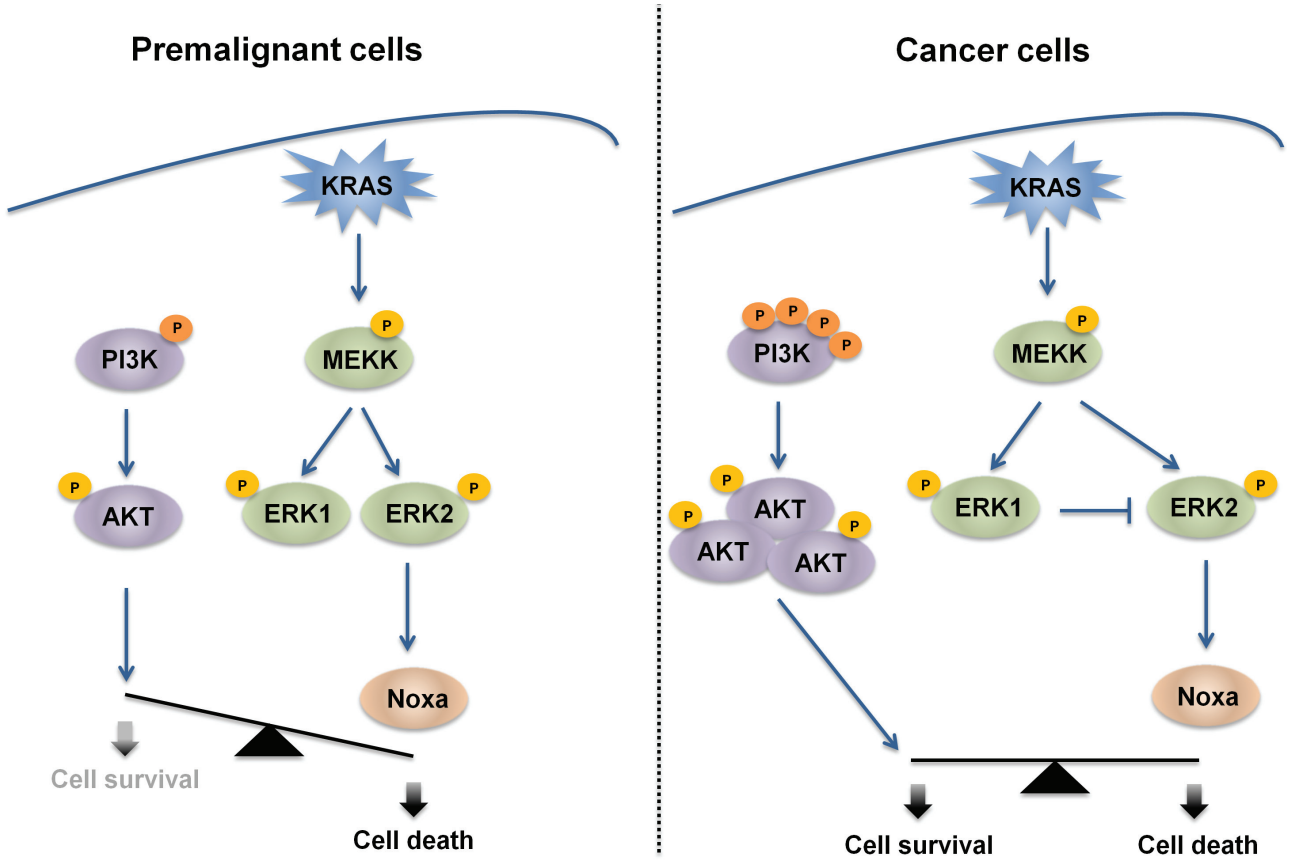

Figure 7: Proposed mechanism for oncogenic KRAS-mediated sensitization to cell death. In premalignant models, normal epithelial cells expressing endogenous or ectopic mutated KRAS express high levels of Noxa due to the hyper-activation of MAPK kinases and in particular of ERK2. In these settings, the basal activation of the PI3K/AKT pathway is not sufficient to protect from this pro-death stimulus and treatment with several cytotoxic agents results in Noxa-dependent cell killing. In contrast, in CRC cells, Noxa levels are independent of KRAS status and oncogenic KRAS-bearing cells respond to treatment to the same extent as in the presence of wild-type KRAS. In fact, mutated PI3K and up-stream stimuli likely deriving from the tyrosine kinase receptors activate AKT, which counterbalances the potential pro-death stimulus deriving from oncogenic KRAS.

METHODS

Cell lines

The human isogenic hTERT-immortalized mammary epithelial cell lines HME +/+ and HME D13/+, and the human epithelial mammary MCF10A together with the isogenic pairs of colorectal cancer cell lines SW48 +/+ and SW48 D13/+, HCT116 +/- and HCT116 D13/-, Lim1215 +/+ and Lim1215 D13/+, DLD1 D13/- and DLD1 +/- have already been described [4, 27]. HME isogenic pairs and MCF10A cell lines were cultured in DMEM-F12 (Gibco), supplemented with 10% FBS (LONZA), 2 mM glutamine (LONZA), 20 ng/ml EGF (Immunological Science), 10 µg/ml insulin (Sigma), 500 µg/ml hydrocortisone (Sigma-Aldrich). SW48 and DLD1 isogenic pairs were cultured with DMEM (Gibco) supplemented with 10% FBS and 2 mM glutamine. Lim1215 isogenic pairs were cultured with RPMI (LONZA) supplemented with 10% FBS, 2 mM glutamine and 1 µg/ml insulin. HCT116 were cultured in RPMI, supplemented with 2 mM glutamine, sodium pyruvate (LONZA), and non-essential amino acids (LONZA). HeLa cells for the high-throughput screening and packaging HEK293FT (Life Technologies) for lentiviral production were cultured in DMEM with 10% FBS. All cell lines were mycoplasma-free as determined by Takara Mycoplasma Detection Kit (Clontech).

Reagents

Antibodies targeting pan-RAS, Noxa (CalBiochem), Actin and ERK1/2 (Sigma), cleaved-PARP, cleaved caspase-3, phosphoERK1/2 (Thr202/Tyr204), pAKT and AKT (Cell Signaling), cIAP1 (R&D Systems), cIAP2 and XIAP (BD Biosciences), caspase-8 (Enzo Life Sciences) and Mcl-1 (Santa Cruz Biotechnology) were employed in western blot experiments. z-VAD(OMe)-FMK was purchased by BIOMOL, Necrostatin-1 from Enzo Life Sciences. PD98059 and UO126 were purchased from CalBiochem, LY294002 from Sigma, GDC-0941 and Triciribine from Selleckem. Infliximab (Schering-Plough) and Enbrel (Wyeth Pharmaceuticals) were used as TNF blockers. CPT and neocarzinostatin were purchased from Sigma-Aldrich, etoposide by Teva. SM83 synthesis has been described elsewhere [25, 28], while izTRAIL was purified as already shown [29]. Mutant KRAS (G13D) was cloned in the pINDUCER20 and lentiviral particles prepared modifying an already described protocol [30] and using Lipofectamine 2000 as transfection reagent. Expression of the transgene was induced by doxycycline (Sigma-Aldrich) at the indicated concentrations.

High-throughput screening

On day 1, 350 HeLa cells/well were seeded in 384-well white plates in 20 µl medium. At day 2, media was changed with cells being exposed to 100 nM SM83 in addition to FDA-approved drug libraries (ENZO Life Sciences, MicroSource Discovery Systems Inc. and Prestwick Chemical, France) with the drug library compounds present at a final concentration of 1 µM. At day 3, cells exposed to SM83 were also exposed to 20 pg/ml izTRAIL. Cell viability was estimated on day 5 by CellTiter-Glo (Promega). Hits were selected due to their capability to enhance the cytotoxic activity of SM83/izTRAIL and then validated using the same HeLa cells employed in the screening. In validation experiments, SM83 and izTRAIL were administered alone and in combination, also changing the schedule and pre-treating cells with SM83 24 h before izTRAIL or administrating these compounds simultaneously. On the basis of these results, validated hits were tested in a panel of premalignant and cancer cell lines.

Western blot

Cells were harvested by centrifugation at 4500 rpm for 5 min at 4°C. After washing once with PBS, lysates were prepared by resuspending cell pellets in 60-100 µl lysis buffer (125 mM Tris HCl pH 6.8, 5 % SDS) supplemented with 1x complete protease (Roche Diagnostics) and phosphatase inhibitors (Sigma-Aldrich). Lysates were boiled at 99°C, sonicated for 20 seconds at RT. Then lysates were centrifuged at 13000 rpm for 20 min at RT and cleared supernatants were transferred into a new tube and frozen at -20°C. Cell lysates were mixed with 4x reducing SDS-Sample buffer containing 10% β-mercaptoethanol (Sigma-Aldrich) and heated for 10 min at 99°C. Proteins (50 µg) were separated by SDS-PAGE using pre-cast 4-12% BisTris NuPAGE gels (Life Technologies), blotted to PVDF membranes (Millipore), which were washed with PBS-tween for 5 min, blocking buffer made of 4% non-fat milk in PBS-tween for 30 min and then incubated overnight with the indicated primary antibodies. Proteins were detected after hybridization with appropriate horseradish peroxidase (hrp)-conjugated secondary antibodies by adding a chemiluminescent substrate (EuroClone).

Cell viability assays

96-well optical bottom, polymer base white plates (Thermo Scientific) were used for viability tests. At day 1, 10000 cells per well were seeded in 100 µl medium. At day 2, cells were treated adding the indicated drug(s) in 10 µl volume per well. At day 3, cell viability was

determined using the CellTiter-Glo assay according to the manufacturer's instructions. Statistical analysis was performed with GraphPad Prism 5.02 using the two-tailed unpaired t-test.

Transfection and lentiviral transduction

To achieve transient knock-down of target proteins in HME cells, a reverse transfection protocol employing siRNAs (Qiagen) and RNAiMAX (Life technologies) was used. Briefly, 3.25 µl RNAiMAX and 200 µl Optimem (GIBCO) were mixed and incubated for 5 min at RT. Subsequently, 3.25 µl siRNA of a 20 µM stock were added, mixed and incubated for further 30 min at RT. The transfection mix was placed in a 6-well plate and 0.15 x 10^6 cells seeded in 800 µl on top.

Tumor cells were seeded the day before transfection and the same transfection mix as for reverse transfection was added on top of cells 24 h later. The cells were then incubated for 48 h before being drug-treated for further 24 h or cultured for 72 h before stopping the experiment. In each experiment, scramble siRNAs (siCtr) were used as a control.

Cells transduced with lentiviral particles were cultured in the presence of medium collected from HEK293FT packaging cells transfected with pINDUCER20-KRAS G13D (referred to as G13D) or empty vector (Mock). After 48 h, medium was replaced and fresh medium added in the presence of 500 µg/ml G418 (Life Technologies).

Ras-GTP pull-down assay

2.5 x 10^6 cells were seeded into 10 cm dishes. The next day, cells were incubated with and without 250 ng/ml of Dox. Cell lysis and RAS-GTP pulldown was performed. Cells were lysed in 500 µl of IP-lysis buffer supplemented with a cocktail of protease inhibitors. To fully detach lysed cells, they were scratched using a cell scraper and transferred into tubes for a 30-minute lysis at 4 °C on a rotator. Lysates were centrifuged at 13000 rpm for 30 min and cleared supernatants were transferred to a new tube. RAS-GTP was precipitated using beads coated with the RAF1-binding domain RBD recombinant protein. The following day, beads were washed 5 times with IP-lysis buffer and precipitated protein complexes were eluted from the beads via boiling in SDS-Sample buffer for 10 minutes at 80°C. Proteins were separated by SDS-PAGE and analyzed by western blot. As a loading control, proteins were stained by blue coomassie (Thermo Scientific Pierce).

ACKNOWLEDGMENTS

The inducible pINDUCER20 plasmid was kindly provided by Stephen Elledge (Howard Hughes Medical Institute), TNF blockers by Emilio Berti (Ospedale Maggiore Policlinico), the GST-RBD plasmid by Maria Grazia Borrello (Fondazione IRCCS Istituto Nazionale dei Tumori).

This study was supported by the Italian Association for Cancer Research (AIRC, MCO – 9998, D.D.).

REFERENCES

1. Pylayeva-Gupta Y, Grabocka E and Bar-Sagi D. RAS oncogenes: weaving a tumorigenic web. Nat Rev Cancer. 2011; 11: 761-774.
2. Eser S, Schnieke A, Schneider G and Saur D. Oncogenic KRAS signalling in pancreatic cancer. Br J Cancer. 2014; 111: 817-822.
3. Meyerhardt JA and Mayer RJ. Systemic therapy for colorectal cancer. N Engl J Med. 2005; 352: 476-487.
4. Misale S, Yaeger R, Hobor S, Scala E, Janakiraman M, Liska D, Valtorta E, Schiavo R, Buscarino M, Siravegna G, Bencardino K, Cercek A, Chen CT, et al. Emergence of KRAS mutations and acquired resistance to anti-EGFR therapy in colorectal cancer. Nature. 2012; 486: 532-536.
5. Weidle UH, Maisel D and Eick D. Synthetic lethality-based targets for discovery of new cancer therapeutics. Cancer Genomics Proteomics. 2011; 8: 159-171.
6. Steckel M, Molina-Arcas M, Weigelt B, Marani M, Warne PH, Kuznetsov H, Kelly G, Saunders B, Howell M, Downward J and Hancock DC. Determination of synthetic lethal interactions in KRAS oncogene-dependent cancer cells reveals novel therapeutic targeting strategies. Cell Res. 2012; 22: 1227-1245.
7. Corcoran RB, Cheng KA, Hata AN, Faber AC, Ebi H, Coffee EM, Greninger P, Brown RD, Godfrey JT, Cohoon TJ, Song Y, Lifshits E, Hung KE, et al. Synthetic lethal interaction of combined BCL-XL and MEK inhibition promotes tumor regressions in KRAS mutant cancer models. Cancer Cell. 2013; 23: 121-128.
8. Lamba S, Russo M, Sun C, Lazzari L, Cancelliere C, Grernrum W, Lieftink C, Bernards R, Di Nicolantonio F and Bardelli A. RAF suppression synergizes with MEK inhibition in KRAS mutant cancer cells. Cell Rep. 2014; 8: 1475-1483.
9. Huang S, Ren X, Wang L, Zhang L and Wu X. Lung-cancer chemoprevention by induction of synthetic lethality in mutant KRAS premalignant cells in vitro and in vivo. Cancer Prev Res (Phila). 2011; 4: 666-673.
10. de Bruijn MT, Raats DA, Hoogwater FJ, van Houdt WJ, Cameron K, Medema JP, Borel Rinkes IH and Kranenburg O. Oncogenic KRAS sensitises colorectal tumour cells to chemotherapy by p53-dependent induction of Noxa. Br J Cancer. 2010; 102: 1254-1264.
11. Di Nicolantonio F, Arena S, Tabernero J, Grosso S, Molinari F, Macarulla T, Russo M, Cancelliere C, Zecchin

D, Mazzucchelli L, Sasazuki T, Shirasawa S, Geuna M, et al. Deregulation of the PI3K and KRAS signaling pathways in human cancer cells determines their response to everolimus. J Clin Invest. 2010; 120: 2858-2866.

12. Tao S, Wang S, Moghaddam SJ, Ooi A, Chapman E, Wong PK and Zhang DD. Oncogenic KRAS confers chemoresistance by upregulating NRF2. Cancer Res. 2014;

13. Hata AN, Yeo A, Faber AC, Lifshits E, Chen Z, Cheng KA, Walton Z, Sarosiek KA, Letai A, Heist RS, Mino-Kenudson M, Wong KK and Engelman JA. Failure to induce apoptosis via BCL-2 family proteins underlies lack of efficacy of combined MEK and PI3K inhibitors for KRAS-mutant lung cancers. Cancer Res. 2014; 74: 3146-3156.

14. Hadj-Slimane R, Pamonsinlapatham P, Herbeuval JP, Garbay C, Lepelletier Y and Raynaud F. RasV12 induces Survivin/AuroraB pathway conferring tumor cell apoptosis resistance. Cell Signal. 2010; 22: 1214-1221.

15. Moller Y, Siegemund M, Beyes S, Herr R, Lecis D, Delia D, Kontermann R, Brummer T, Pfizenmaier K and Olayioye MA. EGFR-Targeted TRAIL and a Smac Mimetic Synergize to Overcome Apoptosis Resistance in KRAS Mutant Colorectal Cancer Cells. PLoS One. 2014; 9: e107165.

16. Gyrd-Hansen M and Meier P. IAPs: from caspase inhibitors to modulators of NF-kappaB, inflammation and cancer. Nat Rev Cancer. 2010; 10: 561-574.

17. Eckelman BP, Salvesen GS and Scott FL. Human inhibitor of apoptosis proteins: why XIAP is the black sheep of the family. EMBO Rep. 2006; 7: 988-994.

18. Fulda S. Molecular pathways: targeting inhibitor of apoptosis proteins in cancer--from molecular mechanism to therapeutic application. Clin Cancer Res. 2014; 20: 289-295.

19. Fulda S and Vucic D. Targeting IAP proteins for therapeutic intervention in cancer. Nat Rev Drug Discov. 2012; 11: 109-124.

20. Li L, Thomas RM, Suzuki H, De Brabander JK, Wang X and Harran PG. A Small Molecule Smac Mimic Potentiates TRAIL- and TNF{alpha}-Mediated Cell Death. Science. 2004; 305: 1471-1474.

21. Vince JE, Wong WW, Khan N, Feltham R, Chau D, Ahmed AU, Benetatos CA, Chunduru SK, Condon SM, McKinlay M, Brink R, Leverkus M, Tergaonkar V, et al. IAP Antagonists Target cIAP1 to Induce TNFα-Dependent Apoptosis. Cell. 2007; 131: 682-693.

22. Varfolomeev E, Blankenship JW, Wayson SM, Fedorova AV, Kayagaki N, Garg P, Zobel K, Dynek JN, Elliott LO, Wallweber HJA, Flygare JA, Fairbrother WJ, Deshayes K, et al. IAP Antagonists Induce Autoubiquitination of c-IAPs, NF-κB Activation, and TNFα-Dependent Apoptosis. Cell. 2007; 131: 669-681.

23. Probst BL, Liu L, Ramesh V, Li L, Sun H, Minna JD and Wang L. Smac mimetics increase cancer cell response to chemotherapeutics in a TNF-alpha-dependent manner. Cell Death Differ. 2010; 17: 1645-1654.

24. Lecis D, Drago C, Manzoni L, Seneci P, Scolastico C, Mastrangelo E, Bolognesi M, Anichini A, Kashkar H, Walczak H and Delia D. Novel SMAC-mimetics synergistically stimulate melanoma cell death in combination with TRAIL and Bortezomib. Br J Cancer. 2010; 102: 1707-1716.

25. Lecis D, Mastrangelo E, Belvisi L, Bolognesi M, Civera M, Cossu F, De Cesare M, Delia D, Drago C, Manenti G, Manzoni L, Milani M, Moroni E, et al. Dimeric Smac mimetics/IAP inhibitors as in vivo-active pro-apoptotic agents. Part II: Structural and biological characterization. Bioorg Med Chem. 2012; 20: 6709-6723.

26. Lecis D, De Cesare M, Perego P, Conti A, Corna E, Drago C, Seneci P, Walczak H, Colombo MP, Delia D and Sangaletti S. Smac mimetics induce inflammation and necrotic tumour cell death by modulating macrophage activity. Cell Death Dis. 2013; 4: e920.

27. Di Nicolantonio F, Arena S, Gallicchio M, Zecchin D, Martini M, Flonta SE, Stella GM, Lamba S, Cancelliere C, Russo M, Geuna M, Appendino G, Fantozzi R, et al. Replacement of normal with mutant alleles in the genome of normal human cells unveils mutation-specific drug responses. Proc Natl Acad Sci U S A. 2008; 105: 20864-20869.

28. Manzoni L, Belvisi L, Bianchi A, Conti A, Drago C, de Matteo M, Ferrante L, Mastrangelo E, Perego P, Potenza D, Scolastico C, Servida F, Timpano G, et al. Homo- and heterodimeric Smac mimetics/IAP inhibitors as in vivo-active pro-apoptotic agents. Part I: Synthesis. Bioorg Med Chem. 2012; 20: 6687-6708.

29. Ganten TM, Koschny R, Sykora J, Schulze-Bergkamen H, Buchler P, Haas TL, Schader MB, Untergasser A, Stremmel W and Walczak H. Preclinical Differentiation between Apparently Safe and Potentially Hepatotoxic Applications of TRAIL Either Alone or in Combination with Chemotherapeutic Drugs. Clin Cancer Res. 2006; 12: 2640-2646.

30. Meerbrey KL, Hu G, Kessler JD, Roarty K, Li MZ, Fang JE, Herschkowitz JI, Burrows AE, Ciccia A, Sun T, Schmitt EM, Bernardi RJ, Fu X, et al. The pINDUCER lentiviral toolkit for inducible RNA interference in vitro and in vivo. Proc Natl Acad Sci U S A. 2011; 108: 3665-3670.

31. Arena S, Isella C, Martini M, de Marco A, Medico E and Bardelli A. Knock-in of oncogenic Kras does not transform mouse somatic cells but triggers a transcriptional response that classifies human cancers. Cancer Res. 2007; 67: 8468-8476.

32. Roulston A, Muller WJ and Shore GC. BIM, PUMA, and the achilles' heel of oncogene addiction. Sci Signal. 2013; 6: pe12.

33. Farmer H, McCabe N, Lord CJ, Tutt AN, Johnson DA, Richardson TB, Santarosa M, Dillon KJ, Hickson I, Knights C, Martin NM, Jackson SP, Smith GC, et al. Targeting the DNA repair defect in BRCA mutant cells as a therapeutic

strategy. Nature. 2005; 434: 917-921.

34. Elgendy M, Sheridan C, Brumatti G and Martin SJ. Oncogenic Ras-induced expression of Noxa and Beclin-1 promotes autophagic cell death and limits clonogenic survival. Mol Cell. 2011; 42: 23-35.

35. Guegan JP, Ezan F, Theret N, Langouet S and Baffet G. MAPK signaling in cisplatin-induced death: predominant role of ERK1 over ERK2 in human hepatocellular carcinoma cells. Carcinogenesis. 2013; 34: 38-47.

36. Vantaggiato C, Formentini I, Bondanza A, Bonini C, Naldini L and Brambilla R. ERK1 and ERK2 mitogen-activated protein kinases affect Ras-dependent cell signaling differentially. J Biol. 2006; 5: 14.

37. Janku F, Wheler JJ, Naing A, Stepanek VM, Falchook GS, Fu S, Garrido-Laguna I, Tsimberidou AM, Piha-Paul SA, Moulder SL, Lee JJ, Luthra R, Hong DS, et al. PIK3CA mutations in advanced cancers: characteristics and outcomes. Oncotarget. 2012; 3: 1566-1575.

38. McCubrey JA, Steelman LS, Chappell WH, Abrams SL, Franklin RA, Montalto G, Cervello M, Libra M, Candido S, Malaponte G, Mazzarino MC, Fagone P, Nicoletti F, et al. Ras/Raf/MEK/ERK and PI3K/PTEN/Akt/mTOR cascade inhibitors: how mutations can result in therapy resistance and how to overcome resistance. Oncotarget. 2012; 3: 1068-1111.

39. Belmont PJ, Jiang P, McKee TD, Xie T, Isaacson J, Baryla NE, Roper J, Sinnamon MJ, Lee NV, Kan JL, Guicherit O, Wouters BG, O'Brien CA, et al. Resistance to dual blockade of the kinases PI3K and mTOR in KRAS-mutant colorectal cancer models results in combined sensitivity to inhibition of the receptor tyrosine kinase EGFR. Sci Signal. 2014; 7: ra107.

40. Misale S, Arena S, Lamba S, Siravegna G, Lallo A, Hobor S, Russo M, Buscarino M, Lazzari L, Sartore-Bianchi A, Bencardino K, Amatu A, Lauricella C, et al. Blockade of EGFR and MEK intercepts heterogeneous mechanisms of acquired resistance to anti-EGFR therapies in colorectal cancer. Sci Transl Med. 2014; 6: 224ra26.

41. Prahallad A, Sun C, Huang S, Di Nicolantonio F, Salazar R, Zecchin D, Beijersbergen RL, Bardelli A and Bernards R. Unresponsiveness of colon cancer to BRAF(V600E) inhibition through feedback activation of EGFR. Nature. 2012; 483: 100-103.